



**International Committee for Future Accelerators**

Sponsored by the Particles and Fields Commission of IUPAP

# **Beam Dynamics Newsletter**

**No. 37**

**Issue Editor:  
R. Wanzenberg**

**Editor in Chief:  
W. Chou**

**August 2005**



## Contents

<b>1</b>	<b>FOREWORD.....</b>	<b>9</b>
1.1	FROM THE CHAIRMAN.....	9
1.2	FROM THE EDITOR .....	10
<b>2</b>	<b>LETTERS TO THE EDITOR .....</b>	<b>12</b>
2.1	2004 THE YEAR OF JUBILEES: FIFTY YEARS OF CERN, FORTY YEARS OF ICTP, TEN YEARS OF ESRF USER OPERATION.....	12
	2.1.1 Introduction: .....	12
	2.1.2 50 Years of CERN.....	12
	2.1.3 40 Years of ICTP.....	14
	2.1.4 10 Years of ESRF User Operation .....	17
	2.1.5 Concluding Remarks .....	17
	2.1.6 References: .....	18
<b>3</b>	<b>INTERNATIONAL LINEAR COLLIDER (ILC).....</b>	<b>18</b>
3.1	ILC SCHOOL .....	18
3.2	HIGH GRADIENT SUPERCONDUCTING RF CAVITIES .....	19
	3.2.1 Introduction .....	19
	3.2.2 Review of Progress in Cavity & Cryomodule Gradients .....	19
	3.2.3 35 MV/m by Electropolishing & Mild Baking.....	20
	3.2.4 Designs for higher gradient structures.....	21
	3.2.5 Promising new material.....	23
	3.2.6 Summary.....	24
	3.2.7 References .....	24
<b>4</b>	<b>CYCLOTRONS .....</b>	<b>25</b>
4.1	BEAM DYNAMIC ACTIVITIES AT PSI'S HIGH INTENSITY CYCLOTRONS .....	25
	4.1.1 Introduction .....	25
	4.1.1.1 <i>Steps to increase the beam intensity</i> .....	26
	4.1.1.2 <i>Injector 2 upgrade</i> .....	27
	4.1.1.3 <i>The 72 MeV beam: Transfer and bunching</i> .....	27
	4.1.1.4 <i>Ring Cyclotron upgrade</i> .....	28
	4.1.2 Beam Dynamic Codes and Methods Development.....	28
	4.1.2.1 <i>Space Charge Solvers</i> .....	28
	4.1.2.2 <i>Particle Mesh Solver</i> .....	29
	4.1.2.3 <i>A Novel Massively Parallel Poisson Solver</i> .....	29
	4.1.2.4 <i>The Multigrid Solver</i> .....	30
	4.1.2.5 <i>Mad9p Methodical Accelerator Design Version 9</i> .....	31
	4.1.3 Eigenmode solvers.....	32

4.1.3.1	<i>Solving the matrix eigenvalue problem</i> .....	32
4.1.3.2	<i>Solving the correction equation</i> .....	33
4.1.3.3	<i>Parallelization</i> .....	34
4.1.3.3.1	<i>Trilinos</i> .....	34
4.1.3.3.2	<i>Data structures</i> .....	35
4.1.3.3.3	<i>Data distribution</i> .....	35
4.1.3.4	<i>Numerical experiments</i> .....	35
4.1.4	<i>Beam Dynamics Issues in Transport lines and Cyclotrons</i> .....	38
4.1.4.1	<i>870 keV Line</i> .....	38
4.1.4.2	<i>Injector 2 Coasting Beam</i> .....	39
4.1.4.3	<i>Injector 2 Including Collimation</i> .....	40
4.1.4.4	<i>Calculations in the Ring Cyclotron</i> .....	41
4.1.5	<i>Conclusions</i> .....	42
4.1.6	<i>Acknowledgments</i> .....	43
4.1.7	<i>References</i> .....	43
4.2	<i>DUBNA CYCLOTRONS - STATUS AND PLANS</i> .....	44
4.2.1	<i>Introduction</i> .....	44
4.2.2	<i>The U400 cyclotron</i> .....	45
4.2.3	<i>Modernization of the U400 cyclotron at the FLNR JINR</i> .....	46
4.2.4	<i>The U400M cyclotron</i> .....	47
4.2.5	<i>Beam extraction from U400M cyclotron</i> .....	47
4.2.6	<i>Tritium accelerator</i> .....	48
4.2.7	<i>References</i> .....	50
4.3	<i>COMPUTER SIMULATION OF BEAM DYNAMICS IN JINR PHASOTRON UP TO 650 MeV ENERGY</i> .....	51
4.3.1	<i>Introduction</i> .....	51
4.3.2	<i>Beam acceleration up to energy 650 MeV computer simulation</i> .....	53
4.3.3	<i>Conclusions</i> .....	56
4.3.4	<i>References</i> .....	56
4.4	<i>NEW BEAM DEVELOPMENTS AT IThemba LABS</i> .....	56
4.4.1	<i>Introduction</i> .....	56
4.4.2	<i>Cyclotrons at iThemba LABS</i> .....	57
4.4.2.1	<i>Light-ion solid-pole injector cyclotron (SPC1)</i> .....	57
4.4.2.2	<i>The second solid-pole injector cyclotron (SPC2)</i> .....	58
4.4.2.3	<i>The separated-sector cyclotron (SSC)</i> .....	58
4.4.3	<i>Extension of the facilities for the production of radionuclides</i> .....	60
4.4.3.1	<i>Additonal Buncher</i> .....	60
4.4.3.2	<i>New Vertical Beam Line for Radionuclide Production</i> .....	60
4.4.3.3	<i>Beam Splitting for Radionuclide Production</i> .....	62
4.4.4	<i>Improved Beam Diagnostic Equipment</i> .....	62
4.4.5	<i>Proposed new facilities for proton therapy at iThemba LABS</i> .....	63
4.4.6	<i>References</i> .....	63
4.5	<i>STATUS OF THE RIKEN ACCELERATOR RESEARCH FACILITY AND RI BEAM FACTORY PROJECT</i> .....	64
4.5.1	<i>Introduction</i> .....	64

4.5.2	RARF .....	66
4.5.2.1	<i>General description</i> .....	66
4.5.2.2	<i>Operation</i> .....	67
4.5.2.3	<i>Schedule towards the RIBF</i> .....	69
4.5.3	RIBF .....	70
4.5.3.1	<i>Acceleration modes and performance</i> .....	70
4.5.3.2	<i>Expected primary beam intensities: estimation</i> .....	71
4.5.3.3	<i>fRC</i> .....	72
4.5.3.4	<i>IRC</i> .....	73
4.5.3.5	<i>SRC</i> .....	74
4.5.3.6	<i>BigRIPS</i> .....	76
4.5.3.7	<i>Expansion of the nuclear world in the RIBF: estimation</i> .....	77
4.5.3.8	<i>Experimental installations in the Phase II</i> .....	77
4.5.4	Summary .....	78
4.5.5	References .....	79
<b>5</b>	<b>POLARIZATION .....</b>	<b>80</b>
5.1	POLARIZED BEAM ACCELERATION IN COSY AND FUTURE OPTIONS FOR POLARIZATION AT HESR .....	80
5.1.1	Introduction .....	80
5.1.2	Cooler Synchrotron COSY .....	81
5.1.2.1	<i>Spin Resonances</i> .....	82
5.1.2.2	<i>Polarized Beam Acceleration</i> .....	82
5.1.2.3	<i>Spin Manipulation</i> .....	83
5.1.3	High-Energy Storage Ring HESR .....	83
5.1.3.1	<i>Polarized Antiprotons</i> .....	84
5.1.3.2	<i>Spin Resonances</i> .....	84
5.1.3.3	<i>Siberian Snake</i> .....	85
5.1.4	Conclusion and Outlook .....	86
5.1.5	Acknowledgement .....	87
5.1.6	References .....	87
5.2	SPIN POLARISATION AT DESY .....	88
5.2.1	Introduction .....	88
5.2.2	Longitudinally polarised electron and positron beams in HERA .....	88
5.2.2.1	<i>Generalities and HERA-I</i> .....	88
5.2.2.2	<i>HERA-II</i> .....	89
5.2.2.3	<i>Recent developments</i> .....	90
5.2.3	A new spin-orbit tracking code, SLICKTRACK .....	92
5.2.4	The invariant spin field and spin tunes .....	92
5.2.5	References .....	93
5.3	POLARIZED PROTON ACCELERATION AT RHIC .....	93
5.3.1	Introduction .....	93
5.3.2	Challenge for accelerating polarized protons in RHIC .....	95
5.3.2.1	<i>Polarization</i> .....	95
5.3.2.2	<i>Luminosity</i> .....	96
5.3.3	RHIC performance .....	96

5.3.4	Acknowledgement .....	98
5.3.5	References .....	98
<b>6</b>	<b>ACTIVITY REPORTS .....</b>	<b>99</b>
6.1	BEAM-BEAM COLLISIONS WITH AN ARBITRARY CROSSING ANGLE: ANALYTICAL TUNE SHIFTS, TRACKING ALGORITHM WITHOUT LORENTZ BOOST, CRAB-CROSSING99	
6.1.1	Introduction.....	99
6.1.2	Beam-beam tune shift formulae.....	99
6.1.3	Beam-beam interaction formulae for tracking.....	102
6.1.3.1	<i>Kick from a single slice</i> .....	104
6.1.3.2	<i>Tracking algorithm</i> .....	105
6.1.4	Comparison of analytical tune shifts with numerical simulations.....	106
6.1.5	Conclusions.....	108
6.1.6	References.....	109
6.2	A LONGITUDINAL COUPLED BUNCH FEEDBACK FOR HERA-P.....	109
6.2.1	Introduction.....	109
6.2.2	The Feedback System .....	111
6.2.3	Outlook.....	114
6.2.4	References.....	114
6.3	SIMULATION OF COHERENT SYNCHROTRON RADIATION EFFECTS FOR THE SECOND BUNCH COMPRESSOR CHICANE AT THE VUV-FEL.....	114
6.3.1	Introduction.....	114
6.3.2	Notes on CSR Simulations .....	115
6.3.3	Bunch Compressor Chicanes .....	116
6.3.4	Simulation Results .....	118
6.3.5	Conclusion .....	122
6.3.6	References.....	122
<b>7</b>	<b>WORKSHOP AND CONFERENCE REPORTS .....</b>	<b>123</b>
7.1	SUMMARY OF THE 32ND ICFA ADVANCED BEAM DYNAMICS WORKSHOP ON “ENERGY RECOVERING LINACS” (ERL2005) .....	123
7.1.1	Introduction.....	123
7.1.2	Electron Guns and Injector Designs .....	125
7.1.2.1	<i>DC, Normal -Conducting RF and Superconducting RF Guns</i> .....	125
7.1.2.2	<i>Beam Dynamics in the Gun and Injector</i> .....	127
7.1.2.3	<i>The Cathode and Laser Package</i> .....	128
7.1.2.4	<i>Modeling and Computational Issues</i> .....	130
7.1.2.5	<i>Magnetized Beams and Polarization</i> .....	131
7.1.3	Optics and Beam Transport .....	132
7.1.3.1	<i>Ongoing ERL projects</i> .....	132
7.1.3.2	<i>Emittance Growth</i> .....	133
7.1.3.3	<i>Stability Issues</i> .....	133
7.1.3.4	<i>Longitudinal Phase Space Manipulations</i> .....	134
7.1.3.5	<i>BBU instability and linac optics</i> .....	134
7.1.3.6	<i>Accelerator modeling</i> .....	135

7.1.3.7	<i>Merger Design</i> .....	135
7.1.3.8	<i>Halo formation</i> .....	136
7.1.3.9	<i>Space charge and CSR Modeling</i> .....	136
7.1.3.10	<i>Collaborations</i> .....	137
7.1.3.11	<i>Summary of Recommended Studies</i> .....	137
7.1.4	Superconducting RF and RF Control.....	137
7.1.4.1	<i>Superconducting Modules for ERLs</i> .....	138
7.1.4.2	<i>Cavity Designs for ERLs</i> .....	138
7.1.4.3	<i>Cavity Quality</i> .....	139
7.1.4.4	<i>HOM Damping</i> .....	139
7.1.4.5	<i>Microphonics</i> .....	140
7.1.4.6	<i>Frequency Tuner</i> .....	141
7.1.4.7	<i>RF Control</i> .....	141
7.1.4.8	<i>Input Couplers</i> .....	142
7.1.4.9	<i>RF Power Sources</i> .....	142
7.1.4.10	<i>Cryogenics</i> .....	142
7.1.4.11	<i>Injector Cryomodules</i> .....	143
7.1.4.12	<i>Transfer to Industry</i> .....	143
7.1.5	Synchronization, Diagnostics and Instrumentation.....	144
7.1.5.1	<i>Transverse Beam Profile</i> .....	144
7.1.5.2	<i>Longitudinal Beam Profile</i> .....	145
7.1.5.3	<i>Machine Timing and Synchronization</i> .....	146
7.1.5.4	<i>Beam Position</i> .....	147
7.1.5.5	<i>Machine Protection</i> .....	147
7.1.5.6	<i>Summary</i> .....	148
7.2	SUMMARY OF THE 34TH ICFA ADVANCED BEAM DYNAMICS WORKSHOP “HIGH POWER SUPERCONDUCTING ION, PROTON, AND MULTI-SPECIES LINACS - HPSL 2005”.....	148
7.2.1	Introduction.....	148
7.2.2	Plenary Sessions.....	149
7.2.3	Parallel working group sessions.....	150
7.2.3.1	<i>Beam Dynamics session</i> .....	150
7.2.3.2	<i>Superconducting Radiofrequency Resonators for Ion Linacs</i> .....	151
7.2.3.3	<i>High-power and low level RF</i> .....	151
7.2.4	Summary.....	152
7.3	REPORT ON THE ICFA MINI-WORKSHOP ON “COMMISSIONING OF X-RAY FREE-ELECTRON-LASERS” 18-22 APRIL 2005 AT DESY, ZEUTHEN.....	152
7.3.1	Introduction and Summary.....	152
7.3.2	Background and Goals of the Workshop.....	153
<b>8</b>	<b>FORTHCOMING BEAM DYNAMICS EVENTS</b> .....	<b>155</b>
8.1	THE 35 <sup>TH</sup> ADVANCED BEAM DYNAMICS WORKSHOP: THE PHYSICS AND APPLICATIONS OF HIGH BRIGHTNESS ELECTRON BEAMS.....	155
8.1.1	Workshop background.....	155
8.1.2	Workshop mission.....	155
8.1.3	Program.....	155

8.1.4	Contact and registration .....	156
8.1.5	Committees .....	156
8.2	THE 36 <sup>TH</sup> ICFA ADVANCED BEAM DYNAMICS WORKSHOP: NANOBEAM 2005 .....	157
8.2.1	Topics... ..	157
8.2.2	Sessions.....	157
8.2.3	Committees .....	157
8.2.4	Contact.....	158
8.3	THE 37 <sup>TH</sup> ADVANCED BEAM DYNAMICS WORKSHOP: FUTURE LIGHT SOURCES 2006.....	158
8.4	THE 38 <sup>TH</sup> ADVANCED BEAM DYNAMICS WORKSHOP: LBI-LPA 2005, LASER-BEAM INTERACTIONS AND LASER PLASMA ACCELERATORS .....	158
8.5	MINI-WORKSHOP ON LOW LEVEL RF: LLRF05 .....	159
8.5.1	Topics... ..	159
8.5.2	Registration.....	159
8.5.3	Programme.....	159
8.5.4	Contact.....	160
8.5.5	Committees .....	160
8.6	MINI-WORKSHOP ON “THE FRONTIER OF SHORT BUNCHES IN STORAGE RINGS” .....	160
8.6.1	Topics... ..	160
8.6.2	Organizing Committee.....	161
8.7	AN ONE YEAR INTERNATIONAL SCOPING STUDY ON NEUTRINO FACTORIES AND SUPERBEAMS.....	161
8.7.1	Introduction.....	161
8.7.2	Neutrino Oscillation Physics today .....	161
8.7.3	Future Neutrino Beams .....	162
8.7.4	The International Scoping Study .....	162
8.7.5	References.....	163
<b>9</b>	<b>ANNOUNCEMENTS OF THE BEAM DYNAMICS PANEL .....</b>	<b>163</b>
9.1	ICFA BEAM DYNAMICS NEWSLETTER.....	163
9.1.1	Aim of the Newsletter.....	163
9.1.2	Categories of Articles .....	163
9.1.3	How to Prepare a Manuscript .....	164
9.1.4	Distribution .....	164
9.1.5	Regular Correspondents.....	165
9.2	ICFA BEAM DYNAMICS PANEL MEMBERS .....	166

# 1 Foreword

## 1.1 From the Chairman

Weiren Chou, Fermilab  
mail to: [chou@fnal.gov](mailto:chou@fnal.gov)

At the ICFA meeting held on July 3<sup>rd</sup>, 2005 in Uppsala, Sweden (during Lepton-Photon 2005) ICFA unanimously approved Albrecht Wagner (DESY) to succeed Jonathan Dorfan (SLAC) as the new Chair of ICFA for a 3-year term beginning January 1, 2006. At this meeting it also approved Shin-ichi Kurokawa (KEK) to replace Maury Tigner (Cornell U.) as the new Chair of ILCSC for a 2-year term starting immediately. There are also other membership changes in both ICFA and ILCSC, which can be found on the ICFA web site: [http://www.fnal.gov/directorate/icfa/icfa\\_home.html](http://www.fnal.gov/directorate/icfa/icfa_home.html).

This meeting also approved the replacement of Pisin Chen (SLAC) by Yunhai Cai (SLAC) as a member of the Beam Dynamics Panel. Pisin has served on this Panel for many years and made important contributions, in particular, in the organization of the workshop series titled "Quantum Aspects on Beam Dynamics." On behalf of the Panel, I'd like to express my sincere thanks to Pisin for his work over the past years. Yunhai is a well-known accelerator physicist and plays a major role in the PEP-II project at SLAC. Before that he worked at the SSC. He is now the leader of the SLAC ILC damping ring group. I'd like to welcome Yunhai on board and look forward to working with him in the coming years.

The meeting approved a new workshop: the 39<sup>th</sup> ICFA Advanced Beam Dynamics Workshop (ABDW) on High Intensity and High Brightness Hadron Beams "HB2006." It will be the third in the series following *HB2002* (Fermilab) and *HB2004* (GSI) and will take place May 29 – June 2, 2006 in Tsukuba, Japan. It is sponsored by KEK and JAERI. The organizers are Yong Ho Chin and Masanori Ikegami. More information will be available in the next issue of this Newsletter.

I would like to take this opportunity to announce a change for future ABDWs. This workshop series has joined the JACoW collaboration for online publication of workshop proceedings. This was approved by both ICFA and JACoW and will have an important impact in the organization of new workshops. For example, the program chairs and technical editors will be required to attend the JACoW steering committee meeting in order to learn about online publication. JACoW has certain boundary conditions that we need to meet, which can be found on the web: <http://accelconf.web.cern.ch/AccelConf/>. Most major accelerator conferences are now JACoW members, including PAC, EPAC, APAC, LINAC, FEL, etc. In addition to online publication, JACoW will allow us to share its vast database, which consists of more than 7,500 authors' names. All the papers published by these people at these conferences can be searched via JACoW. This is a main advantage of becoming a member of JACoW.

The ICFA Beam Dynamics Panel held a meeting on May 20, 2005 in Knoxville, Tennessee (USA) during PAC05. Twenty people attended, including Panel members

and their delegates. Barry Barish (Caltech), Director of the ILC GDE, was invited to this meeting for discussions on how this Panel could help the GDE. The ILC is the highest priority of the ICFA at this moment. The Panel expressed its willingness to help. There were two specific issues discussed at the meeting:

1. The Panel will help the GDE to organize an ILC school. (Details can be found in Section 3.1 of this issue.)
2. The Panel will help the GDE on an ILC beam dynamics study. This will be explored at Snowmass during the 2<sup>nd</sup> ILC Workshop in August.

At the Panel meeting, the Panel Chair gave a panel report. Several working group leaders (Caterina Biscari from LNF-INFN, Kwang-Je Kim from ANL, and David Sagan for David Rice from Cornell U.) reported group activities in the past two years. Francois Ostiguy (Fermilab), technical advisor of the *World Accelerator Catalogue* project, gave a progress report. Due to technical difficulties, the project was delayed but should be able to start to take input in the summer. The meeting also decided the Newsletter editors for the next two years:

- No. 38, December 2005: In Soo Ko (PAL)
- No. 39, April 2006: Kwang-Je Kim (ANL)
- No. 40, August 2006: Jiuqing Wang (IHEP, China)
- No. 41, December 2006: Ingo Hofmann (GSI)
- No. 42, April 2007: Yunhai Cai (SLAC)
- No. 43, August 2007: Chris Prior (RAL)

Thanks to editor Rainer Wanzenberg (DESY), this issue is well organized and published on time. Please enjoy!

## 1.2 From the Editor

Rainer Wanzenberg, DESY  
mail to: [Rainer.Wanzenberg@desy.de](mailto:Rainer.Wanzenberg@desy.de)

First and foremost I would like to thank all the authors of the contributions to this issue of the newsletter. This newsletter begins with a letter to the Editor by S. A. Khan reflecting on anniversaries celebrated last year, and looking ahead to the extension of international collaboration on accelerators and beam physics as well as to new regional facilities.

There is a dedicated section on recent activities related to the global effort towards a linear collider. The “Second ILC Accelerator Workshop” will be held in Snowmass, Colorado, August 14-27, 2005. Reports from that workshop are expected for the next issue of this newsletter in December.

This issue contains two theme sections on cyclotrons and on polarized beams. Cyclotrons have not been in the focus in recent issues of the newsletter although many cyclotrons are operated worldwide for different purposes. These include medical applications, nuclear physics and the operation of a spallation neutron source. The contributions to this topic, received from different regions of the world, demonstrate that cyclotrons are interesting with respect to beam dynamics, which includes not only aspects of beam optics but also three-dimensional modeling of complicated accelerator structures and space charge dominated beams. I am particularly pleased by receiving an article by IJ. L. Conradie from South Africa, which reports new beam developments in the iThemba Labs (see Section 4.4).

The section on polarization covers achievements with respect to polarized beams as well as recent progress in spin-orbit tracking codes. The Cooler Synchrotron COSY is accelerating polarized proton and deuteron beams up to a momentum of 3.7 GeV/c. The attainment and handling of spin polarization of electron and positron beams has a long tradition at DESY. Presently longitudinal polarized electrons of energy of 27.5 GeV are delivered to three HERA experiments. RHIC has shown an impressive increase in polarized proton (100 GeV) performance over the last few years.

There are interesting and well-written activity reports on beam-beam effects, a longitudinal feedback system and on coherent synchrotron radiation effects in bunch compressors.

There are several workshop and conference reports, including a well-prepared comprehensive report of the ERL2005.

The forthcoming beam dynamics workshops can be found in section 8 of this newsletter.

Last but not least I would like report that Dr. Anton Piwinski, one of the founders of this newsletter, has received the USPAS Prize for his achievements in accelerator physics and technology. I include the text and a photo from the DESY Telegram with kind permission of the DESY Public Relations Department:

On May 18th, 2005, the USPAS (US Particle Accelerator School) Prize for Achievement in Accelerator Physics and Technology was awarded to Dr. Anton Piwinski during the US Particle Accelerator Conference in Knoxville, Tennessee.

He received the Prize in acknowledgement of his “fundamental contribution to the understanding of charged particle beams in circular accelerators, in particular of intrabeam scattering, beam-beam effects and synchro-betatron resonances.”



Dr. Anton Piwinski (right)

Besides these important contributions to accelerator physics and the resulting quantitative understanding of beam instabilities and emittance growth, he also played a leading role in the successful commissioning and subsequent improvements of accelerators like DORIS, PETRA, HERA and LEP during his 34 year long scientific career at DESY.

His scientific work at DESY began in 1966. From the end of 1984 to the beginning of 1986, he was a scientific associate at CERN. Today, almost 6 years after his retirement, he is still scientifically active and can be seen almost every day at DESY.

We are especially grateful to Anton when he made some effort and found three early issues of the newsletter in his file and gave them to us. These issues had publication dates but no issue numbers. Anton suspected they were No. 2, 3 and 4. These are valuable ICFA documents. We have scanned them and added to the newsletter archive (<http://icfa-usa.jlab.org/archive/newsletter.shtml>).

## 2 Letters to the Editor

### 2.1 2004 the Year of Jubilees: Fifty Years of CERN, Forty Years of ICTP, Ten Years of ESRF User Operation

Sameen Ahmed KHAN  
Middle East College of Information Technology (MECIT)  
PO Box 79, Al Rusayl, Postal Code 124  
Technowledge Corridor, Knowledge Oasis  
Muscat, Sultanate of Oman  
mail to: [sakhan@mecit.edu.om](mailto:sakhan@mecit.edu.om),  
<http://www.pd.infn.it/~khan/>

#### 2.1.1 Introduction:

Physicists love to celebrate anniversaries. It enables them to get together, to evaluate, reflect and look ahead. The year 2004 provided three anniversaries in a row from the life of institutions. We shall briefly review the origins and achievements of the three institutions: CERN (European Laboratory for Particle Physics, in Geneva, Switzerland); ESRF (European Synchrotron Radiation Facility, in Grenoble, France); and ICTP (Abdus Salam International Centre for Theoretical Physics, in Trieste, Italy) respectively.

#### 2.1.2 50 Years of CERN

On 29 September 2004, CERN (the European Laboratory for Particle Physics, in Geneva, Switzerland) celebrated its 50th birthday. The origins of a European laboratory can be traced back to the 1940's. The idea was publicly voiced before the larger scientific community and policy makers, through the message of the Nobel Laureate Louis de Broglie read out at the "European Cultural Conference" held in Lousanne in December 1949. Louis de Broglie proposed setting up a *new* European laboratory to halt the exodus of physics talent from Europe to North America. In June 1950 at the UNESCO General Assembly held in Florence, Italy, the Nobel Laureate Isodor Isaac Rabi put forward a resolution calling on UNESCO (United Nations Educational, Scientific and Cultural Organization) "to assist and encourage the formation and organization of regional centres and laboratories in order to increase and make more fruitful the international collaboration of scientists". The Florence resolution was carried forward with support from many quarters and persuasion in some instances. The idea of a European laboratory was *not* readily accepted by all--scientists and governments. Specifically, Niels Bohr, James Chadwick, and Hendrick Kramers, some of the most eminent members of the European physics establishment, questioned the practicality of starting a new laboratory from scratch (see Page No. 12 in [1]). The conventions establishing CERN came into force on 29 September 1954. It was signed

by twelve countries then and has twenty member states now: Austria, Belgium, Bulgaria, the Czech Republic, Denmark, Finland, France, Germany, Greece, Hungary, Italy, the Netherlands, Norway, Poland, Portugal, The Slovak Republic, Spain, Sweden, Switzerland and the United Kingdom. It was the effort of several scientists & diplomats which made the above possible. Here, it would be relevant to cite the efforts of Edoardo Amaldi [1-2]. Rest is a very interesting and voluminous piece of history beyond the scope of this short note. Amaldi divides the *prehistory* of CERN in three parts: the first one extending from about 1948 to 15th February 1952. At that date eleven European countries had signed in Geneva the so-called “Agreement” establishing a provisional organization; the second period the so-called “Planning Stage” extends from February 1952 to 1st July 1953 when the convention establishing the permanent Organization was signed by the twelve European governments; the third period called the “Interim Stage” runs from July 1953 to 29 September 1954, when the Convention entered into force.

CERN has developed into the largest physics research centre in the world. CERN employs about three thousand people, representatives of a wide range of skills: physicists, engineers, technicians, craftsmen, administrators, secretaries, workmen. Some seven thousand scientists, over half the world's particle physicists use CERN's facilities. They represent some 500 universities and over 80 nationalities [3].

Besides advancing the understanding of nature, CERN has produced practical technology and feats of engineering that have pushed the state of the art to its outer limits. Among the laboratory's most noteworthy technical accomplishments are:

- **World Wide Web:**

The enormously numerous and complex data generated in CERN's accelerators were of limited value if they could not be shared with physicists around the world. So it was at CERN that Tim Berners-Lee invented a file sharing protocol and added it to his hyper text mark-up language (HTML), to form the basis of the Web.

- **Grid Computing:**

Today, together with the Argonne National Laboratory in Illinois, CERN is leading the way in the development of distributed supercomputing for numerous large-scale applications: from climate prediction to genome analysis.

- **Superconducting Magnets:**

These developed for CERN's accelerators have produced fields unequalled in any other large-scale applications. The ones for the LHC (Large Hadron Collider), cooled with liquid helium, are designed to generate fields of nine Tesla! This is to be compared with the fields in a typical MRI (Magnetic Resonance Imaging) device, which generates 1.5 Tesla.

- **The All-Electronic Detector:**

A generation ago, particle collisions were tracked in a cloud chamber. Images had to be analyzed manually and could not be produced by specific sought-after events. Working at CERN in the late 1960's the physicist George Charpak invented the first all-electronic detector. Called a multiwire proportional

chamber, the detector is in trials now for use in medical X-ray imaging, where it could greatly reduce the amount of radiation needed to form an image.

- **Stochastic Cooling:**

CERN engineer Simon van der Meer developed arcane control techniques to make bundles of particles that tend to fly apart cohere, so as to boost the probability of collisions in a particle detector. Together with Charpak's detector, the technique led to the discovery of the W and Z particles.

The Swiss Post Office issued a stamp to commemorate the 50 years of CERN. It was designed by the Swiss artists, Christian Stuker and Beat Trummer. This stamp is much different from the other stamps as it does **not** use any of the existing CERN's imagery and is very symbolic. The radiating design portrays an opening, a spreading out towards infinity, which reflects CERN's fundamental goals of research and the transmission of knowledge.



### 2.1.3 40 Years of ICTP

On 4-5 October 2004, ICTP (Abdus Salam International Centre for Theoretical Physics, in Trieste, Italy) celebrated its 40th anniversary with an international conference, *Legacy of the Future*. The conference attracted more than three hundred scientists and policy makers around the world. Significantly, the conference held a roundtable discussion on the future of science in the developing world. It is this concern for the developing world, since its inception in 1964, which makes ICTP unique.

The name of ICTP is forever linked to its founder Abdus Salam, a co-winner of the 1979 Nobel Prize in Physics, the founder and long-time director of ICTP. Salam was born in 1926 in Jhang, then part of India. Jhang became part of Pakistan after the division of the subcontinent in 1947. Salam returned to Pakistan in 1951 after a brilliant start to a research career in Britain. In Pakistan he experienced the dilemma of trying to perform scientific research and advanced studies in the relative isolation of a developing country. Without access to conferences, journals and other forms of support, Salam made the very difficult decision of to leave his home country to continue his work in physics. He joined Imperial College in London and established a research group with extraordinary distinction. Salam's first hand experience in coping with scarce resources and the remote location of his country prompted him to create ICTP with an aim to foster the growth of advanced scientific studies and research in developing countries. Salam's vision has been fulfilled.

Abdus Salam decided to create an international centre dedicated to theoretical physics that would pay special attention to the needs of scientists from the developing world. In 1960, Salam outlined a proposal for the Centre, at the *Tenth Annual International Conference on High Energy Physics*, in Rochester, USA. The same year

he presented the proposal before the delegates attending the General Conference of the IAEA (International Atomic Energy Commission), in Vienna, Austria.

Salam's brainchild met with enthusiastic support from eminent physicists including the Nobel Laureate Niels Bohr (who had earlier expressed reservations about crating CERN) and later his son Aage Bohr (who later received the Nobel Prize in Physics in 1975). But Salam's ongoing efforts to secure support for the creation of the Centre encountered a series of obstacles set in place by the IAEA's *Scientific Advisory Committee* (SAC). The Committee (including Nobel Laureate Isidor Isaac Rabi) suggested that the creation of the fellowship programmes at existing centres of theoretical physics could prove more cost-effective and easier-to-implement, than creating a *new* Centre from the scratch. Committee members also expressed concerns that a centre in theoretical physics would have no practical applications for developing countries struggling to improve their living standards (see Page No.7 in [4]). It is very glaring that Rabi who had drafted the Florence resolution urging UNESCO to create regional science centres, had opposed the creation of ICTP.

Sigvard Eklund, a strong believer in Abdus Salam's vision, was appointed the Director-General of IAEA in 1961. This was the turning point and Salam's idea triumphed. The IAEA soon realized that the new Centre could not be created solely with its own funds. Financial offers came from the governments of Italy with Trieste as the candidate site; from Denmark for Copenhagen; from Pakistan for Lahore; and from Turkey for Ankara. The most generous offer came from Italy and the man behind this was Professor Paolo Budinich, a famous theoretical physicist in Italy. Budinich argued that the Centre would help ease East-West tensions due to the Cold War.

After a slow but clear sailing for four years in the corridors of policymakers, Salam's proposal became a reality. On 5 October 1964, a group of high officials, mostly from Italy, joined eminent physicists from around the world for the inaugural meeting of the newly-created International Centre for Theoretical Physics (ICTP). A seminar on plasma physics served as a platform from which ICTP was officially launched. Abdus Salam, who spearheaded the drive for the creation of ICTP by working through IAEA, became the Centre's director. Paolo Budinich, who worked tirelessly to bring the Centre to Trieste, became ICTP's deputy director. After residing for four years in downtown Trieste, ICTP moved to its permanent location near the Miramare Park in 1968. Soon UNESCO also joined in extending support to the new Centre. Over the four decades ICTP has accomplished its goals.

ICTP has been in close contacts with the accelerator laboratories from the very beginning. Some of the accelerator-related topics are covered in the various ICTP activities (such as *Free Electron Lasers* in the *Winter College on Optics*). ICTP has hosted several accelerator related activities including: *ICFA Panel* in June 1986; *ICFA School on Instrumentation in Elementary Particle Physics* four times during 1987-1991; and *ICFA School on Beam Dynamics and Engineering of Synchrotron Light Sources* in May 1991. Since 1991, ICTP has been regularly hosting the *School on the use of Synchrotron Radiation in Science and Technology*; the next School in the series is scheduled to be held in May 2006 (see the ICTP Calendar in [5]). The close vicinity of the 2.4GeV ELETTRA synchrotron to the ICTP has led to collaborations. Since several years there has been a formal arrangement between the two institutions. The ICTP-ELETTRA Users Programme is offers access to the synchrotron radiation facility ELETTRA in Trieste, to scientists who are citizens of developing countries and work in

those countries. Up to an annual total of 1500 hours has been made available within this programme for beam time applications at any of the existing ELETTRA beam lines.

Since its birth four decades ago, several scientific bodies have spawned with headquarters in and around ICTP. Collectively, they are known as the “Trieste Science System”, which include SISSA (International School of Advanced Study); TWAS (Third World Academy of Sciences). ICTP is encouraging science in the developing countries through its various visiting programmes. It is also recognizing their talent through the prizes and medals it has instituted. This is reflected in:

- Around two thousand scientific activities (from introductory schools to advanced workshops) have been organized on the ICTP’s premises.
- Around hundred thousand scientific visitors have been to ICTP. About half of them came from developing countries and many of them regard ICTP as scientific home away from home.
- Thousands of research papers have resulted from the work of the ICTP community.
- Almost every physics PhD in the continent of Africa has some link with ICTP.
- Over eighty Nobel Laureates have given lectures at ICTP, as well as many prestigious scientists.

In 2004, ICTP had 7134 participants in about fifty meetings totalling to 4327 person-months. 69% came from developing countries. In all 124 countries were represented. ICTP has successfully evolved from a *vision to a system* [5]. ICTP was renamed as Abdus Salam ICTP on the occasion of Salam’s first death anniversary in November 1997.

CERN and ICTP are international institutions of advanced scientific research with similar aspirations and understandably, their histories are intertwined. Two members of the CERN Theory Division, Jacques Prentki and Léon van Hove, took part in the panels of experts that encouraged the setting up of ICTP. The Scientific Council of the ICTP (after it was setup) has been served by Léon van Hove, Victor Weisskopf and Herwig Schopper (all three were Director-General of CERN). Alvaro de Rújula, a researcher from ICTP became the director of the CERN Theory Division. Abdus Salam the founding director of ICTP served for several years on CERN’s scientific policy committee.

There is a deep and strange link between ICTP and particle physics. In the year 1964 (the year ICTP came into being) the Nobel Laureate Murray Gell-Mann introduced the term *quarks* for the subnuclear particles. Gell-Mann was inspired by the Dublin born poet James Joyce’s poem *Finnegans Wake*, which had the line “Three Quarks for the Muster Mark”. Joyce had spent over a decade in Trieste, where he wrote his masterpiece *Ulysses*. Joyce was driven by rhyme and Gell-Mann by symmetry!

### 2.1.4 10 Years of ESRF User Operation

Inauguration of the ESRF (European Synchrotron Radiation Facility, in Grenoble, France) on 30 September 1994 marked the end of its construction period. However, the idea of joint European facility dates back to 1975. Its construction began in 1988 and the first fifteen beamlines were opened to users in 1994. ESRF is supported by eighteen countries. Twelve of them are ‘Contracting Party’ countries: France, Germany, Italy, United Kingdom, Spain, Switzerland, Belgium, The Netherlands, Denmark, Finland, Norway and Sweden. The remaining six (Portugal, Israel, Austria, Poland, Czech Republic and Hungary) have been associated through ‘Bilateral Agreements’. All of them contribute to the annual budget of about seventy million US dollars. The 6.0GeV facility is constantly pushing experimental possibilities to new limits. It is one of the three most powerful hard X-ray facilities along with the 8.0GeV SPring-8 (Super Photon Ring, in Japan) and the 7.0GeV APS (Advanced Photon Source, in Argonne, USA). Owing to their extremely high energy these synchrotrons have their specific problems, and have forced the development of new techniques in the field of optics and detectors to ensure the required high stability of the electron beam. In view of the very unique challenges arising due to the extremely high energy, the three most powerful synchrotron laboratories have signed a ‘Framework of Agreement for Collaboration’.

Now, ESRF has forty beamlines. Every year over three thousand scientists use the facility carrying out research in physics, chemistry, materials and life sciences. In the year 2003 there were 5140 user visits for 1282 experimental sessions with 14,273 shifts. These figures are steadily on the rise [6].

### 2.1.5 Concluding Remarks

The anniversaries were celebrated not only by physicists but by the global scientific community. They drew attention of the media and the public at large. It is time to look ahead.

CERN is one of Europe's first joint ventures. It has become a shining example of international collaboration. Its success paved the way for other joint initiatives such as the ESRF and the ESA (European Space Agency). All the three institutions provided a common platform, where the governments across Europe could work jointly towards common goals. This definitely had a bearing on the formation of the European Union. CERN is continually adopting by carrying out new experiments to test new species of theories, each tested for survival against further experimental evidence. Particle physicists are trying to explore the frontiers beyond the reach of CERN. The proposed International Linear Collider (ILC) is a likely candidate for a joint initiative in accelerator physics and will possibly involve participation from all the continents. Global projects rely on collaboration. Historically particle physics has developed an exemplary culture of international collaboration to build and operate large-scale experimental facilities. ILC is also known as the Global Linear Collider (GLC). Building the ILC/GLC will herald a new era in the scientific collaboration among nations and in developing new technologies.

The generous support by the Italian government for ICTP has set a unique example in the North-South cooperation. From the very beginning ICTP has been addressing the problems being faced by the developing countries. ICTP held a “Conference on Physics of Tsunamis” in March-2005, which is another evidence of its deep involvement in the

developing countries. Salam had dreamt of creating twenty ICTPs around the world. As part of that vision, he actively promoted the idea of advancing the cause of science & technology in the developing countries, not only by having researchers from the region work with their colleagues in the developed world, but also by having the region develop its own facilities. For the region of the Middle East he had suggested facilities including a *synchrotron laboratory*. SESAME (Synchrotron-light for Experimental Science and Applications in the Middle East) synchrotron facility, hosted by Jordan, has been a significant development. Regional Synchrotron Radiation Facilities (RSRF) modelled after ESRF, in the continents of Africa, Asia and South America can be a step towards that dream [7]. We need more *Accelerator & Beam Physics Forums* in the underrepresented regions [8].

### 2.1.6 References:

1. Carlo Rubbia, “Edoardo Amaldi: Scientific Statesman”, CERN Report, **CERN-91-09** (1991), 46 pages.
2. Herwig Schopper, Sameen Ahmed Khan and John Krige, “CERN’s Early History Revisited”, *Letters in Physics Today*, **58** (4), 87-89 (April 2005).
3. CERN Website: <http://www.cern.ch/>
4. André-Marie Hamende, “The Birth of the Centre”, *News from ICTP*, **No. 107**, pp. 6-7 (Winter 2003-2004).
5. Abdus Salam ICTP Website: <http://www.ictp.it/>
6. ESRF Website: <http://www.esrf.fr/>
7. Sameen Ahmed Khan, “Need to Create Regional Synchrotron Radiation Facilities (RSRF)”, *IRPS Bulletin*, **17** (2), 7-13 (July 2003). (IRPS: International Radiation Physics Society).
8. Sameen Ahmed Khan, “Call for Creation of Accelerator & Beam Physics Forums”, *ICFA Beam Dynamics Newsletter*, **17**, pp. 5-6 (August 1998); *Europhysics News*, **30** (2), pp. 49-50 (March/April 1999).

## 3 International Linear Collider (ILC)

### 3.1 ILC School

Barry Barish, Weiren Chou and Shin-ichi Kurokawa  
 mail to: [barish@ligo.caltech.edu](mailto:barish@ligo.caltech.edu), [chou@fnal.gov](mailto:chou@fnal.gov), [shin-ichi.kurokawa@kek.jp](mailto:shin-ichi.kurokawa@kek.jp)

The International Linear Collider (ILC) is the next major accelerator project proposed by the world particle physics community. In order to train young generations for this project, there will be an *International School for Linear Colliders*. The school is co-sponsored by the GDE, ICFA Beam Dynamics Panel and ICFA ILCSC. An Organizing Committee has been formed. It has nine members:

- GDE – Barry Barish (Caltech, Chair)
- ICFA Beam Dynamics Panel – Weiren Chou (Fermilab)
- ICFA ILCSC – Shin-ichi Kurokawa (KEK)
- Europe – Jean-Pierre Delahaye (CERN), Rolf-Dieter Heuer (DESY)

Asia – In Soo Ko (PAL), Kaoru Yokoya (KEK)

Northe America – Alex Chao (SLAC), Paul Grannis (Stony Brook / DOE)

The committee had its first meeting on August 17, 2006 at Snowmass during the 2<sup>nd</sup> ILC Workshop. It decided that the school will take place May 19-25, 2006 in Sokendai, Hayama, Japan. (Sokendai is a graduate university located about 70 km south of Tokyo.) The students and lecturers will be chosen from three regions: Asia, Europe and North America. A Curriculum Committee and a Local Committee will be set up soon. The former will be responsible for selecting courses and students, identifying lecturers and sending out invitations; the latter for web site, posters, budgeting and on-site organization of the school. A more detailed announcement of this school will appear in the December issue of this newsletter.

## 3.2 High Gradient Superconducting RF Cavities

Hasan Padamsee, [Cornell University](http://Cornell University), Ithaca, NY 14853

mail to: [hsp3@cornell.edu](mailto:hsp3@cornell.edu)

### 3.2.1 Introduction

Gradients and Q's in the dominant ILC candidate structure have shown steady improvement, reaching 35 – 40 MV/m over the last two years using the best techniques of electropolishing, high pressure rinsing and 120° C baking for 48 hours. Above 40 MV/m, the surface magnetic field encroaches the range of the rf critical magnetic field, believed to fall between 1750 and 2000 Oe, depending on the theory. One way to circumvent the limit is to modify the cavity shape to reduce the ratio of peak surface magnetic to accelerating field. Two candidate shapes have evolved: the Re-Entrant shape (RE) and the Low-Loss (LL) shape. Although field emission is aggravated by higher electric fields, it does not present a brick wall limit because high pressure water rinsing at 100 bar eliminates micro-particles which cause field emission. The record field in a single cell re-entrant cavity is now 47 MV/m corresponding to a surface magnetic field of 1790 Oe and a surface electric field of 103 MV/m.

### 3.2.2 Review of Progress in Cavity & Cryomodule Gradients

The superconducting linear collider collaboration has made significant advances during the past decade. More than a hundred 9-cell structures have been produced by industry. There has been a steady rise in 9-cell cavity performance at the TESLA TEST FACILITY (TTF) due to material and process improvements. Chief among these have been high purity, starting niobium sheet material (residual resistivity ratio, RRR  $\approx$  300), eddy current screening of niobium sheets to eliminate large ( $>$  100  $\mu$ m diameter) defects, careful electron beam welding procedures in a good vacuum ( $\approx$   $10^{-5}$  torr), controlled ( $<$  15° C) buffered chemical polishing (BCP) in a mixture of acids (HF, HNO<sub>3</sub> and H<sub>3</sub>PO<sub>4</sub>) to remove 100  $\mu$ m of surface damage layer, 1350° C titanium heat treatment to post purify the niobium to RRR values of 600 or higher, BCP of the inside and outside to remove titanium deposited during the post purification, high pressure rinsing with 100 bar water to remove micro-particle contaminants that cause field emission, followed by drying and assembly in a Class 10 clean room environment.

As cavity gradients advanced, clean assembly techniques for cavity strings with input couplers and cryomodules continued to improve so that cryomodule performance has also been rising steadily [1]. The difference between vertical test results and cryomodule results is decreasing as is the spread in gradients. Measured dark currents (average: 20 nA) are below acceptable values, the goal being  $< 50$  nA at 35 MV/m per cavity, which would correspond to a 250 mW heat load.

### 3.2.3 35 MV/m by Electropolishing & Mild Baking

Over the last three years, the use of electropolishing combined with mild baking ( $100^\circ - 120^\circ$  C, for 50 hours) has yielded CW gradients between 35 - 40 MV/m to meet the one TeV upgrade requirement for the ILC. Fig. 1 shows the performance of six best 9-cell cavities at TTF[1] as tested in a vertical dewar.

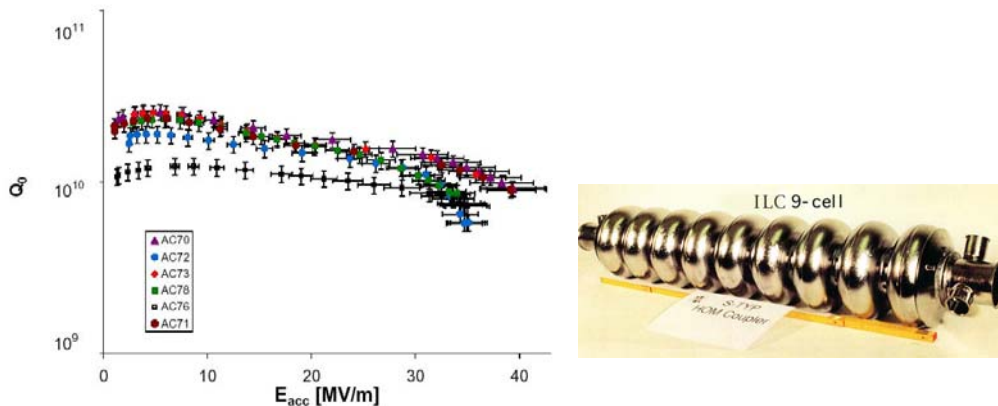


**Figure 1:** (Left) Vertical test results at TTF for six 9-cell cavities after electropolishing and baking. (Right) 9-cell cavity, dominant candidate for ILC.

For a niobium surface prepared by BCP the Q starts to drop steeply above accelerating fields of 20 MV/m, and eventually a quench occurs. The Q-drop occurs even when there is no field emission, as judged by the absence of x-rays. For want of a better term, the phenomenon carries the label “high-field Q-slope,” a phenomenon which has become one of the hottest topics in the field of RF superconductivity. Temperature maps show that losses take place in high magnetic field regions of the cavity [2]. Although the understanding is not yet complete, there has been much progress in identifying the contributing factors, such as roughness due to steps at grain boundaries, and excess oxygen impurity at the metal-oxide interface. The good news is that electropolishing reduces the roughness and  $100 - 120^\circ$  C baking for 50 hours eliminates the Q-slope for cavities prepared by EP. It is suspected that baking heals the RF penetration layer by redistributing the excess oxygen impurities from the oxide-metal interface.

Among the electropolished and baked cavities, several 9-cell units equipped with input couplers, higher order mode (HOM) couplers and tuners have been operated at TTF inside a single-cavity test cryomodule (called CHECHIA) with a high power klystron to reach gradients between 35 - 38 MV/m[1]. One of the three CHECHIA tests was a long-term test. The cavity operated without quench or trips for more than 1100

hours at 35 MV/m at a Q value of  $7 \times 10^9$ . Another fully equipped cavity was installed in a complete TTF cryomodule after its CHECHIA test. It operated at 35 MV/m at a Q of  $6 \times 10^9$ .

### 3.2.4 Designs for higher gradient structures

Several laboratories are pursuing gradients above 35 MV/m with multiple goals: larger operating margin, lower cost, smaller site, or higher final energy for the ILC upgrade (e.g. 1.2 TeV). The best single-cell cavities of the TTF shape at many laboratories reach 40–42 MV/m. Above these gradients, the magnetic field at the surface approaches the fundamental limit where superconductivity breaks down. One way to circumvent this limit is to modify the shape of the cavity to reduce the ratio of peak magnetic to accelerating fields. Two new shapes have emerged, as shown in Fig. 2, the Low Loss (LL) shape [3] and the Re-entrant (RE) shape [4]. Table 1 compares the apertures, peak surface electric and peak surface magnetic fields of the new shapes with those of the TTF shape. Both Jlab and KEK have adopted the LL structure to push for higher gradients in multi-cells. Cornell is pursuing the RE structure. Fig. 3 shows a multi-cell LL structure built at KEK, now undergoing tests

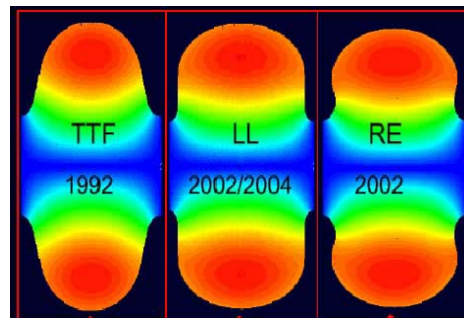


**Figure 2:** Comparison of the TTF shape (left) with the LL (middle) and re-entrant shape (right).



**Figure 3:** A Low Loss multi-cell cavity under development at KEK.

**Table 1:** Comparison of aperture, and surface fields for three shapes.

Design	TTF	LL	RE
Aperture	70 mm	60 mm	70 mm
E <sub>pk</sub> /E <sub>acc</sub>	2.0	2.36	2.2
H <sub>pk</sub> /E <sub>acc</sub>	4.2	3.61	3.76

Simulations show that the RE and LL shapes are as resilient against multipacting as the TTF shape. The Lorentz force detuning coefficient of the new shapes is slightly higher than for the TTF shape [5]. A downside of the new shapes is the higher accompanying surface electric field, which enhances “field emission” of electrons from regions of high electric field. For example, to reach  $E_{acc} = 45$  MV/m, the peak surface electric field would approach 100 MV/m. Field emission does not present a brick-wall limit, however, because techniques such as high-pressure water rinsing at pressures of about 100 bars eliminate the microparticle contaminants that cause field emission. Another important aspect of cavity shape is beam aperture. Smaller apertures produce stronger wakefields. For example the LL shape has 18% higher longitudinal and 65% higher transverse wakefields [3]. The re-entrant shape has the same aperture as the TTF shape and therefore comparable wakes.

New ideas are usually proved in single-cell cavities before the technical challenges of multi-cell accelerating units are addressed. A LL single cell cavity built at Jlab [6] reached  $E_{acc} = 40$  MV/m at a  $Q$  value of  $6 \times 10^9$  after EP and bake. Cornell built two RE cavities; one was sent to KEK. The first 70 mm-aperture re-entrant single-cell cavity reached a world record accelerating field at Cornell of 46 MV/m CW with a  $Q$  value of  $10^{10}$ , and 47 MV/m in the pulsed mode [7]. In a very recent test [8] KEK also achieved a CW gradient of 47 MV/m with a  $Q$  above  $10^{10}$ . Fig. 4 compares the re-entrant single cell with a TTF shape cavity, and Fig. 5 shows the  $Q$  vs  $E$  curves for tests conducted at Cornell and KEK on RE single-cell cavities.

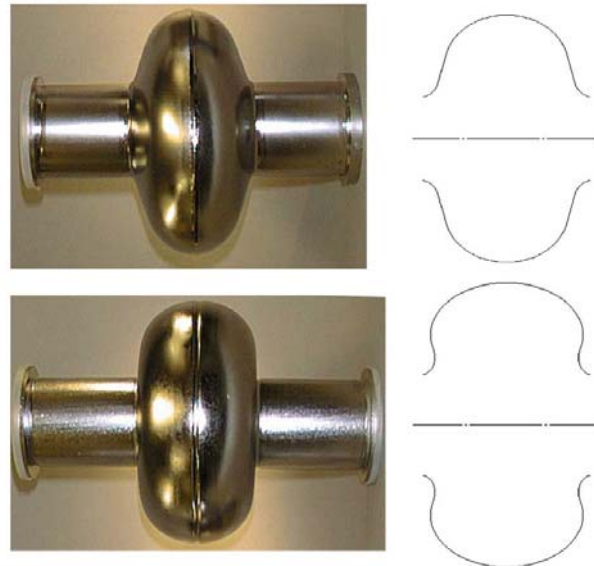


**Figure 4:** (Upper) TTF niobium cavity and profile. (Lower) Reentrant cavity and profile.

To reach record performance levels, the first RE cavity was made from high-purity niobium (with RRR = 300), the cavity halves post purified to RRR > 600 with yttrium at 1200° C to avoid premature thermal breakdown of the superconductivity. Electropolishing the halves as well as the finished cavity provided a smooth surface. For the finished cavity, the EP took place in a vertical orientation which is somewhat simpler than the usual horizontal method where the cavity must be rotated. High-pressure rinsing at 100 bar scrubbed the surface free of the microparticles that cause

field emission. In addition, baking at 100 °C for 50 hours promoted a redistribution of the oxygen in the RF layer. A second identical cavity was fabricated at Cornell, post purified as a completed cavity with titanium (2 hours at 1300 and 4 hours at 1200C) and sent to KEK. Here it was electropolished in the standard horizontal configuration, HPR rinsed and tested in a vertical dewar.

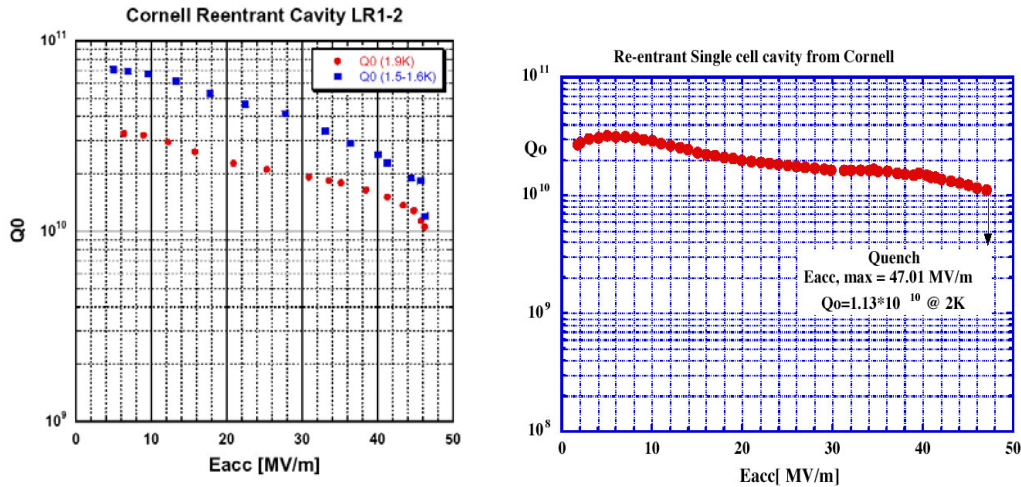


**Figure 5:** (Left) Record performance of the re-entrant cavity prepared and tested at Cornell (Right) Record performance of an identical re-entrant cavity fabricated at Cornell, prepared and tested at KEK.

### 3.2.5 Promising new material

Another approach to higher gradients is to improve the material. Jefferson Lab [9] has started investigation of very large grain and single crystal niobium sheets cut by electro discharge machining (EDM) directly from the melted ingot (Fig. 6). The highly annealed and large grain material shows that the Q-slope starts at a higher magnetic field (presumably due to the sharply reduced density of grain boundaries) and the onset moves to an even higher field for the single crystal cavity. A single cell cavity (at 2.2 GHz) of the LL shape fabricated from single crystal reached  $E_{acc} = 45$  MV/m at  $Q = 7 \times 10^9$  after BCP and bake (Fig. 6). With the absence of grain boundaries, just BCP treatment provides a surface smoothness of the order of 20 nm in the single grain material. It is remarkable that the single crystal integrity was not destroyed by deep drawing the cups from the sheet or by electron beam welding the two cavity halves together. No grain boundaries were found in the weld seam. Large grain material does have grains in the weld seam.

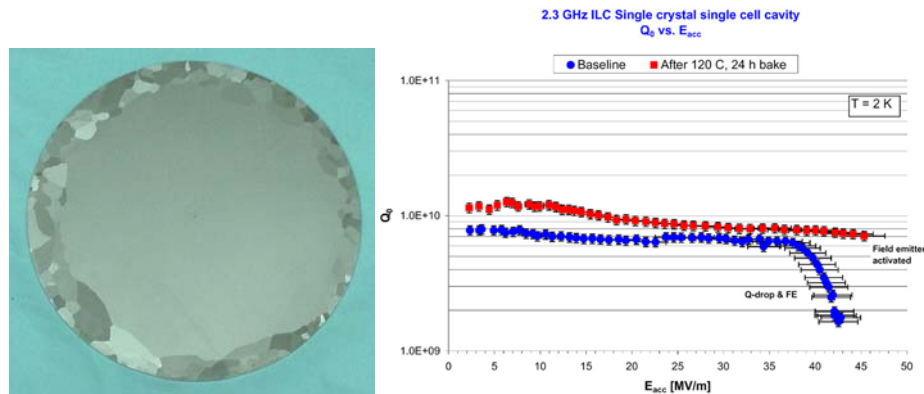


**Figure 6:** (Left) Disk sliced from ingot, the center region is single crystal. (Right)  $Q$  vs.  $E$  before and after baking for BCP treated 2.2 GHz single cell cavity.

There are many advantages to using ingot slices of large and single grains over standard sheet material. Skipping the many steps (forging, grinding, rolling and annealing) between ingot and poly-crystal sheet reduces cost and maintains the purity and RRR of the ingot. Rather than EP, the simpler (and less expensive) BCP procedure provides a smooth surface. In fact the BCP smoothness was better (27nm) than the EP smoothness on a fine grained polycrystal material (250 nm).

### 3.2.6 Summary

Steady advances in science and technology are responsible for spectacular increases in superconducting cavity performance since the large installations of CEBAF (Jefferson Lab) and LEP-II (CERN) during the 1990's. The gradient range for these accelerators was  $< 10$  MV/m. The gradient of niobium cavities has more than tripled over the last decade, spurring new accelerator applications. SRF technology efforts are expanding rapidly world-wide to meet ILC goals, for which cavities must be capable of 35 MV/m gradient before installation to be suitable for the later 1 TeV upgrade. (While still under discussion, the starting gradient choice for the 500 GeV machine could be lower (e.g. 30 MV/m) for more operation margin, and less risk.) New cavity shapes and new materials for high gradients are on the horizon for reaching higher energies for the ILC upgrade to one TeV and beyond. Single cell cavities are now reaching 45 – 47 MV/m.

### 3.2.7 References

1. L. Lilje, 2005 Particle Accelerator Conference, Knoxville, TN, paper TOPE00.
2. H. Padamsee, et al., "Cornell Status Report" in The 10th Workshop on RF Superconductivity, p. 15, Tsukuba, Japan (2001).
3. J. Sekutowicz et al, Particle Accelerator Conference, Knoxville, TN, paper, TPPT056
4. V. Shemelin, 2005 Particle Accelerator Conference, Knoxville, TN, paper, TPPT068
5. N. Solyak, Fermilab, priv. comm.
6. P. Kneisel, Jlab, priv. comm.
7. R. Geng, et al., 2005 Particle Accelerator Conference, Knoxville, TN, paper, ROAC009
8. K. Saito, KEK, Private communication.
9. P. Kneisel et al., 2005 Particle Accelerator Conference, Knoxville, TN, paper, TPPT076

## 4 Cyclotrons

### 4.1 Beam Dynamic Activities at PSI's High Intensity Cyclotrons

A.Adelmann, R.Geus, P.A Schmelzbach, L. Stingelin

[PSI](#), Paul Scherrer Institut

mail to: [Andreas.Adelmann@psi.ch](mailto:Andreas.Adelmann@psi.ch)

#### 4.1.1 Introduction

PSI operates the most powerful cyclotron worldwide for the benefit of a multi-user, cross-disciplinary research facility. The accelerator complex consists now of a Cockcroft-Walton pre-injector, a 72-MeV separated sector injector cyclotron and a 590 MeV separated sector Ring Cyclotron. The beam production started in 1974 with a Philips Cyclotron as injector. The commissioning of the dedicated, more powerful Injector 2 in 1984, the reconstruction of the target stations in 1985 and 1990 and the upgrade of the rf-system of the Ring Cyclotron from 1992 to 1995 allowed for the stepwise increase of the overall performance. The spallation neutron source SINQ was taken into operation in 1996. Technical information on the accelerator can be found in reference [1].

A beam current of 1.8 to 1.85 mA is now routinely extracted from the Ring Cyclotron, delivered to the production targets M and E for secondary pion and muon beams in 6 experimental areas, and partially transported to SINQ, which, in turn, feeds 7 neutron guides with a total of 14 instruments (in 2005). With a 4 cm thick Target E the transmission to the spallation neutron source SINQ amounts to about 70%, thus a beam of 1.2 mA is available at this facility. In addition, parts of the beam are split in the 72 MeV and 590 MeV beam lines for isotope production, proton therapy and materials irradiation. The layout of the facility is shown in Figure 1.

The facility has a considerable potential for further improvements, especially for the advantage of users of the neutron beams. Since the cooling system of SINQ can accommodate a load of 2 mA the main proton beam could be increased to 2.7 to 2.8 mA without major modification of the spallation target. For higher currents an improved design is required, which, however, is within the reach of present technology. Therefore, the ongoing upgrade project aims at a beam current of 3 mA. The total power will be 1.8 MW, of which about 1.3 MW will be delivered to the SINQ-Target. The limit for the primary beam is essentially set by the maximal acceptable load on Target E. A reconstruction of Target E to accommodate higher currents is not foreseen in this upgrade program.

The planned improvements of the accelerator complex are summarized in this introduction. Several aspects of the beam dynamical work performed in the frame of this project will be discussed in the following chapters.

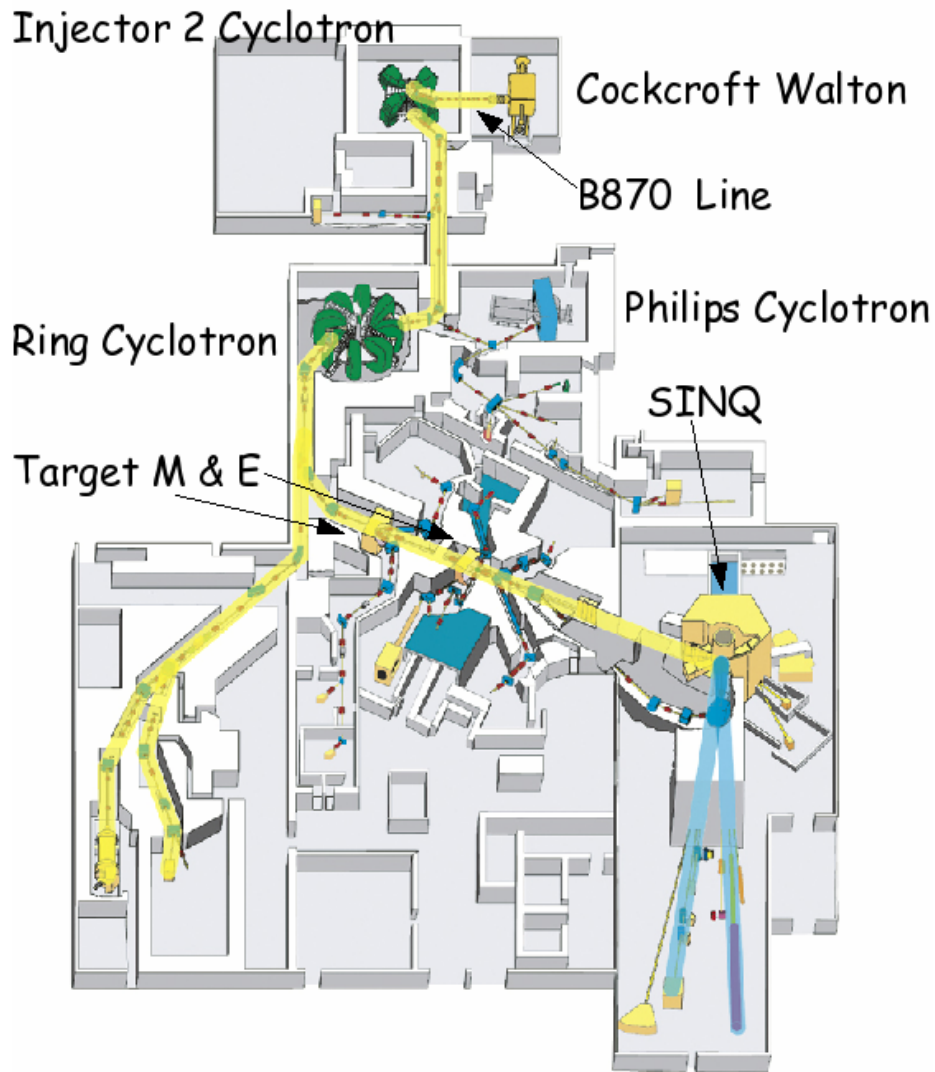


**Figure 1:** The PSI proton accelerator facility

#### 4.1.1.1 *Steps to increase the beam intensity*

The performance of the PSI cyclotrons is based on low beam losses due to the large turn separation at the extraction, i.e. the high energy gain per turn achieved by the use of powerful rf-cavities.

The installation in the Ring Cyclotron of a new copper rf-cavity allowing for an increase of the accelerating voltage from 750 to 1000 kV opens the way to a significant gain in beam intensity. The prototype cavity was installed in the Ring Cyclotron in 2004. A second cavity will be put in operation in 2006, thus allowing soon first attempts to raise the beam current. The installation of all 4 cavities will be completed in 2008.

The Injector 2 Cyclotron is now able to deliver beam currents up to 2.2 mA. Therefore, its performance must also be improved. Since the extraction losses of this machine are the main source of the sky shine radiation around the facility, the success of the upgrade program depends strongly on the way we can deal with this limiting parameter.

The prediction of the performance of a high power accelerator is a difficult task since the relevant factors are not accessible by usual beam dynamical calculations. The current limit is given by the losses due to tails and halos several orders of magnitude smaller than the beam itself. In the routine operation at 1.8 mA for example, the tolerated injection and extraction losses are in the range of 0.02 % of the beam intensity. A reliable beam simulation requires tracking of millions of particles, a good knowledge of the initial conditions, the consideration of higher order effects, and detailed beam diagnostics for comparison and validation of the calculations. The development of the computational tools needed for such simulations is in progress, and the results recently obtained for Injector 2 are very promising. This approach however is time consuming and, at present, projections have still to rely on extrapolation and scaling based on the performance observed at different steps of the development of the facility.

#### 4.1.1.2 *Injector 2 upgrade*

The quality of the beam extracted from the Injector 2 Cyclotron depends crucially on the initial conditions at injection. In the past few years, significant progress has been made (in fact an increase of the beam current from 1.5 to 2 mA) mainly by better handling the space charge effects on the bunching of the 870 kV beam from the Cockroft-Walton pre-accelerator. New calculations show that the installation of a second buncher operated at the third harmonic (150 MHz) can significantly increase the beam intensity in the phase space defined by the collimators at the injection point, and generate the conditions required for acceleration in the “round beam” mode. It will, for example, be possible to reach 3.4 mA with a DC beam of 9 mA, compared with the present 2.2 mA at 12 mA DC. The operation at lower currents allows for beams of higher quality, less space charge problems in the beam transport line and a reduced load on the CW. The confirmation of the buncher calculations by a full 6-dimensional simulation including also the beam cleaning at the phase collimators is under way. The new buncher will be installed in 2006.

The injector cyclotron was equipped with two flat-topping cavities. They are obsolete with the presently used “round beam” mode of operation which is characterized by a stable, almost spherical shape of the bunch with a very narrow phase width (2 degree rf at the extraction). These cavities will be replaced by new 50 MHz systems, thus almost doubling the energy gain per turn. The concept study led to the choice of single-gap cavities, as discussed in a previous publication [2]. They are expected to be installed in 2009. The technical requirements set by this upgrade have already been considered in the recently performed renewal of the vacuum system of Injector 2.

#### 4.1.1.3 *The 72 MeV beam: Transfer and bunching*

A significant reduction of the losses in the Ring Cyclotron can be achieved by judicious beam cleaning by collimators in the transfer line. Local shielding of the collimators helps to reduce the contribution to the sky shine and thus allows to cut out up to several  $\mu\text{A}$  of parasitic beam. The layout of the Ring center has also been improved to minimize the losses in this region.

Preliminary calculations show that space charge compensated bunching is applicable to generate a variety of starting conditions at the Ring Cyclotron. A full simulation of the beam injection is in preparation and should show whether the “round beam” acceleration mode is practicable in this accelerator. If this technique does not

work, the “superbuncher” can alternatively be used as phase rotator to improve the matching to the phase acceptance of the Ring Cyclotron.

Phase width measurements [3] between the Injector and Ring Cyclotrons confirm that a “superbuncher” working at the 10<sup>th</sup> harmonic is a suitable choice. The construction of a device based on drift tube cavities is in progress. It is described in Ref. [4].

#### 4.1.1.4 *Ring Cyclotron upgrade*

In the “round beam” acceleration mode a flat-topping cavity would no longer be required in the Ring Cyclotron. However, since results from a reliable simulation are not at hand at the moment, the further use of such a system should be also considered.

The current limits, observed during the previous stepwise reductions of the turn number, show an  $N^{-3}$  dependence, which corresponds to the rule proposed by W. Joho for the strength of the longitudinal space charge effects. In addition, considering the  $I^{1/3}$  width dependence of the beam from Injector 2, one can infer that, for a matched beam, the emittance term entering the calculation of the beam width in the Ring contributes the same way to the current limit. Since the emittance of the injected beam is known, both parts can be disentangled, and a calibration is obtained for the space charge contribution itself. With this model, the beam width for any combination of emittance, space charge distribution and accelerating voltage shape can be evaluated.

For identical conditions for the compensation of the space charge effect by means of a tilted flat-top, the maximum current achievable with the present beam quality delivered to the Ring will be 5 mA with four accelerating cavities at 1 MV. However, the present flat-top system is already operated close to its thermal limit and will not be able to provide the optimal correction when the new cavities are operated at the rated voltage. Using a very simplified model to evaluate the shape of the longitudinal phase space one can estimate that beam currents up to 2.7 mA should be already achievable with the present flat-top performance in combination with the “superbuncher”. Therefore, the decision whether the development of a new flat-top system should be undertaken will be delayed until results of the simulation and/or first experimental tests confirm or deny the applicability of the “round beam” technique in the Ring Cyclotron.

### 4.1.2 **Beam Dynamic Codes and Methods Development**

The aim of our code and methods development is to make the step from *qualitative* to *quantitative* predictions. This requires the accurate three-dimensional modeling of large and complicated accelerator structures including space charge, beam lines, collimation, and in the future secondary effects.

The required three-dimensional modeling will ultimately demand high performance computing (HPC) resources such as clusters of workstations or symmetric multiprocessor systems (SMP). In order to efficiently integrate existing code, we use the object oriented programming (OOP) paradigm throughout all our code development, resulting in clearly structured and reusable software or software-components.

#### 4.1.2.1 *Space Charge Solvers*

When modeling space-charge-dominated beams, one of the key elements is accurate and fast Poisson solvers. The fundamental steps in calculating  $E$ , the electric self field are: a Lorentz transformation to the beams rest frame  $\mathbf{x}'=L(\mathbf{x})$ , interpolation of the

charges  $q_i(\mathbf{x}')$  to obtain the charge density  $\rho$ , on a discrete space (grid). Then we solve:

$$\begin{aligned} -\Delta u &= \frac{\rho}{\varepsilon_0} \quad \text{on } \Omega, \\ u &= 0 \quad \text{on } \partial\Omega, \end{aligned} \tag{1}$$

where  $\Omega \subset \mathbb{R}^3$  is a bounded domain, and  $\varepsilon_0$  is the permittivity of vacuum. We then obtain the fields in the beam frame:

$$E' = -\nabla u, \quad B' = 0,$$

followed by an interpolation at particle positions  $x'$  from the  $E'$  on the grid. The back transformation to the beam frame  $\{E, B\} = L(E')$ , ends the field calculation. Dirichlet, open or periodic boundary can be used.

#### 4.1.2.2 Particle Mesh Solver

Some of the most used solvers are direct FFT based solvers (no discretization of the  $\nabla$ -operator). We show here the differences with respect to the general scheme previously presented.  $G$  denotes the Greens function in open space, while variables with hats are in Fourier space. To obtain the scalar potential in the beam frame, we interpolate  $\rho$  and  $G$  onto a rectangular grid, followed by a Fourier transform to obtain  $\hat{\rho}$  and  $\hat{G}$ . Determining  $\hat{u} = \hat{G} \otimes \hat{\rho}$  and transforming back gives  $u = FFT^{-1}(\hat{u})$ . To compute finally the electric and magnetic fields we follow the procedure described in the previous section. The use of FFT reduces the computational complexity from  $O(N^2)$  to  $O(N \log N)$  with  $N$  denoting the grid size. Using parallel FFT's one can easily parallelize this scheme and integrate it into a particle tracking program [10]. Open or periodic boundary conditions can be used.

#### 4.1.2.3 A Novel Massively Parallel Poisson Solver

In the case of large and complicated boundaries we propose a finite element based Poisson solver (using trilinear finite elements) with a semi unstructured grid. The resulting linear system of equations is then solved with a multigrid. The same steps apply as for the previously described solver with the exception that Eq. (1) is treated differently.

The use of a structured grid  $\Omega_h$  has several advantages in comparison to a pure unstructured grid. One of them is the small storage requirement, since the discretisation stencil is a fixed stencil independent of the grid point. Other advantages are the super convergence of the gradient and the natural construction of coarse grids. To be able to discretize more general domains, we apply so called *semi-unstructured* or embedded structured grids as depicted in Figure 2. These grids consist of a large structured grid in the interior of the domain, and an unstructured grid, which is only contained in boundary cells. A detailed description of semi-unstructured grids for general domains is given in [7].

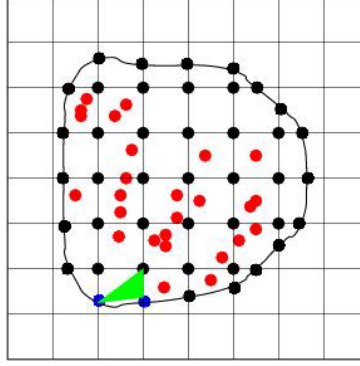


**Figure 2:** Semi-unstructured grid with particles (red) and edge cells (green)

Here, we describe only the main properties of semi-unstructured grids. A semi-unstructured grid generation is based on the structured grid  $\Omega_h$ , and leads to the following objects: *interior cells*, *boundary cells* and *exterior cells*. The boundary of  $\Omega$  cuts the boundary cells. This cut is approximated by triangles for every boundary cell. The union of all these triangles and all interior cells is the *discretization domain*  $\Omega_h$ . The semi-unstructured grid is the set of *nodal points*

$$N_n = N_{n,i} \cup \partial N_n \quad (2)$$

where  $\partial N_n$  are the boundary nodal points and  $N_{n,i} \subset \Omega_h$  are the interior nodal points. The boundary nodal points are constructed in such a way that every boundary nodal point  $p \in N_n$  is contained in the interior of an edge of a boundary cell. Several advantages of the structured grid  $\Omega_h$  still remain for the semi-unstructured grid  $N_n$ . One of them is the low storage requirement, since the discretization stencils of the structured grid are constant. Another is the natural construction of coarse grids up to a very coarse grid. Such constructions are important for obtaining an optimal multilevel iterative solver. Furthermore, the structured grid inside of the domain leads to a local super-convergence of the gradient. To obtain a finite element discretization of (2) we use linear elements. The discretized  $\Delta$ -operator results in a sparse linear system of equations.

#### 4.1.2.4 The Multigrid Solver

A multigrid algorithm [9] is used to solve the linear system of equations resulting from the finite element discretization of  $N_n$  and the corresponding differential operator is based on a sequence of fine and coarse grids

$$\Omega_{h_1} \subset \Omega_{h_2} \subset \dots \subset \Omega_{h_n}$$

and restriction and prolongation operators

$$R_{h_i} : \Omega_{h_{i+1}} \rightarrow \Omega_{h_i}$$

$$P_{h_i} : \Omega_{h_{i-1}} \rightarrow \Omega_{h_i}.$$

Restriction and prolongation has to be applied to FEM-spaces and to the differential operators from fine to coarse grid (and vice versa). Depending on the grid and the

operator, additional structures must be provided. Performance results of the parallel Poisson solver and the parallel grid generators is shown in Table 1 for a toy Poisson problem where  $\Omega = S^3$  (sphere). We show in Table 1 the scalability of the grid generator and the solver. The scalability defined as product of execution time (T) and number of processors (P) divided by the problem size (M) is given for the grid generation (in column 3) and for one multigrid iteration (in column 5) with a Gauss-Seidel smoother. We observe excellent scalability with respect to the problem size  $M$  which is equivalent to say we can handle in the order  $10^{11}$  macro particles in a simulation with reasonable computing time.

**Table 1:** Scalability of the parallel grid generator  $T_g P/M$  and the Poisson solver (TP/M) showing also T, the time in seconds for one Multigrid (V-cycle) step

P	M	$T_g P/M$	T	TP/M
8	625464	3.5e-3	3.1	3.9e-5
32	306080	8.5e-3	0.78	8.1e-5
248	4751744	5.9e-3	1.2	6.2e-5
248	36998619	7.5e-3	7.7	5.1e-5
960	23312735	4.85e-3	4	1.64e-4
2035	405242845	6.60e-3	10.7	5.3e-5
4075	7166171845	8.7e-3	160	9.9e-5

Automatic parallelization of a code can only be achieved if the code is implemented in a suitable language, for example C++ and MPI (Message Passing Interface) augmented with the concept of expression templates. Using expression templates, one can implement operators like  $+$ ,  $-$ , ... in such a way that expressions like  $\mathbf{u} = \mathbf{a} + \mathbf{b} + \mathbf{c}$  are evaluated in an efficient way for vectors  $\mathbf{a}, \mathbf{b}, \mathbf{c}$ . The main idea of this concept is to implement the operator  $+$  such that  $\mathbf{a} + \mathbf{b}$  does not return the resulting vector, but a template object which is able to evaluate  $\mathbf{a} + \mathbf{b}$  efficiently for every component of the vector, originally proposed in [8]. This ansatz allows C++ to achieve the same performance on vector and matrix expressions as with Fortran. Expression templates are also used in Mad9p, explained in the subsequent section.

#### 4.1.2.5 Mad9p Methodical Accelerator Design Version 9

Mad9p is a general purpose parallel particle tracking program including three-dimensional space charge calculation [10]. Mad9p is based on the Vlasov-Maxwell equations. In this model particle motion is governed by external fields, with a mean-field approach for the space-charge fields. Particle collisions and radiation are neglected. The total Hamiltonian for a beam line element can be written as a sum of two parts,  $H = H_1 + H_2$  which correspond to the external and space charge contributions. A second-order integration algorithm (split operator) for a single step is then given by

$$M_k(\tau) = M_k^1(\tau/2)M_k^2(\tau)M_k^1(\tau/2) + O(\tau^3)$$

where  $\tau$  denotes the step size,  $M_k^1$  is the map corresponding to  $H_1$  obtained by differential algebra methods from a general relativistic Hamiltonian and  $M_k^2$  is the map corresponding to  $H_2$ , is obtained by discretizing the resulting Poisson problem on a

rectangular mesh using Fourier techniques, as previously described. Open and periodic boundary conditions can be chosen.

### 4.1.3 Eigenmode solvers

Many applications in electromagnetics require the computation of some of the eigenpairs of the curl-curl operator,

$$\mathbf{curl} \mu_r^{-1} \mathbf{curl} \mathbf{e}(\mathbf{x}) - k_0^2 \varepsilon_r \mathbf{e}(\mathbf{x}) = \mathbf{0}, \quad \mathbf{div} \mathbf{e}(\mathbf{x}) = 0, \quad \mathbf{x} \in \Omega, \quad (3)$$

in a bounded simply-connected, three-dimensional domain  $\Omega$  with homogeneous boundary conditions  $\mathbf{e} \times \mathbf{n} = \mathbf{0}$  imposed on the connected boundary  $\partial\Omega$ .  $\varepsilon_r$  and  $\mu_r$  are the relative permittivity and permeability. Equations (3) are obtained from the Maxwell equations after separation of the time and space variables and after elimination of the magnetic field intensity. While  $\varepsilon_r$  and  $\mu_r$  are complex numbers in problems from waveguide or laser design, in simulations of accelerator cavities the materials can be assumed to be loss-free, thus admitting real  $\varepsilon_r$  and  $\mu_r$ , whence all eigenvalues are real. Here, we will assume  $\varepsilon_r = \mu_r = 1$ . Thus, the discretization of (3) by finite elements leads to a real symmetric generalized matrix eigenvalue problem

$$A\mathbf{x} = \lambda M\mathbf{x}, \quad C^T \mathbf{x} = \mathbf{0}, \quad (4)$$

where  $A$  is positive semidefinite and  $M$  is positive definite. In order to avoid spurious modes we approximate the electric field  $\mathbf{e}$  by Nédélec (or edge) elements [22]. The Lagrange multiplier (a function) introduced to treat properly the divergence-free condition is approximated by Lagrange (or nodal) finite elements [13].

In the following we describe *femaXX*, a parallel simulation tool for efficiently computing a few of the smallest eigenvalues and corresponding eigenvectors of (4). *femaXX* includes postprocessing features like visualisation of eigenfields and calculation of quality factors and gap voltages of accelerator cavities. Here we mainly focus on the eigensolver.

#### 4.1.3.1 Solving the matrix eigenvalue problem

We review the symmetric Jacobi-Davidson eigensolver and the preconditioner that is needed for its efficient application. This algorithm is well-suited since it does not require the factorization of the matrices  $A$  or  $M$ . In [13, 14] we found JDSYM to be the method of choice for this problem.

The Jacobi–Davidson algorithm has been introduced by Sleijpen and van der Vorst [23]. There are variants for all types of eigenvalue problems [15]. Here we use a variant adapted to the generalized symmetric eigenvalue problem (4) as described in detail in [12].

We just sketch the algorithm. Let us assume that we have already computed  $q$  eigenvalues of (4) and have the corresponding eigenvectors available in the  $n \times q$  matrix  $Q$ . (Initially,  $Q$  is ‘empty’.) Of course,  $C^T Q = \mathbf{0}$ . Let us further assume that we have available a search space  $\mathcal{R}(V_k)$  where  $V_k = [\mathbf{v}_1, \dots, \mathbf{v}_k]$  with  $V_k^T M V_k = I_k$ ,  $C^T V_k = \mathbf{0}$ , and  $Q^T M V_k = \mathbf{0}$ . JDSYM proceeds in three steps to expand the search space by one dimension.

1. **Extraction.** In the extraction phase, a Ritz pair of (4) restricted to  $\mathcal{R}(V_k)$  is computed. This amounts to computing the spectral decomposition of  $V_k^T A V_k$  and selecting a particular Ritz pair  $(\tilde{\rho}, \tilde{\mathbf{q}})$  in  $\mathcal{R}(V_k)$  that best approximates the searched eigenpair in the sense that  $\tilde{\rho}$  is the Ritz value closest to some given target value. Here,  $\tilde{\rho} = \rho(\tilde{\mathbf{q}})$  denotes the Rayleigh quotient of  $\tilde{\mathbf{q}}$ .
2. **Correction.** Let  $\tilde{Q} \equiv [Q, \tilde{\mathbf{q}}]$ . In order to improve the actual best approximation  $(\tilde{\rho}, \tilde{\mathbf{q}})$  a correction  $\mathbf{t}$  is determined that satisfies the *correction equation*

$$(I - M\tilde{Q}\tilde{Q}^T)(A - \tilde{\rho}M)(I - \tilde{Q}\tilde{Q}^T M)\mathbf{t} = -\mathbf{r}, \quad \tilde{Q}^T M\mathbf{t} = \mathbf{0}, \quad (5)$$

where  $\mathbf{r} = A\tilde{\mathbf{q}} - \tilde{\rho}M\tilde{\mathbf{q}}$  is the residual at  $\tilde{\mathbf{q}}$ .  $\mathbf{t}$  can be interpreted as a Newton correction at  $\tilde{\mathbf{q}}$  for solving  $A\mathbf{x} - \rho(\mathbf{x})M\mathbf{x} = \mathbf{0}$ . For efficiency reasons, the correction equation is solved only approximately by a Krylov subspace method.

3. **Extension.** The solution  $\mathbf{t}$  of (5) is made  $M$ -orthogonal to  $V_k$  and orthogonal to  $C$ ,

$$\hat{\mathbf{t}} = (I - V_k V_k^T M)(I - YH^{-1}C^T)\mathbf{t}. \quad (6)$$

After  $M$ -normalization,  $\hat{\mathbf{t}}$  is appended to  $V_k$  to yield  $V_{k+1}$ . Note that  $Y = M^{-1}C$  is a (very sparse) basis of the null space of  $A$  and that  $H = Y^T C$  is the discretization of the Laplace operator in the nodal element space [13].

In order to limit the memory costs, the dimension of  $V_k$  is limited. If  $\dim(V_k) = j_{max}$  then the iteration is *restarted* meaning that the vectors  $\mathbf{v}_1, \dots, \mathbf{v}_{j_{max}}$  are replaced by the *jmin* best Ritz vectors in  $V_k$ .

#### 4.1.3.2 Solving the correction equation

For the Krylov subspace method to be efficient, a preconditioner is a prerequisite. Following Fokkema et al. [17] for solving (5) we use preconditioners of the form

$$(I - M\tilde{Q}\tilde{Q}^T)K(I - \tilde{Q}\tilde{Q}^T M), \quad (7)$$

where  $K$  is a symmetric preconditioner of  $A - \tilde{\rho}M$ . For efficiency reasons, we compute  $K$  only once for a fixed shift  $\sigma$  such that  $K \approx A - \sigma M$ . We experienced best results when  $\sigma$  is in the middle of the set of desired eigenvalues.

Both the system matrix and the preconditioner are symmetric. However, because of the dynamic shift  $\tilde{\rho}$ , they can become indefinite. For this reason, the QMRS iterative solver [18] is suited particularly well.

Our preconditioner  $K$ , cf. (7), is a combination of a hierarchical basis preconditioner and an algebraic multigrid (AMG) preconditioner.

Since our finite element spaces consist of Nédélec and Lagrange finite elements of degree 2 and since we are using hierarchical bases, we employ a hierarchical basis preconditioner. Numbering the linear before the quadratic degrees of freedom, the matrices  $A$  and  $M$  in (4) get a 2-by-2 block structure,

$$A = \begin{bmatrix} A_{11} & A_{12} \\ A_{21} & A_{22} \end{bmatrix}, \quad M = \begin{bmatrix} M_{11} & M_{12} \\ M_{21} & M_{22} \end{bmatrix}. \quad (8)$$

Here the (1,1)-blocks, i.e.  $A_{11}$  and  $M_{11}$ , correspond to the bilinear forms involving linear basis functions. The hierarchical basis preconditioners are stationary iteration methods for solving

$$\begin{bmatrix} K_{11} & K_{12} \\ K_{21} & K_{22} \end{bmatrix} \begin{pmatrix} \mathbf{x}_1 \\ \mathbf{x}_2 \end{pmatrix} = \begin{pmatrix} \mathbf{b}_1 \\ \mathbf{b}_2 \end{pmatrix}, \quad K_{ij} = A_{ij} - \sigma M_{ij}.$$

that respect the 2-by-2 block structure of  $A$  and  $M$ . In sequential computations we chose the symmetric block Gauss–Seidel iteration as the underlying stationary method [13]. In the present parallel setting we fared better with the block Jacobi iteration,

$$K = \begin{bmatrix} \tilde{K}_{11} & \\ & \tilde{K}_{22} \end{bmatrix},$$

where the approximation  $\tilde{K}_{22}$  of  $K_{22}$  again represents a stationary iteration method of which we execute a single iteration step. We implemented two iterations that access local information only. First, the Jacobi iteration

$$\tilde{K}_{22} = \text{diag}(K_{22}), \tag{9}$$

and, second, an iteration that executes a symmetric Gauss-Seidel step on the largest diagonal block owned by a processor. Both, approaches are quite efficient in a parallel environment and easy to implement. The latter is more powerful than the former. It deteriorates with increasing numbers of processor, though.

$\tilde{K}_{11}$  represents an AMG preconditioner, of which we execute a single V-cycle. This makes our preconditioner a true multilevel preconditioner.

We found the Multilevel Preconditioner Package ML [21] the AMG solver of choice as it can handle unstructured systems that originate from the Maxwell equation discretized by linear Nédélec finite elements. ML implements a smoothed aggregation AMG method [24] that extends the straightforward aggregation approach of Reitzinger and Schöberl [20]. ML is part of Trilinos which is discussed in the next section.

#### 4.1.3.3 Parallelization

For very large problems, the data must be distributed over a series of processors. To make the solution of these large problems feasible, an efficient parallel implementation of the algorithm is necessary. Such a parallelization of the algorithm requires proper data structures and data layout, some parallel direct and iterative solvers, and some parallel preconditioners. For our project, we found the Trilinos Project [19] to be an efficient environment to develop such a complex parallel application.

##### 4.1.3.3.1 Trilinos

Trilinos is an object-oriented software framework for the solution of large-scale, complex multi-physics engineering and scientific applications written in C++. Its capabilities include parallel linear algebra computations, the solution of linear and non-linear equations, parallel algebraic preconditioners, and related capabilities.

Our parallel implementation of JDSYM eigensolver makes use of the following Trilinos packages

- Epetra, the fundamental Trilinos package for basic parallel algebraic operations. It provides a common infrastructure to the higher level packages,
- Amesos, the Trilinos wrapper for linear direct solvers (SuperLU, UMFPACK, KLU, etc.),
- AztecOO, an object-oriented descendant of the Aztec library of parallel iterative solvers and preconditioners,
- ML, the multilevel preconditioner package that implements a smoothed aggregation AMG preconditioner capable of handling Maxwell equations [16, 21].

For a detailed overview of Trilinos and its packages, we refer the reader to [19].

#### 4.1.3.3.2 Data structures

Real valued double precision distributed vectors, multivectors (collections of one or more vectors) and (sparse) matrices are fundamental data structures, which are implemented in Epetra.

Vectors, multivectors and matrices are distributed row wise. The distribution is defined by means of a map. A map can be defined as the distribution of a set of integers across the processes that relate the global and local row indices. A map completely describes the distribution of vector elements or matrix rows. Note that rows can be stored on several processors redundantly.

Trilinos supports dense and sparse matrices. Sparse matrices are stored locally in the compressed row storage (CRS) format. Some algorithms require only the application of a linear operator, such that the underlying matrix need not be available as an object. Epetra handles this by means of a virtual operator class. Epetra also supports block sparse matrices. Unfortunately, there is no particular support for symmetric matrices.

To *redistribute* data, one defines a new, so-called target map and creates an empty data object according to this new map as well as an Epetra's import/export object from the original and the new map. The new data object can be filled with the values of the original data object using the import/export object, which describes the communication plan.

#### 4.1.3.3.3 Data distribution

A suitable data distribution can reduce communication costs and balance the computational load. The gain from such redistribution can, in general, overcome the cost of this preprocessing step.

We use the ParMetis library to distribute the matrices across the processors. The partitioner tries to distribute a graph such that a) the number of graph vertices per processor is balanced and b) the number of edge cuts is minimized. The former balances the work load. The latter minimizes the communication overhead by concentrating elements in diagonal blocks and minimizing the number of non-zero off-diagonal blocks.

#### 4.1.3.4 Numerical experiments

We report on experiments that we conducted by means of problems originating in the design of the RF cavity of the 590 MeV Ring cyclotron installed at the Paul Scherrer Institut (PSI) in Villigen, Switzerland.

We discuss the numerical experiments used to assess the parallel implementation.

The experiments have been executed on a 32 dual-node Linux PC cluster in dedicated mode. Each node has 2 AMD Athlon 1.4 GHz processors, 2 GB main memory, and 160 GB local disk. The nodes are connected by a Myrinet providing a communication bandwidth of 2000 Mbit/s.

For these experiments, we use Trilinos version 5.0 on top of MPICH 1.2.6. We compare the execution times for computing the 5 smallest positive eigenvalues and corresponding eigenvectors using JDSYM with the multilevel preconditioner defined previously. We set  $j_{min} = 6$  and  $j_{max} = 15$ . An approximate eigenpair  $(\rho, \mathbf{q})$  is considered converged when the norm of the residual  $\mathbf{r} = A\mathbf{q} - \rho M\mathbf{q}$  satisfies

$$\|\mathbf{r}\|_2 \leq \varepsilon \|\mathbf{q}\|_M,$$

where  $\varepsilon$  is set to  $10^{-8}$ .

The projector (6) is applied only once per outer iteration. For this projector, applying  $H^{-1}$  amounts to solving a Poisson equation [13]. In order to do so, we use the preconditioned conjugate gradient method (PCG), combined with a multilevel preconditioner. We require high accuracy from this iterative solver (residual norm reduction by a factor  $10^{10}$ ), so that the solution vector  $\mathbf{x}$  satisfies the constraints  $C^T\mathbf{x} = \mathbf{0}$ .

The accuracy of the results was satisfactory. The computed eigenvectors were  $M$ -orthogonal and also orthogonal to  $C$  to machine precision. The 2-norm of the residuals of the computed eigenpairs was below  $10^{-9}$ .

We deal with two problem sizes. They are labelled `cop40k` and `cop300k`.

**Table 2:** Matrix characteristics

Grid	$n_{A-\sigma M}$	$nnz_{A-\sigma M}$	$n_H$	$nnz_H$
cop40k	231,668	4,811,786	46,288	1,163,834
cop300k	1,822,854	39,298,588	373,990	10,098,456

Their characteristics are given in Table 2, where we list the order  $n$  and the number of non-zeros  $nnz$  for the shifted operator  $A-\sigma M$  and for the discrete Laplacian  $H$ . Here the eigenvalues to be computed are

$$\lambda_1 \approx 1.13, \quad \lambda_2 \approx 4.05, \quad \lambda_3 \approx 9.89, \quad \lambda_4 \approx 11.3, \quad \lambda_5 \approx 14.2.$$

We set  $\sigma = 1.5$ .

**Table 3:** `cop40k`: Comparison of the block Gauss-Seidel (left) and the Jacobi (right) preconditioners for  $K_{22}$

$p$	$t$ [sec]	$E(p)$	$t_{prec}$ [%]	$t_{proj}$ [%]	$n_{outer}$	$n_{inneravg}$
1	1806 2092	1.001.00	45	37 18 18	48 53	12.62 19.02
2	1142 1219	0.790.86	47	38 16 17	51 54	15.47 18.96
4	634 642	0.71 0.81	46	37 16 17	51 54	16.29 19.43
8	327 321	0.690.81	46	38 17 18	51 53	16.24 19.23
12	216 227	0.700.77	47	40 19 19	51 53	15.51 19.47
16	175 174	0.65 0.75	50	43 19 20	51 53	16.35 18.96

In Table 3, we report the execution times  $t = t(p)$  for solving the eigenvalue problem with various numbers  $p$  of processors. These times do not include preparatory work, such as the assembly of matrices or the data redistribution.  $E(p)$  describes the parallel efficiency with respect to the simulation run with the smallest number of processors.  $t_{prec}$  and  $t_{proj}$  indicate the percentage of the time the solver spent applying the preconditioner and the projector, respectively.  $ninneravg$  is the average number of QMRS iterations per outer iteration. The total number of applications of the preconditioner  $K$  is approximately  $nouter \cdot ninneravg$ . Note that not only the symmetric block Gauss-Seidel preconditioner varies with  $p$ . Also the multilevel preconditioner depends on the processor number because the formation of the aggregates respects the distributed data layout.

In Table 3, we use AMG preconditioners for the block  $K_{11}$  and for the whole  $H$ . However, we distinguish, in the table, the results obtained by applying, to the block  $K_{22}$ , one symmetric Gauss-Seidel (SGS) step with the diagonal block owned by a processor (left columns) or one Jacobi step (right columns). The block SGS reduces the number of QMRS iterations. However, each iteration is more expensive than one iteration with the Jacobi step.

For this case, the overall computation times are better with the Gauss-Seidel steps. However, the quality of the preconditioner  $K$  deteriorates with the number of processors as  $ninneravg$  increases with  $p$ .

**Table 4:** cop40k: Comparison of results with (left) and without (right) redistribution

$p$	$t$ [sec]		$E(p)$		$nouter$		$ninneravg$	
1	1957	2005	1.00	1.00	53	53	19.02	19.02
2	1159	1297	0.84	0.77	54	53	19.06	19.66
4	622	845	0.79	0.59	54	55	19.43	19.18
8	318	549	0.77	0.45	53	54	19.23	19.67
12	231	451	0.71	0.37	53	54	20.47	19.78
16	184	366	0.66	0.34	53	54	19.00	19.04

In Table 4, we use the AMG preconditioner for the block  $K_{11}$ , Jacobi steps for  $K_{22}$ , and a similar strategy for  $H$  (AMG preconditioner for  $H_{11}$  and Jacobi steps for  $H_{22}$ ). We investigate the effect of redistributing the matrices. Results in Table 3 show that the quality of data distribution is important. For the largest number of processors ( $p=16$ ), the execution time with the redistributed matrices is half the time obtained with the original matrices. These were straightforward block distributions of the matrices given in (8).

**Table 5:** cop300k: Results with the best parameters

$p$	$t$ [sec]	$E(p)$	$nouter$	$ninneravg$
8	4346	1.00	62	28.42
12	3160	0.91	62	28.23
16	2370	0.92	61	28.52

Finally, in Table 5, we report results for our largest problem size `cop300k`. We use the 2-level preconditioner for  $K$  and  $H$ : an appropriate AMG preconditioner for the blocks  $K_{11}$  and  $H_{11}$  and one step of Jacobi for the blocks  $K_{22}$  and  $H_{22}$ . Table 5 shows that, for these experiments, the iteration counts behave nicely and those efficiencies stay high.

#### 4.1.4 Beam Dynamics Issues in Transport lines and Cyclotrons

##### 4.1.4.1 870 keV Line

The starting point for all B870 injection line calculations is a 4-dimensional transverse phase space distribution, which has been proven to be physically satisfactory in the daily operation of the beam line. The longitudinal dimensions are uniform in space and momenta. The initially DC beam is modeled by using a characteristic longitudinal beam length of  $\beta\lambda$ , where  $\lambda$  is the wavelength of the RF. The double gap buncher is modeled by (analytic) sinusoidal momenta modulation of the beam.

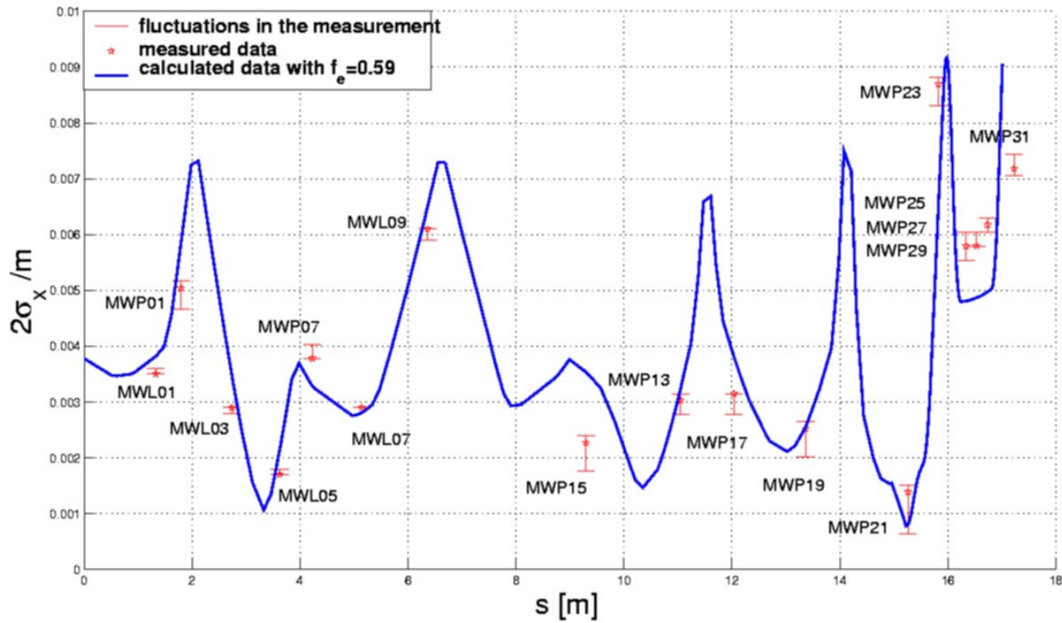


**Figure 3** (color): Horizontal beam envelope

Figure 3 shows the horizontal beam envelope (similar results are obtained in the vertical direction) after fitting the 4-dimensional transverse distribution and a global space-charge neutralisation factor  $f_e$  using a stochastic fit algorithm based on Simulated Annealing.

Define  $F$  as

$$F = \sum_{n=1}^{\#Monitors} [X_{mea}(s_n) - X_{sim}(s_n)]^2 \quad (10)$$

This function is a measure of the degree of conformity between simulation and profile monitor measurements, where  $X_{mea}(s_n)$  is a measured rms quantity at the position  $s_n$  along the beam line and  $X_{sim}(s_n)$  is the corresponding calculated quantity obtained by Mad9p. The fitting procedure then minimizes  $F$  in (10). As shown in Figure 3 we obtain good agreement between measurement and simulation. The space-charge neutralisation factor  $f_e = 0.59$  obtained is in the expected range (for reference see [10]). The discrepancy in MWP15 is not fully understood. The deviations seen at MWP25 to MWP31 are related to the buncher and the high dispersive region in this part of the beam line. More detailed modelling is needed in order to minimize the gap between theory and observation.

#### 4.1.4.2 Injector 2 Coasting Beam

A model of the Injector 2 lattice based on hardedge elements is used for various coasting beam simulations. The 2D results of Adam [5], which predict a stable round distribution in horizontal- longitudinal configuration space has been verified (see Figures 4 and 5) with the full three-dimensional model. The data shown are for 5MeV and 1mA.

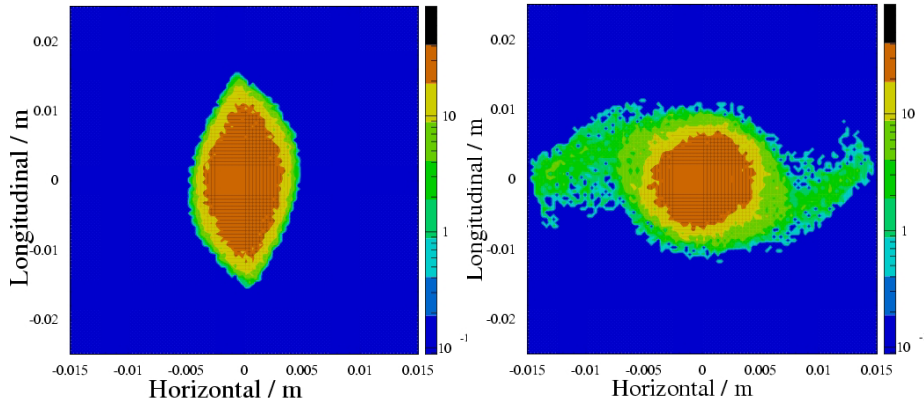


**Figure 4** (color): Charge density in a.u.: Turn 1 and 6.

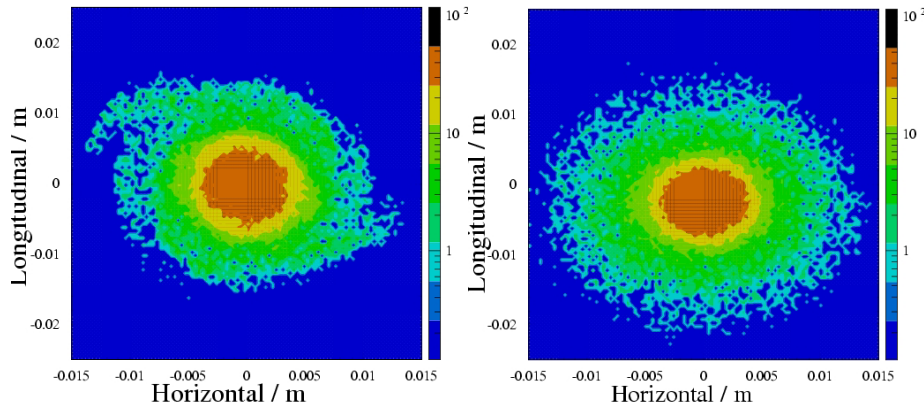


**Figure 5** (color): Charge density in a.u.: Turn 10 and 60.

The effect of the beam intensity on the development of the rms beam sizes in the horizontal and longitudinal directions is shown in Figure 6 for 60 turns. The strong oscillations in the first few turns are due to an initial 'mismatch' of the beam. The fact that the rms beam size increases with increasing beam current strongly suggests that the matching of the incoming beam has to be adapted to the beam intensity and might be the key to a very fast development of the desired round and stable distribution. Those simulations suggest again that the concept of an isochronous cyclotron is well suited for high intensity operation. More research is needed in order to make predictions for the redesign of the B870 line, and to allow operation beyond the 2 mA presently achieved.

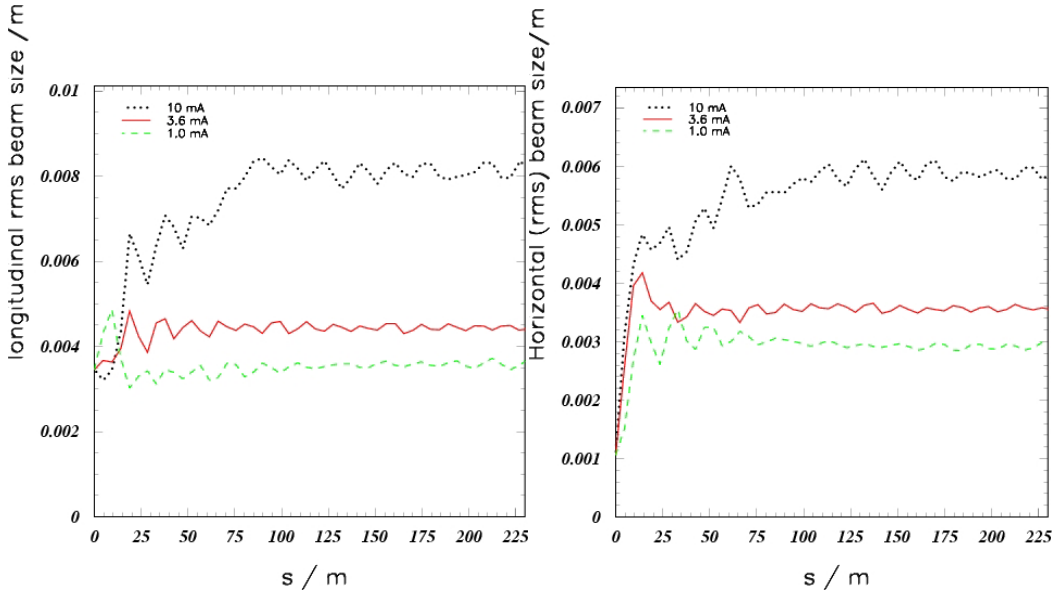


**Figure 6** (color): Horizontal and Longitudinal rms beam sizes at different intensities over 60 turns.

#### 4.1.4.3 *Injector 2 Including Collimation*

To fix the non-trivial initial conditions we start with one turn and the estimated particle distribution from [10]. After lengthy precision work on positioning the collimators and fine-tuning details of injections, we were able to simulate the very beginning of Injector 2 with satisfactory results. The amount of beam deposition on some collimators (KIP1 and KIP2), as well as the collimation process shown in Figure 7, are well in agreement with observation. The z-axis is the direction of beam propagation and the x-axis points to the center of the cyclotron. Looking at Figure 7 makes it clear that the bunch center rotates itself, the lower arm is expanding and the bunch has been collimated at the right place.

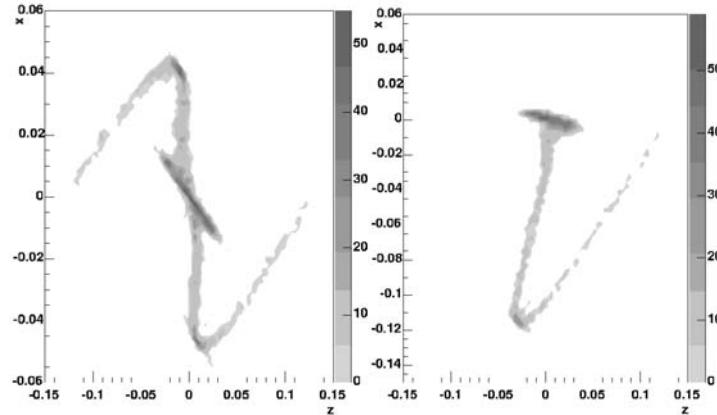


**Figure 7:** Spatial particle density in a.u before KIP1 and after KIP1  
 In figure 8 we show the situation of an extrapolated four resonator operation of Injector 2 which is nicely confirmed by three dimensional simulations.

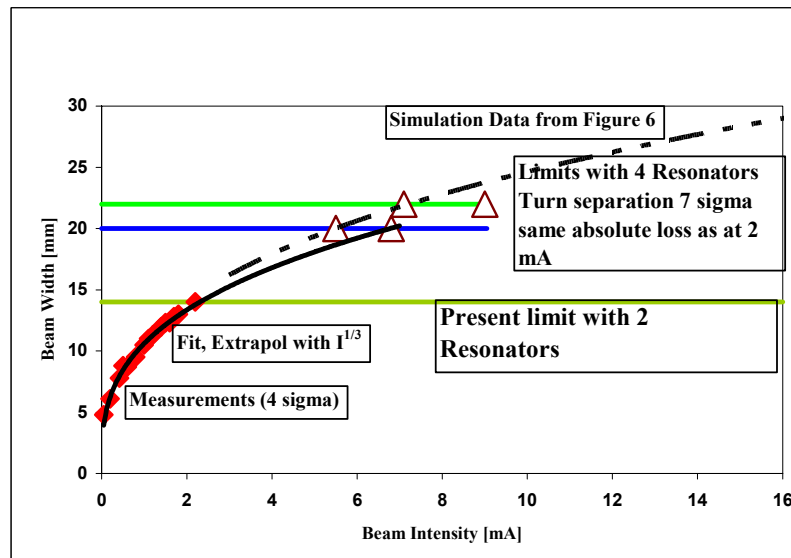


**Figure 8 (color):** Extrapolating current measurements, including rf hardware upgrade plans and comparing with simulations

#### 4.1.4.4 Calculations in the Ring Cyclotron

A mode-expansion method [11] is used for the representation of beam-excited fields in the ring cyclotron. For the determination of the mode amplitudes and phases it is required to calculate the parameters of zero beam-current trajectories from cyclotron injection to extraction.

These particle motions are integrated by a fourth order Runge-Kutta algorithm based on a third order Taylor-expansion of the static magnetic fields.

The ESIL eigenmode solver in Omega3P allows calculating Higher Order Modes (HOMs) of the entire cyclotron-structure as basis functions for the mode-expansion. A set of 280 eigenmodes with resonance frequencies close to harmonics of the beam-

crossing frequency is found and 30 particularly critical modes are selected. Their eigenfields are interpolated onto a structured, cylindrical grid, located in the midplane.

Subsequent tracking of about 100000 macro-particles with 2d space-charge corrections (see Figure 9) and comparing the beam-shapes of a simulation with consideration of HOMs to results from a HOMless simulation indicates that the effect of beam-excited fields onto the beam-quality is relatively small for the beam-currents of about 2mA.

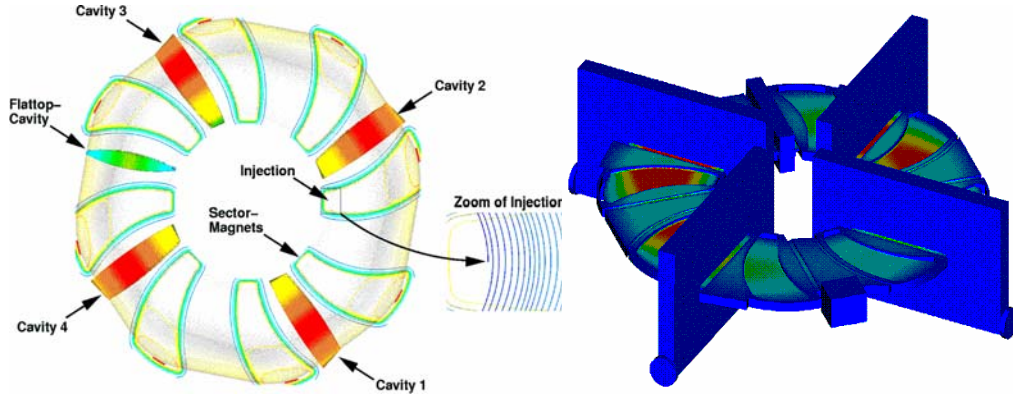


**Figure 9** (color): Left, schematics the Ring cyclotron with selected orbits at injection and on the right side is shown the leakage of the HOM's into the vacuum chamber

#### 4.1.5 Conclusions

With the upgrade of various components a substantial increase of the beam current delivered by the PSI Proton Accelerators seems feasible in a medium time range. While the prediction of the expected performance is based on simple models or on extrapolations, comprehensive simulations are under way to improve our understanding of the beam dynamical aspects of high power cyclotrons. The transport and the injection of the beam into the injector cyclotron have been investigated and the results are in good agreement with the observed beam behavior. The influence of HOMs in the Ring Cyclotron was evaluated.

The focus on our beam dynamics code and methods development is on the quantitative modeling of large and complicated accelerator structures. This can be achieved by combining latest numerical and computational methods such as state-of-the-art parallel Particle-In-Cell (PIC), as well as large-scale parallel computing capabilities. Beside this “main street” development we also recognize the need for tools enabling large-scale data management and visualization [25, 26].

In the cases considered, the parallel eigenmode solver of femaXX shows a very satisfactory behavior. The efficiency of the parallelized code does not get below 65 percent for 16 processors. We usually have a big efficiency loss when going from one to two processors. Then efficiency decreases only slowly as the number of processors is further increased. This is natural due to the growing communication-to-computation ratio.

The accuracy of the results is satisfactory. The computed eigenvectors were  $M$ -orthogonal and orthogonal to  $C$  to machine precision. The 2-norms of the residuals of the computed eigenpairs were below  $10^{-9}$ .

We are currently working on coupling femaXX with particle tracking. This will allow our particle tracking simulations to use accurate eigenfields, when pushing particles through cavities.

We are confident that a full 3D start-to-end simulations of the coupled Cyclotrons (see Figure 1) including collimations and taking into account measured rms beam sizes as well as information from beam loss monitors will be available in the near future.

#### 4.1.6 Acknowledgments

We gratefully acknowledge the work of our colleagues at ETH Zurich, Sandia National Laboratories, Lawrence Berkeley Laboratory and the University of Erlangen, Peter Arbenz, Martin Becka, Ulrich Hetmaniuk, Tiziano Mengotti, M. A. Furman, Robert D. Ryne and Christoph Pflaum. Many thanks go to the PSI proton acceleration operation staff for providing excellent experimental data.

#### 4.1.7 References

1. Proc.16th Conf. on Cyclotrons and their Applications, East Lansing , p 526, 527
2. M. Bopp et al. ,*Upgrade Concepts of the PSI Accelerator RF Systems for a Projected 3 mA Operation*, Proc. 16<sup>th</sup> Conf. on Cyclotrons and their Applications, East Lansing, 2001, p. 300.
3. R. Dölling, New Time Structure Probes between Injector and Ring Cyclotron, PSI Annual Report 2004.
4. J.-Y. Raguin et al., 500 MHz Buncher for the 72 MeV Injection Line, EPAC 2004.
5. S.R. Adam, ``Methoden zur Berechnung der Longitudinalen Raumladungs Effekte in Isochronzyklotrons'', PhD Thesis, ETH Zurich (1985).
6. H.R. Fitze, ``Developments at PSI (including new RF cavity)'' Cyclotrons 2004.
7. C. Pflaum, ``Semi-unstructured grids, Computing'' (2001) 67.
8. T. Veldhuizen, ``Expression templates'', C++ Report (1995) 7.
9. U. Trottenberg, C.W. Oosterlee, A. Schüller, ``Multigrid'', Academic Press (2001).
10. A. Adelmann, ``3D Simulations of Space Charge Effects in Particle Beams'', PhD Thesis, ETH Zurich (2002).
11. L. Stingelin et al., "Beam Cavity Interaction Simulation for the PSI Ring-Cyclotron'', Cyclotrons 2004.
12. P. Arbenz and R. Geus. A comparison of solvers for large eigenvalue problems originating from Maxwell's equations. *Numer. Linear Algebra Appl.*, 6(1):3–16, 1999.
13. P. Arbenz and R. Geus. Multilevel preconditioners for solving eigenvalue problems occuring in the design of resonant cavities. *Applied Numerical Mathematics*, 2004.
14. P. Arbenz, R. Geus, and S. Adam. Solving Maxwell eigenvalue problems for accelerating cavities. *Phys. Rev. ST Accel. Beams*, 4:022001, 2001.
15. Z. Bai, J. Demmel, J. Dongarra, A. Ruhe, and H. van der Vorst. *Templates for the Solution of Algebraic Eigenvalue Problems: A Practical Guide*. SIAM, Philadelphia, PA, 2000.
16. P. B. Bochev, C. J. Garasi, J. J. Hu, A. C. Robinson, and R. S. Tuminaro. An improved algebraic multigrid method for solving Maxwell's equations. *SIAM J. Sci. Comput.*, 25(2):623–642, 2003.
17. D. R. Fokkema, G. L. G. Sleijpen, and H. A. van der Vorst. Jacobi–Davidson style QR and QZ algorithms for the partial reduction of matrix pencils. *SIAM J. Sci. Comput.*, 20(1):94–125, 1998.
18. R. Freund and N. M. Nachtigal. Software for simplified Lanczos and QMR algorithms. *Appl. Numer. Math.*, 19:319–341, 1995.

19. M. Heroux, R. Bartlett, V. Howle, R. Hoekstra, J. Hu, T. Kolda, R. Lehoucq, K. Long, R. Pawlowski, E. Phipps, A. Salinger, H. Thornquist, R. Tuminaro, J. Willenbring, and A. Williams. An overview of the Trilinos Project. *ACM Trans. Math. Softw.*, 5:1–23, 2003.
20. S. Reitzinger and J. Schöberl. An algebraic multigrid method for finite element discretizations with edge elements. *Numer. Linear Algebra Appl.*, 9(3):223–238, 2002.
21. M. Sala, J. Hu, and R. S. Tuminaro. ML 3.1 Smoothed Aggregation User’s Guide. Tech. Report SAND2004-4819, Sandia National Laboratories, September 2004.
22. P. P. Silvester and R. L. Ferrari. *Finite Elements for Electrical Engineers*. Cambridge University Press, Cambridge, 3rd edition, 1996.
23. G. L. G. Sleijpen and H. A. van der Vorst. A Jacobi–Davidson iteration method for linear eigenvalue problems. *SIAM J. Matrix Anal. Appl.*, 17(2):401–425, 1996.
24. P. Vanek, J. Mandel, and M. Brezina. Algebraic multigrid based on smoothed aggregation for second and fourth order problems. *Computing*, 56(3):179–196, 1996.
25. A. Adelman, R.D. Ryne, J.M. Shalf, and C. Siegerist, H5Part: A Portable High Performance Parallel Data Interface for Particle Simulations, *PAC 05 Knoxville*
26. A. Adelman, R.D. Ryne, J.M. Shalf, and C. Siegerist, From Visualisation to Data Mining with Large Data Sets, *PAC 05 Knoxville*

## 4.2 Dubna cyclotrons - status and plans

S.L. Bogomolov, S.N. Dmitriev, B.N. Gikal, G.G. Gulbekyan, M.G. Itkis,  
V.V. Kalagin, Yu.Ts. Oganessian, V.A. Sokolov  
mail to: [gikal@nrmail.jinr.ru](mailto:gikal@nrmail.jinr.ru)

FLNR JINR, Joint Institute for Nuclear Research, Dubna, Moscow region, Russia

### 4.2.1 Introduction

Presently the Flerov Laboratory of Nuclear Reactions (FLNR) of the Joint Institute for Nuclear Research (JINR) has four cyclotrons of heavy ions, U400, U400M, U200, DC40, which provide performance of the basic and applied researches. Total operating time of cyclotrons is about 8000 hours/year.

The FLNR scientific program on heavy ion physics included experiments on the synthesis of heavy and exotic nuclei using ion beams of stable and radioactive isotopes and studies of nuclear reactions, acceleration technology and applied research.

The intensive beams of  $^{48}\text{Ca}$  ions on the cyclotron U400 have provided performance of the program on synthesis of a number of new isotopes of the super heavy elements.

The Tritium beam with the energy of 19 MeV/n and intensity of  $10^9$  pps was accelerated on the cyclotrons U400. The beams of  $\text{He}^6$  (28 MeV/n) and  $\text{He}^8$  (25 MeV/n) with intensity  $3 \cdot 10^5$  pps and  $3 \cdot 10^4$  pps respectively were received in flight method using a thin Beryllium production target in the separation channel.

The realization of the project DRIBs (Dubna Radioactive Ion Beams) based on ISOL scheme is completed at the Laboratory. It will allow increasing the intensity of the  $\text{He}^6$  and  $\text{He}^8$  beams up to  $10^{10}$  pps and  $10^8$  pps respectively. The first physical experiment is being planned to carry out by the end of this year.

Last year the modernization of DC40 cyclotron was carried out. The task of modernization is acceleration of an intensive beam of Kr with energy about 1.2 MeV/n that will be used for irradiation of deferent polymer materials.

The FLNR works on creation of the cyclotron DC72 for the Slovak Cyclotron Center in Bratislava are being conducted. The accelerator is developed for acceleration

of protons with energy up to 72 MeV and heavy ions with energy from 3.5 up to 18 MeV/n. The first beam is being planned to obtain in 2005.

The Flerov Laboratory of Nuclear Reactions in collaboration with the Nuclear Physics Institute (Almaty, Kazakhstan) the cyclotron DC60 for applied researches has been developed for the Research Center at the L.N. Gumilev Euroasia State University in Astana (Kazakhstan). The cyclotron is capable to accelerate ions from Carbon to Xenon with energies  $0.35 \div 1.67$  MeV/n.

#### 4.2.2 The U400 cyclotron

The U400 has 12 experimental channels, the main experimental setups are [1]: GFRS - gas filled recoil separator, VASILISSA - the electrostatic separator, CORSET/DEMON - the setup for study of fusion-fission reactions, U600 - the setup for production the track membranes, MSP144 - the magnetic separator.

The diagram of U400 operation in 1997-2004 and using the beams is shown Figure 1. In 1998-2004, the U400 was mainly used for experiments with  ${}_{48}\text{Ca}^{5+}$  ions for the purpose of synthesis the new super heavy elements.

The isochronous U400 cyclotron has been in operation since 1978 [2]. Until 1996, the PIG - ion source has been used for ion production. Since 1996, the ECR-4M ion source (made in GANIL, France) has been installed at the U400. The axial injection system was created to inject ions from the ECR-4M to the U400 center [3]. To increase the capture into acceleration the sine and linear bunchers were installed into the axial injection canal [4].

The essential modernization of the U400 axial injection in 2002 included sharp shortening of the horizontal part of the injection canal [5]. To increase the capture in acceleration efficiency, the combination of line and sine bunchers are used [6]. The linear buncher is situated at 4.4m and the sine one is placed at 0.8 m above the median plane.

The modernization gave us the possibility to increase the  ${}_{48}\text{Ca}^{+5}$  current into the injection line from  $40 \div 60$  to  $80 \div 100$   $\mu\text{A}$  at the similar capture in acceleration efficiency. Correspondingly, the average output  ${}_{48}\text{Ca}^{+18}$  ion current was increased from 15 to 25  $\mu\text{A}$ .

The average intensity of  ${}_{48}\text{Ca}^{+5}$  ions at the U400 extraction radius is about 4.3  $\mu\text{A}$  (21.5  $\mu\text{A}$ ). The typical  ${}_{48}\text{Ca}^{+5}$  ion energy is  $250 \div 270$  MeV. Since 2003, the TOF method [7] with two capacitive pickup electrodes has been used at the U400 to measure the extracted ion energy and to adjust the ion acceleration regime.

The required energy of extracted ions received by means of changing the charge of accelerated particle (rough method) and by means of changing the stripping foil position, or changing the RF frequency and the magnetic field level (fluent method). To realize the  ${}_{48}\text{Ca}^{+5}$  ion extraction with energies more than 260 MeV with keeping the beam intensity, the special magnetic channel has been constructed and situated at the hill outer edge. The aim of the channel is additional focusing of the extracted ion beam at the second turn after the stripping foil, when the foil is moved to the big radius.

In experiments on synthesis the new super heavy elements, the average intensity of the  ${}_{48}\text{Ca}^{+18}$  before the experimental target is about 1.4  $\mu\text{A}$  (25  $\mu\text{A}$ ). The main  ${}_{48}\text{Ca}^{+18}$  line of the ion spectrum after the stripping foil is mainly used for the physical experiments. The results of  ${}_{48}\text{Ca}$  acceleration in 2003 presented in [8]. In the regimes, the average consumption of solid  ${}_{48}\text{Ca}$  is about 0.8 mg/hour,

- $I_{\Sigma} = 8,2 \cdot 10^{14}$  pps,
- matter consumption  $-0,8$  mg/hour,
- utilization  $-0,16$  mg/hour (20%),
- $^{48}\text{Ca}$  enrichment (60% in matter),
- $dN/dt (^{48}\text{Ca}) = 12 \cdot 10^{14}$  pps (0,4 mg/hour),
- efficiency  $\varepsilon (0 \rightarrow n) \approx 65\%$
- efficiency  $\varepsilon (0 \rightarrow 5^+) = 10\%$

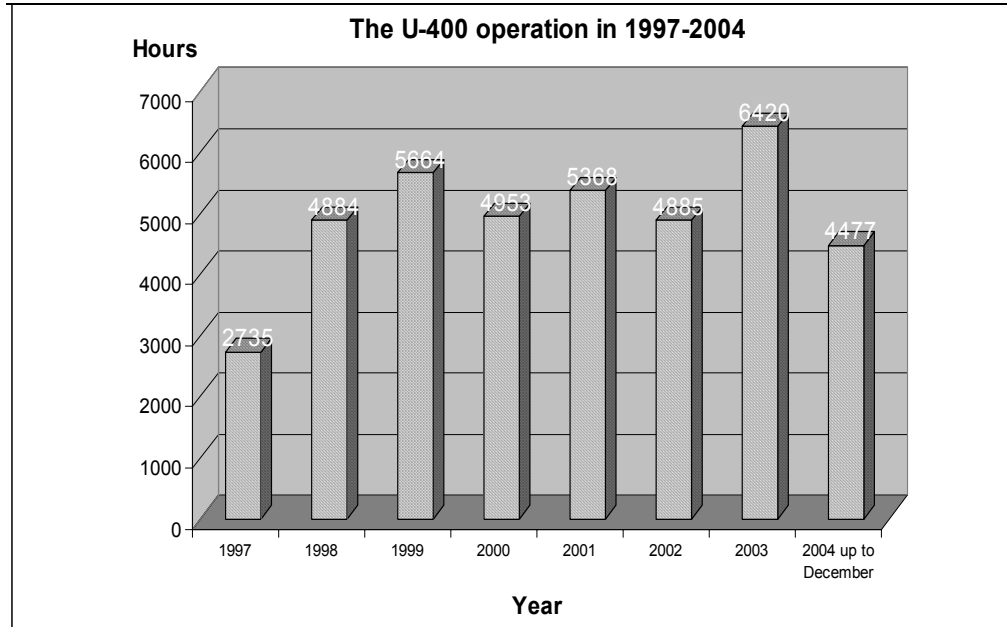


**Figure 1:** The diagram of U400 operation in 1997-2004

### 4.2.3 Modernization of the U400 cyclotron at the FLNR JINR

The modernization of the U400 has been suggested to improve the cyclotron parameters. The aims of the modernization are:

- decreasing the magnetic field level at the cyclotron center from the region of  $1.93 \div 2.1$  T to  $0.8 \div 1.8$  T, that allows us to decrease the electrical power of the U400R main coil power supply in four times;
- providing the fluent ion energy variation at factor 5 for every mass to charge ratio  $A/Z$  at accuracy of  $\Delta E/E = 5 \times 10^{-3}$ ;
- increasing the intensity of accelerated ions of rare stable isotopes at factor 3.

The beginning modernization of the U400 axial injection included sharp shortening the injection canal horizontal part. As the result, the distance from the ECR to the AM90 bending magnet became equal to 730 mm. The changes allow us to increase the  $^{48}\text{Ca}^{+18}$  ion intensity at the U400 output from 0.9 to 1.4  $\mu\text{A}$ . Further modernization intends decreasing ion losses by means of increasing the SL solenoid inner diameter from 68 to 100 mm and the AM90 bending magnet horizontal aperture from 70 to 94 mm.

In the future, we are planning to search possibility of increasing the injection voltage from the range of 13÷20 kV to 40÷50 kV. As we estimated, the changes can give us increasing the U400R accelerating efficiency in 1.5÷2 times, it is particularly important for  $^{48}\text{Ca}$  ions.

To extract ions out of the U400R we suppose to use two ways: electrostatic deflector and stripping foil method.

Both the methods allow us to extract ions in the directions of the existing ion transport channels.

The RF system of U400R will consist of two RF generators that will excite two separated RF dee resonators. The RF resonators will be made from iron with copper coating to decrease the outgassing rate from the vacuum surface.

The modernization of vacuum system will include changing five diffusion pumps VA-8-7 with  $\text{N}_2$  pumping rate of  $Q=4250$  l/s each to five cryopumps with  $Q=3000$  l/s each and two turbopumps with 1900 l/s each. In addition the materials of the cyclotron vacuum chamber and RF resonators will be changed to decrease their outgassing rate. The given changes allow us to improve vacuum in the cyclotron chamber from  $(1.5\div 2) \cdot 10^{-7}$  Torr to  $10^{-7}$  Torr.

#### 4.2.4 The U400M cyclotron

The axial injection system of the U400M [9] was put into operation in 1995. The design of the axial injection system of the U400M cyclotron is similar to that of the U400 cyclotron, but on cyclotron two sources of ions are installed. ECR is for production of heavy ions and high-frequency source of ions, which in our case was used for generation of Tritium ion beam. The DECRIS-2 (Dubna ECR Ion Source) installed at the cyclotron is created at the FLNR [10]. The beam is focused by a lenses and three solenoids placed in the axial channel. The channel is pumped out by two turbomolecular and three cryogenic pumps, which provide vacuum of  $2.5 \cdot 10^{-7}$  Torr.

Due to good vacuum in the cyclotron chamber (better than  $1 \cdot 10^{-7}$  Torr) and high acceleration rate, the beam loss during the process of acceleration up to the final radius is less than 10%.

The diagram of U400M operation in 1997-2004 and using the beams is shown in Figure 2.

#### 4.2.5 Beam extraction from U400M cyclotron

The beam is extracted from the cyclotron by a stripping foil. The beam extraction system allows the beam to be extracted with a stripping ratio  $Z_{\text{int}}/Z_{\text{ext}} = 1.4 \div 1.7$  ( $Z_{\text{int}}$  - the charge of ions of the internal beam,  $Z_{\text{ext}}$  - the charge of ions of the extracted beam). Main ion energy range of extracted ions is 30 ÷ 50 MeV/n. The beam extraction efficiency constitutes of 70-80%.

At present a number of new set-ups have been mounted, including the ACCULINNA [11] channel, intended for the production of radioactive ion beams. To carry out these experiments, the ECR source has been specially adjusted, which has enabled the production of high intensity beams of light ions both of gaseous and solid materials.

The intensity of beams of light ions in the range from Li to Ne with an energy of 30÷50 MeV/nucl was  $3\div 5 \cdot 10^{13}$  pps. This was achieved with using a bunching system,

which increases the intensity of the beam by a factor of 3÷5. Table 1 shows the efficiency of the beam transportation from the ECR source to the physical target obtained for  $^{11}\text{B}^{3+}$ .

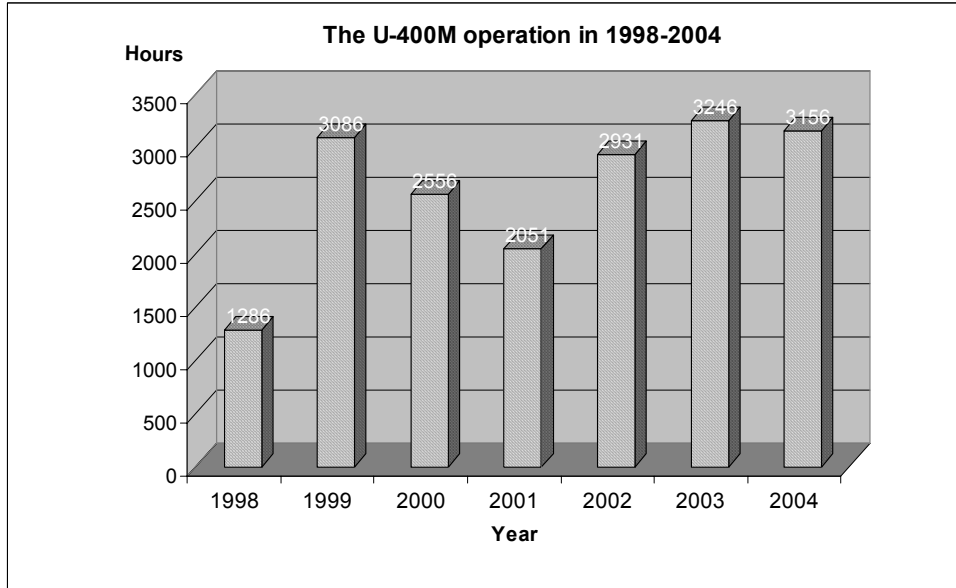


**Figure 2:** The diagram of U400M operation in 1997-2004

**Table 1:** The efficiency of the  $^{11}\text{B}^{3+}$  beam transportation from the ECR source to the physical target.

$I_{\text{ECR}}$ $^{11}\text{B}^{3+}$	$I_s$ in the center $^{11}\text{B}^{3+}$	$I_s$ at final radius $^{11}\text{B}^{3+}$	$I_s$ extracted $^{11}\text{B}^{5+}$	$I_s$ on the target $^{11}\text{B}^{5+}$
86 $\mu\text{A}$	22 $\mu\text{A}$	20 $\mu\text{A}$	30 $\mu\text{A}$	30 $\mu\text{A}$
$1.7 \cdot 10^{14}$ pps	$4.4 \cdot 10^{13}$ pps	$4 \cdot 10^{13}$ pps	$3.6 \cdot 10^{13}$ pps	$3.6 \cdot 10^{13}$ pps
26%				
	90%			
		90%		
			100%	
21%				

#### 4.2.6 Tritium accelerator

The tritium ion beam was required for study of  $^4\text{H}$  and  $^5\text{H}$  resonance states in neutron transfer reactions  $t+t \rightarrow ^5\text{H}+p$  and  $t+t \rightarrow ^4\text{H}+d$ . Experiments were performed at the separator ACCULINNA [11].

At the U400M cyclotron the tritium ions should be accelerated as molecular ions  $(\text{DT})^+$  from the point of view beam extraction by stripping. The required beam intensity on the liquid tritium target was about  $10^8$  pps. Taking into account the beam losses on transport and monochromatisation the intensity of the accelerated beam should be about 10 nA ( $6 \times 10^{10}$  pps).

The main requirements to the ion source were:

- minimal consumption of radioactive tritium;
- high output of molecular ions;
- long lifetime.

For production of molecular ions the RF ion source was chosen. During the operation at the test bench the ion source was optimized for production of  $\text{H}_2^+$  ions.

The schematic view of the RF ion source with electrostatic optics is shown in Figure 3.

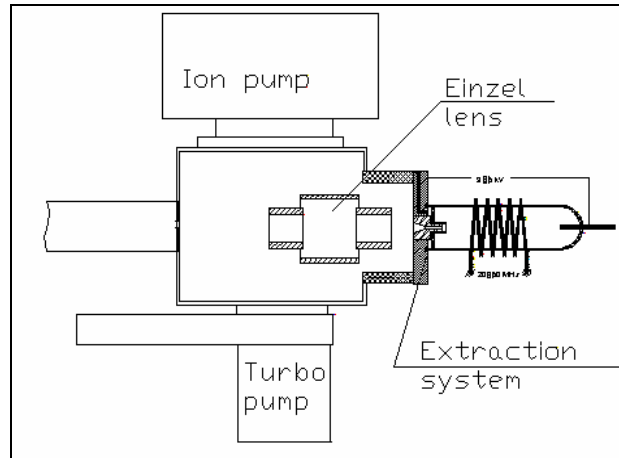


**Figure 3:** The schematic view of the RF ion source

For feeding of the tritium atoms into the ion source the special gas feed system was developed in RFNC – VNIIEPh (Sarov, Russia) that provides fine regulation of gas flow and safety handling with tritium. The system has two channels for the gas feed: one was used for feeding of deuterium-tritium mixture with the tritium content of 1%, and the second one was used for the main gas - deuterium.

A beam of 58 MeV tritons was obtained from the U400M cyclotron and delivered to the tritium target. The ACCULINNA separator ion optics was used to select the beam having an energy spread smaller than 0.5%, angular dispersion of  $\Delta\theta < 0.5^\circ$  and a 4 mm beam spot in the final focus plane. The average intensity of the delivered beam was around  $2 \cdot 10^7 \text{ s}^{-1}$  [12]. Table 2 shows the efficiency of the tritium beam transportation from the ion source to the physical target.

All together, the beam quality, target parameters and performance of detector telescopes, allow one to have an experimental resolution of  $\sim 500 \text{ keV}$  for the widths of  $^5\text{H}$  resonance states which could result from the  $t+t$  reaction.

**Table 2:** Efficiency of acceleration and extraction of tritium ion beam

$I_{is}$ , nA	$I_{int}$ , nA	$I_{ext}$ , nA	$I_{target}$ , nA
12	5	4,7	4,5
42 %			
	94 %		
		96 %	

A series of experiments on the production of radioactive ion beams from Li to O with energy of  $30 \div 50 \text{ MeV/nucl}$  was carried out at the ACCULINNA facility [11]. On

the focal plane of the facility spots of  ${}^6\text{He}$ ,  ${}^8\text{He}$ ,  ${}^{11}\text{Li}$ ,  ${}^{12}\text{Be}$  beams were about 10 mm in diameter, the ion energy spread -  $\Delta E/E = 5\%$ . The obtained results are presented in Table 3.

**Table 3:** Radioactive ion beams produced by ACCULINNA facility at the Be target (primary beam intensity -  $6.25 \times 10^{12}$  pps)

RIB, $E_{\text{RIB}}$	Yields, pps	Reaction
${}^6\text{He}$ (25 MeV/A)	$9.0 \cdot 10^5$	$\text{Be} + {}^7\text{Li}$ (32 MeV/A)
${}^8\text{He}$ (25 MeV/A)	$2.5 \cdot 10^3$	$\text{Be} + {}^{13}\text{C}$ (43 MeV/A)
${}^{11}\text{Li}$ (35 MeV/A)	$2.6 \cdot 10^2$	$\text{Be} + {}^{15}\text{N}$ (47 MeV/A)
${}^{12}\text{Be}$ (27 MeV/A)	$1.3 \cdot 10^4$	$\text{Be} + {}^{18}\text{O}$ (35 MeV/A)

In 2000 ÷ 2002 the first stage of the DRIBs project has been realized at the U400-U400M accelerator complex.

This year a series of experiments on  ${}^6\text{He}$  ion beam will be started.

#### 4.2.7 References

1. "JINR FLNR Scientific report 1995-1996", Dubna (1997), "JINR FLNR Scientific report 1997-1998", Dubna (2000).
2. G. Gulbekian and CYCLOTRON Group, "Status of the FLNR JINR Heavy Ion Cyclotrons" in Proc. Of 14th Int. Conf. On Cyclotrons and Their Applications, Cape Town, South Africa, 1995, p. 95.
3. Yu.Ts. Oganessian, G.G. Gulbekian, B.N. Gikal, M. El-Shazly et al., "Axial injection system for the U-400 cyclotron with the ECR-4M ion source", in JINR FLNR sci. rep.1995-1996, Heavy Ion Physics, Dubna 1997, p. 270.
4. O. Borisov, B. Gikal, G. Gulbekyan, I. Ivanenko, I. Kalagin, "Optimization of the axial injection system for U400 cyclotron (linear buncher)", in Proc. of EPAC2000, Vienna, Austria, 2000, p. 1468.
5. Yu.Ts. Oganessian, G.G. Gulbekyan, B.N. Gikal, I.V. Kalagin et al. "Status of the U400 cyclotron at the FLNR JINR", in Proc. of APAC-2004 Conf., Gyeongju, Korea, 2004.
6. I. Kalagin, I. Ivanenko, G. Gulbekian "The experimental investigation of the beam transportation efficiency through the axial injection system of the U400 cyclotron", in Proc. of the 2001 Particle Accelerator Conf., Chicago, 2001, p. 1568.
7. B. Wolf, "Handbook of ion sources", CRC Press, 1995.
8. Yu.Ts. Oganessian, <http://flerovlab.jinr.ru/flnr>.
9. G.G. Gulbekian, I.V. Kolesov, V.V. Bekhterev et al. "Axial injection system for the U400M cyclotron with an ECR ion source" in JINR FLNR Sci. Rep.1993-1994, Heavy Ion Physics, Dubna 1995, p. 227.
10. A. Efremov, V. Behterev, S.L. Bogomolov, V.B. Kutner, A.N. Lebedev, V.N. Loginov, N.Yu. Yazvitsky "Performance of the ion source DECRIS-14-2". Rev. Sci. Instrum. 69(2) (1998) 662.
11. A.M. Rodin et al., NIM B126 (1997) 236.
12. Yu.Ts. Oganessian, G.G. Gulbekian, S.L. Bogomolov et al. "Production and acceleration of tritium ion beam at the U400M cyclotron", Proc. of the 16th Int. Conf. On Cyclotrons and Their Applications, East Lansing, USA, ( 2001), p. 466.

### 4.3 Computer Simulation of Beam Dynamics in JINR Phasotron up to 650 MeV Energy

L.M.Onischenko, E.V. Samsonov  
 Dzhelepov Laboratory of Nuclear Problems  
 Joint Institute for Nuclear Research, Dubna, Russia  
 mail to: [olm@jinr.ru](mailto:olm@jinr.ru)

#### 4.3.1 Introduction

The project [1, 2] of the external injection of a beam is developed for an increase in the intensity of the JINR synchrocyclotron (Phasotron) from 5 to 50  $\mu\text{A}$ . It is supposed that the beam with current 6-8 mA and energy 5 MeV, delivered from the cyclotron, after additional bunching and neutralization ( $\text{H}^- \rightarrow \text{H}^0$ ) is injected at the central region of the Phasotron. Carbon foil will be used in order to get proton beam ( $\text{H}^0 \rightarrow \text{p}$ ). Some parameters of the Phasotron central region for the scheme of external injection (Fig. 1) are given in Table 1.

**Table 1:** Data of the Phasotron central region.

Type of accelerated particle		p
Initial energy	(MeV)	5.0
Radius of injection	(cm)	27.0
Average magnetic field	(T)	1.2
Betatron frequencies:	$\nu_r$	1.01
	$\nu_z$	0.12
Orbital frequency	(MHz)	18.124
Phase width of the bunch	(RF)	20-30
Harmonic number		1
Number of acceleration gaps		2
Accelerating voltage	(kV)	37

Some preliminary results concerning an efficiency of beam capture into acceleration not taking into account space charge effects were described earlier in [3, 4]. But at such high intensity of the injected beam it is necessary to know detailed information about space-charge effects (SCE) on the particle dynamics.

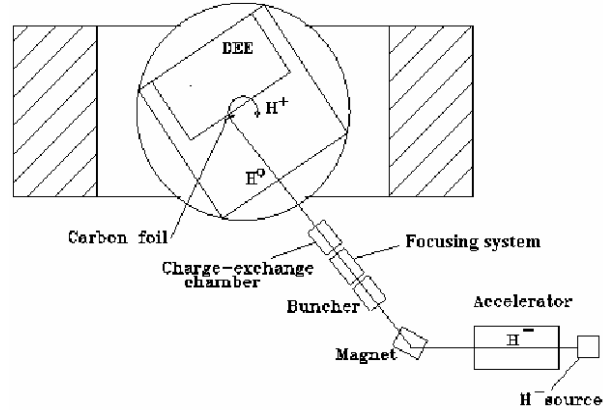


**Figure 1:** Scheme of the external injection.

More detailed investigation shows that the injection efficiency with taking into account space charge effects [5, 6] is equal 49.2 %. After 3000 turns 5080 particles from 10000 were lost mainly due to vertical losses. It is seen on the fig. 3, that vertical losses take place mainly near injection energy.

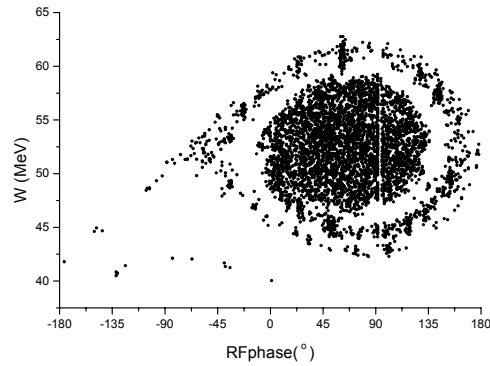


**Figure 2:** Position of 4923 particles captured into acceleration on plane (W-RF phase).

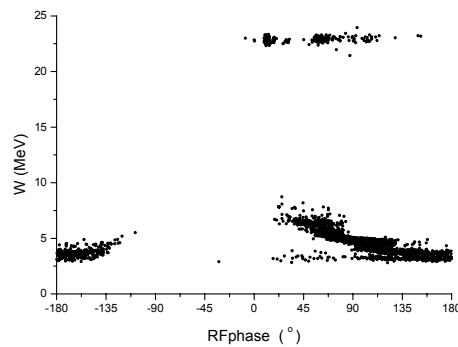


**Figure 3:** Position of 4000 vertically lost particles on plane (W-RF phase).

#### 4.3.2 Beam acceleration up to energy 650 MeV computer simulation

Investigation of the beam acceleration process up to the final energy has two main objectives:

- to investigate (calculate) the beam acceleration process;
- to determine (find) beam quality (emittances, energy spread) at the end of acceleration before the beam extraction.

Due to the small energy gain in Phasotron (near 25 keV per turn) the acceleration process continues 37000 turns. To have an available calculation time we have used in our calculations only 2000 particles (instead of 4920) and did not take into account space charge effects. Even with these conditions the calculation time was about 120 hours.

These 2000 particles used in calculation were chosen from the 4920 captured particles by the uniform random procedure. Main results of calculations are shown on Fig. 4 - 11.

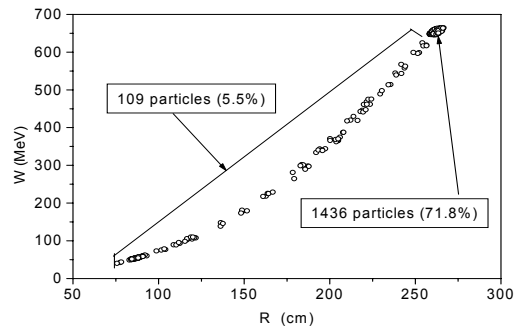


**Figure 4:** Final particles position on plane (R-W).

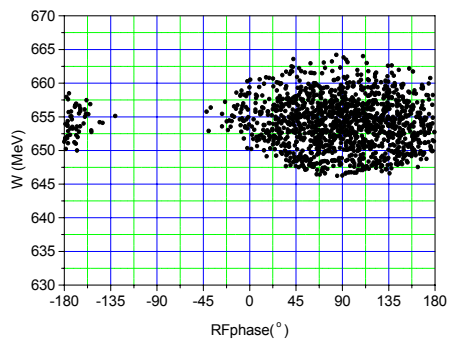


**Figure 5:** Final particles position on plane (W-RF phase).

It is seen from fig. 3 that the phase losses are distributed uniformly along the all acceleration cycle. Number of particles inside separatrix is equal 1436 (71.8 % of 2000).

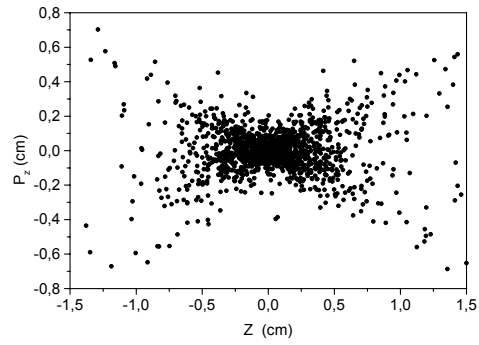


**Figure 6:** Final particles position on vertical phase plane.

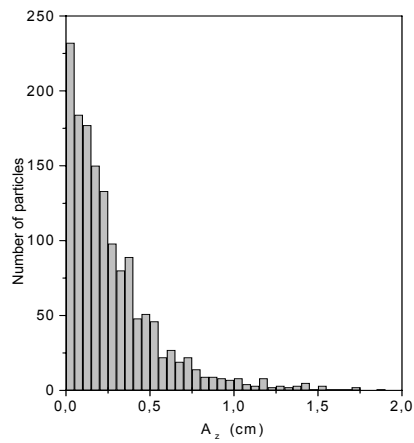


**Figure 7:** Vertical amplitudes final distribution of the particles free oscillations.

The Fig. 6 illustrates the vertical position and angle of each particle at the end of acceleration, which are entirely determined by the vertical free oscillations.

The amplitude distribution of these oscillations is shown on fig. 7. More than 95 % of particles have vertical amplitudes less than 1 cm.

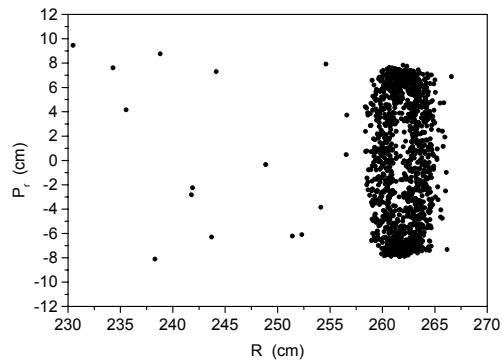


**Figure 8:** Final particle positions on radial plane.

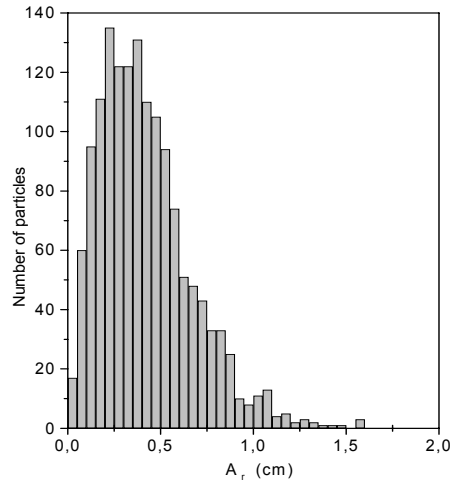


**Figure 9:** Radial amplitudes of free oscillations final distribution.

The radial particles position (Fig. 8) is determined not only by the free oscillations but also by the synchrotron oscillations. Special procedure is used to separate the free oscillations amplitude; free oscillation amplitude distribution at the end of acceleration is shown on Fig. 9. Main parts of particles have the amplitudes less than 1 cm.

On fig. 10 it is shown the distribution of the vertical beam losses on radius and on fig. 11 it is shown dependence of the free oscillations frequencies on radius. It is evident the coincidence of the maximum beam losses radial position on fig. 10 and minimum of the vertical oscillation frequency  $Q_z$ .

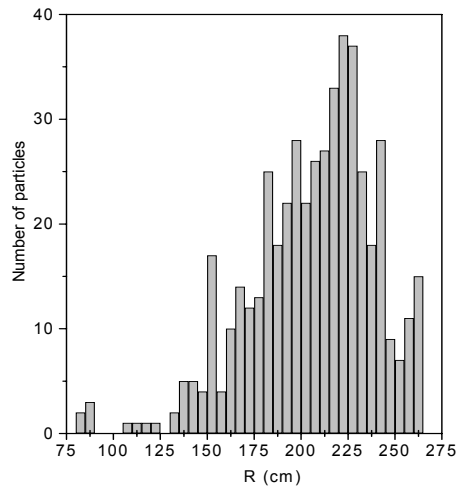


**Figure 10:** Vertical losses dependence on radius.

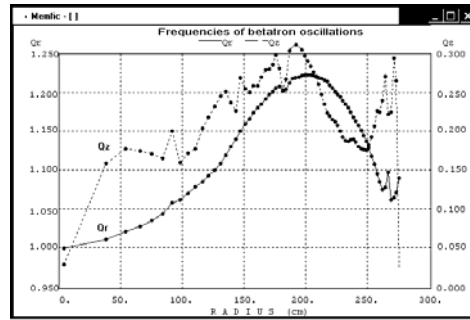


**Figure 11:** Free oscillation frequency dependence on radial.

### 4.3.3 Conclusions

Computer simulation of the beam dynamics along the whole acceleration cycle is demonstrated the almost 23 % of beam losses including 22.7 % vertical losses and 5.5 % phase losses. The final beam intensity is equal 21.5  $\mu\text{A}$  as follows from this simulation. The vertical beam losses along acceleration could be ruled out (eliminated) by increasing the vertical oscillation frequencies in the (200  $\div$  250) cm radial range. The losses at the injection (fig. 3) could be decreased by increasing the injection energy.

### 4.3.4 References

1. O.V. Savchenko, Program of experiments at the JINR Phasotron, JINR D1-90-480, p. 17, (in Russian).
2. O.N. Borisov, L.M. Onischenko, Proc. of EPAC 1998, Stockholm, p. 2097.
3. L.M. Onischenko, E.V. Samsonov, Proc. of the 16-th Cyclotron Conference, 2001, East Lansing, p. 393.
4. L.M. Onischenko, E.V. Samsonov, Problems of atomic science and technology, 2001, N3, p. 155, Ukraine, Charkov.
5. L.M. Onischenko, E.V. Samsonov. Problems of atomic science and technology 2004 N1 Series NPI (42), p. 140-143.
6. E.V. Samsonov. Internal report, Dubna, DLNP, 2004.

## 4.4 New Beam Developments at iThemba LABS

IJ.L. Conradie

[iThembaLABS](http://iThembaLABS), P. O. Box 722, Somerset West, 7129, South Africa

mail to: [lowry@tlabs.ac.za](mailto:lowry@tlabs.ac.za)

### 4.4.1 Introduction

At iThemba LABS (previously the National Accelerator Centre) proton beams, accelerated in a K=200 separated-sector cyclotron with a K=8 solid-pole cyclotron as injector [1,2], to an energy of 66 MeV are utilized for the production of radioisotopes and for neutron therapy. Proton therapy is done at 200 MeV. Low-intensity beams of light and heavy ions, as well as polarized protons, pre-accelerated in a second injector

cyclotron with a K-value of 11 [3], are available for nuclear physics research. Additions and improvements to the cyclotrons and beam lines currently in progress, for increasing the beam intensity for radioisotope production, include flat-topping systems for the light-ion injector and separated-sector cyclotrons, and an additional buncher. A new vertical beam line is under construction and beam splitting in the existing beam lines is being planned to extend the facilities for the production of radioisotopes.

The cyclotrons at iThemba LABS are operated 24 hours per day and 7 days per week [4], except for the planned shutdowns (four weekends during the year, a week in July and four weeks in January). Proton therapy is scheduled for Mondays and Fridays from 08h00 to 16h00. Beam is available for production of radioisotopes from 16h00 until 06h00 the next day from Monday until Friday morning and for neutron therapy during normal working hours on Tuesdays, Wednesdays and Thursdays. Beams of light and heavy ions as well as polarized protons, pre-accelerated in a second solid-pole injector cyclotron, are used for nuclear physics experiments over the weekends.

The 66 MeV proton beam time is optimized by automatically switching the beam between treatments to the radioisotope production vault and the intensity is increased to between 100  $\mu\text{A}$  and 150  $\mu\text{A}$ . It nevertheless remains difficult to meet the beam time requirements of the different disciplines. An increase in the intensity of the 66 MeV proton beam delivered by the existing cyclotrons and more diverse facilities for the production of radioisotopes would alleviate this problem to some extent. External beam intensities of up to 180  $\mu\text{A}$  have been used for radionuclide production with the 66 MeV proton beam, with beam losses of less than 0.8  $\mu\text{A}$ . Due to overheating of the production targets the beam current is normally limited to 100  $\mu\text{A}$ . At present the beam intensity is limited to 150  $\mu\text{A}$  by excessive beam losses at extraction in the separated-sector cyclotron. The maximum beam intensity that can be obtained from the injector cyclotron is 320  $\mu\text{A}$ . At this intensity the effect of longitudinal space-charge forces is noticeable and an increase in the internal beam intensity does not lead to an increase in the external beam current.

Experiments with a flat-topping system in the injector cyclotron showed that a 600  $\mu\text{A}$  proton beam can be extracted with an extraction efficiency of 94% [5]. The longer beam pulses extracted with a flat-topping system fall outside the linear range of the buncher in the transfer beam line. A second buncher, operating at a harmonic frequency of the existing one, is therefore being built. To prevent the longer beam pulses from acquiring excessive energy spread in the separated-sector cyclotron, a flat-topping system for this cyclotron has also been installed. With these modifications implemented it is expected that a 400  $\mu\text{A}$  beam will be available from the SSC. At present radioisotopes are produced in only one vault. A vertical beam line is under construction and beam splitting is being planned to irradiate more than one target at a time.

To increase the availability of beam for proton therapy an additional accelerator seems to be the only solution and is being investigated.

#### **4.4.2 Cyclotrons at iThemba LABS**

##### *4.4.2.1 Light-ion solid-pole injector cyclotron (SPC1)*

SPC1 pre-accelerates and provides beams of light ions, mainly protons, for injection into the separated-sector cyclotron (SSC) and further acceleration. The two 90°-dees are connected to quarter-wave resonators that can be tuned with short-circuit plates in the

frequency range 8.6 MHz to 27.5 MHz for acceleration on harmonic numbers either 2 or 6 to obtain a maximum energy gain per turn. Dee voltages of up to 60 kV, at a power level of 20 kW per resonator, and three constant orbit geometries are used to accommodate the desired energy ranges and beam currents for light ions. The magnet has four radial sectors. The beam is extracted with an electrostatic channel and two magnetic channels at a radius of 0.476 m. Feedback systems stabilize amplitude and phase of the dee voltage. An internal PIG ion source is used to pre-accelerate a proton beam to an energy of 3.14 MeV and then finally in the separated-sector cyclotron to an energy of 66 MeV at an RF frequency of 16.37 MHz for neutron therapy and radioisotope production. The maximum proton energy in SPC1 is 8 MeV.

Additional resonators are coupled capacitively to the two main resonators to superimpose a fifth harmonic, 81.8 MHz, of the main RF frequency on the main dee voltage. The flat-topping resonators are tuned with moveable short-circuit plates and are driven by power amplifiers through 50 ohm cables. The main and flat-top dee voltages are 49 kV and 1.96 kV, respectively. The power consumption is 900 W for a flat-topping dee voltage of 1.96 kV. The measured beam orbit pattern in the SPC1, with and without flat-topping is shown in figure 1. Although both the main and harmonic power amplifiers deliver power to the same dees care has been taken that power is not fed from one amplifier into the other.

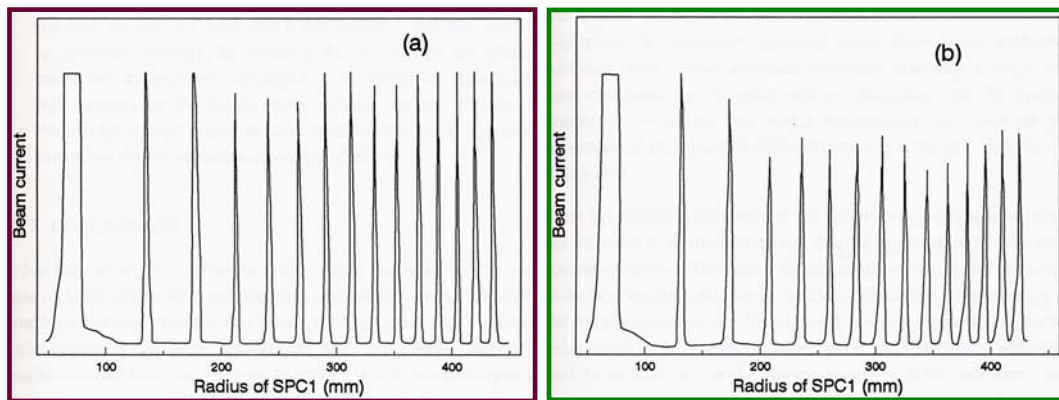


**Figure 1:** The beam orbit pattern in SPC1 (a) with (b) without flat-topping

#### 4.4.2.2 The second solid-pole injector cyclotron (SPC2)

SPC2 is, apart from its axial injection system, almost identical to SPC1 and has a K-value of 11 for heavy ions. It pre-accelerates and provides beams of both heavy ions and polarized hydrogen ions for the SSC, from an external ECR ion source and an atomic beam polarized ion source. Beams from the ion sources are inflected with spiral inflectors, one for each of the three orbit geometries. The diagnostic equipment includes a harp, which can be positioned near the extraction radius for optimization of the magnetic field and minimization of the energy spread.

#### 4.4.2.3 The separated-sector cyclotron (SSC)

The variable-energy SSC, the main accelerator at iThemba LABS, that has been designed to accelerate protons up to 200 MeV [6], has occasionally been used to

accelerate protons to 227 MeV for special purposes. The four radial magnet sectors, with a total weight of 1300 ton, a diameter of 13.2 meters and a height of 7 m have been positioned to an accuracy of 0.1 mm. The maximum magnetic flux density of 1.3 T in the 66 mm pole gaps is obtained with main coils around the poles and additional coils, which are also used for compensation of differences between the sectors, around the central yoke pieces. The sector angle of  $34^\circ$  has been chosen to avoid crossing of the  $2\nu_z + \nu_x = 4$  inherent resonance and the  $\nu_z = 1$  resonance near extraction for 200 MeV protons. The  $\nu_z = \nu_x$  resonance near injection and the  $3\nu_x = 4$  inherent resonance could not be avoided. The magnet vacuum chambers are mounted in the pole gaps with the 29 trim coils, for isochronization of the magnetic field, outside the vacuum system in the gaps between the poles and the vacuum chamber walls, thereby eliminating the need for hundreds of water and power feedthroughs. Each magnet vacuum chamber is supported with 96 studs from the top and bottom poles of a magnet sector [7]. Two  $\lambda/2$ -resonators, capacitively coupled through 50 ohm cables to 150 kW power amplifiers provide a maximum dee voltage of 220 kV in the frequency range of 6 to 26 MHz [8]. With the dees located outside the pole gaps of the magnets, in the valleys between the magnet sectors, the pole gaps could be made small to obtain strong vertical beam focusing. Several feedback systems keep the dee voltage and phase of the high Q-value resonators stable and tuned by compensating for beam loading and temperature changes. The injection system of the SSC consists of two bending magnets and a magnetic inflection channel. The beam is extracted with two septum magnets. An electrostatic extraction channel is also available for extraction but has seldom been used, since the large spaces between magnet sectors allow operation with high dee voltages and good orbit separation at extraction. The sharp drop-off in the magnetic field at the extraction radius, due to the small pole gap, and the relatively large spaces available for extraction components in the two valleys between magnet sectors not occupied by resonators allows much easier beam extraction than in the case of solid-pole cyclotrons.

The SSC accelerates beams of light and heavy ions as well as beams of polarized protons. Proton beam intensities of more than  $100 \mu\text{A}$ , at 66 MeV, are extracted from the SSC for the production of radioisotopes. Activation of the components of the SSC is limited because of the high extraction and transmission efficiency of the SSC, which is more than 99.2%. Upgrading of the iThemba LABS isotope production facilities to accommodate higher beam intensities, necessitated the installation of a horizontal half-wave flat-topping resonator that will operate at the third harmonic (49.1 MHz) of the main frequency [9]. With short-circuit plates at injection and extraction, the injection and extraction orbits will not be affected by the flat-topping voltage of the resonator. The flat-topping voltage has a maximum value of 62 kV about halfway between the injection and extraction radii. The calculated beam width due to energy spread for a  $40^\circ$  long beam pulse in the SSC with flat-topping is shown in figure 2. The height of the resonator is 0.465 m and the length is 3.017 m. The acceleration gap increases from 60 mm at injection to 100 mm at extraction. The calculated power dissipation and Q-value are 8.6 kW and 11000, respectively, with no beam. The measured Q-value is 8300. During operation with beam, power will be transferred from the beam to the resonator.

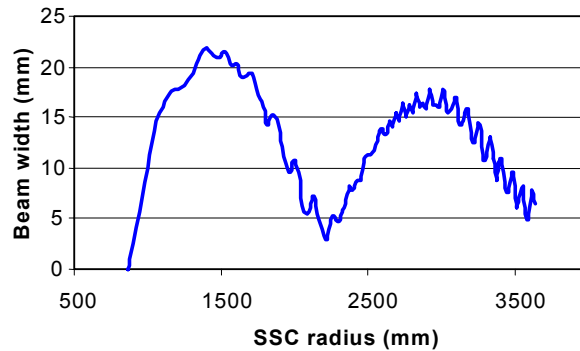


**Figure 2:** Beam width due to energy spread as a function of radius in the SSC for a 40° long beam pulse with flat-topping.

#### 4.4.3 Extension of the facilities for the production of radionuclides

##### 4.4.3.1 *Additional Buncher*

An additional buncher [4] is under construction to handle the larger beam pulses from SPC1. This new double-gap buncher will be installed in the transfer beam line between SPC1 and the SSC and will operate at 65.5 MHz, i.e. four times the main cyclotron RF frequency and twice the frequency of the existing buncher. The power consumption in the quarter-wave resonator at a voltage of 14 kV is 190 W. The distance between the two gaps is 187 mm. Calculations have shown that beam pulse lengths of 40°, in terms of the main RF frequency, from SPC1 are within the linear range of the double-drift system formed by the two bunchers together.

##### 4.4.3.2 *New Vertical Beam Line for Radionuclide Production*

In order to utilize the increased beam intensity for radionuclide production at 66 MeV a new vertical beam line [10], shown in figure 3, was installed.

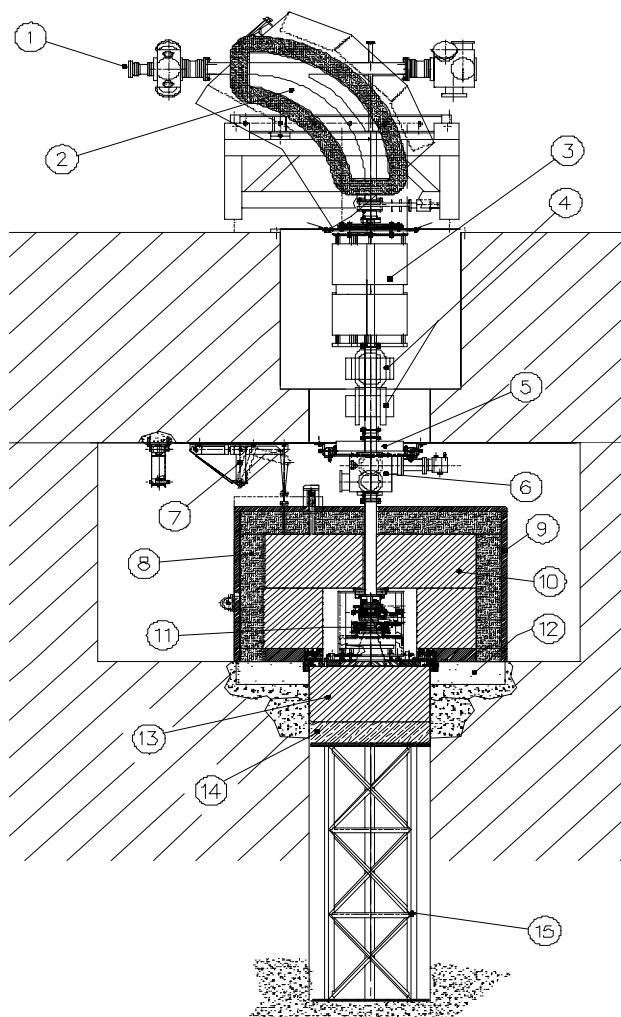


**Figure 3:** Layout of the vertical beam line for the production of radionuclides showing:

1. the horizontal beam line
2. the 90° bending magnet
3. two quadrupole magnets
4. sweeper magnets
5. steerer magnet
6. vacuum chamber for diagnostic equipment with a Faraday cup, harp and capacitive probe for current measurement
7. shielding lift mechanism for target exchanges
8. 9. and 10. inner iron shield
11. target
12. water tanks with a 4% ammonium pentaborate solution
13. iron shield
14. borated paraffin-wax shield
15. support structure.

The 90° bending magnet, with zero degree entrance and exit angle, directs the beam away from the horizontal line. The beam then passes through two quadrupole magnets and two H-type sweeper magnets, the purpose of which is to sweep the beam in a circular pattern with a radius of 10 mm over the target at a rate of 3 kHz. The coils of the sweeper magnets are tuned with capacitors and are driven by audio power amplifiers. The steering magnets together with a diagnostic vacuum chamber that contains a harp, a Faraday cup and a phase probe for non-destructive beam current measurements are positioned downstream from the sweeper magnets. The beam is focused on the target that has a diameter of 40 mm.

#### 4.4.3.3 Beam Splitting for Radionuclide Production

The irradiation of two targets at the same time can be accomplished by splitting the beam [7] as shown in figure 4. The beam will be deflected with an 800 mm long electrostatic channel, which operates with a negative deflector voltage of 70 kV across a 30 mm gap. Only two thirds of the beam will be used in the vertical beam line. The deflected beam will be diverted around the 90° bending magnet before it is taken to the radionuclide production vault. The beam loss is expected to be about 1  $\mu\text{A}$  for a 400  $\mu\text{A}$  total beam current. The septum magnet deflects the beam through 20°.

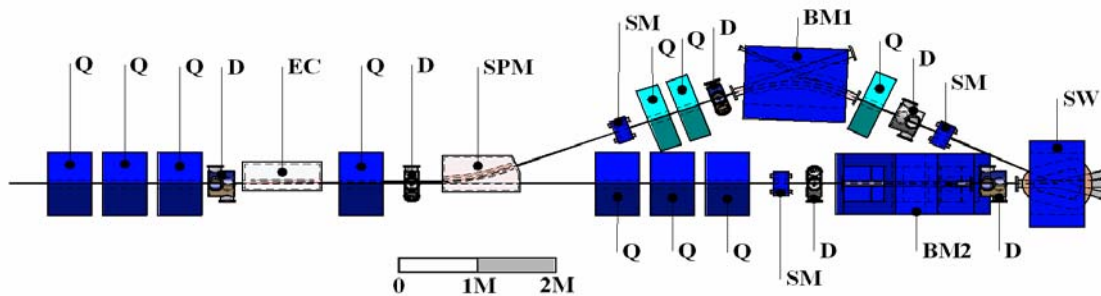


**Figure 4:** Layout of the planned beam lines for supplying two targets for radionuclide production simultaneously with beam. The main components are the electrostatic channel EC, the septum magnet SPM, the bending magnet BM1 and the existing switcher magnet SW. The bending magnet BM2 deflects the beam downward into the vertical beam line. Q, SM and D designate quadrupole magnets, steering magnets and diagnostic vacuum chambers, respectively.

To adjust the beam height in the septum magnet, a quadrupole magnet positioned directly after the electrostatic channel is used. The deflected beam is focused by three quadrupole magnets to a double waist in the switcher magnet with zero entrance and exit angles.

#### 4.4.4 Improved Beam Diagnostic Equipment

Non-destructive beam position monitors were developed [11] and have been installed at eleven positions in the transfer beam line between SPC1 and the SSC and the high-energy beam lines to align and monitor the high-intensity beams. The monitors have been designed to measure the beam position in both the horizontal and vertical directions and to fit in the diagnostic vacuum chambers together with existing equipment. In order to prevent modifications to the chambers the monitors are installed through the beam ports and are fixed with an internal clamp. The electronic signal processing equipment, for each monitor, consists of an RF signal processing module and a data acquisition and control module, and has been developed by Forschungszentrum, Jülich as part of a collaboration agreement\* with iThemba LABS.

In the transfer beam line proton beams with intensities as low as 40 nA could be aligned. In the high-energy beam line proton beams of about 0.7  $\mu\text{A}$  are used for alignment. Pickup from the main RF systems and buncher has been reduced to -135

\* Supported by BMBF and NRF, project-code 39.1.B0A.2.B.

dBm. The signal strength at the fourth harmonic of the main RF frequency, at which some measurements are made, is  $-90$  dBm for a  $1 \mu\text{A}$  beam. A remote-controlled shielded beam stop for optimization of the beam transmission through the separated-sector cyclotron at high beam intensities has been installed in the high-energy beam line close to the cyclotron. The beam stop has been designed for a maximum beam power of 32 kW.

#### 4.4.5 Proposed new facilities for proton therapy at iThemba LABS

New facilities, based on a commercial 230 MeV cyclotron, for proton therapy are proposed for iThemba LABS [12]. In addition to the existing two vaults for proton therapy, three further vaults will be provided. Four of these vaults will be equipped with, respectively, an iso-centric spot-scanning system, a fixed horizontal line for spot-scanning and two fixed lines for scattering systems enabling treatment from two angles each. Proton beams from the new cyclotron will be switched between the different vaults. It is estimated that about 1000 patients will be treated annually with the new facilities, which will be operated on a commercial basis. The existing 200 MeV cyclotron will be retained for nuclear physics research, production of radio nuclides and neutron therapy and will in future also be used for eye treatment with protons in one of the existing vaults for proton therapy.

#### 4.4.6 References

1. A. H. Botha et al., Commissioning of the NAC Separated-Sector Cyclotron, Proc. of the 11<sup>th</sup> Int. Conf. on Cyclotrons and their Applications, (Ionics Publishing Company, Tokyo 1987), p. 9.
2. A.H. Botha et al., Operation and Development of the NAC Accelerator Facilities, Proc. of the 12<sup>th</sup> Int. Conf. on Cyclotrons and their Applications, (World Scientific 1991), p. 80.
3. Z. B. du Toit et al., Commissioning of the Injector Cyclotron for Polarised and Heavy Ions at NAC, Proc. of the 14<sup>th</sup> Int. Conf. on Cyclotrons and their Applications, (World Scientific 1996), p. 28.
4. J.L. Conradie et al., "New Priorities and Developments at NAC", Proc. of the 16th Int. Conf. on Cyclotrons and their Applications, AIP Conference Proceedings, Volume 600, East Lansing, May 2001, p. 120.
5. J.L. Conradie et al., "Cyclotrons at iThemba LABS", Proc. 17th Int. Conf. on Cycl. and their Appl., Tokyo, 2004, to be published. "
6. H.N. Jungwirth, et al., "Design of Magnets for an Open-Sector Cyclotron, Proc. 7<sup>th</sup> International Conference on Cyclotrons and their Applications, Zurich, Switzerland, 1975, p.193-196.
7. F.J. Munford et al., "Design of a Vacuum Chamber for the magnets of a Separated-sector Cyclotron", Proc. Of the 8<sup>th</sup> International Conference on Cyclotrons and their Appl., Bloomington, Indiana, USA, 1978, p.1934-1937
8. A.H. Botha, et.al., "The Status of the South African National Accelerator Centre", Proceedings of the 8<sup>th</sup> International Conference on Cyclotrons and their Appl., Bloomington, Indiana, USA, 1978
9. J.G. de Villiers, et al., "A Flat-topping System for the Separated-sector Cyclotron at iThemba LABS", Proc. 17th Int. Conf. on Cycl. and their Appl., Tokyo, 2004, to be published.

10. D.T.Fourie, et al., “New Beam Lines for the Production of Radionuclides at iThemba LABS”, Proc. 17th Int. Conf. on Cycl. and their Appl., Tokyo, 2004, to be published.
11. J. Dietrich et al., Beam Position Monitor Development for iThemba LABS Cyclotron Beam Lines, EPAC’2004, Lucerne, July 2004, p.2589.
12. J.L. Conradie et al, “Proposed new Facilities for Proton Therapy at iThemba LABS”, EPAC’2002, Paris, June 2002, p. 560.

## **4.5 Status of the RIKEN Accelerator Research Facility and RI Beam Factory Project**

Y. Yano, M. Kase and A. Goto

Cyclotron Center, RIKEN, Hirosawa 2-1, Wako-shi, Saitama 351-0198, Japan

mail to: [yano@riken.jp](mailto:yano@riken.jp)

### **4.5.1 Introduction**

The advent of a radioactive isotope (RI) beam in the last half of 1980’s has opened up a new fascinating discipline in the nuclear science and technology. To further develop this new promising field, the RIKEN Accelerator Research Facility (RARF) has undertaken construction of an “RI Beam Factory,” or simply “RIBF” since April 1997 aiming to realize a next generation facility that is capable of providing the world’s most intense RI beams at energies of several hundreds MeV/nucleon over the whole range of atomic masses.

Figure 1 shows a schematic layout of the existing facility and the RIBF under construction. At present, the RARF has the world-class heavy-ion accelerator complex consisting of a K540-MeV ring cyclotron (RRC) [1] and a couple of different types of the injectors: a variable-frequency heavy-ion linac (RILAC) [2] and a K70-MeV AVF cyclotron (AVF) [3]. Moreover, its projectile-fragment separator (RIPS) [4] provides the world’s most intense light-atomic-mass (less than nearly 60) RI beams.

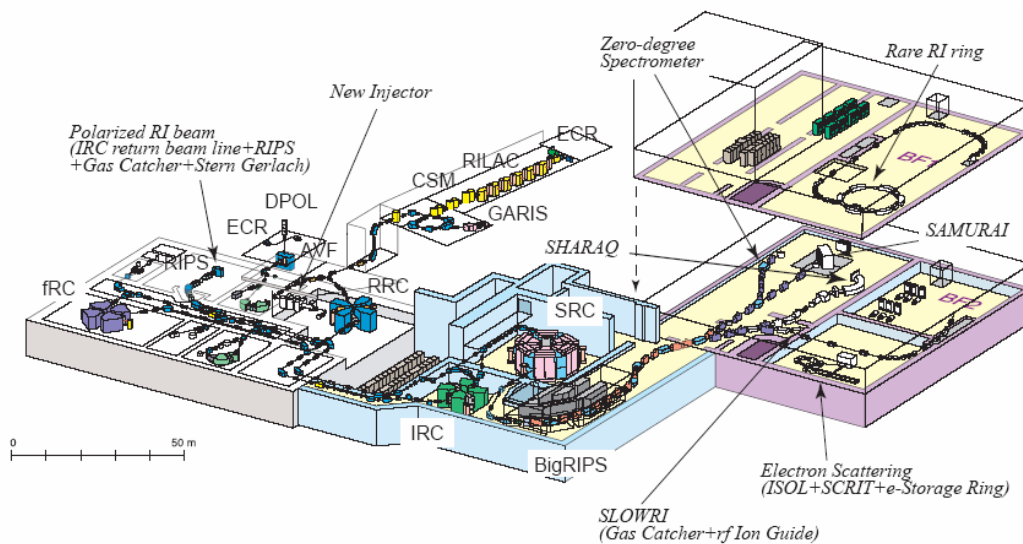


**Figure 1:** A schematic bird's-eye view of the existing facility (left-hand side) and the RIBF under construction (right-hand side). The arrows indicate major experimental installations planned in the second-phase program of the RIBF project. The experimental installations other than the zero-degree spectrometer have not been approved yet.

The RIBF will add new dimensions to the RARF's present capabilities: a new high-power heavy-ion booster system consisting of three ring cyclotrons with  $K=570$  MeV (fixed frequency, fRC [5]), 980 MeV (intermediate stage, IRC [6]) and 2500 MeV (superconducting, SRC [7]), respectively, will boost energies of the output beams from the RRC up to 440 MeV/nucleon for light ions and 350 MeV/nucleon for very heavy ions. An 880 MeV polarized deuteron beam will also be available. The goal of the available intensity is set to be 1  $\mu\text{A}$ , which is limited due to presently planned radiation shielding power around a primary-beam dump. These energetic heavy-ion beams will be converted into intense RI beams via the projectile fragmentation of stable ions or the in-flight fission of uranium ions by the superconducting isotope separator, BigRIPS [8]. The combination of the SRC and the BigRIPS will expand our nuclear world on the nuclear chart into presently unreachable region.

Now (as of August, 2005) the assembling of the SRC, the IRC and the BigRIPS is under way at their respective sites in the RIBF accelerator building completed in April 2003. The assembling of the fRC has just started. The construction of the RIBF experimental building was complete in May 2005. The first beam (a 350 MeV/nucleon uranium beam with nearly ten pA) is scheduled for late 2006. The routine operation for the users will begin in April 2007.

The RIBF project is divided into the phase I already approved and the phase II not yet approved. In the phase I, the booster ring cyclotrons, the BigRIPS and, in addition, a zero-degree forward spectrometer will be completed. Major experimental installations planned to be constructed in the phase II are under priority discussion. They are: a large acceptance superconducting spectrometer (SAMURAI), a gamma-ray detector array, a facility utilizing very slow RIBs provided via a gas-catcher and rf ion guide system (SLOWRI), a low-to-medium energy polarized RIB facility consisting of a gas catcher and a Stern-Gerlach separator at the RIPS (Polarized RI beams), a high-resolution RI-

beam spectrometer (SHARAQ), a rare RI precision mass measurement apparatus consisting of an isochronous storage ring and an individual injection system (Rare RI ring), and an electron-scattering experimental apparatus consisting of a self-confining RI-ion target (SCRIT) in an electron storage ring and a uranium-photo-fission ISOL system. A new additional injector linac to the RRC to make it possible to concurrently conduct RIBF experiments and super-heavy-element experiments is also planned. It is our hope that the phase II will be approved and the construction will be undertaken in 2006. The details of each planned experimental installation are described in Ref. [9]. In this report, the status of the RARF activities and the RIBF project will be described.

## 4.5.2 RARF

### 4.5.2.1 *General description*

As shown in Fig.1, the RARF has three kinds of accelerators: the RILAC, the RRC, and the AVF.

The RILAC, which was completed in 1981, is a heavy-ion linac having six variable-frequency resonators. The frequency range is 17 – 45 MHz. It was designed as the first injector to the RRC. It had been providing heavy-ion beams with almost the entire mass range with energies up to 2.5 MeV/nucleon. At the beginning, the pre-injector of the RILAC was a 500 kV Cockcroft-Walton high-voltage terminal equipped with a PIG heavy ion source. It was converted into the combination of a powerful ion source of 18 GHz ECR ion source [10] and a variable-frequency RFQ (FCRFQ) linac [11] in 1996. Heavy ion beams with high intensities more than 1  $\mu$ A became available. Six second-harmonic resonators were added as an energy booster after the RILAC in 2000. As the result, the maximum energy has been upgraded to 6 MeV/nucleon. These energy boosters were introduced as the acceleration part of the Charge-State Multiplier (CSM) [12], which was constructed in collaboration with the Center for Nuclear Study (CNS). The RRC, which was completed in 1986 as the main accelerator, is a K540 ring cyclotron having four separated-sector magnets and two rf resonators. The first beam of 26 MeV/nucleon  $^{40}\text{Ar}$  was successfully extracted from the RRC in December 1986 operated together with the RILAC as its injector. In the case of the RILAC-RRC mode, the operational frequencies of the two accelerators are the same, and the harmonic number of the RRC is 9, 10, 11, or 12 according to injection energy. In 1987, the RRC began to deliver beams for experiments and then the RARF officially started. The RRC reached to its full performance in 1989, when the AVF was completed. After the energy booster was installed in the RILAC, the operation of the RRC with the harmonic number of 8 has become available.

The AVF, which was designed as the second injector of the RRC, was completed in 1989. It is a K70 AVF cyclotron, having four spiral sectors and two rf dees with an angle of 85 degrees. The rf is tunable from 12 to 24 MHz. The AVF can accelerate ions having a mass-to-charge ratio smaller than 4, up to 3.8 MeV/nucleon (at 12 MHz) and to 14.5 MeV/nucleon (at 24 MHz). Its mean extraction radius of 71.4 cm is the four-fifth of the mean injection radius of the RRC. In the case of the AVF-RRC operation, the rf of the AVF is 1/2 sub-harmonic of that of the RRC, and the harmonic number of the RRC is five. Two types of ion sources, a 10 GHz ECR ion source and a polarized ion source are placed on the floor above the cyclotron vault. In the collaboration with the CNS, a new 14 GHz ECR ion source was installed in the injection line of the AVF

and a flattop resonator [3] was added to the rf system of the AVF. Recently the K-value of the AVF was upgraded from 70 up to 78 by improving the magnet power supplies.

The beam lines of these three accelerators as of 2004 are shown in Fig.1. The RRC has six target rooms from E1 to E6. The RIPS, which aims at production of RI beams, has been in operation in E6. The magnetic spectrometer called SMART, which had been located in E4 since 1991, terminated its use in the spring of 2005. The fRC will be installed in this room. The GAs-filled Recoil Isotope Separator (GARIS), which had been initially installed in the E1 target room of the RRC, is now sitting in the target room of the RILAC. A low-energy RI-beam separator (CRIB) has been installed in the AVF beam line of E7, in collaboration with the CNS. There has been an irradiation facility for biological samples and dosimetry in E5 and an irradiation apparatus producing a large variety of RI's as multi-tracers in E3. The particle analyzer (PA) has been installed in E2 in collaboration with the CNS.

#### 4.5.2.2 Operation

The RRC have been supplying a number of kinds of beams since 1986. They are plotted in a mass-energy plane as shown in Fig. 2. The accelerated beams cover the entire energy-mass range according to the initial design for both the RILAC-RRC and AVF-RRC schemes. The beams with the top energy of 135 MeV/nucleon for ions with

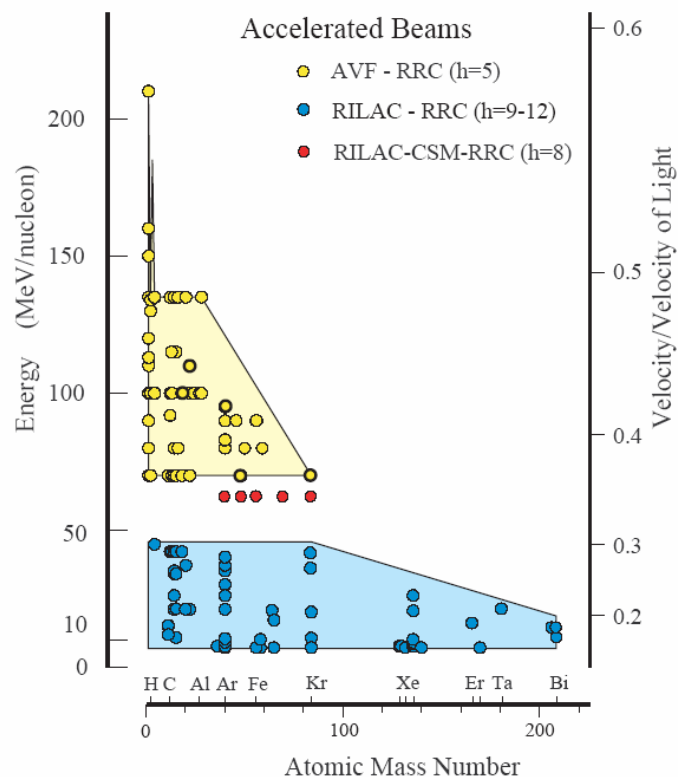


**Figure 2:** Performance of the RPC.

a mass-to-charge ratio of 2 have been frequently used for the applications to biology and medicine in E5 and the RI production in E3. Especially these beams have been

applied to an ion-beam breeding on plant business. The polarized deuteron beams with energies ranging 70 to 135 MeV/nucleon had been used at the SMART in E4. Because an orientation of spin at the SMART target is adjusted with a Wien filter in the injection beam line of the AVF, a single turn extraction should be realized in both the AVF and RRC, and it should be kept during the experiment.

About 70% of the total beam time has been devoted into experiments using RI beams produced at the RIPS by the projectile fragmentation method. For the efficient production of the RI beams, the intense primary beams of neutron-rich isotopes are frequently required, such as 110 MeV/nucleon  $^{18}\text{O}$ , 100 MeV/nucleon  $^{22}\text{Ne}$ , 70 MeV/nucleon  $^{48}\text{Ca}$ , and 70 MeV/nucleon  $^{86}\text{Kr}$ . These beams are marked in terms of emphasized-circles in Fig.2. The AVF-RRC scheme supplies enough beam intensities ( $>100$  pnA) for  $^{18}\text{O}$  and  $^{22}\text{Ne}$ , but poor intensities for beams heavier than  $^{48}\text{Ca}$  (only several pnA).

The RRC had been designed to operate with a harmonics of 9 in the case of the RILAC-RRC scheme with the top energy of the RILAC. Using a part of energy booster of the CSM, the RRC operation with a harmonics of 8 was tried and successfully done in 2002. It gives energy of 63 MeV/nucleon at the RRC with a frequency of 38 MHz. The beams of  $^{40}\text{Ar}$ ,  $^{48}\text{Ca}$ ,  $^{58}\text{Fe}$ , and  $^{86}\text{Kr}$  were accelerated in this scheme so far. In the most cases, the beam intensities are drastically increased, while their energies are somewhat lower (63 MeV/nucleon) compared with those in the AVF-RRC scheme.

**Table 1:** Upgrade of beam intensities with the CSM

Ion	AVF => RRC					RILAC => CSM => RRC				
	$E_{\text{RRC}}$ ( $h_{\text{RRC}}$ ) MeV/n	Stripping after AVF			$I_{\text{RRC}}$ pnA	$E_{\text{RRC}}$ ( $h_{\text{RRC}}$ ) MeV/n	Stripping after CSM			$I_{\text{RRC}}$ pnA
		$Q_i$	$Q_f$	$E_{\text{AVF}}$ MeV/n			$Q_i$	$Q_f$	$E_{\text{CSM}}$ MeV/n	
$^{40}\text{Ar}$	95 (5)	11	17	5.2	90	63 (8)	11	15	3.6	1000
$^{48}\text{Ca}$	70 (5)	11	18	4.0	7	63 (8)	11	17	3.6	150
$^{58}\text{Fe}$	90 (5)	13	24	5.0	4	63 (8)	13	21	3.6	80
$^{70}\text{Zn}$						63 (8)	16	25	3.6	120
$^{86}\text{Kr}$	70 (5)	20	31	4.0	4	63 (8)	16	30	3.6	90

The beam intensities of these beams are compared in Table 1 for the AVF-RRC and RILAC-RRC operations. This increase in beam intensities is owing to that the performance of the ECR ion source and the beam transmission for the RILAC is much better than those for the AVF. As the beam intensity is sometimes more important than these energy-degrades for the RI beam production, this new scheme has recently been frequently used for RIPS experiments.

At the beginning, the RRC beams with bottom energy were frequently used for super-heavy element research at E1. Considering the acceleration efficiency, the GARIS was moved to a RILAC target room. The research experiments on a  $Z=113$  element have been carried out at the GARIS since 2003. The high-intensity  $^{70}\text{Zr}$  beam with energy of 5 MeV/nucleon has been supplied on a rotating bismuth target of the GARIS in the e3 beam line of the RILAC more than 110 days from September 2003 to April 2005. Eventually two candidates of  $Z=113$  element were detected so far. [13]

We measured the longitudinal emittance for various beams accelerated by the RRC using the SMART. [14] The energy spread and time spread measured for a 95-MeV/nucleon  $^{40}\text{Ar}$  beam were 0.13 % (FWHM) and 700 ps (FWHM), respectively. We also estimated phase space distributions of beams of the RIBF at every stage of the acceleration scheme based on the measured emittance. We have thus confirmed that our accelerator complex will allow us to accelerate heavy-ion beams without any serious beam loss under their careful tunings.

Figure 3 shows the statistics of the RRC operation since 1987. A total of the operation hours per year had gradually but steadily increased, with reaching in 1990 to 6800 hr per year, which is considered to be a practical limit. After that, the operation time decreased slightly due to the RIBF construction work and slight reduction of the operation budget.

#### 4.5.2.3 Schedule towards the RIBF

As the RIBF project is approaching to the commissioning, the RARC needs to start its preparations as follows. The production of uranium ions at the RILAC ion source began in June 2005, and its acceleration test will start in autumn 2005. To realize these, the ion source area was separated, in summer 2004, from the other accelerator areas into an independent room for the treatment of uranium material. In autumn 2004, we obtained the official permission by the government for the acceleration of uranium ion beam. The developments of charge-stripper for the uranium beams are in progress [15].

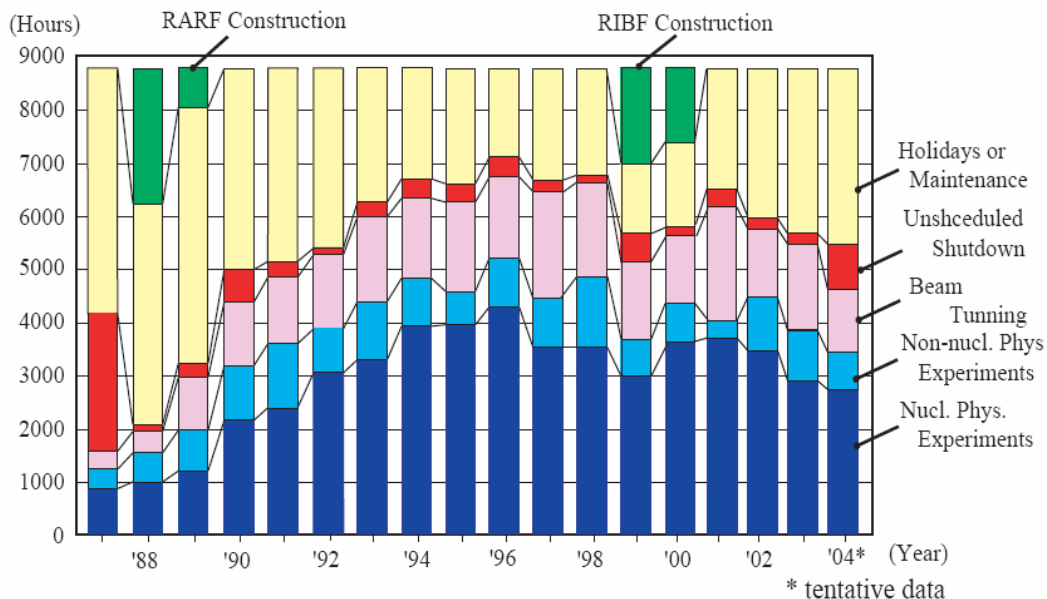


**Figure 3:** Statistics of the RRC operation since 1987.

The extraction beam lines of the fRC will appear in the D room, the RRC room and the E1 room as shown in Fig.1. The operation of the RRC will be interrupted due to the construction of these beam lines from April to June 2006. In autumn 2006, the RILAC and RRC will begin to provide beams into the RIBF accelerators (fRC, IRC and SRC.)

### 4.5.3 RIBF

#### 4.5.3.1 Acceleration modes and performance

Figure 4 shows a schematic diagram of the RIBF heavy-ion accelerator system. In this diagram, a K-value and a velocity gain factor of each cyclotron are shown. Several acceleration modes will be available. Mode (1): RILAC+ RRC+ (stripper2) + fRC+ (stripper3)+ IRC+ SRC is used for the RI-beam generation at 350 MeV/nucleon (fixed energy). 115 MeV/nucleon output beams from the IRC can be transferred to the existing RIPS in the phase II. Mode (2): RILAC+ (stripper1) + RRC+ (stripper3)+ IRC+ SRC is used for variable energy experiments. Mode (3): AVF+ RRC+ SRC is used for polarized deuteron beam generation at 880 MeV in the phase II. The harmonic numbers for respective operation modes are also shown. Figure 5 summarizes the acceleration performance of the RIBF.

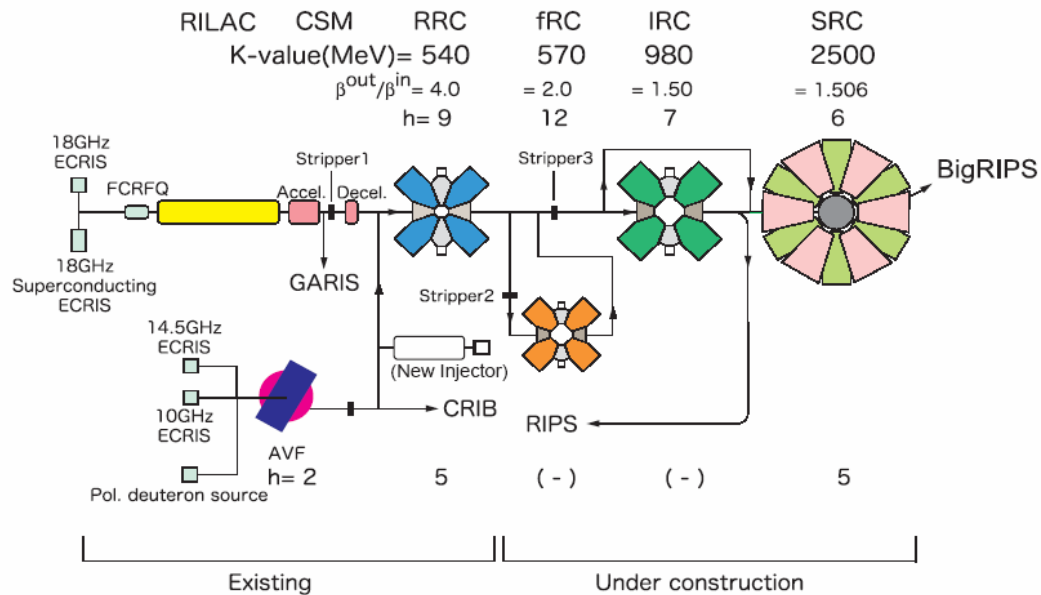


**Figure 4:** A schematic diagram of the RIBF heavy-ion accelerator system.

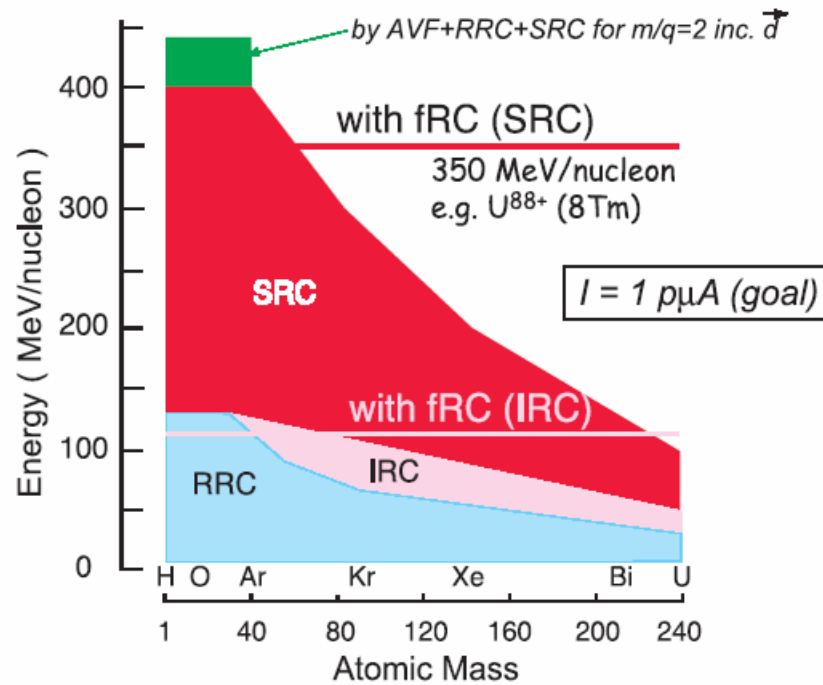


**Figure 5:** A diagram of the RIBF acceleration performance (MeV/nucleon) for each atomic mass.

#### 4.5.3.2 Expected primary beam intensities: estimation

At present, the beam transmission efficiency through the RILAC (between the exit of the mass-to-charge analyzing slit for the beam extracted from the 18 GHz ECRIS and the injection point to the RRC) and that through the RRC (between the injection point to the RRC and the extraction point from the RRC) are nearly 70% and also nearly 70%, respectively.

We conjecture that the former unsatisfactory efficiency is attributed mainly to: (1) the emittance broadening of the ECRIS beams caused by the strong space-charge effect and (2) the optical astigmatism due to the nonlinear aberration in the analyzer magnet section, and that the latter one is attributed mainly to: (3) the insufficient longitudinal focusing power of the present rebuncher system between the RILAC and the RRC.

Nevertheless, assuming that the 100 % transmission efficiency can be realized for all of the fRC, the IRC and the SRC, 1 pμA beam will be achieved, for example, for <sup>48</sup>Ca, <sup>86</sup>Kr, <sup>136</sup>Xe beams at 350 MeV/nucleon, as shown in Table 2. And also nearly 10 pA is expected for <sup>238</sup>U beam at 350 MeV/nucleon without use of the first charge stripper (between the RILAC and the RRC) when 8 eμA of U<sup>35+</sup> beam estimated may be obtained from the present 18 GHz ECRIS [10].

**Table 2:** Expected intensities ( $\mu\text{A}$ ) of primary beams  $^{48}\text{Ca}$ ,  $^{86}\text{Kr}$ ,  $^{136}\text{Xe}$  and  $^{238}\text{U}$  at the exits of the 18 GHz ECRIS, the RILAC, the RRC, the fRC, the IRC, the SRC when these beams are finally accelerated by the SRC to 350 MeV/nucleon. Both of the transmission efficiencies through the RILAC and through the RRC are assumed to be 70%. As for the fractions of the charge state after the charge strippers, see Ref. 16. The expected intensity of  $^{238}\text{U}$  beam from the 28 GHz ECRIS under the conceptual design is given in Ref. 10.

	18GHz ECRIS	RILAC	RRC	Charge Stripper2	fRC	Charge Stripper3	IRC	SRC
$^{48}\text{Ca}$	8+	8+	8+	19+	19+		19+	19+
( $\mu\text{A}$ )	10	7.0	4.9	2.0	2.0		2.0	2.0
$^{86}\text{Kr}$	14+	14+	14+	33+	33+		33+	33+
	10	7.0	4.9	2.0	2.0		2.0	2.0
$^{136}\text{Xe}$	20+	20+	20+	44+	44+	52+	52+	52+
	15	10.5	7.3	2.2	2.2	0.97	0.97	0.97
$^{238}\text{U}$	35+	35+	35+	72+	72+	88+	88+	88+
18GHz>	0.23	0.16	0.11	0.021	0.021	0.007	0.007	0.007
Super>	16	11.2	7.8	1.5	1.5	0.51	0.51	0.51

In the near future, we plan to remedy the respective problems (1)-(3) listed above to improve the present unsatisfactory transmission efficiencies by taking the following measures: (1) We will raise the extraction voltage a few times higher to reduce the emittance growth and implement the neutralizing solenoid just after the exit of the ECRIS to reduce the space charge force; (2) We will modify the analyzing dipole magnet to have an appropriate sextupole field to compensate the non-linear optics; and (3) We will install a new double-rebuncher system between the RILAC and the RRC to produce an enough focusing power in the longitudinal direction and will modify the present sinusoidal rf system of the RRC into a flat-top acceleration system.

In order to realize the 1  $\mu\text{A}$  uranium beam at 350 MeV/nucleon, in addition to these remedies, we will have to develop a new 28 GHz superconducting ECRIS [10].

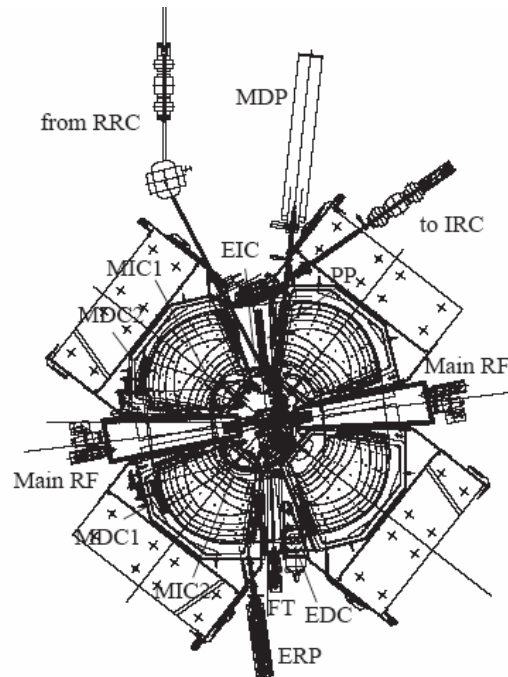
#### 4.5.3.3 fRC

Figure 6 shows a layout of the fRC. The fRC is a four-sector room-temperature ring cyclotron, which is designed as a fixed frequency machine, unlike other cyclotrons in the RIBF, so as to minimize its construction cost. Moreover, in order to minimize magnetic field correction to form isochronous fields, ion beams are accelerated with charge-to-mass ratios within a narrow band of their values.

The mean injection and extraction radii are 1.55 m and 3.30 m, respectively. Injection and extraction energies (10.5 and 50.7 MeV/nucleon) of the fRC are determined to compensate energy losses in the charge strippers in upstream and downstream of the fRC. [16] The K-value of the fRC is 570 MeV, which corresponds to the bending power of 50.7 MeV/nucleon  $^{238}\text{U}^{71+}$ . The frequency of the fRC is determined at 55 MHz, which is three times those of the RILAC and the RRC, so as to obtain high acceleration voltage in the main rf resonator with small mechanical size and low rf power. Acceleration voltage per one turn is expected to be 1 MV by use of two rf resonators to obtain large turn separation. Since the fRC is operated at the frequency

three times that of the RRC, the fRC is also equipped with a flattop resonator to make the phase acceptance large ( $\pm 10^\circ$ ).

The fRC will be placed in the E4 experimental room of the present building after evacuating the existing magnetic spectrometer. The beam is sent to the IRC after extracted through a hole in a yoke of the sector magnet.



**Figure 6:** Layout of the fRC.

#### 4.5.3.4 IRC

Figure 7 shows a layout of the IRC. The IRC is a room temperature ring cyclotron with K-980 MeV, which is placed upstream of the SRC. The injector of the IRC is the RRC (variable energy acceleration mode) or the fRC (350 MeV/nucleon mode). The maximum energy is 127 MeV/nucleon. The IRC mainly consists of four sector magnets, beam injection and extraction elements, two acceleration resonators and one flattop rf resonator. The mean injection and extraction radii are 2.77 m and 4.15 m, respectively. Acceleration RF frequency is variable from 18.0 MHz to 38.2 MHz according to the energy of the accelerated ions. Maximum sector field is as high as 1.9 T, which is achieved with rather low power consumption of 0.5 MW.

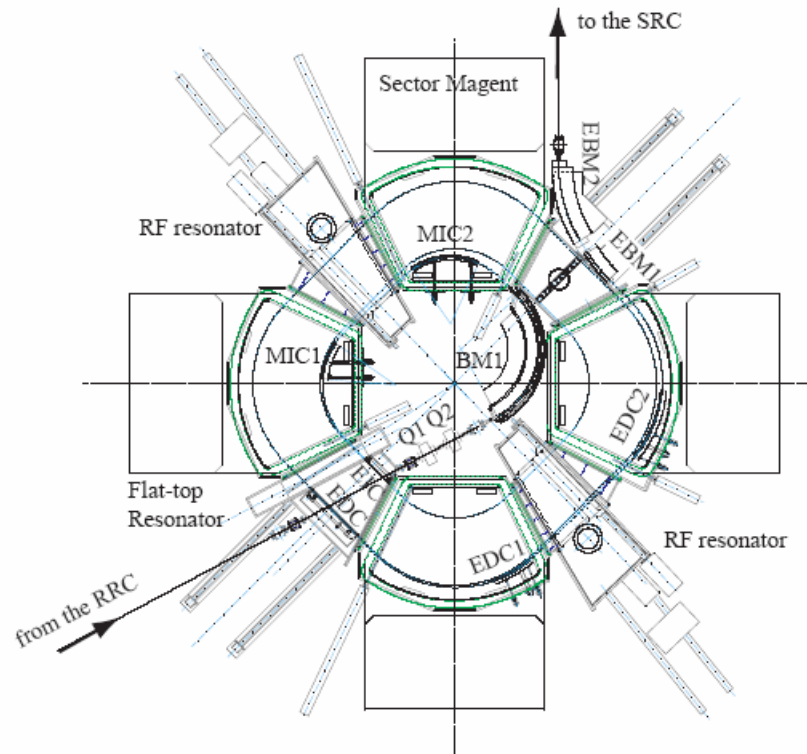


**Figure 7:** Layout of the IRC.

#### 4.5.3.5 SRC

A plan view of the SRC is shown in Fig. 8. The SRC mainly consists of six superconducting sector magnets, four main rf resonators, one flattop rf resonator, injection and extraction elements (among them the injection bending magnet (SBM) is superconducting). The valley regions are covered with magnetic shield irons in order to reduce the stray field. Some of the iron slabs of the magnetic shield are bridged on the top and bottom of the valley regions between the sector magnets, and the others are placed vertically between these top and bottom slabs. The total weight of these six falling-U-shaped structures is about 3,000 t; the total weight of the SRC amounts to 8,300 t. The K-value is 2,500 MeV. The outer radius and height of the SRC are 9.2 m and 7.6 m, respectively. The mean injection and extraction radii are 3.56 m and 5.36 m, respectively. The SRC allows us to accelerate light heavy-ions at 440 MeV/nucleon and very heavy ions at 350 MeV/nucleon. A photograph of the SRC under assembling in the vault is shown in Fig. 9.

The sector magnet is 7.2 m in length and 6 m in height. The weight is about 800 t per each. The sector angle is 25 deg. The maximum sector field is 3.8 T, which is required to accelerate  $U^{88+}$  ions at 350 MeV/nucleon (8 Tm). Main components of the sector magnet are: a pair of superconducting main coils, four sets of superconducting trim coils, their cryostat, thermal insulation support links, twenty-two pairs of normal conducting trim coils, warm-poles and a yoke.

This K2500-MeV SRC will be the world's first superconducting ring cyclotron with the ever largest K-value. In the course of design of the sector magnet, significant changes were made from the original design: (1) a pair of large active magnetic-shield coils have been replaced with soft iron slabs that cover the valley regions, which results

in the self radiation shielding and the self leakage-magnetic-flux shielding structure, and (2) the cold-pole scheme have been replaced with the warm pole scheme, which results in the shorter cooling time structure.

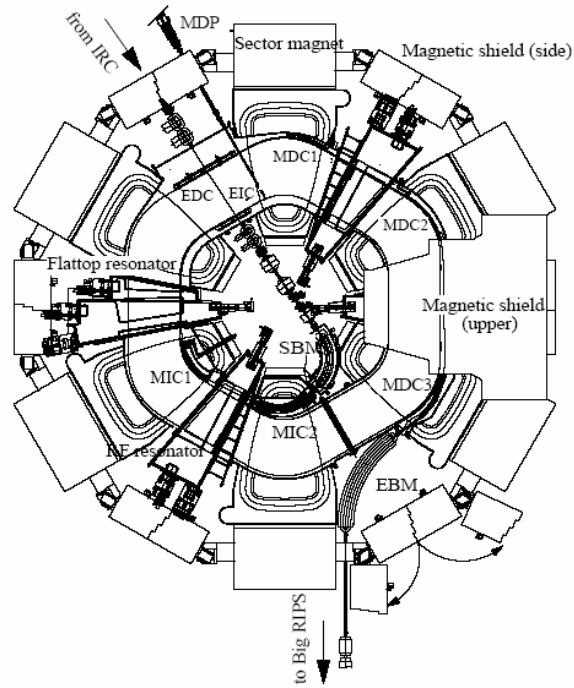


**Figure 8:** Layout of the SRC.



**Figure 9:** Photograph of the SRC under assembling in the vault. The control dewar for the liquid He vessel can be seen on the top of the central region of the cyclotron.

#### 4.5.3.6 *BigRIPS*

The BigRIPS is designed to be of a two-stage RI beam separation scheme as shown in Fig. 10. The first stage from the production target to the F2 focus comprises a two-bend achromatic spectrometer, consisting of four superconducting quadrupole triplets (STQs) and two room-temperature dipoles (RTDs). This first stage serves to produce and separate RI beams. The in-flight fission of a uranium beam as well as the projectile fragmentation of various heavy ion beams are used to produce RI beams. A wedge-shaped degrader is inserted at the momentum-dispersive focus F1 to make achromatic isotopic separation based on the so-called dispersion matching technique. A high-power beam dump is placed inside of the gap of the first dipole to stop 100 kW primary beams. Thick concrete blocks of about 9,000 t surround the first stage to shield neutron radiation from the target and beam dump. The second stage from the F3 focus to the F7 focus consists of eight STQs and four RTDs, comprising a four-bend achromatic spectrometer. Since our energy domain is not so high, the purity of RI beams is expected to be poor due to the nature of energy loss as well as the mixture of charge state. Several isotopes are mixed in an RI beam. To overcome this difficulty, the second stage is employed to identify RI-beam species (the atomic number, the mass-to-charge ratio and the momentum) in an event-by-event mode, making it possible to deliver tagged RI beams to experimental setups placed downstream of the BigRIPS.

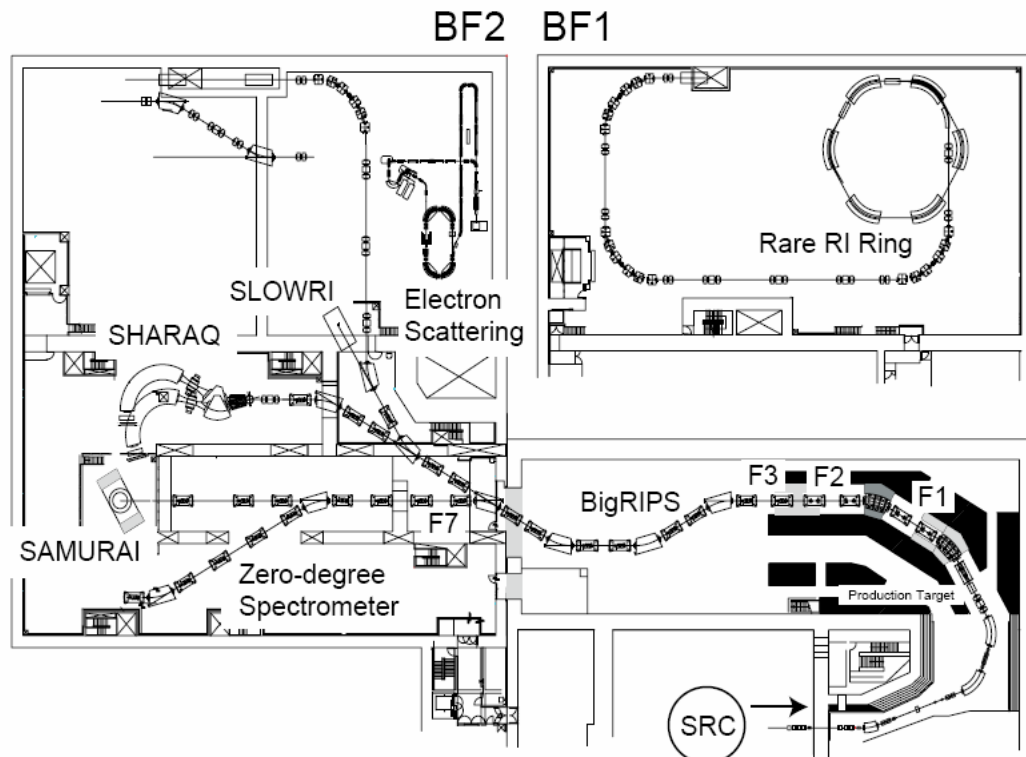


**Figure 10:** Layout of the BigRIPS and the major experimental installations planned in the second phase.

The angular acceptances of the BigRIPS are designed to be 80 mrad horizontally and 100 mrad vertically, while the momentum acceptance to be 6 %. The maximum

bending power is 9 Tm. The total length is 77 m. The angular and momentum spreads of fission fragments at 350 MeV/nucleon uranium ions are estimated to be about 100 mrad and 10 %, respectively. The acceptances of BigRIPS are comparable to those values, allowing one to achieve high collection efficiency for the in-flight fission fragments: almost half of the produced fission fragments may be accepted. These high acceptances are made possible by the use of superconducting quadrupoles with large apertures and room-temperature dipoles with large gaps.

The beam-line spectrometer called the zero-degree spectrometer will be constructed in the first phase. This spectrometer is specified for inclusive and semi-exclusive measurements equipped with gamma detectors around secondary targets.

#### 4.5.3.7 Expansion of the nuclear world in the RIBF: estimation

The expected yields of RI beam have been estimated assuming the primary beam current and energy of 1  $\mu\text{A}$  and 350 MeV/nucleon, respectively. The EPAX2 has been employed to obtain the production yields of unstable nuclei of interest, taking into account the BigRIPS angular- and momentum- acceptances.

The region on the nuclear chart where the production rate exceeding 1 particle/day, which will be enough to confirm the existence, can be obtained is indicated in Fig. 11 for the projectile fragmentation of appropriate stable nuclei and the in-flight fission of a uranium beam.

The expected intensity of doubly magic nuclei  $^{78}\text{Ni}$  is found to be 10 particles/sec, which enables the detailed internal structure studies of this intriguing nucleus.

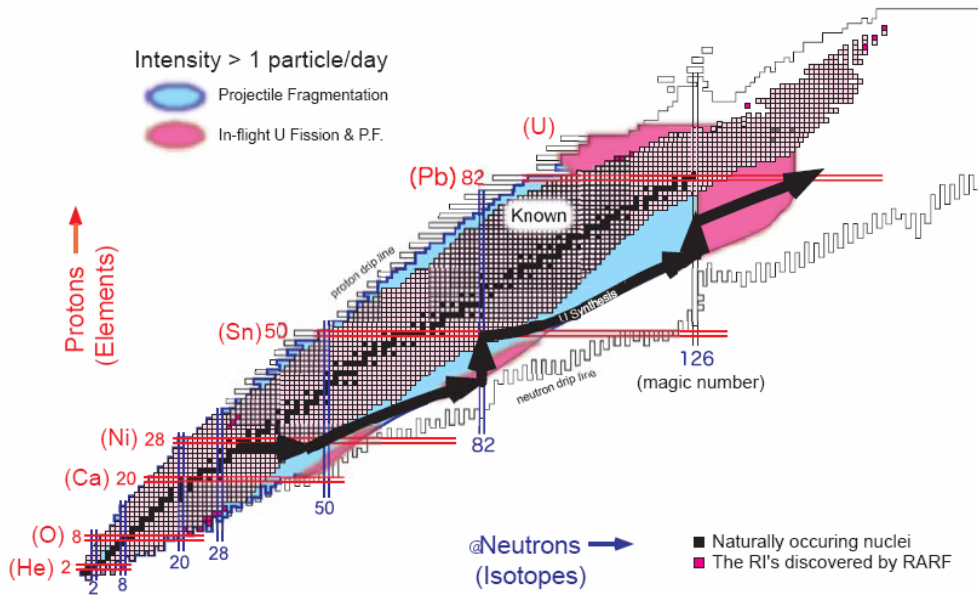


**Figure 11:** Great expansion of the nuclear world on the nuclear chart by the RIBF. The new region to be expanded will cover the hypothetical pathway to uranium synthesis in the supernova explosion.

#### 4.5.3.8 Experimental installations in the Phase II

Various experimental installations are planned as shown in Fig. 10.

The large-acceptance multi particle spectrometer (SAMURAI) is proposed. The main part of the spectrometer system is a large-gap superconducting magnet with bending power of 7 Tm for momentum analysis of heavy projectile fragments and projectile-rapidity protons with large angular and momentum acceptance. The large gap also enables measurements of projectile-rapidity neutrons with large angular acceptance in coincidence with heavy projectile fragments.

The high-resolution RI-beam spectrometer (SHARAQ) with momentum resolution of 15,000 is proposed.

The slow RI-beam facility (SLOWRI) is proposed aiming to provide universal slow or trapped RI of high purity by combining the BigRIPS and a gas-catcher system utilizing the so-called rf ion-guide technique. This will allow a unique opportunity to perform precision atomic spectroscopy for a wide variety of RI's, not available in so far existing facilities worldwide.

The new system of electron scattering experiment for unstable nuclei using the SCRTI is proposed. The SCRIT (Self-Confining Radioactive Ion Target) is the trapped-ion cloud formed at local position in an electron storage ring. Ions are three-dimensionally confined in the transverse potential well produced by the projectile electron beam itself and additionally applied longitudinal mirror potential. RI ions are injected into the potential well from outside. Therefore we need slow RI ion source like an ISOL. In our numerical calculation, the luminosity of e-RI collision is achievable to be more than  $10^{28} \text{ s}^{-1}\text{cm}^{-2}$ , which is enough to determine the charge distribution of unstable nuclei.

The new precision mass measurement system (Rare RI ring) consisting of individual injection and a precisely tuned isochronous ring is proposed for energetic rare RI beams. In the scheme, we measure a time-of-flight of a particle in the ring and its velocity before injected into the ring (on the long transport line) by combining individual injection. The accuracy of the mass measurement can be achieved at the order of  $10^{-6}$  for the momentum acceptance of the order of  $10^{-2}$ . Individual injection also allows us to identify the mass-measured RI particles event-by-event.

The recent great success of the discovery of the new super heavy element (SHE),  $^{278}_{113}$  using the RILAC, the CSM and the GARIS strongly encourages us to further pursue the heavier SHE search and to more extensively study nuclear physical and chemical properties of the SHEs. This compels us to provide a longer machine time for these experiments. However, this SHE research and the RIBF research are incompatible with each other, because both of these two researches use the RILAC. Thus, we propose to construct a new additional injector linac to the RRC which is planned to place in the RRC vault. The new injector will be used exclusively to produce the 350 MeV/nucleon primary beams (It is operated at the fixed frequency like the fRC.) This linac will make it possible to concurrently conduct the SHE and the RIBF researches.

#### 4.5.4 Summary

The world-top-class radioactive-isotope-beam (RIB) facility, which is called "RI beam factory (RIBF)", is under construction at RIKEN. This facility is based on the so-called "in-flight RI beam separation" scheme. Commissioning of a new high-power heavy-ion booster system consisting of a cascade of three ring cyclotrons with K=570 MeV (fixed frequency, fRC), 980 MeV (intermediate stage, IRC) and 2500 MeV (superconducting, SRC), respectively, is scheduled for late in 2006. This new ring-

cyclotron cascade system boosts energies of the output beams from the existing K540-MeV ring cyclotron up to 440 MeV/nucleon for light ions and 350 MeV/nucleon for very heavy ions. These energetic heavy-ion beams are converted into intense RI beams via the projectile fragmentation of stable ions or in-flight fission of uranium ions by a superconducting isotope separator, BigRIPS. The combination of the SRC and the BigRIPS will expand our nuclear world into presently unreachable region. Major experimental installations are under priority discussion as the second-phase program of the RIBF project. Construction of the second phase is expected to start in 2006.

#### 4.5.5 References

1. M. Kase *et al.*, "Present Status of the RIKEN Ring Cyclotron", proceedings of the 17th Int. Conf. on Cyclotrons and Their Applications, Yoyogi, Tokyo (2004).
2. O. Kamigaito *et al.*, "Upgrade of RILAC Injector", *ibid.*
3. S. Kohara *et al.*, Nucl. Instrum. Methods Phys. Rev. A526 (2004) 230.
4. T. Kubo *et al.*, Nucl. Instrum. Methods Phys. Rev. B70 (1992) 309.
5. N. Inabe *et al.*, "Fixed-Frequency Ring Cyclotron (fRC) in RIBF", proceedings of the 17th Int. Conf. on Cyclotrons and Their Applications, Yoyogi, Tokyo (2004);  
13. T. Mitsumoto *et al.*, "Construction of the fRC Sector Magnet for RIKEN RI Beam Factory", *ibid.*
6. J. Ohnishi *et al.*, "Construction Status of the RIKEN Intermediate-Stage Ring Cyclotron (IRC)", *ibid.*
7. H. Okuno *et al.*, "Magnets for the RIKEN Superconducting Ring Cyclotron", *ibid.*
8. T. Kubo, Nucl. Instrum. Methods Phys. Rev. B204 (2003) 97.
9. Reports on RIKEN RI Beam Factory Project for RIBF International Advisory Committee 2004, to be published.
10. T. Nakagawa *et al.*, "Intense Heavy Ion Beam Production from RIKEN ECRIS", proceedings of the 17th Int. Conf. on Cyclotrons and Their Applications, Yoyogi, Tokyo (2004).
11. O. Kamigaito *et al.*, "Construction of a variable-frequency quadrupole linac for the RIKEN heavy-ion linac", Rev. Sci. Instrum. 70, 4523 (1999).
12. O. Kamigaito *et al.*, "Construction of a booster linac for the RIKEN heavy-ion linac", Rev. Sci. Instrum. 76, 013306-1-11 (2005).
13. K. Morita *et al.*, J. Phys. Soc. Jpn. 73 (2004) 2593.
14. N. Fukunishi *et al.*, "Beam Quality Studies on RIKEN Ring Cyclotron and RI Beam Factory", proceedings of the 17th Int. Conf. on Cyclotrons and Their Applications, Yoyogi, Tokyo (2004).
15. H. Hasebe *et al.*, "Long-lived Carbon Stripper Foils for Intense Heavy-ion Beams", *ibid.*;  
14. H. Ryuto *et al.*, "Rotating carbon Disk Stripper for Intense Heavy-ion Beams", *ibid.*
16. H. Ryuto *et al.*, "Charge Stripping Plan of the RIKEN RI-beam factory", *ibid.*

## 5 Polarization

### 5.1 Polarized Beam Acceleration in COSY and Future Options for Polarization at HESR

A. Lehrach, [Forschungszentrum Jülich](http://www.fz-juelich.de)  
 mail to: [a.lehrach@fz-juelich.de](mailto:a.lehrach@fz-juelich.de)

#### 5.1.1 Introduction

Spin motion in an external electro-magnetic field of a circular accelerator is described by the so-called Thomas-BMT equation [1], resulting in a closed-orbit spin tune of  $\nu_{sp} = \gamma G$  for a transverse magnetic guiding field.  $G = (g-2)/2$  is the anomalous magnetic moment of the particle (e.g. 1.7928 for protons, 1.800(8) for antiprotons, and -0.1423 for deuterons), and  $\gamma = E/m$  the Lorentz factor. The closed-orbit spin tune specifies the number of spin precessions performed during one turn along the closed orbit (for amplitude dependent spin tune see [2]). During acceleration depolarizing spin resonances are crossed if the spin's precession frequency is equal to the frequency of encountered spin-perturbing magnetic fields. In a strong-focusing ring two different types of first-order spin resonances are excited, imperfection resonances caused by field errors and misalignments of the magnets, and intrinsic resonances excited by focusing magnetic fields. Imperfection resonances are crossed whenever the spin tune is an integer ( $\gamma G = k$ ,  $k$ : integer). The number of intrinsic resonances depends on the superperiodicity  $P$  of the lattice, given by the number of identical periods in the accelerator. One obtains for the resonance condition of intrinsic resonances\*  $\gamma G = kP \pm Q_y$ , where  $Q_y$  is the vertical betatron tune. The amount of depolarization (ratio of initial to final polarization) after uniformly crossing an isolated spin resonance is described by the Froissart-Stora formula [3].

Polarized beams have been accelerated to medium energies in several hadron machines, like the ZGS [4], SATURNE II [5], AGS [6], and KeK PS [7]. In the early days, the polarization was preserved by non-adiabatic methods: tune jumps at intrinsic resonances and harmonic orbit correction at imperfection resonances. Over the years, several novel schemes have been developed. Coherent betatron oscillations are excited by an RF dipole to adiabatically flip the spin without polarization losses at strong intrinsic resonances [8]. Partial snakes or correcting dipoles are routinely utilized to overcome imperfection resonances by exciting adiabatic spin-flips [9, 10]. Ya.S. Derbenev and A.M. Kondratenko introduced the concept of Siberian snakes to overcome spin resonances in circular accelerators [11], experimentally proved at IUCF [12]. The spin is rotated by  $180^\circ$  around a horizontal axis in the snake per turn around the ring, forcing the spin tune to be a half integer, independent of beam energy. First-order spin resonances are not crossed. Siberian snakes are the essential part of RHIC to preserve polarization during acceleration [13].

In this article the status of the polarized beams acceleration at the Cooler Synchrotron COSY in Jülich is described and future options for polarized beams at the

---

\*In this equation the amplitude dependent spin tune is approximated by  $\gamma G$ .

High-Energy Storage Ring HESR of the Facility for Antiproton and Ion Research FAIR at GSI Darmstadt are discussed.

### 5.1.2 Cooler Synchrotron COSY

The COSY cooler synchrotron and storage ring accelerates polarized and unpolarized proton (deuteron) beams in the momentum range from 300 (600) MeV/c to 3.7 GeV/c (see Fig. 1) [14]. The COSY accelerator complex includes H<sup>-</sup>/D<sup>-</sup> sources and the cyclotron JULIC for pre-acceleration. The negative charged ions are injected via charge exchange into the COSY ring. The Low-Energy polarimeter monitors the beam polarization before injection to ensure stable operation of ion source and cyclotron. The main diagnostics tool for polarization development in COSY is the EDDA detector [15], primarily designed to measure the pp-scattering excitation function. The polarization is determined by measuring the asymmetry of scattering between the circulating COSY beam and carbon or CH<sub>2</sub>-fiber targets.

COSY's lattice has a racetrack design, consisting of two 180° arc sections connected by straight sections. The total length of the ring is 183.47 m. The betatron tunes are ranging from 3.55 to 3.7 in routine operation. The straight sections can be tuned as telescopes with  $2\pi$  betatron phase advance. The super periodicity of the lattice can be adjusted to  $P = 2$  or  $6$ . Usually a  $P = 6$  optics is applied at injection and changed to  $P = 2$  during acceleration to avoid crossing the transition energy. However, due to symmetry-breaking installations (e.g. ANKE spectrometer and electron-cooler magnets) the super period of the lattice in COSY is reduced to  $P = 1$ .

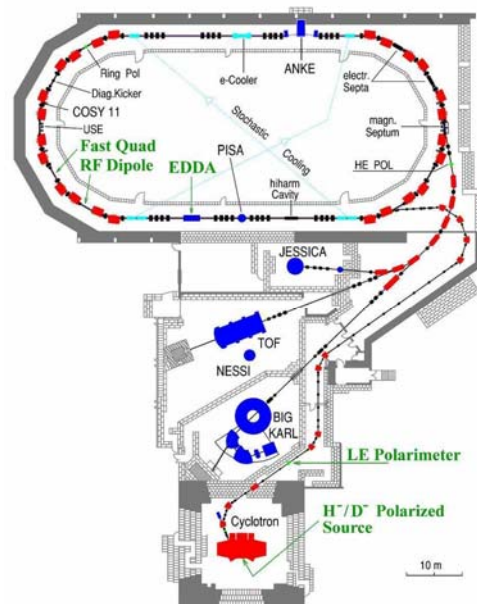


**Figure 1:** COSY accelerator complex including ion sources and cyclotron. Also shown are the Low-Energy (LE) polarimeter and the EDDA detector, RF dipole and tune-jump quadrupole.

### 5.1.2.1 Spin Resonances

First-order spin resonances for protons are listed in Table 1. Five imperfection resonances are crossed in the momentum range of COSY. Simulations indicate that an excitation of the vertical orbit with existing correction dipoles by  $1\text{ mrad}$  is sufficient to adiabatically flip the spin at all imperfection resonances. In addition, the solenoids of the electron-cooler system inside COSY are available for use as a partial snake. A rotation angle of less than  $1^\circ$  of the spin around the longitudinal axis already leads to a spin-flip without polarization losses at the existing imperfection resonances. In case of intrinsic resonances the resonance condition is given by  $\gamma G = kP \pm (Q_y - 2)$  for  $2\pi$  betatron phase advance in the straight sections [16]. Five intrinsic resonances have to be crossed for superperiodicity  $P = 2$ . Additional intrinsic resonances are excited for superperiodicity  $P = 1$ :  $\gamma G = -1 + Q_y$  ( $992.4\text{ MeV}/c$ ),  $7 - Q_y$  ( $1505.3\text{ MeV}/c$ ),  $1 + Q_y$  ( $2222.0\text{ MeV}/c$ ),  $9 - Q_y$  ( $2659.4\text{ MeV}/c$ ),  $3 + Q_y$  ( $3328.6\text{ MeV}/c$ ).

**Table 1:** Imperfection and intrinsic resonances for protons at COSY. Intrinsic resonances are listed for a vertical tune of  $Q_y = 3.61$  and different superperiodicities  $P$ .

P	$\gamma G$	Kin. Energy / MeV	Momentum / MeV/c
	2	108.4	463.8
2	6- $Q_y$	312.4	826.9
	3	631.8	1258.7
2	0+ $Q_y$	950.7	1639.3
	4	1155.1	1871.2
2,6	8- $Q_y$	1358.8	2096.5
	5	1678.5	2442.6
2	2+ $Q_y$	1997.1	2781.2
	6	2201.8	2996.4
2	10- $Q_y$	2405.2	3208.9

A tune-jump system was developed to preserve polarization at intrinsic resonances [17]. It consists of a pulsed air-core quadrupole, designed to reduce polarization losses to less than 5% at the strongest intrinsic resonance, and less than 1% at all other intrinsic resonances in COSY. To meet this goal, a vertical tune jump of more than  $\Delta Q_y = 0.06$  in  $10\ \mu\text{s}$  was specified.

For deuterons the spin tune is about 25 times lower than for protons at the same energy and therefore spin resonances are 25 times further apart from each other [18]. No first-order spin resonance is crossed in the momentum range of COSY at an ordinary betatron tune below 3.7. The polarized source at COSY is designed to provide a sequence of vector and tensor polarized beams [19], to be selected by the user out of the variety of possible combinations.

### 5.1.2.2 Polarized Beam Acceleration

In recent years, vertically polarized proton beams have routinely been accelerated and delivered to internal as well as external experiments at different momenta with polarization above 80% at COSY. Provisions to preserve polarization during acceleration are shown in the left plot of Fig. 2. The spin is flipped at imperfection resonances by exiting the vertical closed orbit using correction dipoles. To avoid polarization losses at intrinsic resonance tune jumps were applied.

The measured polarization after optimization for polarized beam is shown in the right plot of Fig. 2. Some polarization losses have been observed at the coupling resonance  $\gamma G = 8 - Q_x$ . By separating the two transverse tunes, the polarization losses could significantly be reduced. More than  $10^{10}$  polarized protons have been stored at final momentum.

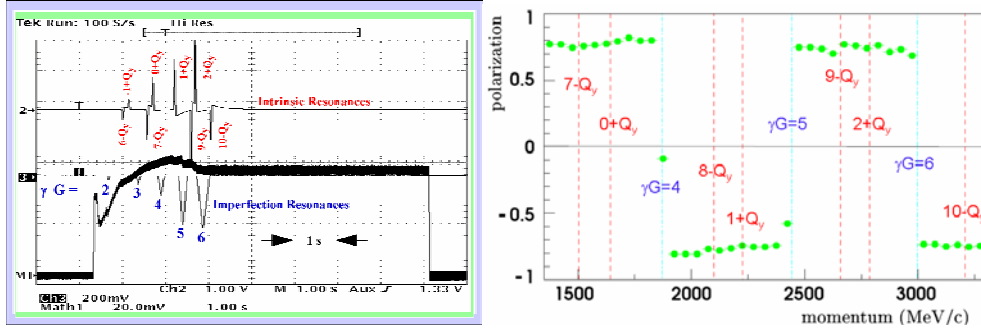


**Figure 2:** Left plot: Provisions to preserve polarization during acceleration. Trace 1 shows the beam current, trace 2 the current of vertical correction dipoles, and trace 3 the current of the tune-jump system versus time, applied at various spin resonances. Right plot: Vertical beam polarization during acceleration measured with the EDDA detector in the momentum range between 1100 MeV/c and 3300 MeV/c.

Up to 70% of deuteron polarization has been reached without additional provisions.

### 5.1.2.3 Spin Manipulation

Spin manipulation studies of vertical polarized protons, vector and tensor polarized deuterons, and investigations of higher-order resonances were carried out by the international SPIN@COSY collaboration [20]. A remarkably high measured proton spin-flip efficiency of  $99.92 \pm 0.04\%$  was achieved by using a strong ferrite-core water-cooled RF dipole, which provides a magnetic field of  $0.54 \pm 0.03$  T-mm (rms) at 916 kHz. For polarized deuterons a high spin-flip efficiency of  $97 \pm 1\%$  was measured, and the dynamics of tensor polarization was studied in detail. The striking behavior of the spin-1 tensor polarization during spin-flips recently found at IUCF was confirmed [21]. For higher-order spin resonance studies, a well-elaborated procedure to move betatron tunes during the COSY cycle was developed and applied. As expected, a total spin-flip was observed at the strong first-order intrinsic spin resonance  $\gamma G = 8 - Q_y$ . Third-order spin resonances were measured to be much stronger than the second-order spin resonance for our conditions.

## 5.1.3 High-Energy Storage Ring HESR

The High-Energy Storage Ring HESR is dedicated to Strong Interaction studies with antiprotons in the momentum range from 1.5 to 15 GeV/c (see Fig. 3.). The total length of the ring is about 574 m. According to the Conceptual Design Report and Technical Report [22] the HESR is a storage ring for one internal interaction point, equipped with the PANDA detector [23]. The antiproton beam is accelerated in SIS100 to the desired energy before being injected and stored in the HESR. Recently, a synchrotron mode was added [24], transferring 3.8 GeV/c antiprotons directly from the

accumulator rings to the HESR. This allows to accelerate polarized beams in the HESR with a ramping rate of about  $25 \text{ mT/s}$ .

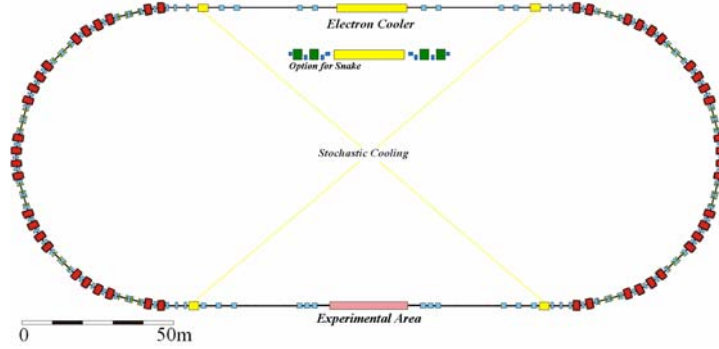


**Figure 3:** Schematic view of the HESR with a six-fold symmetry lattice in the arcs. Tentative positions for beam cooling devices, Siberian snake and experimental installations are indicated.

#### 5.1.3.1 Polarized Antiprotons

The PAX collaboration [25] proposed a method to prepare intense beams of polarized antiprotons. Polarized antiprotons can be produced in a storage ring by spin-dependent interaction in a pure hydrogen gas target. The polarizing process is based on spin transfer from the polarized electrons of the target atoms to the orbiting antiprotons in a dedicated large acceptance Antiproton-Polarizer Ring (APR) [26, 27]. Spin Filtering has been established experimentally at the Test Storage Ring (MPI Heidelberg) in 1992 [28] and by the subsequent theoretical analysis [29]. The beam lifetime in the APR can be expressed as function of the Coulomb-Loss cross section and the total hadronic proton-antiproton cross section. A polarized atomic beam is injected into a storage cell, located in a low-beta section. The diameter of the beam tube of the storage cell should match the ring acceptance angle at the target. As discussed in [26], the magnitude of the antiproton beam polarization depends on the acceptance angle of the ring. The optimum beam energies for different acceptance angles at which the polarization build-up works best can be obtained from the maximum figure of merit (FOM) of the polarized antiproton beam:  $FOM = P^2 \cdot N \cdot f_{rev}$ , where  $P$  denotes the beam polarization,  $N$  the number of particles stored in the APR and  $f_{rev}$  the revolution frequency. To perform spin-physics experiments in antiproton-proton interactions, the polarized beam would have to be accelerated and stored in the HESR [30].

#### 5.1.3.2 Spin Resonances

Due to the PANDA dipole chicane and the electron-cooler magnets the super periodicity of the HESR lattice is reduced to  $P = 1$ . In total 25 imperfection resonances and 50 intrinsic resonances would have to be crossed during acceleration (see Table 2). The strength of the resonances depends on the orbit excursions for imperfection resonances and focusing structure of the lattice and beam emittance for intrinsic resonances and is ranging from  $10^{-2}$  to  $10^{-6}$  for the expected beam parameter. Due to phase-space coupling introduced by the 15 Tm solenoid of the electron-cooler also strong coupling spin resonances are excited. The large number of resonances in the

HESR makes it very hard to apply techniques of single spin resonances correction. Siberian snakes seem to be to only option to guarantee a setup with low polarization losses during acceleration and deceleration.

**Table 2:** Imperfection and intrinsic resonances for a vertical tune of  $Q_y = 12.14$

P	$\gamma G$	Kin. Energy / GeV	Momentum / GeV/c
1,2	$16 - Q_y$	1.082	1.789
	4	1.155	1.871
1,2	$-8 + Q_y$	1.228	1.953
1	$17 - Q_y$	1.605	2.364
	5	1.678	2.443
1	$-7 + Q_y$	1.752	2.521
1,2,6	$18 - Q_y$	2.129	2.920
	6	2.202	2.997
	...		
1	$15 + Q_y$	13.265	14.172
1,2	$40 - Q_y$	13.642	14.550
	28	13.715	14.624
1,2	$16 + Q_y$	13.789	14.697

### 5.1.3.3 Siberian Snake

In the HESR momentum range it is difficult use a RHIC-type helical dipole snake [31] due to large orbit excursions. The maximum orbit excursion would be larger than  $25\text{cm}$  at the lowest momentum of the HESR (see left of Fig. 4). Therefore a magnet system with a combination of helical and solenoidal fields was investigated, consisting of four RHIC-type helical dipole magnets with a maximum field of  $2.5\text{ T}$  and a  $15\text{ Tm}$  solenoid (see middle plot in Fig. 4) [30]. If the snake magnets are ramped, this system provides a full spin-flip in the whole momentum range by keeping the maximum closed orbit excursion below  $5\text{ cm}$  (see left plot of Fig 4).

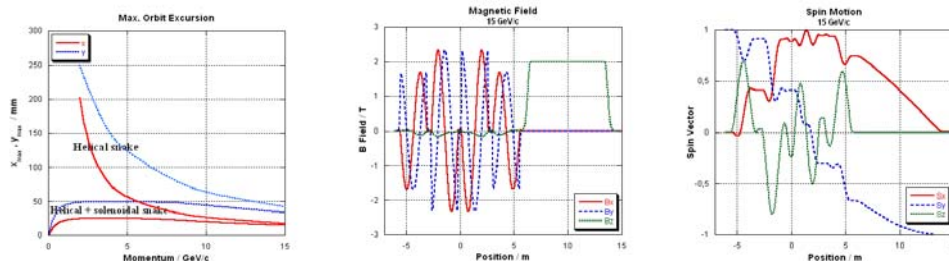


**Figure 4:** Maximum closed orbit distortions (left), magnetic field distribution (middle), and spin motion (right) for a Siberian snake with combined magnetic fields.

The spin motion at  $15\text{ GeV}/c$  is shown in the right plot of Fig. 4. Spin rotation induced by the DC electron-cooler solenoid at any possible field level can be compensated by the rampable  $15\text{ Tm}$  snake solenoid, if snake and electron-cooler are installed in the same straight section. A scheme to compensate phase-space coupling introduced by the snake and electron-cooler magnets has to be worked out. The most

serious drawback of a combined field scheme is large orbit excursion inside the helical dipoles, which could be a major restriction for the beam quality in the HESR.

Y. Shatunov proposed a second scheme for the HESR, which contains four additional solenoids grouped on either side of the DC electron-cooler solenoid (see Fig. 5), providing a maximum integrated solenoidal field strength of  $60 Tm$  [32].

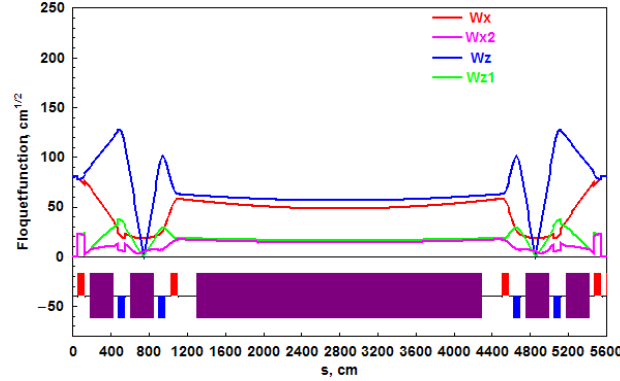


**Figure 5:** Eigen modes of the optical functions and magnet arrangement of the solenoidal Siberian snake. In purple the solenoid of the electron-cooler (middle) and snake solenoids are shown, red and blue bars indicate the position of skew quadrupoles.

To compensate phase-space coupling introduced by the solenoids, two groups of four skew quadrupole magnets are needed. The rotation angles of the quadrupoles have to be adjusted for different solenoid fields of the electron-cooler and beam momenta. Since the rotation angles of the skew quadrupoles are only slightly changing with momentum by less than  $0.1 rad$ , the field rotation can be arranged by superimposing two set of coils, applying a regular gradient coil and a  $45^\circ$  rotated one with separate power supplies. The whole magnet insertion provides a betatron phase advance of  $\pi$  and  $2\pi$  in the two transverse planes and has a total length of  $56 m$ . It fits into the existing HESR lattice. Compared to the combined snake it has the great advantage, that this snake arrangement does not excite large orbit excursion and lattice perturbation.

#### 5.1.4 Conclusion and Outlook

The solenoids of the electron-cooler, acting as a partial snake, and vertical correction dipoles are successfully applied at COSY to overcome imperfection resonances by exciting adiabatic spin-flips. For intrinsic resonances a tune-jump system has been developed and is suitable to handle all intrinsic resonances. Highly polarized proton and deuteron beams are routinely delivered to internal and external experiments at different momenta at COSY.

Due to the large number of spin resonances, a Siberian snake is proposed to preserve polarization during acceleration in the HESR. Two different schemes have been investigated. The snake arrangement with combined fields causes large orbit excursions. The solenoidal snake fits into the HESR lattice and fulfills all requirements in terms of beam and spin dynamics, but requires an integral solenoid field of  $60 Tm$ . Rampability of the super-conducting snake magnets has to be insured in both cases.

The PAX collaboration is aiming for Proton-Antiproton Scattering Experiments with Polarization at FAIR. Different experimental stages are proposed, where major

milestones of the project can be reached before the final goal is approached: a polarized proton–antiproton asymmetric collider [25].

### 5.1.5 Acknowledgement

The author would like to acknowledge the work of all members of the COSY team, SPIN@COSY collaboration, HESR consortium, and PAX collaboration. I'm also very grateful to R. Maier, D. Prasuhn, B. Lorentz, H. Stockhorst, F. Rathmann, A.D. Krisch, Yu.M. Shatunov, D.B. Barber, M. Bai, A.U. Luccio, and T. Roser for valuable suggestions and fruitful discussions on spin dynamics in circular accelerators.

### 5.1.6 References

1. L.H. Thomas, *Phil. Mag.* 3, 1 (1927); V. Bargmann, L. Michel, V.L. Telegdi, *Phys. Rev. Lett.* 2, 435 (1959).
2. D.P. Barber, G.H. Hoffstätter, M. Vogt, *AIP Conf. Proc.* 570, 751 (2001); D.P. Barber, J.A. Ellison, K. Heinemann, *Phys. Rev. ST Accel. Beams* 7, 124002 (2004).
3. M.Froissart, R.Stora, *Nucl. Inst. and Meth.* 7, 297 (1960).
4. T. Khoe et al., *Part. Accel.* 6, 213 (1975).
5. J.L. Laclare et al., *Jour. de Phys. Tome 46 No. 2*, 499 (1985).
6. F.Z. Khiari et al., *Phys. Rev. D* 39, 45(1989).
7. H. Sato et al., *Nucl. Inst. and Meth. A* 272, 617 (1988); KEK Report 87-22 (1987).
8. M. Bai et al., *Phys. Rev. Lett.* 80, 4673 (1998).
9. H. Huang et al., *Phys. Rev. Lett.* 73, 2982 (1994).
10. A. Lehrach et al., *Acceleration of the Polarized Proton Beam in the Cooler Synchrotron COSY*, Proc. of the Particle Accelerator Conference PAC99, New York, 2292 (1999).
11. Ya.S. Derbenev, A.M. Kondratenko, *Part. Accel.* 8, 115 (1978); Ya.S. Derbenev, A.M. Kondratenko, *Sov. Phys. JETP* 37 (6), 968 (1973).
12. A.D. Krisch et al., *Phys. Rev. Lett.* 63, 1137 (1989); B.B. Blinov et al., *Phys. Rev. Lett.* 73, 1621 (1994).
13. I. Alekseev et al., *Nucl. Inst. and Meth. A* 499, 392 (2003); K. Brown et al., *Conceptual design for the acceleration of polarized protons in RHIC*, technical report, RHIC (1995).
14. R. Maier, *Nucl. Inst. and Meth. A* 390, 1 (1997); H. Stockhorst et al., *Progress and Developments at the Cooler Synchrotron COSY*, Proc. of the 8th European Part. Acc. Conf. EPAC 2002, Paris, 629 (2002).
15. M. Altmeier et al. (EDDA Collaboration), *Phys. Rev. Lett.* 85, 1819 (2000).
16. A. Lehrach et al., *AIP Conf. Proc.* 675, 153 (2003); A. Lehrach, R. Gebel, R. Maier, D. Prasuhn, H. Stockhorst, *Nucl. Inst. and Meth. A* 439, 26 (2000).
17. A. Lehrach, PhD thesis, Jül-3501 (Bericht des Forschungszentrums Jülich), ISSN 0944-2952 (1998).
18. J.S. Bell J.S., CERN yellow reports 75-11; H. Huang, S.Y. Lee, L. Ratner, Proc. of the Part. Acc. Conf. PAC 1993, Washington, 432 (1993).
19. P.D. Eversheim et al., *AIP Conf. Proc.* 339, 668 (1994), R. Weidmann et al., *Rev. Sci. Ins.* 67, 2 (1996).
20. V.S. Morozov et al., *Phys. Rev. ST Accel. Beams* 7, 024002 (2004); M.A. Leonova et al., *Phys. Rev. Lett.* 93, 224801 (2004); V.S. Morozov et al., *Phys. Rev. ST Accel. Beams* 8, 061001 (2005).
21. V.S. Morozov et al., *Phys. Rev. Lett.* 91, 214801 (2003).
22. An International Accelerator Facility for Beams of Ions and Antiprotons, *Conceptual Design Report*, GSI Darmstadt, November 2001, see <http://www.gsi.de/GSI-Future/cdr/>;

- FAIR Project, Technical Report, submitted to the international FAIR project committees, January 2005, to be published.
23. Strong Interaction Studies with Antiprotons, Letter-of-Intent, PANDA collaboration, January 2004, see <http://www.gsi.de/documents/DOC-2004-Jan-115-1.pdf>.
  24. Meeting on Concepts for the HESR, GSI Darmstadt, March 31<sup>st</sup> to April 1<sup>st</sup> 2005, minutes unpublished.
  25. Antiproton-Proton Scattering Experiments with Polarization, Technical Report, PAX collaboration, May 2005, see <http://www.fz-juelich.de/ikp/pax/>.
  26. F. Rathmann, P. Lenisa, E. Steffens, M. Contalbrigo, P.F. Dalpiaz, A. Kacharava, A. Lehrach, B. Lorentz, R. Maier, D. Prasuhn, H. Stroeher, Phys. Rev. Lett. 94, 014801 (2005).
  27. A. Lehrach, S. Martin, F. Rathmann, P. Lenisa, I.N. Meshkov, A. Sidorin, A. Smirnov, C. Montag, E. Steffens, C. Wiedner, A Method to Polarize Stored Antiprotons to a High Degree, Proc. of the Particle Accelerator Conference, Knoxville, TN (2005).
  28. F. Rathmann et al., Phys. Rev. Lett. 71, 1379 (1993).
  29. C. J. Horowitz and H. O. Meyer, Phys. Rev. Lett. 72 (1994) 3981; H. O. Meyer, Phys. Rev. E 50, 1485 (1994).
  30. A. Lehrach, I. Koop, A.U. Luccio, R. Maier, A. Otbojev, D. Prasuhn, Yu.M. Shatunov, Polarized beams in the high-energy storage ring of the future GSI project, Proc. of the 16th International Spin Physics Symposium, SPIN2004, Trieste, Italy (2004).
  31. see <http://www.agsrhichome.bnl.gov/RHIC/Spin>.
  32. Y. Shatunov, Siberian Snake at HESR, internal report (2005), unpublished.

## 5.2 Spin polarisation at DESY

D.P. Barber, E. Gianfelice-Wendt\* and M. Vogt  
 DESY, Notkestrasse 85, 22607 Hamburg, Germany  
 mail to: [mpybar@mail.desy.de](mailto:mpybar@mail.desy.de)

### 5.2.1 Introduction

The attainment and handling of spin polarisation of electron and positron beams has a long tradition at DESY. In this article we give an overview of polarisation in HERA and of some other recent typical activities.

### 5.2.2 Longitudinally polarised electron and positron beams in HERA

#### 5.2.2.1 Generalities and HERA-I

In HERA, the 6.3 km electron(positron)-proton double ring collider at DESY in Hamburg, Germany, the proton and electron(positron) beams are accelerated to 920 GeV and 27.5 GeV respectively and collide head—on at the IP's North and South, where the experiments H1 and ZEUS are located. The internal gas target experiment HERMES joined the collider experiments in 1994.

An integral part of the original HERA design (HERA-I) was the provision of longitudinally spin polarised electron(positron) beams for the collider experiments and we succeeded: the HERA electron(positron) ring is the first and only high energy

---

\* Now at Fermi National Accelerator Laboratory, Batavia, Illinois, U.S.A.

electron(positron) storage ring to provide longitudinal polarization, and, moreover, at three collision points

The electrons (positrons) become spin polarized through the emission of synchrotron radiation (the Sokolov-Ternov effect [1]). The polarization direction is given by the periodic solution, of the Thomas-BMT equation for the spin on the closed orbit, and it is vertical in a perfectly planar ring with no solenoids. The periodic spin solution is rotated into the longitudinal direction at the experiments by special magnet insertions (“spin rotators”) which, at HERA, make use of radial fields [2]. The ring is therefore no longer planar everywhere. In a ring where, by design, the periodic spin solution is not everywhere vertical and/or there is, by design, vertical dispersion, stochastic photon emission causes the single particle spins to diffuse away from the periodic solution with a consequent decrease of polarization. This source of spin diffusion is partially neutralized in “spin matched” optics [1]. Spin diffusion is also caused when the tilt of the periodic spin solution and the vertical dispersion are non-zero due to the unavoidable magnet misalignments and field errors [1]. As predicted by simulations, for HERA a tilt of some tens of mrad leads to very large depolarization. Thus in addition to the usual orbit correction, a dedicated minimization of the tilt is needed. At HERA this is realized empirically by minimizing the most important Fourier components of the tilt by means of vertical orbit bumps (“harmonic bumps” [3]) on the basis of polarization measurements. Spin diffusion is particularly strong when the spin tune on the closed orbit (the number of precessions around periodic solution per revolution) is near resonance with the orbital motion. In HERA at 27.5 GeV it is about 62.5. The lowest order resonances are the strongest.

Finally, in a collider like HERA, the interaction with the counter-rotating proton beam is also expected to be a source of depolarization. The proton bunches act as non-linear lenses causing a shift and a spread of the electron (positron) tunes. In addition the fields of the proton bunches directly perturb the orbital and spin motion of the electrons (positrons) thereby disturbing the spin matching. The orbital tunes are chosen so as to optimize the polarization. Due to the large beam-beam tune spreads it can happen that the tunes of the pilot bunches (i.e. the few non-colliding bunches used for the background correction of the luminosity measurement) then lie on a spin-orbit resonance. This explains the apparently surprising observation that the polarization of the pilot bunches is sometimes lower than the polarization of the colliding ones, in spite of the fact that they are not subject to the beam-beam force.

After high transverse polarization was demonstrated at HERA, the HERMES experiment was installed at the East interaction point during the 1993-1994 shut down together with a pair of spin rotators around that IP to provide the experiment with longitudinally polarized electrons (positrons) [3]. The spin helicity can be inverted at the IP by inverting the directions of the radial fields of the rotator magnets. Until August 2000, careful machine tuning (orbit, energy, orbital tunes) allowed high (between 50 and 70 percent) longitudinal electron and positron polarization to be delivered to HERMES, as well as luminosity for H1 and ZEUS. The steadily increasing strength of the beam-beam interaction [4] could also be handled.

### 5.2.2.2 *HERA-II*

Then, in response to the wish for higher luminosity, between September 2000 and July 2001, the North and South interaction regions (IR) were rebuilt [5]. With this new design the luminosity was increased by a factor of about 2.5-3. The opportunity was

also taken to install two more pairs of spin rotators so that H1 and Zeus could also, at long last, benefit from longitudinal polarization. Thus HERA-II was born.

The insertion of the two extra pairs of spin rotators, was expected to decrease the maximum attainable level of Sokolov-Ternov polarization from 89 to 83 percent and to introduce further potential depolarization. However, the latter was not expected to be serious with the original layout of the IR's. But now, the modifications needed for the increased luminosity meant that some measures that had been taken to ensure high polarization for HERA-I had to be unraveled: optimization for the highest improvement in luminosity in HERA is not helpful for polarization.

The main concerns were the removal of the experiment anti-solenoids, the overlapping of the strong combined function magnet GO and the H1 solenoid field, the increased strength of the IR and arc quadrupoles resulting in a larger sensitivity to magnet misalignment, and the increased beam-beam interaction strength. With 140 mA of protons the incoherent horizontal and vertical beam-beam parameter per IP, were expected to increase w.r.t. year 2000 from 0.012 to 0.034 and from 0.029 to 0.052 respectively. These large values give not only a measure of the strength of the beam-beam force but clearly also set limits to the choice of the optimal tunes for polarization. After removal of the anti-solenoids, the insertion of the two more pairs of spin rotators was also necessary for the survival of polarization. The H1 solenoid, for example, would tilt an initially vertical polarization by about 86 mrad, thus destroying polarization. The GO/H1 solenoid field overlap leads to a small tilt of the periodic spin solution even in the presence of the rotator. In the current design the betatron coupling resulting from the solenoids is corrected by four independently powered skew quadrupoles per IP. Their strengths are trivially computed by requiring the off diagonal blocks of the transport matrix through the IR to vanish. Since the solenoids are relatively weak (7.6 Tm and 4.4 Tm for the H1 and Zeus solenoids respectively) their treatment as small perturbations is adequate. Because knowledge of these fields is not very accurate, orthogonal knobs for an empirical correction of the coupling were also provided [6] and proved to work well.

A detailed account of HERA-II and the polarization calculations for HERA-II is given in [6]. See [5] too. The expected polarization in the presence of full 3-D spin motion, computed by SITROS [7] is between 54 and 60 percent. This number does not include beam-beam effects, since the code could not deliver convincing results for the upgraded machine in the presence of the beam-beam interaction. But on the basis of the observations with HERA-I the maximum attainable polarization in the presence of the beam-beam interaction was estimated to be around 45-50 percent.

The first polarization studies with all three rotators running took place with positrons and without collisions, in March 2003. After optimizing the harmonic bumps the maximum longitudinal polarization attained (with experiment solenoids turned on) was 54 percent, close to expectations.

In the Summer of 2004 the longitudinal positron polarization delivered in the presence of collisions was around 40 percent, increasing to 50 percent towards the end of a run as the proton emittance increased. More details can be found in [8].

### 5.2.2.3 *Recent developments*

In September 2004 we switched to running with electrons. Since the proton beam and the electron beam share magnets at H1 and Zeus, in HERA-II this required a realignment of the magnets and the detectors and a consequent running-in period before

the machine could realize its full potential. But then, after high luminosity was re-established difficulties were encountered with attaining high polarization. This was traced to the effect on the orbital tunes of the beam-beam force. With positrons, the beam-beam force defocuses the beam and in addition the positron tunes spread to lower values than the nominal tunes. But with electrons the beam-beam force focuses the beam and the electron tunes spread to values higher than the nominal tunes. If the fractional part of the closed orbit spin tune is close enough to  $\frac{1}{2}$ , then moving the orbital tunes towards the nearest integer increases the distance from (strong) low order spin-orbit resonances and thus generally improves the polarization. Our standard working point has nominal tunes slightly above the integer (about 0.12 and 0.2 in the horizontal and vertical plane respectively). With typical beam—beam tune shift parameters of 0.04 to 0.06 horizontally and 0.06 to 0.09 vertically the effect on the equilibrium polarization of the colliding bunches is significant. In standard operation and with a well tuned machine the polarization of the pilot bunches quickly increases to above 50 percent while the polarization of the colliding bunches typically reaches 30 percent in the first hour and then slowly increases while the beam-beam effect decreases due to the growing proton emittances. The difference between the early polarizations of the colliding and the pilot bunches is strongly correlated with the initial proton intensities.

To roughly quantify the relative effect of tune shift compared to residual nonlinear effects due to the beam-beam lens, we measured the coherent beam-beam tune shift at the end of a regular run, estimated the incoherent tune shift, dumped the proton beam and then moved the nominal tunes to values corresponding to the central tunes with collisions. After attaining equilibrium the polarization was almost exactly equal to the polarization with collisions. We therefore concluded that, at least for moderate strength of the beam-beam parameter (at the end of a run) the major effect on polarization is in fact the tune shift.

Thus during June 2005 we operated HERA-e with so-called mirror tunes, i.e. the working point was shifted from slightly above to slightly below the integer. With mirror tunes the positive beam-beam tune shift moves the tunes in the cores of the electron bunches closer towards the integer thereby moving the colliding bunches away from low order spin-orbit resonances and promising higher polarization. After executing all standard procedures for the new working point and after carefully optimizing the polarization we indeed achieved higher polarization of the colliding bunches already early in the run. Polarizations of 40 percent to 45 percent could easily be achieved with the colliding bunches – and with most aggressive tuning even 50 percent. However, when the tunes were optimized for polarization the specific luminosity was significantly reduced, while with mirror tunes optimized for maximum luminosity the improvement of polarization was marginal. Part of the reason is that electron-proton collisions with mirror tunes are to some extent very similar to positron/proton collisions with standard tunes. For example the dynamic beta-beat is proportional to the beam-beam tune shift parameter but also to the reciprocal of the sine of the phase advance over one turn. In fact while HERA delivers peak luminosities of  $2.2 \times 10^{30}$  Hz/cm<sup>2</sup>/mA<sup>2</sup> in electron-proton operation with standard tunes, the peak luminosities achieved with mirror tunes were between  $1.5$  and  $1.8 \times 10^{30}$  Hz/cm<sup>2</sup>/mA<sup>2</sup> which are comparable to the luminosities achieved with positrons at standard tunes. In addition the luminosity-lifetime was reduced in mirror tune operation. Thus it was decided to give priority to getting the highest possible integrated luminosity by moving the working point back to standard tunes. However, the June 2005 operation of HERA showed that in principle,

when the conditions are optimized for polarization, HERA-II can deliver high longitudinal electron polarization at three interaction points in the presence of strong beam-beam forces.

### 5.2.3 A new spin-orbit tracking code, SLICKTRACK

As a result of earlier experience with the effects of the beam-beam force we had decided to upgrade our software for simulating depolarization. This led to the code SLICKTRACK.

First estimates of attainable equilibrium polarization are usually made with computer codes of the SLIM family [1]. However, such codes only predict the strengths of the first order spin-orbit resonances. The best way to estimate the effects of higher order resonances, including the effects of nonlinear orbit motion and beam—beam forces, is to simulate the effects of stochastic photon emission in a Monte-Carlo (M-C) spin-orbit tracking code which operates on a large ensemble of particles and includes the full 3-D spin motion. Analytical methods [1] lack the required power and generality. Therefore, a new M-C algorithm has been implemented in the code SLICKTRACK, an extended version of SLICK, the thick lens version of SLIM [1]. The M-C approach was pioneered in the early 1980's in the code SITROS [7, 1] but with SLICKTRACK, advantage has been taken of the subsequent huge increase in available computer power and of experience, to create a new, much simpler software architecture. This in turn facilitates detailed investigation of the depolarization process and of the effect of lack of spin transparency of sections of the ring under the heading: “diagnostics”, so that the potential for unreliable results is minimized. Analytical methods give some useful insights but the M-C algorithm employs much simpler mathematics than analytical algorithms and it is therefore much less susceptible to errors. The M-C algorithm is also subject to fewer assumptions and is more flexible. For example, it is easy to include strong beam-beam forces.

SLICKTRACK is already in service for HERA. It is also in service for eRHIC [9] and of course it provides a powerful general tool for studying (de)polarization in any electron (positron) ring. Thus it will be used also for checking depolarization in the damping rings of the ILC.

### 5.2.4 The invariant spin field and spin tunes

Apart from the practical matters surrounding attaining high longitudinal electron (positron) polarization in HERA, we continue to work on various aspects of theoretical spin dynamics. Thus, for example, we have devoted effort to understanding and systematizing the concept of spin tune on integrable syncho-betatron orbits and the conditions for its existence. In particular we have introduced the concepts of well-tuned and ill-tuned tori as a way of classifying the spectra of spin motion. This work [10] was done in collaboration with J.A. Ellison of the University of New Mexico. The bibliography in [10] contains a list of typical papers on theoretical work at DESY including reference to our extensive studies of the feasibility of attaining high proton polarization at 920 GeV in HERA. For the latter see [11, 12] too.

As another example from our studies we point to our finding that in the simple mathematical model used in the discussion of the so-called “snake resonances” [13] which can occur in rings with Siberian Snakes, the invariant spin field is irreducibly

discontinuous at the vertical orbital tunes at which the snake “resonances” occur [14]. As a consequence it is clear that although such models gave the first warning of the problems caused by snake “resonances” [13], they probably have limited applicability for calculation of the invariant spin field in real rings. Then, the invariant spin field should be calculated using stroboscopic averaging [15] with a realistic description of the ring and the orbital motion.

### 5.2.5 References

1. D.P. Barber and G. Ripken, in Handbook of Accelerator Physics and Engineering, Eds. A.W. Chao and M. Tigner, World Scientific, 2nd edition 155-167 (2002).
2. D.P. Barber et al., Phys. Lett., B343, 436-443 {1995}.
3. D.P. Barber et al., Nucl. Inst. Meth., A338, 166-184 {1994}.
4. E. Gianfelice, in Polarised protons at high energies, DESY-PROC-1999-03, 77-91 (1999).
5. M. Seidel and F. Willeke, EPAC'00, Vienna, June 2000.
6. G.Z.M. Berglund, “Spin-orbit maps and electron spin dynamics for the luminosity upgrade project at HERA”, DESY-THESIS-2001-044 (2001).
7. J.Kewisch, Ph.D. Thesis, University of Hamburg, DESY 85-109 (1985).
8. E. Gianfelice-Wendt et al., EPAC'04, Lucerne, July 2004.
9. eRHIC Zeroth-Order Design Report. Eds. M. Farkhondeh and V.Ptitsyn, BNL Report C-A/AP/142 (2004).
10. D.P. Barber, J.A. Ellison and K. Heinemann, Phys. Rev. ST Accel. Beams 7(12), 124002 (2004).
11. M. Vogt, Ph.D. Thesis, University of Hamburg, DESY-THESIS-2000-054 (2000).
12. G.H. Hoffstaetter, “A modern view of high energy polarized proton beams”. To be published as a Springer Tract in Modern Physics.
13. S.Y. Lee, “Spin Dynamics and Snakes in Synchrotrons”, World Scientific (1997).
14. D.P. Barber, R. Jaganathan and M. Vogt, e-print physics/0502121.
15. K. Heinemann and G.H. Hoffstaetter, Phys. Rev. E 54(4), 4240 (1996).

## 5.3 Polarized proton acceleration at RHIC

M. Bai, W. Fischer, T. Roser  
BNL, Collider Accelerator Department, Upton, NY 11973  
mail to: [mbai@bnl.gov](mailto:mbai@bnl.gov)

### 5.3.1 Introduction

The Relativistic Heavy Ion Collider (RHIC) is a high energy collider designed to provide not only collisions of heavy ions but also of polarized protons. Table 1 lists the RHIC machine parameters for polarized protons [1].

**Table 1:** Latest machine parameters for p-p collisions.

Parameter	Unit	p-p
relativistic $\gamma$ , injection	...	25.9
relativistic $\gamma$ , store	...	266.5
no of bunches, $n_b$	...	112
ions per bunch, $N_b$	$10^{11}$	2.0
emittance $\epsilon_{N,x,y}$ 95%	mm·mrad	20
luminosity	$\text{cm}^{-2}\text{s}^{-1} 10^{30}$	150
polarization,store	...	70%

Fig. 1 shows the polarized proton accelerating chain. The polarized  $H^-$  ion beam from the Optical Pumped Polarized Ion Source (OPPIS) gets accelerated up to a kinetic energy of 200 MeV in the LINAC, and then injected into the Booster through a striping foil. The Booster then accelerates the polarized proton beam to a total energy of 2.35 GeV and injects the beam into the Brookhaven AGS where beam is accelerated to 24.3 GeV.

The acceleration of polarized H- in LINAC is spin transparent. There are a total of 2 imperfection spin resonances in the Booster from its injection energy to the extraction energy. They are overcome by correcting the individual harmonics of the vertical orbit distortion. No intrinsic spin resonance is encountered during the acceleration because the vertical betatron tune in Booster is set at 4.8 just above the spin precession tune at the Booster extraction energy.

The polarized proton acceleration in the AGS encounters a total of 41 imperfection resonances and seven intrinsic resonances [2]. A 5% helical partial snake is employed to overcome all the imperfection spin resonances [3,4,5], and an rf dipole which kicks the beam at a frequency near the vertical betatron frequency is used to induce a full spin flip through the four strong intrinsic spin resonances at  $G\gamma = 0 + Q_y$ ,  $G\gamma = 12 + Q_y$  and  $G\gamma = 36 \pm Q_y$  [6]. Here,  $G$  is the anomalous g-factor,  $\gamma$  is the Lorentz factor and  $Q_y$  is the vertical betatron tune. In a circular accelerator, the spin precession tune is  $G\gamma$  [2].

In RHIC, two full Siberian snakes are placed  $180^\circ$  apart from each other in either of the two rings to keep the spin precession tune at 0.5 so that neither imperfection resonances nor intrinsic resonances are encountered during the acceleration [1]. The Siberian snakes have worked successfully. With the proper setting of snakes and the careful control of betatron tune and closed orbit during the energy ramp, no polarization loss was observed from RHIC injection energy to 100 GeV.

The two pairs of spin rotators on either side of STAR and PHENIX also allow one to independently orient the beam polarization longitudinally at the experiments [1].



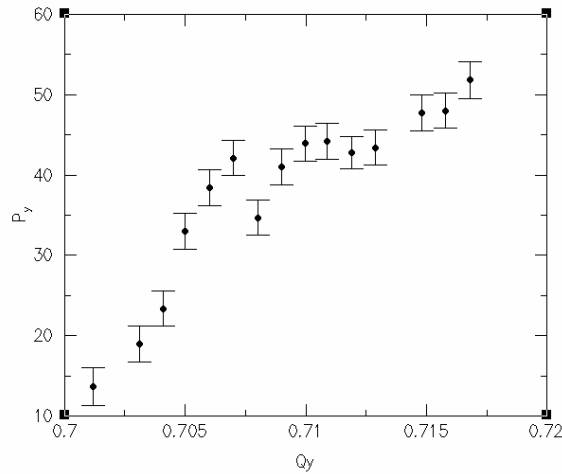


**Figure 2:** snake resonance at  $Q_y = 0.7$

To avoid snake resonances, it is very critical to have both the vertical orbit distortion as well as the betatron working point under control. Currently, the RHIC polarized proton's working point is set at (0.72, 0.73) through the entire energy ramp up to an energy of 100 GeV.

With the current RHIC BPM (Beam Position Monitor) system, an rms value of 0.5 mm vertical orbit distortion has been achieved. To preserve the polarization beyond 100 GeV, the vertical orbit distortion needs to be controlled within 0.3 mm. A realignment of the whole ring is scheduled during the summer shutdown of 2005.

### 5.3.2.2 Luminosity

Currently, the polarized proton luminosity in RHIC is limited by the beam-beam interaction [8] as well as achievable bunch intensity from the AGS in order to maintain the maximum polarization. Three possible working points were carefully studied during the RHIC polarized proton run in 2004 and a working point at (0.695, 0.685) was chosen which optimized beam-beam effect as well as had the best polarization performance [8].

In the past, RHIC also experienced a limitation on the total beam intensity due to the dynamic pressure rise. For the RHIC 2006 run, more NEG coated piped will be installed. Upgrades of the RHIC CNI polarimeters will also improve the local vacuum pressure rise. With the new 25% super-conducting partial Siberian snake in the AGS, it is expected that the beam polarization dependence on the bunch intensity will be removed. To minimize the beam-beam effects, our current plan is to reduce the non-linearities of the triplets as well as other sources. Reducing the non-linear chromaticity should also help to mitigate the beam-beam effect. A 10 Hz vibration of the beam orbit is also observed in RHIC [9] and a feedback system to compensate the 10 Hz vibration of the local orbit at the collision point has been tested and is now being implemented for the two interaction regions [10].

### 5.3.3 RHIC performance

The polarized proton beam acceleration in RHIC was first started in 2000. Table 2 lists the milestones of the RHIC polarized proton development over the past years.

The RHIC polarized proton beam run in 2000 was dedicated to prove the principle of Siberian snake with only one snake installed in the RHIC Blue ring. Since the AGS stable spin direction is vertical and the RHIC stable spin direction with only one full snake lies in the horizontal plane, the polarized proton beam was injected with the snake off. The snake was then adiabatically turned on in order to preserve the beam polarization. A non-zero radial polarization was then measured and confirmed that the snake was working properly.

**Table 2:** RHIC spin program milestone

	Milestone
2000	<ul style="list-style-type: none"> <li>- New polarized proton source(OPPIS) commissioned</li> <li>- One snake was installed in the sector 9 in Blue ring.</li> <li>- CNI polarimeter in Blue installed and commissioned</li> </ul>
2002	<ul style="list-style-type: none"> <li>- All snakes for both rings installed and commissioned</li> <li>- CNI polarimeter in Yellow installed and commissioned</li> </ul>
2003	<ul style="list-style-type: none"> <li>- Spin rotators installed and commissioned</li> <li>- provided longitudinal polarizations at STAR and PHENIX for physics data taking</li> </ul>
2004	<ul style="list-style-type: none"> <li>- RHIC absolute polarimeter using Hydrogen Jet target installed and commissioned</li> <li>- AGS 5% helical warm snake installed and commissioned</li> <li>- RHIC new working point was commissioned</li> </ul>
2005	<ul style="list-style-type: none"> <li>- New superconducting solenoid was installed in the polarized source OPPIS</li> <li>- AGS helical cold snake was installed and commissioning was started</li> <li>- Polarized proton beam in RHIC was accelerated to 205 GeV with 30% polarization measured at this energy</li> </ul>

The RHIC polarized proton run in 2003 showed that the luminosity performance was limited by the beam-beam effect. In order to mitigate the beam-beam effect, couple of new working points were investigated and commissioned during the RHIC 2004 run.

With the 300 m of NEG coated pipes installed during the summer shut-down time of 2004, the RHIC 2005 polarized proton run achieved a total of 106 bunches per ring with  $0.9 \times 10^{11}$  protons per bunch. The improvement of the online model as well as the RHIC BPM system also improved the polarization transmission efficiency.

During the RHIC 2005 polarized proton run, polarized proton beam was also first accelerated to 205 GeV. A polarization of 30% was measured in both rings at 205 GeV with a measured polarization of 50% at injection. The polarization measurement during the energy ramp confirms that the polarization loss occurred beyond 100 GeV.

Table 3 shows the achieved performance of RHIC during the past polarized proton runs.

**Table 3:** RHIC achieved performance

Parameter	Unit	2002	2003	2004	2005
No. Of bunches	...	55	55	56	106
protons/per bunch	$10^{11}$	0.7	0.7	0.7	0.9
store energy	GeV	100.2	100.2	100.2	100.2
$\beta^*$	m	1	1	1	1
peak luminosity	$10^{30} \text{cm}^{-2} \text{s}^{-1}$	2	6	6	10
average luminosity		1.5	3	4	6
Time in store	%	30	41	38	56
average polarization, at store	%	15	35	46	47

### 5.3.4 Acknowledgement

The authors would like to thank both RHIC and AGS shift leaders as well as the operation team of the Collider Accelerator department. The authors would also like to thank all the personnel who are involved in the RHIC polarized proton operations.

### 5.3.5 References

1. RHIC Spin Design Manual
2. S. Y. Lee, Spin Dynamics, World Scientific, Singapore, 1997.
3. T. Roser, Properties of Partially Excited Siberian Snake, in High Energy Spin Physics: 8th International Symposium, ed. K. J. Heller, Minneapolis, 1988, AIP Conference Proceedings No. 187(AIP, New York,1989), p.1442.
4. H. Huang, et al., The Partial Siberian Snake Experiment at the Brookhaven AGS, Proceedings of the third European Particle Accelerator Conference, p.729 (1992).
5. Junpei Takano et al, Optimization of AGS Polarized Proton Operation with the Warm Helical Snake, proceedings of Particle Accelerator Conference, Knoxville, TN (2005)
6. M. Bai, et al., Overcoming Intrinsic Spin Resonance by Using an AC Dipole, in 1997 IEEE Particle Accelerator Conference and International Conference on High-Energy Accelerators, Vancouver, May, 1997.
7. S. Y. Lee and S. Tepikian, Resonance due to a Local Spin Rotator in High-Energy Accelerators, Physical Review Letters, 1635 Vol. 56, Num. 16, 1986.
8. W. Fischer, M. Blaskiewicz, J.M. Brennan, P. Cameron, R. Connolly, C. Montag, S. Peggs, F. Pilat, V. Ptitsyn, S. Tepikian, D. Trbojevic, and J. van Zeijts, "Observation of Strong-Strong and Other Beam-Beam Effects in RHIC", proceedings of the 2003 Particle Accelerator Conference, Portland, Oregon (2003).
9. R. Toma, et al, Quest for a New Working Point in RHIC, proceedings of the 2004 European Particle Accelerator Conference, Lucerne, Switzerland (2004).
10. C. Montag, et al, Helium Flow Induced Orbit Jitter at RHIC, proceedings of Particle Accelerator Conference, Knoxville, TN (2005)
11. C. Montag, et al, Fast IR orbit feedback at RHIC, proceedings of Particle Accelerator Conference, Knoxville, TN (2005)

## 6 Activity Reports

### 6.1 Beam-Beam Collisions with an Arbitrary Crossing Angle: Analytical tune shifts, tracking algorithm without Lorentz boost, Crab-Crossing

D.N. Shatilov, BINP and M. Zobov, INFN-LNF

Mail to: [D.N.Shatilov@inp.nsk.su](mailto:D.N.Shatilov@inp.nsk.su)

#### 6.1.1 Introduction

The beam-beam collision with a finite crossing angle has become a reality since the DAΦNE [1] and KEKB [2] colliders were put in operation. Nowadays, designs or/and upgrade options for a number of colliders and particle factories are based on lattices having a crossing angle (see, for example, [3, 4]). Recently new innovative schemes were proposed, such as crab-crossing for KEKB [5] and very large crossing angle for DAΦNE-II [6]. Hence it is clear that the beam physics related to the crossing angle has become critically important. In this paper we would like to continue discussing these questions, already raised in ICFA Beam Dynamics Letter 34 by Y.Cai [7]. Actually, the Introduction given in [7] can be applied to our paper as well, so we decided not to repeat it here. As compared to [7], we derived the final formulae for 3D Gaussian beams which can be directly used in estimates and simulations of beam-beam collisions with a crossing angle and that can be easily generalized on a Crab-Crossing scheme of collision. Initially we were focused on the analytical expressions for the beam-beam tune shifts with arbitrary crossing angles. These expressions were obtained in 2003 (see [8,9]) and partially checked with simulations. The full implementation of arbitrary crossing angle in the simulation code was performed by the end of 2003, that allowed us to complete the comparison for large crossing angles. Actually, this paper is a joining of [9] (that is a generalization of [8]) and a detailed explanation of the tracking algorithm without Lorentz boost. These two parts are closely connected, use the same notations, and crosscheck each other, so we decided to present them together as a whole.

#### 6.1.2 Beam-beam tune shift formulae

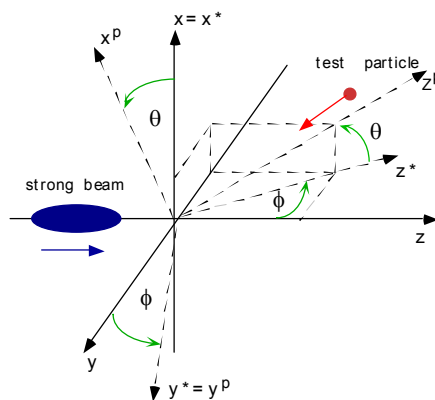


Figure 1: Scheme of beam-beam collision under a crossing angle.

Let us consider two ultra relativistic bunches colliding at an arbitrary angle, as shown in Fig. 1. The strong beam moves along z-axis of the right laboratory coordinate system. The coordinate system connected with the test particles of the weak beam is denoted with the index 'p' in Fig. 1. The coordinate transformations between the two systems are obtained, first, by a rotation of the strong bunch coordinate system by the angle  $\phi$  around x-axis and, second, by a rotation of the resulting system  $x^*-y^*-z^*$  around  $y^*$ -axis by the angle  $\theta$ .

The coordinate transformations from one system to the other are as follows:

$$\begin{aligned}
 x &= x^p \cos(\theta) + z^p \sin(\theta) \\
 y &= y^p \cos(\phi) - (z^p \cos(\theta) - x^p \sin(\theta)) \sin(\phi) \\
 z &= y^p \sin(\phi) + (z^p \cos(\theta) - x^p \sin(\theta)) \cos(\phi) \\
 \text{and} \\
 x^p &= x \cos(\theta) - (z \cos(\phi) - y \sin(\phi)) \sin(\theta) \\
 y^p &= y \cos(\phi) + z \sin(\phi) \\
 z^p &= (z \cos(\phi) - y \sin(\phi)) \cos(\theta) + x \sin(\theta)
 \end{aligned} \tag{1}$$

In the laboratory system components of the electromagnetic field, created by a 3D Gaussian bunch (strong bunch) moving with a velocity  $\sim c$  is given by [10]:

$$\begin{aligned}
 E_x &= \frac{eN\gamma}{2\pi^{3/2}\epsilon_0} x \int_0^\infty dw \frac{\exp\left\{-\frac{x^2}{(2\sigma_x^2+w)} - \frac{y^2}{(2\sigma_y^2+w)} - \frac{\gamma^2(z-ct)^2}{(2\gamma^2\sigma_z^2+w)}\right\}}{(2\sigma_x^2+w)^{3/2} \sqrt{(2\sigma_y^2+w)(2\gamma^2\sigma_z^2+w)}} \\
 E_y &= \frac{eN\gamma}{2\pi^{3/2}\epsilon_0} y \int_0^\infty dw \frac{\exp\left\{-\frac{x^2}{(2\sigma_x^2+w)} - \frac{y^2}{(2\sigma_y^2+w)} - \frac{\gamma^2(z-ct)^2}{(2\gamma^2\sigma_z^2+w)}\right\}}{(2\sigma_y^2+w)^{3/2} \sqrt{(2\sigma_x^2+w)(2\gamma^2\sigma_z^2+w)}} \\
 B_x &= -\frac{E_y}{c} \\
 B_y &= \frac{E_x}{c}
 \end{aligned} \tag{2}$$

Equations of motion of a test particle belonging to the weak beam in this system are:

$$\begin{aligned}
 x(t) &= -c \sin(\theta)t + x_0 & v_x &= -c \sin(\theta) \\
 y(t) &= c \cos(\theta) \sin(\phi)t + y_0 & v_y &= c \cos(\theta) \sin(\phi) \\
 z(t) &= -c \cos(\theta) \cos(\phi)t + z_0 & v_z &= -c \cos(\theta) \cos(\phi)
 \end{aligned} \tag{3}$$

The Lorentz force acting on the test particle due to the electromagnetic fields produced by the strong beam:

$$\vec{F} = e(\vec{E} + \vec{v} \times \vec{B}) \quad \text{with} \quad \vec{v} \times \vec{B} = -v_z B_y \vec{i} + v_z B_x \vec{j} + (v_x B_y - v_y B_x) \vec{k} \quad (4)$$

has the following components:

$$\begin{aligned} F_x &= e(E_x - v_z B_y) = e(E_x + c \cos(\theta) \cos(\phi) B_y) = eE_x (1 + \cos(\theta) \cos(\phi)) \\ F_y &= e(E_y + v_z B_x) = e(E_y - c \cos(\theta) B_x) = eE_y (1 + \cos(\theta) \cos(\phi)) \\ F_z &= e(v_x B_y - v_y B_x) = e \left( -c \sin(\theta) \frac{E_x}{c} + c \cos(\theta) \sin(\phi) \frac{E_y}{c} \right) = e(E_y \cos(\theta) \sin(\phi) - E_x \sin(\theta)) \end{aligned} \quad (5)$$

The force projected onto the axes of the test particle coordinate system has:

$$\begin{aligned} F_x^p &= F_x \cos(\theta) + F_y \sin(\phi) \sin(\theta) - F_z \cos(\phi) \sin(\theta) = eE_x (\cos(\phi) + \cos(\theta)) + eE_y \sin(\theta) \sin(\phi) \\ F_y^p &= F_y \cos(\phi) + F_z \sin(\phi) = eE_y (\cos(\phi) + \cos(\theta)) - eE_x \sin(\theta) \sin(\phi) \end{aligned} \quad (6)$$

According to the tune shift definitions:

$$\begin{aligned} \xi_{x^p} &= \Delta Q_{x^p} = \frac{1}{4\pi} \int_{-\infty}^{+\infty} dz^p \beta_x \frac{\partial F_x^p(x(x^p, y^p, z^p), y(x^p, y^p, z^p), z(x^p, y^p, z^p)))}{\partial x^p} \Big|_{x^p=y^p=0} \\ \xi_{y^p} &= \Delta Q_{y^p} = \frac{1}{4\pi} \int_{-\infty}^{+\infty} dz^p \beta_y \frac{\partial F_y^p(x(x^p, y^p, z^p), y(x^p, y^p, z^p), z(x^p, y^p, z^p)))}{\partial y^p} \Big|_{x^p=y^p=0} \end{aligned} \quad (7)$$

Combining eqs. (1), (2) and (6), differentiating with respect to the transverse coordinate (eq. (7)) and integrating along  $z^p$ , one gets:

$$\begin{aligned} \xi_{x^p} &= \frac{r_e N \beta_x}{2\pi\gamma} \times \\ & \int_0^\infty dw \frac{\left\{ (\cos\theta + \cos\phi)^2 (1 + \cos\theta \cos\phi) (2\sigma_y^2 + w) + \sin^2\phi (1 + \cos\theta \cos\phi) (2\sigma_z^2 + \frac{w}{\gamma^2}) \right.}{\left. + \sin^2\theta \sin^2\phi (1 - \cos^2\theta \cos^2\phi) (2\sigma_x^2 + w) \right\}}{\left( (1 + \cos\theta \cos\phi)^2 (2\sigma_x^2 + w) (2\sigma_y^2 + w) + \cos^2\theta \sin^2\phi (2\sigma_x^2 + w) (2\sigma_z^2 + \frac{w}{\gamma^2}) + \sin^2\theta (2\sigma_y^2 + w) (2\sigma_z^2 + \frac{w}{\gamma^2}) \right)^{3/2}} \quad (8) \\ \xi_{y^p} &= \frac{r_e N \beta_y}{2\pi\gamma} \times \\ & \int_0^\infty dw \frac{\left\{ (\cos\theta + \cos\phi)^2 (1 + \cos\theta \cos\phi) (2\sigma_x^2 + w) + \sin^2\phi \sin^2\theta (1 + \cos\theta \cos\phi) (2\sigma_y^2 + w) \right.}{\left. + \sin^2\theta \cos\phi (\cos\phi + \cos\theta - \cos\theta \sin^2\phi) (2\sigma_z^2 + \frac{w}{\gamma^2}) \right\}}{\left( (1 + \cos\theta \cos\phi)^2 (2\sigma_x^2 + w) (2\sigma_y^2 + w) + \cos^2\theta \sin^2\phi (2\sigma_x^2 + w) (2\sigma_z^2 + \frac{w}{\gamma^2}) + \sin^2\theta (2\sigma_y^2 + w) (2\sigma_z^2 + \frac{w}{\gamma^2}) \right)^{3/2}} \end{aligned}$$

Note, that for combinations  $(\theta = 0; \phi = 0)$  and  $(\theta = \pi; \phi = \pi)$  the above expressions are reduced to the well know formulae for the head-on collision. Besides, for arbitrary  $\theta$  and  $\phi = 0$  eq. (8) reproduces the formulae (9) in [8] for the tune shifts with a horizontal crossing angle.

In case when  $\gamma \gg tg(\theta/2)$  we can neglect the term  $w/(\gamma^2 ctg^2(\theta))$  and for the case of a horizontal crossing angle ( $\phi = 0$ ) we obtain:

$$\begin{aligned}\xi_{x,p} &= \frac{r_e N}{2\pi\gamma} \frac{\beta_x}{\sqrt{(\sigma_z^2 tg^2(\theta/2) + \sigma_x^2)} \left( \sqrt{(\sigma_z^2 tg^2(\theta/2) + \sigma_x^2)} + \sigma_y \right)} \\ \xi_{y,p} &= \frac{r_e N}{2\pi\gamma} \frac{\beta_y}{\sigma_y \left( \sqrt{(\sigma_z^2 tg^2(\theta/2) + \sigma_x^2)} + \sigma_y \right)}\end{aligned}\quad (9)$$

Similarly, for the vertical crossing angle ( $\theta = 0$ ) we get:

$$\begin{aligned}\xi_{x,p} &= \frac{r_e N}{2\pi\gamma} \frac{\beta_x}{\sigma_x \left( \sqrt{(\sigma_z^2 tg^2(\phi/2) + \sigma_y^2)} + \sigma_x \right)} \\ \xi_{y,p} &= \frac{r_e N}{2\pi\gamma} \frac{\beta_y}{\sqrt{(\sigma_z^2 tg^2(\phi/2) + \sigma_y^2)} \left( \sqrt{(\sigma_z^2 tg^2(\phi/2) + \sigma_y^2)} + \sigma_x \right)}\end{aligned}\quad (10)$$

Considering the last expressions (8)-(9) and the luminosity formula given in [11]:

$$L = \frac{N^2}{4\pi\sigma_y \sqrt{(\sigma_z^2 tg^2(\theta/2) + \sigma_x^2)}}\quad (11)$$

We can see that both eqs. (9) and (11) can be obtained from similar formulae for the head-on collision by simply substituting:

$$\sigma_x \rightarrow \sqrt{(\sigma_z^2 tg^2(\theta/2) + \sigma_x^2)}\quad (12)$$

in case of collisions with a horizontal crossing angle and:

$$\sigma_y \rightarrow \sqrt{(\sigma_z^2 tg^2(\phi/2) + \sigma_y^2)}\quad (13)$$

for the collisions at a vertical angle.

### 6.1.3 Beam-beam interaction formulae for tracking

There is no need in sophisticated formulae in the case of small crossing angles. Indeed, after the test particle arrival to the Interaction Point (IP) we know its 6D coordinates. Then we simply add the crossing angles to the particle betatron angles ( $X'$  and  $Y'$ ) and can imagine that the particle belongs to the beam colliding with the strong bunch head-on. Now we can employ the well-known formulae for Beam-Beam Interaction [12, 13]. Despite the strong bunch has some longitudinal length and usually

is represented as a number of slices, after these transformations we again will have the particle at the nominal IP. Finally, we have to subtract the crossing angles from the particle coordinates  $X'$  and  $Y'$  in order to get the particle 6D coordinates in its own frame, and continue tracking through the machine lattice. Nevertheless, some authors of Beam-Beam codes (K. Hirata for BBC code) prefer to perform the transformation through IP in the special frame where the collision is head-on, even for small crossing angles, that requires Lorentz transformations [14]. It was shown in [15] that for small crossing angles both approaches are in good agreement. In fact, the crossing angles used in the older versions of beam-beam code LIFETRAC [16] were  $-\theta$  and  $\phi$ . In this case, for small crossing angles, the particle coordinates  $X'$  and  $Y'$  in the laboratory frame are just equal to the coordinates  $X$ ,  $Y$  in the “p” frame plus the corresponding crossing angles.

In this paper we consider the case of arbitrary crossing angles. Besides, the bunches can be rotated in crab-cavities in order to make the longitudinal axes of both colliding bunches co-parallel. For that, the crab angle should be equal to the minus half crossing angle. However, in general case we shall consider they are independent.

It is well known that in the ultra relativistic case the charged particle creates an electro-magnetic field only in the plane perpendicular to its velocity. In order to track the test particle through the charged “strong” bunch, the following approximation is used. The strong bunch is represented as a number of thin slices (pancakes), the plane of a slice must be perpendicular to its velocity. The test particle experiences a beam-beam kick when it crosses the slice’s plane. This is a “zero-time” interaction, which simplifies the transformation and makes it symplectic. The test particle interacts sequentially with all the slices, with a simple drift space transformation between them. Usually it is said that the strong bunch is divided by slices longitudinally. However, with a crab-crossing collision the slices are not perpendicular to the bunch’s longitudinal axis since it is not parallel to the bunch velocity.

We do not consider here the transformations through the crab-cavities, if any. For the test particle it is implemented by constant  $6 \times 6$  matrixes placed at the correct locations before and after IP. As for this paper, we assume that we know the 6D particle coordinates when it arrives to the nominal IP. Then, the beam-beam transformation is applied to the particle, after that it is tracked through the machine lattice, and so on. The only thing we shall consider concerning the crab-crossing – that is how it affects the strong bunch shape and distribution in the laboratory frame. It is important that the crab rotation is not equivalent to the normal rotation of the strong bunch as a solid body. Instead, it can be imagined as transverse shifts of the slices, where the shift value is proportional to the longitudinal slice coordinate. The particle transverse distributions within slices do not change after such transformation. It is convenient to define the crab angle by two angles in the polar coordinate system:  $\theta_{cr}$  is the total deflection angle and  $\phi_{cr}$  is the azimuth angle in XY plane. After the crab rotation the slice coordinates will be:

$$\begin{aligned}\Delta x &= z_0 \sin(\theta_{cr}) \cos(\phi_{cr}) \\ \Delta y &= z_0 \sin(\theta_{cr}) \sin(\phi_{cr}) \\ z_{cr} &= z_0 \cos(\theta_{cr})\end{aligned}\tag{14}$$

where  $Z_0$  and  $Z_{cr}$  are the longitudinal slice coordinates (with regard to the center of bunch) before and after the crab cavity,  $\Delta x$  and  $\Delta y$  are the transverse slice shifts.

### 6.1.3.1 Kick from a single slice

It is convenient to apply the beam-beam kick in the coordinate system connected with the strong bunch. So, first of all we have to find the test particle coordinates in this system using (1). However, the standard formulae for head-on collision cannot be directly used for large crossing angles. There are at least three factors, which must be considered. First, the contribution of magnetic field is not equal now to the electric one. Second, the “time-of-flight” factor, which can vary in a wide range depending on the crossing angle. And third, the particle energy  $dE/E$  cannot be more calculated in assumption that the transverse momentum is much smaller than the longitudinal one: for large crossing angles it can be comparable or even larger. Fortunately, for the transverse kicks the first two factors exactly compensate each other. Indeed, the Lorentz force acting on the test particle due to the electromagnetic fields produced by the strong slice has the following components (see eqs. 4,5):

$$\begin{aligned} F_x &= e(E_x - v_z B_y) = eE_x(1 - v_z/c) \\ F_y &= e(E_y + v_z B_x) = eE_y(1 - v_z/c) \\ F_z &= e(E_z + v_x B_y - v_y B_x) = e(E_z + E_x v_x/c + E_y v_y/c) \end{aligned} \quad (15)$$

The kick (momentum change) gained by the test particle is proportional to the product of the force and the time of interaction, which is inversely proportional to the relative longitudinal speed of the slice and the particle. Thus, in the case of Gaussian beams, for the transverse kicks we can simply use the Bassetti-Erskine formulae [13] written in assumption that  $|v_z| = c$ .

$$\frac{\Delta p_y}{p_0} = -\frac{Nr_e}{\gamma_0} \sqrt{\frac{2\pi}{\sigma_x^2 - \sigma_y^2}} \cdot \text{Re}(F(x,y)) \quad \frac{\Delta p_x}{p_0} = -\frac{Nr_e}{\gamma_0} \sqrt{\frac{2\pi}{\sigma_x^2 - \sigma_y^2}} \cdot \text{Im}(F(x,y)) \quad (16)$$

where  $p_0$  is the total momentum of the test particle,  $N$  is the number of electrons in the strong slice,  $r_e$  is the classical electron radius,  $\gamma_0$  is the relativistic factor of the test particle,  $\sigma_x$  and  $\sigma_y$  are the transverse sizes of the strong slice (it is assumed that  $\sigma_x > \sigma_y$ ), and the function  $F(x,y)$  is represented through the complex error function  $W(z)$  as follows:

$$F(x,y) = W\left(\frac{x + iy}{\sqrt{2(\sigma_x^2 - \sigma_y^2)}}\right) - e^{-\frac{x^2 + y^2}{2\sigma_x^2 + 2\sigma_y^2}} \cdot W\left(\frac{x \frac{\sigma_y}{\sigma_x} + iy \frac{\sigma_x}{\sigma_y}}{\sqrt{2(\sigma_x^2 - \sigma_y^2)}}\right) \quad (17)$$

Now let us consider the longitudinal kick. The part connected with the magnetic field and transverse velocities (see the third row of (15), last two terms in the parentheses) can be rewritten as follows:

$$\frac{\Delta p_{zB}}{p_0} = \frac{1}{1 - p_z/p_0} \left( \frac{\Delta p_x}{p_0} \cdot \frac{p_x + \Delta p_x/2}{p_0} + \frac{\Delta p_y}{p_0} \cdot \frac{p_y + \Delta p_y/2}{p_0} \right) \quad (18)$$

Since the change in the transverse momentum due to the interaction can be comparable with the initial one, we should use the “average transverse momentum during the interaction”. The change in the longitudinal momentum also can be comparable with the initial one (for example, if the crossing angle is  $90^\circ$ , so that  $v_z \approx 0$ ), but in any case it must be much smaller than the total momentum  $p_0$ , and we may neglect the change of  $p_z$  in the right-hand part of (18). The longitudinal electric field  $E_z$  is created by the space charge of the strong slice if the derivatives  $\partial\sigma/\partial s \neq 0$ . For the Gaussian beams, using the corresponding formulae from [14] we obtain the following expression for the electric part of the longitudinal kick (it is called  $\mathbf{g}$  in [14]):

$$\frac{\Delta p_{zE}}{p_0} = \frac{\left( x \cdot \frac{\Delta p_x}{p_0} + y \cdot \frac{\Delta p_y}{p_0} + \frac{2Nr_e}{\gamma_0} \right) \cdot \left( \frac{\partial\sigma_x^2}{\partial s} - \frac{\partial\sigma_y^2}{\partial s} \right) - \frac{2Nr_e}{\gamma_0} e^{-\frac{x^2+y^2}{2\sigma_x^2+2\sigma_y^2}} \cdot \left( \frac{\sigma_x}{\sigma_y} \frac{\partial\sigma_x^2}{\partial s} - \frac{\sigma_y}{\sigma_x} \frac{\partial\sigma_y^2}{\partial s} \right)}{2(1-p_z/p_0) \cdot (\sigma_x^2 - \sigma_y^2)} \quad (19)$$

The only difference with the head-on collision is the “time-of-flight” factor. Since the transverse momentum can be comparable or even larger than the longitudinal one, the energy change gained by the particle after the kick should be calculated by the formula:

$$\frac{\Delta E}{E_0} = \sqrt{\frac{(p_x + \Delta p_x)^2 + (p_y + \Delta p_y)^2 + (p_z + \Delta p_z)^2}{p_x^2 + p_y^2 + p_z^2}} - 1 \quad (20)$$

If the momentum change is much less than the initial one:  $\Delta p \ll p_0$ , that is usually the case, the energy change can be rewritten as:

$$\frac{\Delta E}{E_0} = \frac{\Delta p_x \cdot \left( p_x + \frac{\Delta p_x}{2} \right) + \Delta p_y \cdot \left( p_y + \frac{\Delta p_y}{2} \right) + \Delta p_z \cdot \left( p_z + \frac{\Delta p_z}{2} \right)}{p_0^2} \quad (21)$$

Let us consider, for example, the case without crossing angle:  $p_z = -p_0$  and the change in longitudinal momentum is much less than the transverse kick:  $\Delta p_z \ll \Delta p$ . Then, using (18) and (21), we obtain:

$$\frac{\Delta E}{E_0} \approx \frac{\Delta p_x \cdot \left( p_x + \frac{\Delta p_x}{2} \right) + \Delta p_y \cdot \left( p_y + \frac{\Delta p_y}{2} \right)}{2p_0^2} - \frac{\Delta p_{zE}}{p_0} \quad (22)$$

That is in agreement with equation (38) from [14].

### 6.1.3.2 Tracking algorithm

After all, we describe the algorithm of Beam-Beam Interaction implemented in the tracking code LIFETRAC. We start from the test particle arrival to the nominal IP and mark this moment as  $\tau_p$ , to distinguish it from  $\tau_0$  – the nominal collision time (when the centers of both colliding beams arrive to the IP). First of all, the transformation is made from the “p” to the laboratory coordinate system using (1), but with  $z^p = 0$ . It is important to note that  $z^p$  here is not the test particle’s longitudinal coordinate with

regard to the equilibrium particle of the weak beam, but the “p” azimuth of the point where the transformation is applied. The same transformation (1) is made for the particle velocities.

If there is a constant separation between the colliding beams (for example, at the Parasitic Crossings), the separation values are added to the particle coordinates X and Y. In the case of crab-crossing there is an additional transverse shift (14), which is individual for each slice. Besides, the strong bunch can be rotated in XY plane (a tilt) due to the betatron coupling. If any, the corresponding transformations are applied to the test particle 6D coordinates. Finally, we get the particle coordinates in the frame where the X- and Y-axes are parallel to the strong slice ellipse axes, and the Z-axis goes through the center of slice along its velocity.

The next step is to find the time interval between  $\tau_p$  and the collision time  $\tau_c$  (it can be negative!). The longitudinal slice coordinate at the moment  $\tau_p$  is  $z_s - s$ , where  $z_s$  is the longitudinal slice shift with regard to the center of the strong bunch, and  $s$  is the longitudinal particle coordinate with regard to the center of the weak bunch – the 5<sup>th</sup> component of the standard 6D particle coordinates in the “p” frame. The test particle’s longitudinal coordinate  $z$  at this moment is given by (1). So, we obtain:

$$\tau_c - \tau_p = \frac{z_s - s - z}{c \cdot (1 - p_z/p_0)} \quad (23)$$

where the numerator is the longitudinal distance between the slice and the particle at the time  $\tau_p$ , and the denominator is the longitudinal velocity of rapprochement. Now we can find the particle coordinates at the moment of collision.

To calculate the kicks by the formulae (16–19), we need to know the transverse sizes of the slice and the derivatives  $\partial\sigma/\partial s$ . These can be obtained from the lattice functions of the strong beam at the nominal IP and the longitudinal coordinate of Collision Point (CP). The next CP will be shifted by the value of longitudinal distance between the two sequential slices, divided by  $(1 - p_z/p_0)$ . The transformation between CP’s is a simple drift space, and then the kick from a slice is applied, and so on.

After the last slice passage, we may need to perform a transformation to the laboratory frame: back rotation in the XY plane (if there is a tilt of the strong bunch), and back transverse shifts (in the cases of crab-crossing and constant separation at the PC). Then the transformation from the laboratory to the particle frame is applied using (1). Finally, we need to shift the particle longitudinally to the nominal IP in the “p” frame – this is made as a simple drift space transformation.

#### 6.1.4 Comparison of analytical tune shifts with numerical simulations

In order to check the formulae (8) describing the general case of collisions with an arbitrary crossing angle we use numerical simulations with beam-beam code LIFETRAC. The betatron tunes in the presence of beam-beam effects are calculated by tracking in the following way. First of all a test particle is tracked for one turn with the initial conditions:

$$X_i = \delta(i,j)\sigma_j, \quad i = 1, 2, \dots, 6, \quad q \ll 1, \quad \delta(i,j) = \begin{cases} 0, & \text{if } i \neq j \\ 1, & \text{if } i = j \end{cases} \quad (24)$$

where  $X_i$  are the coordinates in the 6D phase space and  $\sigma_i$  are the respective rms sizes.

Doing this 6 times for  $j = 1, 2, \dots, 6$  we obtain the  $6 \times 6$  revolution matrix. Then, the matrix eigenvalues are calculated those give us the tunes. For these simulations we use a simple model of collider with linear transformations from IP to IP. In order to reproduce correctly the Gaussian longitudinal distribution we divide a strong bunch in much more longitudinal slices than in ordinary beam-beam simulations. Besides, the longitudinal rms bunch length is taken to be much shorter than the transverse beta functions at IP in order to satisfy approximations made to obtain eqs. (8). In these conditions the following equation is valid:

$$\cos(\mu) = \cos(\mu_0) - 2\pi\xi \sin(\mu_0) \quad (25)$$

where  $\mu_0$  is the initial betatron tune (transverse or vertical, without beam-beam), and  $\mu$  is the tune calculated by tracking. Thus, we can find the tune shift  $\xi$ .

First of all, we performed the comparison for rather small crossing angles, but sizeable Piwinski's angles. The following set of parameters was used: bunch length  $\sigma_L = 3$  cm, beta-functions at the IP  $\beta_x = 150$  cm,  $\beta_y = 20$  cm, emittances  $\varepsilon_x = 5 \cdot 10^{-5}$  cm-rad,  $\varepsilon_y = 10^{-7}$  cm-rad. Figures 2 (a) and (b) show the normalised horizontal and vertical tune shifts calculated analytically and numerically for comparison. As it is seen, the agreement between the analytical formulae and the simulations is very much satisfactory.

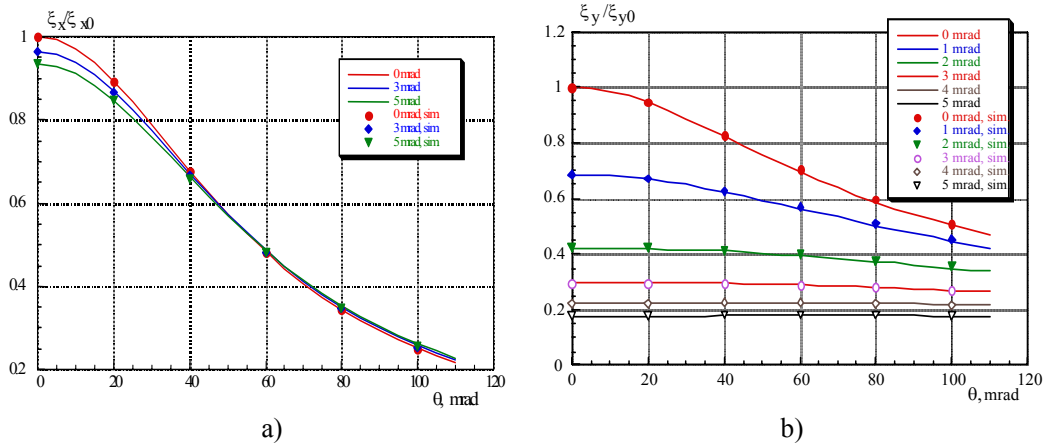


**Figure 2:** The horizontal (a) and vertical (b) tune shifts as a function of angle  $\theta$  for  $\phi = 0, 1, 2, 3, 4$  and 5 mrad (normalised by the value of the horizontal tune shift in head-on collisions). Solid lines – analytical results, dots – simulation results.

Then, we made the comparison for large crossing angles, in the range of 0.1 to 1.0 radians. The choice of parameters was based on the following statements. Bunch length must be much shorter than the beta-functions at the IP. Piwinski's angles of the order of 1-3 (at 1 rad) to have a reasonable and appreciable tune shift reduction in both planes. This also means that the transverse sizes are comparable (not order of magnitude different). Maximum tune shifts have to be reasonable, of the order of 0.02 - 0.05 or so. Finally, we came to the following set of parameters: bunch length  $\sigma_L = 0.3$  cm, beta-functions at the IP  $\beta_x = \beta_y = 100$  cm, emittances  $\varepsilon_x = 2.25 \cdot 10^{-4}$  cm-rad,  $\varepsilon_y = 10^{-4}$  cm-rad.

The comparison results are presented in Figures 3 a) and b) for the horizontal and vertical tune shifts, correspondingly. Some important remarks must be applied to these

results. First of all, since the vector of beam-beam kick (in the laboratory coordinate system) is perpendicular to the strong bunch's velocity, it has a component parallel to the weak bunch's velocity - that results in the energy change (18). The sign of the “energy kick” depends on the sign of the test particle longitudinal coordinate, so that IP behaves like a RF cavity (with rather specific potential shape, however). For large crossing angles, this even can result in the longitudinal instability. Moreover, due to the beam-beam interaction the system becomes 6D coupled, and the coupling depends not only on the  $\xi$  parameters and crossing angles, but on the initial tunes (both betatron and synchrotron) as well. So, the calculated by tracking tune shifts, since they are extracted from the eigenvalues, depend on the initial tunes. For example, in the case of the both crossing angles equal to 1 radian, but the initial tunes changed from (0.12, 0.15) to (0.12, 0.35), we have got the tune shifts changed from (0.01648638, 0.01396790) to (0.01758817, 0.01302020), that is rather big difference. We think, this coupling effect is the main source of discrepancy on large crossing angles, since it is not accounted at all in the analytical formulae (8). So, one can see that when the both angles are large, simulations give larger  $\xi_x$  and smaller  $\xi_y$  than the analytical formulae – it looks like a “redistribution” due to coupling. In these conditions we consider the agreement is quite acceptable.

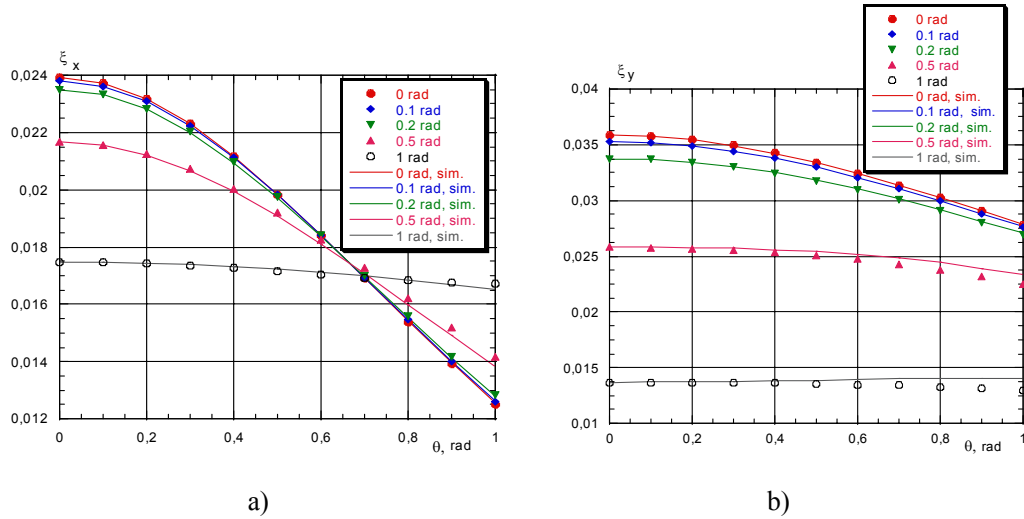


**Figure 3:** The horizontal (a) and vertical (b) tune shifts as a function of angle  $\theta$  for  $\phi = 0, 0.1, 0.2, 0.5,$  and  $1.0$  rad. Solid lines – simulation results, dots – analytical results.

### 6.1.5 Conclusions

1. We have obtained the formulae for the beam-beam tune shifts in collisions with an arbitrary crossing angle. In particular, it has been shown that these formulae can be transformed from the similar formulae for head-on collisions by substituting the horizontal beam size by  $(\sigma_x^2 + \sigma_z^2 \tan^2(\theta/2))^{1/2}$  in case of collisions with a horizontal crossing angle and the vertical beam size by  $(\sigma_y^2 + \sigma_z^2 \tan^2(\phi/2))^{1/2}$  if bunches collide at a vertical crossing angle.

2. The formulae for symplectic 6D beam-beam kick have been derived in the laboratory coordinate system, without Lorentz boost. These are currently implemented in the beam-beam code LIFETRAC.
3. Analysing the tune shift formulae, we see that for flat beams:

- a) The luminosity and the tune shifts are reduced with the horizontal crossing angle. However, since

$$L \sim (\sigma_x^2 + \sigma_z^2 t g^2(\theta/2))^{-1/2}; \quad \xi_x \sim (\sigma_x^2 + \sigma_z^2 t g^2(\theta/2))^{-1}; \quad \xi_y \sim (\sigma_x^2 + \sigma_z^2 t g^2(\theta/2))^{-1/2}$$

the horizontal tune shift drops faster than the luminosity does.

- b) In collisions with the vertical crossing angle the horizontal tune shift practically does not depend on the vertical angle if  $\sigma_x \gg (\sigma_y^2 + \sigma_z^2 t g^2(\phi/2))^{1/2}$  while the vertical tune shift and the luminosity are reduces proportionally to  $(\sigma_y^2 + \sigma_z^2 t g^2(\phi/2))^{-1/2}$ .
4. A comparison of analytical tune shifts calculations with eq. (8) and numerical simulations has shown a good agreement.

### 6.1.6 References

1. M. Zobov et al., PAC05, ROAA001; C. Milardi et al., EPAC04, pp. 233-235.
2. Y. Funakoshi et al., EPAC04, pp. 707-709.
3. C. Zhang et al., EPAC4, pp. 230-232.
4. J. Seeman et al., EPAC04, pp. 878-880.
5. H. Koiso, PAC05, TPPP003, to be published.
6. P. Raimondi, <http://www.lnf.infn.it/conference/d2/TALKS/raimondi.pdf>
7. Y. Cai, ICFA Beam Dyn. Newlett. 34:11-19, 2004.
8. P. Raimondi, M. Zobov, DAΦNE Tech. Note G-58, Frascati, April 30, 2003.
9. D. Shatilov, M. Zobov, DAΦNE Tech. Note G-59, Frascati, May 14, 2003.
10. A.A. Zholents, Preprint 91-18, Novosibirsk, 1991.
11. O. Napoly, Part. Accel. 40:181-203, 1993.
12. K. Hirata, H. Moshhammer, F. Ruggiero, KEK Preprint 92-117.
13. M. Bassetti, G. Erskine, CERN ISR TH /80-06 (1980).
14. K. Hirata, Phys. Rev. Lett. 74:2228-2231, 1995.
15. D. Shatilov, KEK Report 96-14.
16. D. Shatilov, Part. Accel. 52:65-93, 1996.

## 6.2 A longitudinal coupled bunch feedback for HERA-p

Markus Hoffmann  
 DESY, Notkestr. 85, 22607 Hamburg, Germany  
 mail to: [Markus.Hoffmann@desy.de](mailto:Markus.Hoffmann@desy.de)

### 6.2.1 Introduction

A longitudinal broadband damper system to control coupled bunch instabilities is currently under construction to be installed in the 920 GeV proton accelerator HERA-p

at the Deutsches Elektronen-Synchrotron DESY. This represents one of the attempts to increase the specific luminosity at HERA by reducing the bunch length.

Currently the bunch length is about 1.5 ns at the beginning of a luminosity run with 90 mA of protons stored in HERA. The final bunch length is defined by the initial emittance after injection and by the acceleration process where multiply occurring coupled bunch instabilities provoke bunch length blow up at certain energies.

At injection, dipole oscillations are induced by residuals of the beam loading which is not perfectly suppressed by direct RF feedback. There is furthermore a deliberate bucket mismatch in order to increase the Landau damping at injection. This causes longitudinal quadrupole oscillations, thus resulting in an initial emittance of 50 meVs.

During the ca. 30 minutes acceleration ramp (from 40 GeV/c to 920 GeV/c) the bunches are affected by multibunch instabilities, which typically cause the bunch length to blow up twice on the ramp when the bunch length becomes less than 1.5 ns. We end up with bunch lengths about 1.5 ns ( $\varepsilon_s \approx 0.3$  eVs) at the beginning of luminosity run (see Fig. 1). Calculations from the applied voltages of the two RF systems (52 MHz and 208 MHz) and the nominal injected emittance lead us to expect a bunch length of less than 1 ns at the end of the ramp. Three ongoing methods are available to combat bunch lengthening:

1. The double harmonics RF system provides sufficient Landau damping at the nominal energy of 920 GeV. The voltage settings for the 208 MHz RF System at injection have been optimized. We found that a RF voltage of the 4<sup>th</sup> harmonic system (208 MHz) of about 25 % of the main 52 MHz system provides enough Landau damping so that the injection oscillations are adequately damped and the bucket potential still has a good acceptance [2, p. 26ff.]. The voltage is then adiabatically increased during acceleration.
2. We built a device to modulate the amplitude of the four 208 MHz RF systems to set different synchrotron frequencies for each bunch decreasing the coupling between neighbouring bunches. First tests with this method were already done in 2003 with promising results [2]: Modulating 2 out of the 4 RF-Systems could prevent bunch length blow up in most cases or postpone the blow up to higher energies and thus smaller bunch lengths. However the modulation depth was not strong enough to keep the bunches short with nominal fill patterns and high currents. Therefore the hardware has been extended to modulate amplitude and phase of all 4 RF-Systems simultaneously with individual functions. Also a slow feed forward algorithm is foreseen to compensate for beam loading at injection. This will soon be tested.
3. The hardware used for 208 MHz amplitude modulation can also be used to apply a coloured (phase) noise to the beam which could be used to increase the bunch length in a controlled manner to stay just above the threshold where the beam becomes unstable. This method has already been successfully applied at the CERN SPS [3]. At the SPS it leads to less tail population as compared to a beam blown up by instabilities. Hence one may also expect less beam losses during acceleration and at collision. A slightly shorter bunch at 920 GeV/c may also be obtained.

Nevertheless we believe that the bunch length could be further reduced by another factor 1.5 with an active damping system. The feedback system has to measure the phases of all bunches with high accuracy and calculate corrections in real time which are then applied to the beam via a longitudinal feedback kicker. Because transverse and longitudinal emittances of a proton beam are very sensitive to any noise the system must be low noise and also the corrections must be as exact as possible and as moderate as possible. Therefore the feedback system for a hadron beam accelerator is much more challenging than that for electron accelerators where longitudinal coupled bunch feedback systems are widely used.

Studies which deal with the influence of RF noise on coasting beam production and bunch lengthening are in progress. But the feedback system has to be designed and built at the same time because of the limited operation time of HERA which is scheduled to be shut down in 2007. Since we do not know how much noise will be introduced on the beam (the bunch phase detector shows noise (beam plus electronics) of about 0.2 degrees which will be reduced by additional digital filtering) and what the effect will be, all components have to be designed with careful scrutiny of their noise behaviour. Excessive noise induced bunch lengthening could negate the advantages gained.

The theoretical gain in luminosity can be as high as 8 %. The project will be considered successful if the bunch length is held at less than 1 ns for at least 4 hours. At the moment a typical luminosity run lasts 12 hours.

The time frame for this project is slightly more than 1 year commencing September 2004. The last chance to install the new feedback cavity is in the winter shutdown which is scheduled for Nov. 2005. This ambitious time frame implies that we must use the simplest possible solution with the knowledge that the risk due to noise influencing the beam is unknown.

The feedback kicker has to be built with a design simple enough for manufacture and test within the limited time. Higher order modes have to be identified and damped if necessary. Additional unwanted impedance could strengthen multibunch or single bunch instabilities.

### 6.2.2 The Feedback System

The actual design consists of a fast, high precision bunch phase detector, a 1 kW feedback cavity with 104 MHz centre frequency and 5.2 MHz bandwidth, a I/Q-vector modulator, the low level digital FPGA-board with 14 Bit ADCs and DACs and a cavity transient diagnostics.

The high precision bunch phase detector has been in operation since 2003. It was designed as a fast longitudinal diagnostics system [1] and the analog RF hardware can also be used for the feedback system.

Coupled bunch oscillations have been observed for over a year. Considerable archived data have been analysed to reveal, which coupled bunch instability modes occur and at what strength. We frequently observed modes 5 and 11 at lower energies, but also very often the mode 56/164 (HERA has 220 possibly filled buckets) which lead to bunch length blow up at 300 GeV and at  $> 670$  GeV (see Fig. 1 and 2). It is therefore not sufficient to have a near-by-mode feedback or a single mode feedback. A full multibunch mode feedback is necessary. Growth times of the instabilities are typically more than 2 seconds so a relatively moderate kick voltage is needed to damp

the oscillations (the synchrotron frequency of HERA-p is typically 35 Hz but can vary from 20 Hz to 80 Hz during acceleration.)

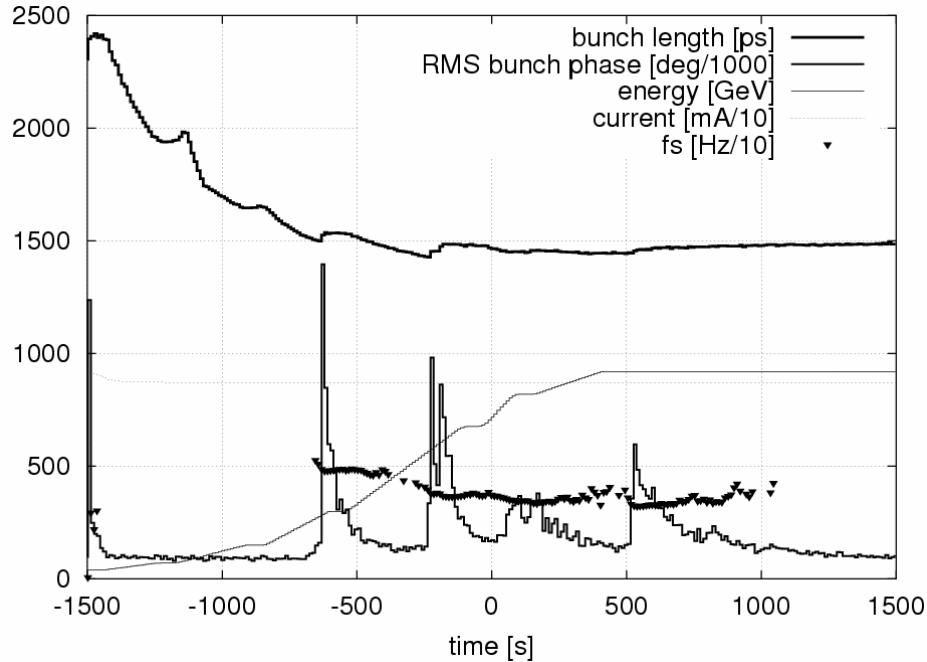


**Figure 1:** Longitudinal parameters on a typical ramp of HERA-p. The data was taken on 26.03.2005 13:58 with 70 mA filled in 150 bunches. The graph shows energy, current, mean bunch length, RMS bunch phases. The initial bunch length after injection is about 2.4 ns. A multibunch instability (mode 164) shows up at 300 GeV and at 600 GeV with correlated bunch length blow up. The instability comes back also at 920 GeV after some time.

A 1 kW cavity system (which can produce longitudinal kicks of about 200 V) is therefore adequate. So a simple cavity without special water cooling will suffice. The cavity itself need not be under vacuum, it surrounds a vacuum chamber with a ceramic gap.

We cannot operate the kicker in base band mode, because of size considerations. We therefore chose a design with 10 times the bunch frequency which is 10.4 MHz (bunch spacing: 96 ns). The resulting 104 MHz kicker is a cylindrical cavity with a diameter of 40 cm and a length of ca. 70 cm. The high bandwidth is achieved by externally loading with a 50 Ohm wave dump. Higher order modes are damped passively with ferrites placed inside the cavity. Special cooling is not foreseen at the moment, but the high power tests are yet to be performed.

After detection, the bunch signals (I and Q components) can be sampled by a digital FPGA board with 10.4 MHz sampling frequency and 14 Bit resolution. Phase calculation for all bunches and offset correction will be done by FPGA software. A digital filter will then be applied to the phase signals to produce the correction kicks, which are the output of the board. The filter has to be able to deal with a slowly changing synchrotron frequency (20 -- 80~Hz). Here we consider a filter design which treats every bunch as an independent oscillator which has to be damped. More sophisticated mode filter algorithms may be required to get better noise performance.

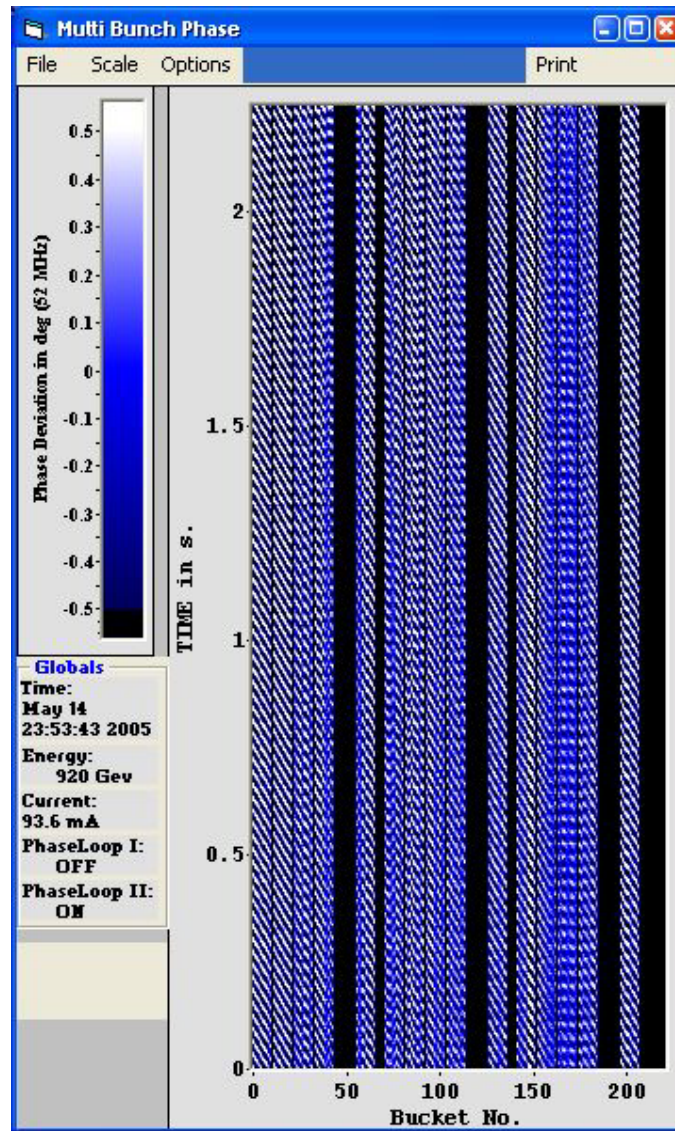


**Figure 2:** Signature of the popular mode 164: The pattern shows 512 samples of the bunchphases of all 220 bunches (only 150 are actually filled). Data was taken on 2005-05-15 00:00h.

In fact the board produces two streams of output which then go to the 104 MHz vector modulator. The modulator input is calculated by the FPGA in such a way that each bunch sees the desired voltage on top of the 104-MHz sine wave when it passes the kicker.

The modulated signal is then amplified by a 1-kW broadband linear amplifier, which will be placed near the HERA tunnel, where the feedback kicker will be installed. The cavity has two symmetrical RF couplers for RF input and a RF load output. For diagnostics and timing adjustment, the cavity transient signals, picked up at the load coupler of the cavity are fed back to a vector demodulator and will be sampled and

archived by the fast longitudinal diagnostic system. We hope that the kicker can also be used as a narrow bandwidth longitudinal beam monitor.

### 6.2.3 Outlook

At the moment the feedback cavity is installed in a test stand. All parameters have been measured and the cavity has been tuned to design values. Parasitic modes have been identified and need now to be damped by ferrites or similar material. Finally high power tests will show if cooling will be necessary.

The vector modulator hardware has been built and tested.

The low level RF digital FPGA board is currently being programmed and tested with the real I/Q beam signals from the fast longitudinal diagnostics system during normal HERA operation.

Theoretical studies concerning noise on the proton beam at HERA are under way. Attempts to understand the sources of bunch coupling in the machine are still in progress.

We are still on schedule so we are optimistic that the feedback system can be installed in the winter shutdown in November this year. The commissioning of the system will take place in January 2006. HERA-p will be the first high energy hadron storage ring in which a longitudinal multibunch feedback system will have been installed.

### 6.2.4 References

1. E. Vogel, Fast Longitudinal Diagnostics for the HERA Proton Ring, Dissertation 2002, DESY-THESIS-2002-010
2. E. Vogel, Status of the Longitudinal Emittance Preservation at the HERA Proton Ring in Spring 2003, Internal Report, DESY-HERA-2003-03, June 2003
3. T. Bohl, et al. Experimental studies of controlled longitudinal emittance blow-up in the SPS as LHC injector and test-bed, EPAC 2004, LHC Project Report 761, Jul 2004

## 6.3 Simulation of Coherent Synchrotron Radiation Effects for the second Bunch Compressor Chicane at the VUV-FEL

Frank Stulle\*, DESY  
mail to: [frank.stulle@desy.de](mailto:frank.stulle@desy.de)

### 6.3.1 Introduction

For the VUV Free-Electron Laser (VUV-FEL), which was built at DESY, the electron beam must meet very tight specifications [1]. To realize the Self-Amplified Spontaneous Emission scheme (SASE) [2,3], on which the VUV-FEL is based, electron bunches with emittances in the order of 1 mm mrad are essential. At the same time very high peak currents are needed, but, unfortunately, the maximum feasible current for the

---

\* Now at PSI, Paul Scherrer Institut

low energy bunches in the gun is limited by the space charge forces. Only high energy bunches can be compressed longitudinally to the needed currents in the order of 1 kA.

The bunch compression at the VUV-FEL is done in two magnetic chicanes by making use of the momentum dependence of the path length  $l_i \approx l_0 + R_{56} \Delta E_i / E_0$ . Here  $l_i$  denotes the path length which the electron with index  $i$  has travelled.  $R_{56}$  is the momentum compaction factor of the chicane and  $\Delta E_i / E_0$  is the relative energy deviation of this electron. Unfortunately, when the electrons pass these chicanes they can produce strong coherent synchrotron radiation (CSR) [4]. Consequently, the six-dimensional phase space distribution will be deformed.

Here results of computer simulations of two different chicanes are presented. These two chicanes have been options for the second bunch compressor chicane at the VUV-FEL. It is shown that the development of the phase space distribution during compression depends strongly on the chicane geometry. Additionally, the influence of different chicane setups is studied by varying the  $R_{56}$ . The energy slope along the bunch is adjusted accordingly to keep the final peak current constant.

Some notes on the CSR tracking codes and on CSR simulations are given the next section. Section 3 describes the geometry of the two chicanes which are compared and the simulation results are presented in section 4. A conclusion is given in section 5.

### 6.3.2 Notes on CSR Simulations

Over the past years several tracking codes have been written or existing codes have been extended to calculate the effect of CSR. These codes are for example Elegant [5], TraFiC<sup>4</sup> [6] and CSRTrack [7]. There is a very important difference between these codes, namely the calculation algorithm for the CSR fields. In Elegant a one-dimensional analytical model is implemented, which is based on Ref. [8]. It is very fast but also neglects several effects, e.g. transverse fields. TraFiC<sup>4</sup> is based on a simplified three-dimensional integration of the electro-magnetic potentials [6]. But already this simplified integration demands a huge calculation effort and thus the number of tracking particles is limited. Two-dimensional integrations using pseudo Green's functions [9] are implemented in CSRTrack, which also includes implementations of the other two methods. The advantages of the Green's function approach are that it is a lot faster than three-dimensional integrations and a lot more accurate than the one-dimensional analytical model. Indeed, its results are usually very close to the three-dimensional integration of scalar and vector potentials [9]. All simulations which are presented here make use of this calculation method.

Like all tracking codes also the CSR tracking codes have to deal with the fact that they cannot track a number of particles comparable to the number of electrons inside a real electron bunch. A bunch of 1 nC consists of more than  $6 \cdot 10^9$  electrons, but even when making use of the one-dimensional model we can track only about one million particles. Using the Green's function approach we can still track about 100000 particles. The integration of the potentials limits the number of particles to some 10000. With such a small number of particles the sampling of the phase space cannot be very accurate. A work-around can be, not to populate all phase space dimensions to get a better sampling of the others. Than of course information is lost. This can be justified for example for the vertical phase space. Since the propagation of the CSR fields will be mainly in the horizontal bending plane of the dipoles, no real impact on vertical coordinates is expected.

When not all phase space dimensions are populated, part of the dynamics can be recovered by tracking additional test particles. They do not radiate themselves but are influenced by the fields of the others, the so called generating particles. Of course a lot of information is lost and with today's computers and codes it is preferable to populate at least longitudinal and horizontal coordinates of the generating distribution for which the CSR fields are calculated.

An effect which is called CSR microbunch instability makes the setup of the generating distribution even more complicated. It was shown in computer simulations [10] and analytically [11] that CSR can amplify small density and energy modulations in the longitudinal phase space distribution. Since the number of generating particles is a lot smaller than the real number of electrons, regardless of which code is used, artificial noise is generated, which in turn can be amplified by CSR in the simulations. Consequently, one should suppress this kind of noise by setting up the generating distribution in an artificially ordered way. On the other hand this might introduce other artificial effects or it can suppress real effects.

In addition, the three codes mentioned above suppress artificial noise in the field calculation by using noise filters (Elegant) or by tracking macroscopic charge distributions, so called sub-bunches, instead of point-like particles (CSRTrack, TraFiC<sup>4</sup>). The user has to take care that the filter parameters are set up correctly or that the sub-bunches give a smooth distribution.

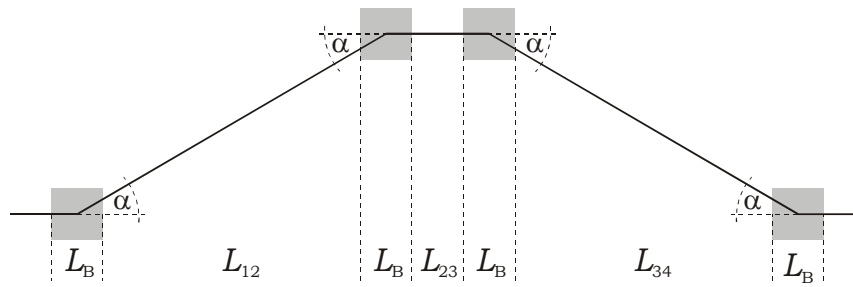
### 6.3.3 Bunch Compressor Chicanes

Two chicanes are compared in the next section. These are a symmetric 4-dipole C-shaped chicane, which I call C-chicane, and a symmetric 6-dipole S-shaped chicane, which I call S-chicane. It is important to note, that an S-chicane is never fully achromatic, but the amount of residual dispersion is usually negligible. A consequence of the symmetry of the chicanes is, that all dipoles in a chicane have the same strength. They are also of the same length. The first and the last drift of the chicanes as well as the drifts which separate the 2<sup>nd</sup> and 3<sup>rd</sup> and the 4<sup>th</sup> and 5<sup>th</sup> dipole of the S-chicane must have the same length. To get comparable results both chicanes have the same overall length of 14.02 m and compress the electron bunches to the same peak current of 2500 A.

In the simulations the momentum compaction factor  $R_{56}$  of the chicanes is varied to study the impact of the varying CSR power. The compression factor  $c_f = \left(1 - R_{56} \frac{1}{E_0} \frac{dE}{ds}\right)^{-1}$  is always kept constant by adjusting the energy slope  $dE/ds$  along the bunch accordingly.

Sketches of the chicanes are shown in Figures 1a and 1b. The basic parameters of both chicanes are given in Table 1. The parameters of the incoming electron beam are given in Table 2.

a)



b)

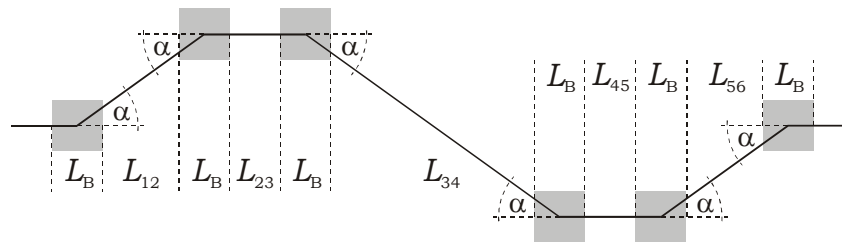


**Figure 1:** Sketches of the C-chicane (a) and the S-chicane (b)

**Table 1:** Chicane parameters used for the simulations

	C-chicane	S-chicane
dipole length $L_B$	0.5 m	0.5 m
1 <sup>st</sup> drift $L_{12}$	5.760 m	2.380 m
2 <sup>nd</sup> drift $L_{23}$	0.5 m	0.5 m
3 <sup>rd</sup> drift $L_{34}$	5.760 m	5.259 m
4 <sup>th</sup> drift $L_{45}$	-	0.5 m
5 <sup>th</sup> drift $L_{56}$	-	2.380 m
bending angle $\alpha$	2.615/3.720/ 4.545/5.205 deg	2.765/3.900/ 4.698/5.314 deg
momentum compaction factor $R_{56}$	-2.5/-5/-7.5/-10 cm	-2.5/-5/-7.5/-10 cm

**Table 2:** Initial electron beam parameters used for the simulations.  
The energy-position correlation varies according to the  $R_{56}$

energy	$E_0$	450 MeV
bunch charge	$Q$	1 nC
bunch length	$\sigma_s$	250 $\mu\text{m}$
peak current	$I_0$	500 A
norm. emittance	$\varepsilon_{x,y}$	$1 \cdot 10^{-6}$ m rad
unc. energy spread (test particles only)	$\sigma_\varepsilon/E_0$	$1 \cdot 10^{-5}$
energy-position correlation	$\frac{1}{E_0} \frac{dE}{ds}$	-32/-16/-10.667/-8 1/m
beta function	$\beta_{x,y}$	40.0 m
alpha	$\alpha_{x,y}$	2.6

### 6.3.4 Simulation Results

For all simulations presented in this section, a charge distribution consisting of about 100000 generating sub-bunches and 20000 test particles has been used. The sub-bunches are distributed over  $\pm 3\sigma$  in each phase space dimension. Longitudinal and horizontal phase space coordinates are ordered, whereas the vertical phase space coordinates are randomly chosen. Uncorrelated energy spread was not included. The test particles are randomly distributed over  $\pm 4\sigma$  in all six phase space dimensions. The tracking was done with the code CSRTrack and makes use of the Green's function method. Tracking always started 1 m in front of the first dipole and stopped 1 m behind the last dipole.

Figures 2 and 3 show the incoming generating distribution for the case with  $R_{56}=5$  cm. For all other cases only the energy slope and, consequently, the rms energy spread is different.

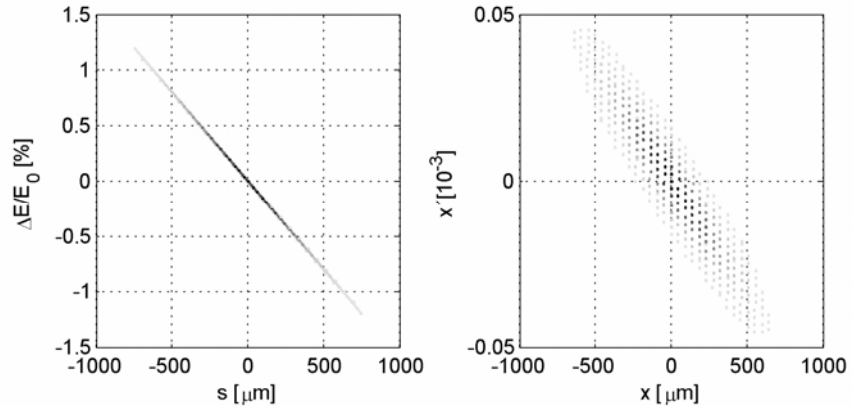


**Figure 2:** Initial longitudinal (left) and horizontal (right) phase space distribution of the generating bunch. Dark dots represent a higher charge than lighter dots.

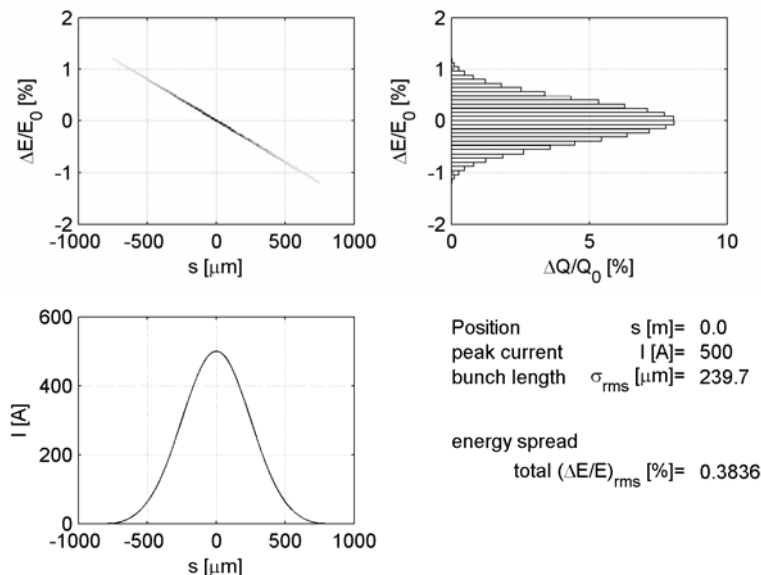


**Figure 3:** Initial longitudinal phase space distribution (upper left), energy profile (upper right) and current profile (lower left) of the generating bunch.

That the chicane geometry has indeed an influence on the deformation of the phase space distribution can be seen in Figures 4 and 5. It becomes especially obvious when one compares the plots of the horizontal coordinates  $x$  and  $x'$  versus the longitudinal position  $s$ . Behind the C-chicane the  $x$ - $s$  plot is strongly bent whereas behind the S-chicane only a wide but straight band is visible. The  $x'$ - $s$  plots look quite similar but the sign of  $x'$  is different. One can also see that the area occupied in the horizontal phase space is smaller behind the S-chicane. That means, the final projected emittance is smaller. This is the most remarkable effect, that the chicane geometry has an effect on the emittance growth. Remember, that both chicanes are of the same length, use the same dipoles and compress the bunches to the same peak current (see also Fig. 6, 7). Without CSR the phase space distributions behind the chicanes would look the same.

In Figures 6 and 7 besides the longitudinal phase space distribution also the energy profile and the current profile together with the slice emittance are plotted. It becomes clear that the chicane geometry has also an effect on the slice emittance. By the way, from Fig. 4, 5 one can also expect the correlated emittance to be different, what it indeed is (Figure 8). Figure 8 shows the dependence of slice and correlated emittance on the  $R_{56}$ . The slice emittance is calculated within a  $5\mu\text{m}$  slice around the peak value of the current. This is also the explanation for the strong growth of the slice emittance for the S-chicane with growing  $R_{56}$ . For small  $R_{56}$  the peak current is slightly shifted with respect to the maximum slice emittance (see also Fig. 6, 7). But with increasing  $R_{56}$  the peak current and the maximum slice emittance move closer together. This behavior is not that strong for the C-chicane. The correlated emittance is always a lot better for the S-chicane. Values for the projected emittance are not given since they also depend on beam optics.

If the peak current and the maximum slice emittance are at the same longitudinal position will not only depend on the chicane geometry but also on beam parameters. Therefore, one cannot use the results for the slice emittance as a argument pro or contra one of the chicanes. Still, when comparing slice emittances along the bunch and correlated emittances, the S-chicane seems to be the better choice.

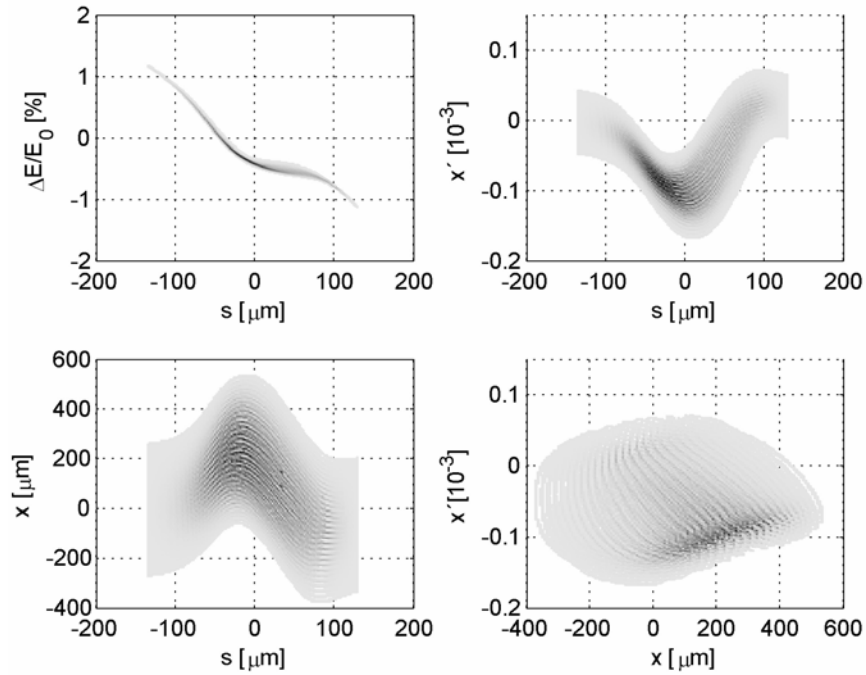


**Figure 4:** Longitudinal phase space distribution (upper left), horizontal angle vs. longitudinal position (upper right), horizontal offset vs. longitudinal position (lower left) and horizontal phase space distribution (lower right) behind the C-chicane.

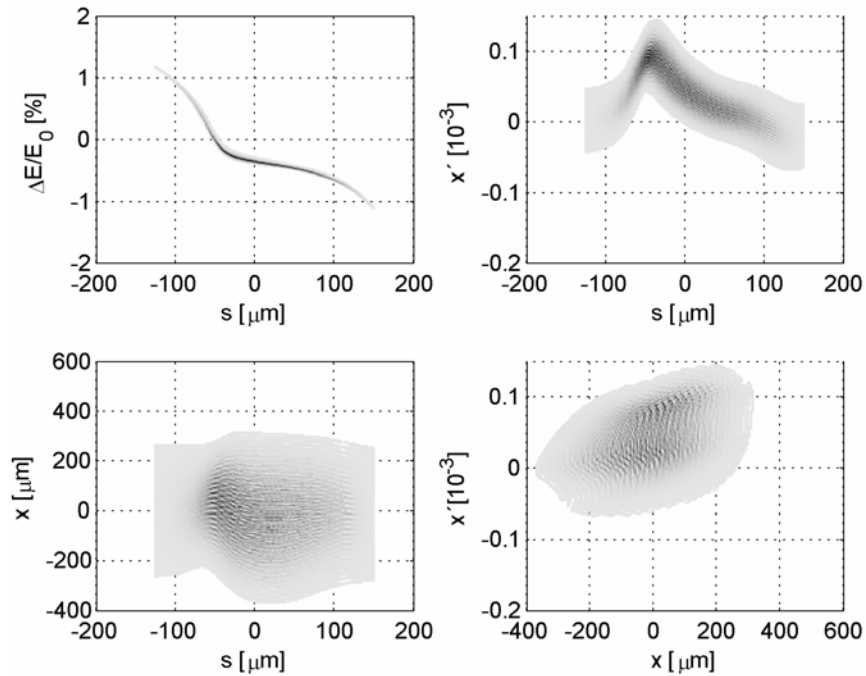


**Figure 5:** Longitudinal phase space distribution (upper left), horizontal angle vs. longitudinal position (upper right), horizontal offset vs. longitudinal position (lower left) and horizontal phase space distribution (lower right) behind the S-chicane.

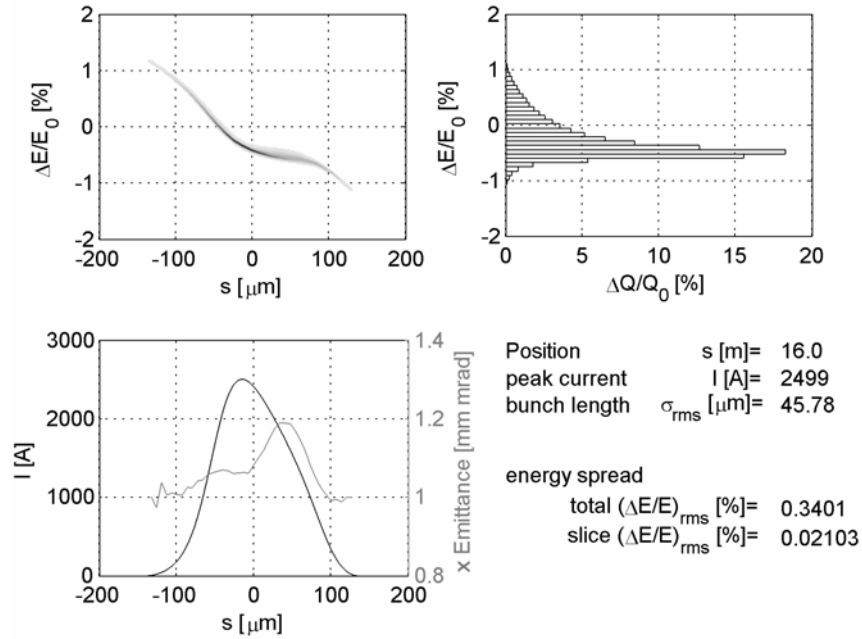


**Figure 6:** Longitudinal phase space distribution (upper left), energy profile (upper right) and current profile (lower left) behind the C-chicane.

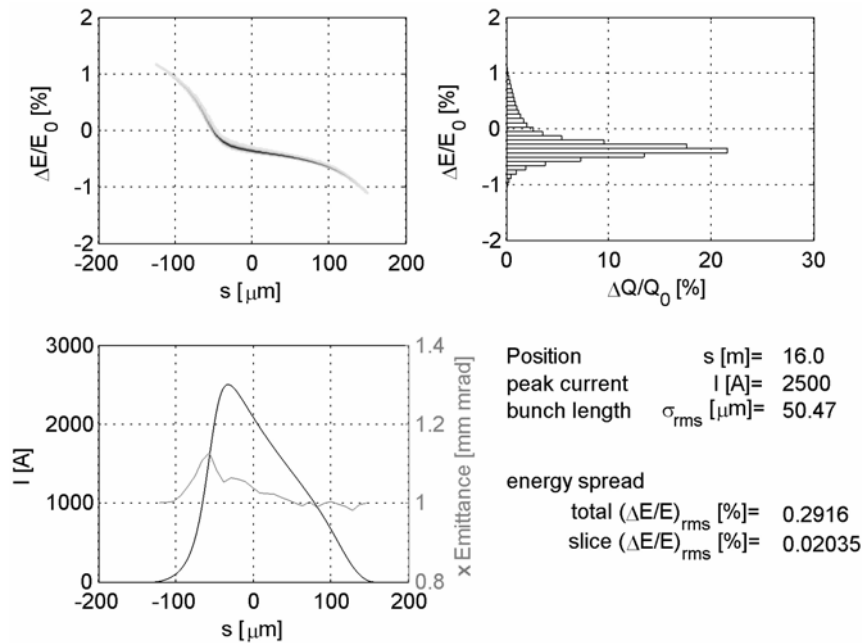


**Figure 7:** Longitudinal phase space distribution (upper left), energy profile (upper right) and current profile (lower left) behind the S-chicane.

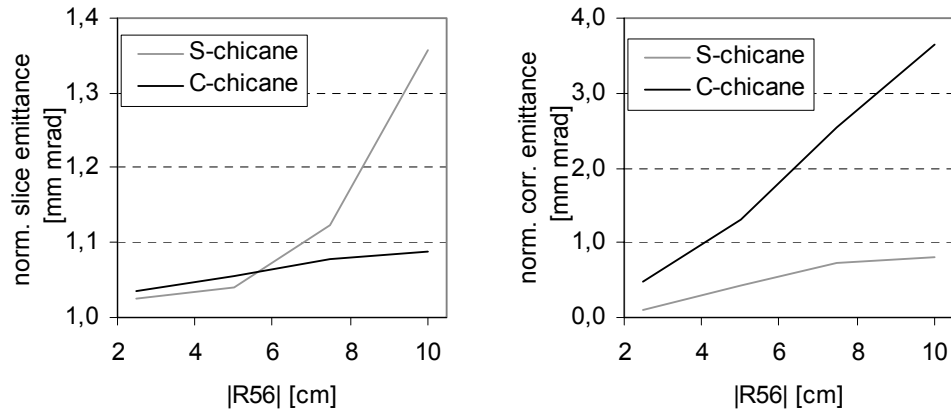


**Figure 8:** Dependence of slice emittance (left) and correlated emittance (right) on  $R_{56}$ .

### 6.3.5 Conclusion

It is shown that the development of the phase space distribution is influenced by coherent synchrotron radiation when electron bunches are compressed in magnetic chicanes. The influence strongly depends on the geometry of the chicane, what is shown here for two layouts, the C-chicane and the S-chicane. When comparing the simulation results the S-chicane induces a smaller deformation of the charge distribution and, consequently, a smaller emittance growth than the C-chicane. This is especially the case for the correlated emittance.

These findings fit to earlier studies and simulations made in Ref. 12. Even though, the simulations performed there have been a lot simpler, most results agree well with the new simulations presented here. But individual parameters, e.g. emittances, can differ a lot.

For a comparison of simulation results to measure data one always has to keep in mind, that the simulations depend strongly on beam parameters. Not only a dense modeling of the charge distribution is needed but also the shape of the beam model must match the real incoming distribution. Gaussian distributions, as used here, can only be used for basic studies.

### 6.3.6 References

1. "SASE FEL at the TESLA Test Facility Phase 2", TESLA-FEL 2002-01, June 2002.
2. A. M. Kondratenko, E. L. Saldin, "Generating of Coherent Radiation by a relativistic Electron Beam in an Undulator", Part. Accel. 10, pp. 207-216, 1980.
3. R. Bonifacio, C. Pellegrini, L. M. Narducci, "Collective Instabilities and high Gain Regime in a Free Electron Laser", Opt. Commun. 50(6), pp. 373-378, July 1984.
4. J. Schwinger, "On Radiation by Electrons in a Betatron", transcribed by M. A. Furman, LBNL-39088, July 1996.
5. M. Borland, "Simple Method for Particle Tracking with Coherent Synchrotron Radiation", Phys. Rev. ST AB 4(070701), July 2001.

6. M. Dohlus, A. Kabel, T. Limberg, "Efficient Field Calculation of 3D Bunches on general Trajectories", NIM A 445, pp. 338-342, 2000.
7. M. Dohlus, private communication.
8. E. L. Saldin, E. A. Schneidmiller, M. V. Yurkov, "On the coherent radiation of an electron bunch moving in an arc of a circle", NIM A 398, pp. 373-394, October 1997.
9. M. Dohlus, "Methods for CSR Tracking", talk given at the ICFA Future Light Sources Sub Panel Mini Workshop on Start-to-End Simulations of X-ray FELs, Berlin, Germany, August 2003
10. M. Borland, "Start-to-End Simulations of SASE FELs from the Gun through the Undulator", in proceedings of FEL2001, Darmstadt, Germany, August 2001
11. E. L. Saldin, E. A. Schneidmiller, M. V. Yurkov, "Klystron Instability of a relativistic Electron Beam in a Bunch Compressor", TESLA-FEL 2002-02, January 2002
12. F. Stulle, "A Bunch Compressor for small Emittances and high Peak Currents at the VUV-Free-Electron Laser", DESY-THESIS 2004-041, October 2004.

## 7 Workshop and Conference Reports

### 7.1 Summary of the 32nd ICFA Advanced Beam Dynamics Workshop on "Energy Recovering Linacs" (ERL2005)

Lia Merminga and Swapan Chattopadhyay  
 Jefferson Lab, Newport News, VA, USA  
 mail to: [merminga@jlab.org](mailto:merminga@jlab.org)

#### 7.1.1 Introduction

The 32<sup>nd</sup> ICFA Advanced Beam Dynamics Workshop on "Energy Recovering Linacs," "ERL2005" was held March 19-23, 2005 in Newport News, Virginia, USA. The workshop was hosted by Jefferson Laboratory, and sponsored by Brookhaven National Laboratory, Cornell University, Daresbury Laboratory and the U.S. Department of Energy Office of Science. The meeting was chaired by Lia Merminga and Swapan Chattopadhyay of Jefferson Lab. ERL2005 was the first international workshop dedicated to energy recovering linacs, their various applications and technical challenges in realizing future ERL-based accelerators.

The four and half-day workshop program opened with a day of plenary talks and broke up into four parallel working group sessions for the following three days. The four working groups were devoted on the topics of: Electron guns and injectors; optics and beam transport; superconducting RF and RF control; diagnostics, instrumentation and synchronization. In the last day of the workshop, a closing plenary session was held in which summaries of the working groups were presented.

The opening plenary session program included presentations on operating ERLs, and on envisioned ERL applications, including ERL-based FELs, x-ray light sources, and ERLs for nuclear and particle physics which include electron cooling devices and electron-ion colliders. Presentations on the state of the art in the four major accelerator physics and technology topics, mapped directly on the four working groups, followed. Armed with the understanding of the present state of ERLs, the community's future

aspirations, and the technical challenges on the way, the charge and program of each working group was presented next, designed to address the technical challenges and draw a road map to resolving them. Three intense days of presentations, information and ideas exchange, and many discussions followed, and the workshop closed with comprehensive reviews of each working group's findings and suggestions for future R&D. An overarching theme was the intensification of collaborative efforts among the various institutions involved in ERL research world-wide. Strong industrial participation was a welcome aspect of the workshop and a sign of times to come. Particularly useful was the cross fertilization with other fields of accelerator physics, such as linear colliders and SASE FELs.

In addition to the intense scientific and technical program, the workshop participants had the opportunity to tour Jefferson Lab's ERL FEL facility, and the superconducting RF Test Facility. Receptions and social events lightened up the spirit of the workshop, and included a piano recital by workshop participant Stefan Simrock and pianist Cathy Combs. The conference banquet was held in the Mariner's Museum with a prelude to the dinner by local cellist Dr. James Preston Herbison, Professor of Music at Norfolk State University and section Cellist with the Virginia Symphony Orchestra.

The workshop attendance was overwhelming and exceeded all expectations of the organizers: 159 registered participants from 9 countries. Thanks to the generous sponsorship of the U.S. Department of Energy, we were able to provide support for 10 students and scholars from 4 countries.

The overwhelming workshop attendance was equally matched by active participation: 81 abstracts were submitted, more than 100 talks were presented throughout the workshop program, and in excess of 50 papers were submitted and will be published.

The program of the each working group was developed primarily by the conveners of the corresponding group in consultation with subsets of the program committee comprised of experts in the particular subject. We are thankful to the program committee members for their expert advice. We are deeply indebted to the conveners of the working groups:

- Electron Guns and Injector Designs – *I. Bazarov (Cornell), I. Ben-Zvi (BNL)*
- Optics and Beam Transport - *G. Hoffstaetter (Cornell), V. Litvinenko (BNL), H. Owen (Daresbury Lab)*
- Superconducting RF and RF Control – *J. Knobloch (BESSY), M. Liepe (Cornell), M. Dykes (Daresbury Lab)*
- Synchronization, Diagnostics, Instrumentation – *W. Graves (MIT), G. Hirst (CCLRC), H. Schlarb (DESY)*

Their expert knowledge, hard work, enthusiasm and truly outstanding performance made this workshop a unique event. We would also like to express our sincere thanks to the team of JLab Staff Services and conference secretaries for the excellent organization.

The proceedings of the workshop will be published as a special issue of *Nuclear Instruments and Methods in Physics Research, Section A* (NIMA). Viewgraphs of all the talks are available on the web page of the conference:

<http://www.jlab.org/intralab/calendar/archive04/erl/program.html>

Abbreviated summaries of the four working group sessions are presented next.

## 7.1.2 Electron Guns and Injector Designs

I. Ben-Zvi and I. Bazarov

The subject of this working group, the electron gun and injector design, is arguably the most critical part of the ERL. It is here that the ultimate performance of the ERL is determined. Working Group 1 dealt with a variety of subjects that is summarized below: The technology of DC, normal-conducting RF and superconducting RF guns; beam dynamics in the gun and injector; the cathode and laser package; modeling and computational issues; magnetized beams and polarization.

Due to the connection to other disciplines represented in the workshop, two joint sessions were held with other working groups on merger design and limiting phenomena with Working Group 2, and on necessary beam diagnostics in the injector with Working Group 4. In the first joint session it became apparent that the advent of the “zigzag” merger leads to a significant brightness improvement in the moderate and high bunch-charge beams. As far as diagnostics are concerned, key injector diagnostic requirements are that most diagnostics must work at low energy (<10 MeV); a need to make the injector as short as possible (and that implies compact diagnostics); and that all diagnostics should be designed for low impedance with CW capability desired at full charge and full repetition rate.

### 7.1.2.1 DC, Normal -Conducting RF and Superconducting RF Guns

A survey of 11 different guns serving in various ERLs was presented by A. Todd (AES), including operating guns such as DC / thermionic emission (JAERI FEL, BINP FEL) and DC / photocathode (JLab FEL); the normal-conducting retired RF gun (Boeing R&D accelerator), which is still state-of-the-art; other RF guns under construction, the LANL/AES normal conducting, the BNL/AES superconducting gun for the R&D ERL, some RF guns under analysis (LUX at LBNL, 4GLS at Daresbury) and DC guns under construction (AES/JLab injector test stand, Cornell injector test stand, Daresbury ERLP). Todd included a list of “requirements”, which are broadly defined with a goal and range of parameters to be found: Output energy ~ 7 MeV (2 – 15); CW average current ~ 200 mA (100 –500); transverse emittance < 6 microns rms normalized (0.1 –6); longitudinal emittance < 145 keV-psec rms (25 –145); bunch length ~ 4 psec (2 –7); energy spread < 0.5 % (0.1 –0.5) @ 7 MeV; RF frequency ~ 700 MHz (500 –1300); 500 kW RF feedthroughs (50 –500).

Todd provided an appraisal of the issues facing the various guns being pursued in the community and concluded with a survey of the three technology options with the observation that we must demonstrate practical, compatible cathode and drive laser options for each injector type, we must pay attention to HOM and CSR issues in injectors and we must successfully demonstrate high RF power handling.

D. Dowell (SLAC) presented a talk on “Technology Challenges for RF Guns as ERL source”. This was a comprehensive and detailed study of RF guns, both normal-conducting (like Dowell’s Boeing gun, which is still state-of-the art for any RF gun for ERLs) and superconducting. The motto of the presentation may be that: “Technical

Challenges are Everywhere! RF Gun; NCRF; SRF; Cathodes; Drive Laser; Bunch Compression; Beam Transport.”

A talk on “Technology Challenges for DC Guns as ERL source” by C. Sinclair (Cornell) followed. Sinclair noted that DC guns with NEA photocathodes, operating between  $\sim 70$  kV and 350 kV, have been used on many research electron accelerators since 1977. He noted the major challenges: There is essentially no experience operating photoemission guns at very high voltages (500-750 kV). Field emission from electrode structures can lead to voltage breakdown, insulator punch-through, and other less serious problems. Good operational lifetime for high quantum efficiency photocathodes requires exceptional vacuum conditions –presently at or near the limits of vacuum technology. Lasers supporting 100 mA operation are presently very much state-of-the-art systems.

Another talk covered the operating experience of GaAs photocathodes at JLab, in the “Performance of the 10 mA DC GaAs photocathode gun in the JLab IR Upgrade FEL”, given by C. Hernandez-Garcia (JLAB).

“Technology Challenges for SRF Guns as ERL Source in View of BNL Work,” was presented by A. Burrill (BNL). Burrill reported about the design, fabrication and commissioning of a 703.75 MHz SRF photoinjector with a retractable multi-alkali photocathode designed to deliver 0.5A average current at 50% duty factor. This is the present undertaking of the electron cooling group in the Collider Accelerator Division of Brookhaven National Labs. This photoinjector represents the state of the art in photoinjector technology, orders of magnitude beyond the presently available technology, and should be commissioned by 2007.

“Technology Challenges for SRF Guns as ERL Source in View of Rossendorf Work,” was presented by D. Janssen (Rossendorf). This presentation came after successful tests of a SRF gun with a superconducting half-cell cavity, and while a new SRF photoinjector for cw operation at the ELBE linac is under development. The conclusion from the successful operation of the SRF injector with a half-cell cavity in 2002 at the Forschungszentrum Rossendorf is addressing the crucial question if the photocathode inside the superconducting cavity reduces the quality factor due to particle pollution. During about 200 hours operation time, such an effect was not seen using CsTe<sub>2</sub> cathodes. It also demonstrates convincingly that a reliable mechanism for inserting a normal-conducting cathode stem into a superconducting cavity does not affect the good performance of the SRF cavity. Following this initial success the Rossendorf group embarked on the design and production of a 3 ½ cell gun which has also various other improvements for getting the smallest emittance out of the device, including careful shape optimization, bunch focusing by a high-order RF mode, symmetrized input coupler and improved tuner system.

An new approach which attempts to bridge the properties of normal and super conducting RF guns was presented in “Novel, Hybrid (Normal-Superconducting) RF Injector for High-Average-Current Electron Sources”, by D. Nguyen (LANL). The proposed solution is a hybrid gun, in which the first 1 ½ cells are normal conducting, followed very closely by an SRF booster. This has the advantages of: cryo-pumping reducing cathode contamination; ohmic loss is reduced with only 1.5 cell NC injector; the gun can now admit a solenoid field for emittance compensation at high bunch charge; and the NC cathode is isolated from SRF cavities, allowing the semiconductor cathode to operate at room temperature.

Table 1 shows a summary of the properties of the 3 main technology choices for ERL guns.

**Table 1:** Photoinjector technology parameters and issues, by the three candidate technologies.

	DC Gun	Normal RF	SRF Gun
Max. gradient achieved	4.3 MV/m	6 MV/m	32 MV/m
Max. gradient planned	>7 MV/m	10 MV/m	>20 MV/m
Max. current demonstrated	10 mA	128 mA at 25% DF	1 mA
Max. current planned	1000 mA	1000 mA	500 mA
Issues	Field emission, vacuum, ion back- bombardment	Thermal management, vacuum	Cathode thermal management, contamination of SRF cavity

#### 7.1.2.2 *Beam Dynamics in the Gun and Injector*

The beam dynamics in the gun and injector are complicated by the low energy (starting actually non-relativistic near the cathode) and the resultant strong space-charge interaction, the process of emittance compensation that starts in the gun and mostly completes in the injector. The aspect ratio of the bunch, which influences its beam dynamics, changes over a large range due to the large relative change in energy. Whatever non-uniformity there is in the charge distribution of the bunch will evolve within a fraction of a plasma oscillation, and that takes place also in the gun and injector area. The merging of the low energy beam from the injector and the returning ERL high energy beam at the linac entrance has significant consequences to the beam dynamics of the machine.

A talk on “Emittance Compensation Theory Overview” was given by J. Rosenzweig (UCLA) concluding that the theory of emittance compensation is a powerful tool that allows one a rational design of a gun and injector for best emittance performance.

The beam merger presents a new problem, a nonlinear coupling between the longitudinal motion and transverse motion in the bending plane. This issue was discussed in “Optimal merger optics and matching to the main linac”, by V. Litvinenko (BNL). The authors offer a new approach to beam merging by devising a system with bi-lateral symmetry, the so-called “zigzag” merger. This idea provides for the first time a solution to how to merge high charge bunches into the accelerator without blowing up the bend-plane emittance. A presentation on “Space charge, CSR, and optimal merger energy”, by S. Lidia (LBNL), made in the framework of the LUX project parameters, concluded that the optimal energy is linked to reducing space charge effects in the compressor, and that CSR induced emittance growth and longitudinal instabilities considerations dominate the design of the arcs and injection lattice. For high energy machines the slice energy spread from the photoinjector beam is too small to prevent

longitudinal instability growth, and thus laser ‘heating’ techniques are useful to introduce a correlated energy spread at high frequency that acts as an uncorrelated spread at frequencies with large gain in the longitudinal CSR instability.

Given the complexity of the photoinjector physics and the large number of parameters that must be adjusted, getting an optimal performance out of this system is a daunting task. The working group participants were very encouraged by two presentations on automated optimization procedures that were developed for this purpose. The first was “Multivariate optimization of Injector Performance”, by I. Bazarov (Cornell), which described the application of a genetic algorithm and parallel computing for the optimization, noting its power and the sometimes unexpected (by simple physics intuition) optimal values for some of the parameters. The second talk was on “Multiple-parameter optimization of ERL injector”, given by R. Hajima (JAERI), a similar task using optimization with PARMELA, step-by-step optimization by down-hill simplex and all-at-once optimization by simulated annealing.

### 7.1.2.3 *The Cathode and Laser Package*

The photocathode and laser are very much related subjects, since the Quantum Efficiency (QE) of the photocathode and the wavelength at which it reaches this QE determine the power of the laser, which may or may not be realizable. The lifetime of the cathode and the vacuum quality that is necessary to achieve this lifetime are also critical considerations, since some gun systems cannot be expected to achieve the vacuum level necessary for some cathodes. A few ground rules were elucidated in the working group. First, it has been agreed that the operational wavelength of the photocathode should be in the visible window; otherwise the conversion of the laser light to shorter wavelength (UV) would present a crucial toll on the overall laser power requirements. The uniformity of the photocathode emission is also critical, since it affects the emittance of the beam. Finally, we note the emergence of a new approach to photocathodes, the diamond amplified photocathode, which was described by a few speakers. The recent experimental results obtained at BNL provide hope that this cathode system is around the corner.

A talk on the “Photocathode options and state-of-the-art”, by Srinivasan-Rao (BNL), presented the requirements from a photocathode: High, uniform QE preferably in fundamental of laser/visible; long life time-tolerant to contamination, ion bombardment; large charge deliverable; prompt response  $\sim 100$  fs electron bunch; short recovery time; operable in High Vacuum; operable in High Field; does not contaminate the injector environment; cryogenic operation; ease of preparation, transport, transfer. Srinivasan-Rao finished by describing some potential laser systems. She concluded that commercial systems are tantalizingly close to meeting a lot of the requirements, however beam shaping and stability requirements may push the parameters to beyond commercial systems, and even if commercial systems are available, project specific custom modification will be needed.

The diamond amplified photocathode system was described in detail in the talk on “Secondary emission cathodes”, by X. Chang (BNL). Following a description of the concept, he explained how it works to provide an extremely long lifetime of the cathode by encapsulation in a hermetically sealed package, how it also serves to protect the gun from the photocathode material, and the specific properties of diamond which are essential for this application, such as extremely good thermal conductivity and easy application of Negative Electron Affinity (NEA). Chang finished by presenting

experimental measurements on gain of up to a few hundreds and transmission through thick diamonds.

A new program at JAERI also embraces the diamond amplification scheme of BNL, as described in “Diamond electron cathodes”, by E. Minehara (JAERI). The speaker presented the equipment and approach taken by JAERI towards gallium arsenide (GaAs) photocathodes in extreme-high vacuum and diamond amplification systems. We heard more of the JAERI program in the talk “DC gun test bench and superlattice GaAs as photocathode”, given by T. Nishitani (JAERI). The fabrication of superlattice GaAs photocathodes is pursued using Molecular Beam Epitaxy, leading to a photocathode DC-gun which satisfies the requirement of long life-time performance. Simulations predict that a superlattice is expected to have higher QE and smaller thermal emittance than a bulk GaAs.

The discussions yielded a list of available photocathodes as a function of required current:

**Over 100 mA:**

Cs:GaAs (demonstrated 9 mA CW in a DC gun at JLab), K<sub>2</sub>CsSb (demonstrated 128 mA at 25% duty factor., in a copper RF gun at Boeing), Cs<sub>3</sub>Sb

**Over 10 mA:**

–Cs: GaAs(polarized), and Cs<sub>2</sub>Te

**Over 1 mA:**

–Metals, Dispenser cathodes

**Technologies to watch (not demonstrated in injectors yet):**

–Cs dispenser cathode, Cs:GaAsP, Cs:GaN, Diamond amplified photocathodes.

On the topic of the associated lasers for photocathodes, the “Laser State-of-the-art: Performance, Stability and Programmable Repetition Rate” was presented by M. Shinn (JLAB). Shinn presented the current laser development, which is specified to deliver ~135 pC charge/bunch, or 100 mA average current. To achieve this current, a laser with these specs is needed: Power: ~ 30 W, at 748.5 MHz, 532 nm. This assumes NEA GaAs with 1% QE @ 532 nm. Pulse-width: ~30 ps FWHM. Amplitude jitter < 0.5% p-p. Timing jitter < 1 ps rms wrt RF master oscillator. Following the description of the approach and the hardware, Shinn concluded that a drive laser system can be a reliable component of an accelerator.

The discussions on beam dynamics and beam quality stressed the need for optimal laser shape. In the past couple of years the technology of laser shaping for photoinjector applications became available. This was exemplified by H. Tomizawa (Spring-8), who reported on “Laser Pulse Shaping for Photoinjectors”. Tomizawa described an impressive system that does laser shaping in 3-D by a variety of advanced optical methods. He concluded that automatic (program driven) shaping of the spatial profile with a deformable mirror and genetic algorithm was successful, achieving either Gaussian or flat-top distributions. However, it takes 1 hour for the system to reach the optimum. He reported that when the spatial profile was improved, the gun emittance was reduced from 6 microns down to 2 microns. Automatic shaping of temporal profile was achieved, yielding rectangular pulse of 2-12 ps with rise-time of 800 fs.

The beam dynamics discussion also pointed out that tri-uniform (or “beer-can”) distributions, while they provide improved emittance over Gaussian distributions, are still not ideal. One desires distributions that have linear space-charge dependence in the bunch as well as being stationary under the beam acceleration and transport, and an

elliptical distribution comes closer to that ideal. This was emphasized in the talk on “Optimal Distributions for Photoinjector RF Guns”, by C. Limborg-Deprey (SLAC). In addition, she described a spectral control technique that exists in the IR and may be even achieved in the UV, leading to arbitrary 3-D shaping using four-gratings with masking arrays in a dispersive environment.

#### 7.1.2.4 *Modeling and Computational Issues*

The beam dynamics of the ERL photoinjector at non-negligible bunch charges is dominated by emittance compensation. Some of this work is being done towards ERL-driven X-ray FELs. Significant work has been done towards the design of an energy recovery linac with 1 MHz repetition rate at 1 nC per bunch driving a potential DESY X-ray FEL, using a superconducting RF gun. “Optimization and Beam Dynamics of an SRF Gun” was then presented by M. Ferrario (INFN). Using the Serafini – Rosenzweig invariant envelope approach and a number of simulation codes, Ferrario described a gun capable of excellent performance in terms of beam brightness. Among his points were the following: Emittance compensation by an external solenoid is possible. 60 MV/m peak field in SC cavity has been already demonstrated.

Another potential ERL based FEL was described in the talk “Conceptual design for the KEK-ERL test accelerator”, by T. Suwada (KEK). Suwada informed the workshop that a conceptual pre-injector design study for the KEK-ERL test accelerator is under development. This work is done using a new, fast simulation code. A demonstration ERL at 200-MeV is being designed.

An unorthodox approach to moderate average beam current (1 –50 mA) guns was presented in the talk “Field-Emission Cathode Gating for RF Electron Guns”, given by J. Lewellen (ANL). He compared the various photocathode options and their salient advantages and disadvantages. Lewellen then described a gun without a laser, which still produces well defined, short electron bunches emitted at the optimum phase for emission in each RF cycle. The idea is to use field emission cathode, which is capable of high current densities (and thus high brightness) from small emitters in the gun. While this idea has been contemplated before, the breakthrough in this novel approach is a particular superposition of a harmonic frequency on top of the fundamental. By a proper selection of the phase and amplitude of the harmonic relative to the fundamental, one creates a waveform that peaks at one place in a way to produce emission in for a short time in the right phase relative to the fundamental.

A comparison done in this Working Group yielded an interesting result summarized in Table 2. This table shows calculated emittances possible from the 3 types: NCRF, DC and SRF. Low thermal emittance of the cathode allows larger illuminated laser spot and consequently reduced space-charge at the cathode. Emittance compensation is efficient in all three gun types. As a result, comparable emittances at the end of the injector can be achieved despite very different electric field values in the guns.

**Table 2:** Emittance compensation simulations for 3 possible guns. Symbol key for this table: \* rms; # Compressed; + Normalized; & Material and assumed electron temperature.

	<b>Bunch Charge</b>	<b>Bunch length<sup>*#</sup></b>	<b>Emittance<sup>*+*</sup></b>	<b>Cathode<sup>&amp;</sup></b>	<b>Peak field</b>
<b>Units</b>	nC	Ps	$\mu\text{m}$	meV	MV/m
<b>RF gun</b>	1/0.2	2.8/1.7	0.72/0.3	Copper, 700	S-band, 120
<b>DC gun</b>	1/0.1	3/3	0.8/0.14	GaAs, 35	15
<b>SRF gun</b>	1/0.1	5.7/2.7	0.8/0.23	Metallic, 184	L-band, 60

### 7.1.2.5 Magnetized Beams and Polarization

Some of the future ERL applications are rather specialized and require specialized electron sources. These include polarized electrons for electron – hadron colliders and magnetized electrons for electron cooling of stored hadron beams.

The subject of “Polarized cathodes and the prospects for high current” was presented by M. Poelker (JLAB). The author posed the question as follows: “What will it take to provide 1 mA at 85% polarization?” Given that this represents an improvement of state-of-the-art by factor of 5 to 10, it is a step in the right direction, yet quite modest compared to the requirements of 30 mA for the ELIC collider, which is planned with beam circulation, and even smaller in comparison to the requirements of eRHIC, based on a few 100’s mA.

To achieve this initial step Poelker calls for good photocathode material; high power mode locked Ti-Sapphire lasers with GHz repetition rate; good gun lifetime, which call for good static vacuum ( $1 \times 10^{-11}$  Torr, using NEG’s + ion pumps); maintain the good vacuum while delivering beam; and last but not least reliable hardware: lasers, gun and diagnostics. He concludes that only superlattice photocathodes have demonstrated polarization  $> 80\%$ , and only superlattice photocathodes can (in principle) provide 1 mA with existing commercial modelocked Ti-Sapphire lasers. However, superlattice photocathodes have good initial QE but lifetime at CEBAF has not been as good as for strained GaAs, the QE falls with increasing laser power. It is clear that more experience is needed.

For scaling to even higher currents, he concluded that gun lifetime is dominated by ion back-bombardment, so it’s reasonable to assume lifetime proportional to current density. Thus the approach to higher currents is to use a large laser spot to drive the gun. This keeps the charge density small, and one may expect to enjoy the same charge density lifetime, despite higher average current operation, with existing vacuum technology.

The “Production of magnetized beams in photoinjectors”, was presented by P. Piot (FNAL). He maintains that understanding the generation of angular-momentum dominated e-beams is a first step toward understanding (and optimizing) the flat beam transformation, which has multiple applications outside an ERL such as beam production towards the ILC at FNAL and the LUX proposal at LBNL, and for ERLs

such as the RHIC e-cooling. Possible techniques for the production of angular momentum dominated beams are by the application of non-zero axial magnetic field on the cathode and ribbon laser transformed into a round beam (Derbenev transform). Piot described the work at his FNAL laboratory on the generation of angular-momentum-dominated electron beams in a photo-injector and studies of the conservation of angular momentum along the beam-line. In their case (up to  $\sim 2$  nC) the beam dynamics is dominated by angular momentum. One diagnostic approach (as well as an application) is to produce a flat beam using a quadrupole triplet. He has shown an excellent agreement of the measurements with simulations, and the production of a very nice emittance ratio of  $\varepsilon_x/\varepsilon_y=85\pm 5$ .

Another item mentioned in this presentation was a plan to test a polarized electron source injector for the ILC based on a cryogenic (but not superconducting) RF gun. FNAL's position is that a DC gun cannot provide a high enough electric field. Polarized injectors have complicated bunching scheme (being a compromise between emittance and bunch length), thus a higher field on the cathode would help. This program will be watched with a lot of interest.

### 7.1.3 Optics and Beam Transport

G. Hoffstaetter, V. Litvinenko and H. Owen

The charge of the working group on "Optics and Beam Transport" was as follows: Perform a survey of the present status of optics and beam transport issues in ERLs and make a list of unsolved problems. The ERLs to be covered include those currently in operation, currently under construction, or envisioned as a possibility for the future anywhere in the world. Special emphasis should be placed on the clear identification of the beam physics limits and accelerator technology limits and an examination of the extent that they have been addressed by past research or need to be addressed by future research. These issues should include linear optics design for the main linac section, linear optics for different ERL applications, nonlinear optics, current dependent effects like BBU and CSR, other sources of emittance growth, halo development and collimation, instrumentation and commissioning techniques. Identify new and promising ideas even though they may need additional work. Finally, the group should summarize in a brief report the highest priority research topics for beam transport in ERLs and provide a list of key experiments and R&D developments.

Electron average currents of 100 mA or more are envisioned, with a good emittance of sub micron (normalized RMS) at the lower current to a few microns at the higher current. Certain applications will require magnetized electron beams or very high charge, lower repetition rate bunches, in which case the emittance can go up another order of magnitude.

#### 7.1.3.1 Ongoing ERL projects

The ERL projects that were developed in recent years worldwide fall into four classes: ERL-FELs, Light sources, Electron coolers, and Colliding beam accelerators.

**ERL-FELs:** The only ERLs in operation provide beams for Free Electron Lasers (FELs). A 10kW light beam has been produced at JLAB, more than 2kW have been produced at JAERI, both using superconducting RF systems. At Novosibirsk an ERL-FEL has been constructed with normal conducting cavities. Under planning at BNL is

an ERL-FEL to be used as the driver laser for the photocathode of the eRHIC linac-ring collider, and finally Hutton from JLAB presented the proposal of the push-pull FEL where two linacs are used, one recovering the energy of the beam that the other has accelerated and vice versa.

**ERL-Light sources:** Several laboratories have proposed high power ERLs for the production of high brightness electromagnetic radiation. Accelerators for different parameter sets and various applications are being worked on by Cornell University, Daresbury, Argonne National Laboratory, Novosibirsk, and KEK. All of these projects had representations at the 2005 ERL workshop. Further there is a project at Saclay and projects had been worked on at BNL and at the University of Erlangen. The Cornell and the Argonne proposals are upgrades to existing light sources.

**Electron Cooling:** The electron cooler that BNL is currently developing for cooling of the ion emittances in RHIC is based on an ERL. Nagaitsev (FNAL) presented the DC electron cooler for the Recycler at FNAL since it recovers the electron energy, albeit not in a linac but in a constant voltage Pelletron, which just recently demonstrated first high energy electron cooling results.

**Nuclear physics ERLs:** JLAB has incorporated an ERL into its design of an electron-ion collider (EIC) for medium energy physics. One version of the eRHIC collider, that is to collide 10GeV electrons with the polarized protons and ions in RHIC is also based on an ERL.

#### 7.1.3.2 *Emittance Growth*

When ERLs provide ultra low emittances in the sub 1~mm-mrad range for insertion devices that are located in the ERL's return loop, the incoherent radiation in these bends can lead to significant emittance increase. In the Cornell ERL design this emittance increase is about 100% for the ultra low initial emittance of 0.1~mm~mrad. It is therefore desirable to equip the return loop with lattices that provide for very little emittance increase. The lattices of ultra low emittance storage ring ideas are good candidates for such designs.

One such lattice was presented by Borland (ANL) which uses very strong permanent magnets with superimposed multipoles and correction coils to produce a very small dispersion in bends. The quadrupoles are very strong but not so high as to be obviously impossible. However, the dynamical aperture is as of yet far too small to be feasible. Furthermore there may be stability and radiation protection issues with permanent magnets. However, such strategies would be useful to limit emittance growth when ultra low emittances from an ERL should be transported for one turn around a return loop. The list of other contributors to emittance growth contains alignment errors, coupler kicks in the linac, wake fields, ion accumulation, space-charge effects, and coherent synchrotron radiation.

#### 7.1.3.3 *Stability Issues*

Third generation storage rings have reduced their emittances and therefore beam-sizes very successfully in recent years. Due to vertical beam sizes of only several micrometers, the stability requirements for these facilities are very strict. Boege (PSI) reported that the tolerable orbit jitter within insertion devices is only 1  $\mu\text{m}$  at the SLS. If ERLs are to be used as x-ray sources, similar stability requirements will apply, since the beams in these sources have similar dimensions, not only in the vertical, but additionally in the horizontal direction. The electron beam that the JLAB linac supplies

to its Nuclear Physics users also has to be very stable. A stabilization of routinely to  $10\mu\text{m}$  has been reported by Lebedev. Improvements of the feedback system could however lead to stability of about  $1\mu\text{m}$ . This has not been tested however, since such stability has not been required for this facility. Furthermore, while the stability at the CEBAF end-stations has been achieved, the electron beam might have significantly less stability in the recirculating linac itself. However, the stability that can be routinely achieved at the end-station should be reproducible at most locations of the accelerator. For a light source with its many insertion devices, beam stability has to be guaranteed at nearly all of the return loop. Since transverse beam oscillation stability is an essential requirement for a future X-ray beam, studies should be initiated that show that the stability requirements can be met.

#### 7.1.3.4 *Longitudinal Phase Space Manipulations*

In contrast to storage rings, the bunch length that ERLs can provide is quite flexible and can be below 100fs. For FEL applications, a very high peak current and therefore a short bunchlength is needed. Some light source applications require very short bunches to provide high time resolution in pump probe experiments. However, short bunches should be avoided within the linac to reduce higher order mode (HOM) heating. Longitudinal optics manipulations are therefore needed to obtain short pulses in the ERL return loop where the undulators are located.

Longitudinal phase space manipulation uses bends as bunch compressors, or at low energy it uses drift spaces and the fact that particles with different velocities have different speeds. Hajima (JAERI) reported that even for a high energy ERL, velocity bunching in the linac can be applied so that the bunch leaves the linac with sub-ps length. Since the residual energy spread after velocity bunching can be smaller than the correlated energy spread required for magnetic compression through a recirculating loop, velocity bunching is useful to realize short pulse and high brightness X-ray ERLs where the current is low enough so that HOM heating is not limiting.

#### 7.1.3.5 *BBU instability and linac optics*

One important limitation to the current that can be accelerated in ERLs or recirculating linear accelerators in general is the multipass beam-breakup (BBU) instability. One and two-dimensional models of BBU, developed by Bisognano, Hoffstaetter and Bazarov, Pozdeyev and Yunn, were discussed along with the respective approximations and regimes of validity.

Collaboration between JLAB and Cornell University has led to a comparison of beam-breakup measurements carried out at the JLAB FEL and computer simulations. These experimental studies were presented by Pozdeyev (JLAB) and the conclusion is that beam breakup can be modeled reasonably well, considering that the optics of the accelerator had not been measured with high precision.

Concepts and experience with BBU suppression techniques were reported by Tennant (JLAB). Several methods were described including an active feedback on BBU, where transverse oscillations are measured at one location and minimized by a kicker at another location in the ERL. Figure 1 summarizes the various BBU suppression techniques that have been tried at the JLAB FEL.

Computer codes to determine the threshold current have been developed at several labs. These codes fall into two classes. Those in the first class perform tracking of

charged bunches with transverse oscillations and find the current above which beam oscillations grow exponentially. The second class of codes is based on the numerical solution of a dispersion relation derived by summing up analytically the excited HOM fields in the cavity. Sawamura (JAERI) presented a comparison of all existing BBU codes, and concluded that they all agree remarkably well for cases where they are mutually applicable. While work on stabilizing BBU and optimizations of optics for large threshold currents is to be encouraged, the state of codes is quite satisfactory already. However, it should be noted that the optics at the lower energy sections of the ERL determines the BBU threshold most strongly. At low energies the cavity focusing is most relevant and therefore has to be understood completely. Currently computed and measured optics within low energy cavities do not seem to agree sufficiently well.

		Effect on 2106 MHz HOM	Considerations for Implementation
Q-Damping	Damping Circuit	$5 \times I_{th}$	<ul style="list-style-type: none"> <li>• Works for only 1 mode per cavity</li> <li>• Not as effective at raising the threshold as beam optical methods</li> <li>• Long term stability of system</li> <li>• Does <b>not</b> effect beam optics</li> </ul>
	3-Stub Tuner	$1.5 \times I_{th}$	
Beam Optics	Phase Trombone	<i>Stabilized</i>	<ul style="list-style-type: none"> <li>• Can stabilize the mode against BBU</li> <li>• What are the effects on other HOMs?</li> <li>• Do they prevent reaching the requirements needed for a suitable lasing configuration?</li> </ul>
	Pseudo-Reflector	<i>Stabilized</i>	

**Figure 1:** Summary of BBU suppression techniques tested at the JLAB FEL.

#### 7.1.3.6 Accelerator modeling

In high energy and nuclear physics accelerators as well as in light source facilities, accelerator modeling has developed to a very high level in recent years. Programs are available that perform optics simulations to various degrees of accuracy, simulate orbit and magnetic field errors, and take into account various beam dynamics effects like coherent synchrotron radiation and space-charge forces. Some of these accelerators have control systems that are closely connected to the accelerator modeling software. A similar step has been taken for the JLAB FEL-ERL, where the simulation program that controls CESR at Cornell University developed by Sagan (Cornell) has been adopted to automatically read out the accelerator state of the FEL and to simulate its optics, and its beam breakup instability current. Beam position data measured at the ERL-FEL are used to refine the optics model and consistency checks allow to locate monitor errors. With this model of the coupled optics, high precision beam breakup instability studies including the polarization direction of each HOM become possible.

#### 7.1.3.7 Merger Design

Every ERL needs a merger between the injection linac and the ERL, and each project has its own proposal. These proposals fall into two classes: A three bend

achromat that puts the injector linac at an angle with the ERL as presented by Hajima (JAERI), and a four bend achromat, also referred to the “zigzag” merger, which puts the injection linac in line with the ERL, presented by Litvinenko (BNL). The four bend achromat has the advantage that it is not only achromatic but compensates the part of the phase space focusing that is linear in the longitudinal coordinate. The space-charge driven emittance increase is therefore reported to be significantly smaller in this layout. Since the four bend merger requires the injector to be in line with the ERL, it is hard to bring the high energy beam into the linac without infringing on the injector linac. Further analysis is needed to decide which merger design is best for each proposed ERL application.

#### 7.1.3.8 *Halo formation*

The formation of a large amplitude beam halo in a high current ERL poses several severe problems. It can create dark current, it can radiate, activate and heat material, notably superconducting structures, it can lead to background radiation in the experiments, and it can produce emittance dilution. Fedotov (BNL) presented mechanisms that lead to halo formation in hadron beams and analyzed these mechanisms that will also apply to electron ERLs. It is pointed out that in ERLs there are two different regions. The first contains the photo injector where the beam is initially fully space-charge dominated, but resonances which for proton beams lead to halo formation do not have time to build up due to rapid acceleration. An effect that remains in this region is the dynamics due to nonlinear time dependent RF fields. The second region contains the rest of the ERL which has emittance dominated beam dynamics, where halo formation is usually small. But for the high beam densities of a ultra low emittance beam, Coulomb scattering becomes relevant. This leads to particle loss in the energy phase space due to single and multiple scattering events, i.e. the Touschek effect and intra beam scattering. Furthermore the nonlinear forces from coherent synchrotron radiation could transport particles to large amplitudes. This field of halo formation due to beam dynamics clearly needs more study. Other sources of beam halo, not related to beam dynamics include a defocused laser spot on the cathode due to light scattering in the laser optics or diffusion of electrons in the cathode's conduction band. Experiments and analysis are needed here in collaboration with laboratories that operate photo-cathode sources.

#### 7.1.3.9 *Space charge and CSR Modeling*

Although space-charge effects are strongest in the source and injector region, longitudinal space charge (LSC) can be important up to energies of many 10MeV and it is therefore an effect that should be understood in existing FELs and should be analyzed for every new design.

Coherent synchrotron radiation is an effect that also stems from the charge distribution of the bunch and is therefore a form of space charge. Accurate computer codes should therefore take both effects into account. Borland (ANL) presented simulations of CSR for a bunch that travels from an ERL once around the APS and can lead to even stronger CSR effects, resulting in a folded longitudinal distribution and in the appearance of charge lumps. It seems likely that if the initial phase space were not Gaussian, much more serious effects would arise, including the micro-bunching instability.

Coherent synchrotron radiation has been a field of intense study in recent years

since bunch compressors for FEL and SASE FEL projects require very short bunches which can produce a destructive amount of coherent synchrotron radiation. Comparison of the energy loss and the energy spread as well as the transverse emittance growth after a bunch compressor for different codes was presented by Kabel (SLAC) and showed that the agreement is very reasonable, considering that all codes use very different formalisms and approximations. However, since the approximations are either very severe, or only very few particles are used to create the CSR fields, work on more accurate computational tools would still be very welcome.

#### 7.1.3.10 *Collaborations*

Since the many laboratories mentioned are working on ERL projects, a strong synergy of collaborations can be expected. Holder (Daresbury) reported on the EUROFEL collaboration, some aspects of which can inspire collaboration on ERL-related issues.

As a start of collaboration on optics and beam transport in ERLs one can mention the JLAB/Cornell work on BBU, and the preparation of articles for the ERL05 workshop. The following papers were prepared as a multi-lab collaboration, rather than as individual contributions corresponding to individual talks: on the optics of different ERL projects, on BBU theory and observations, on all major CSR codes, and on ion clearing in ERLs. For light-source ERLs ion gaps are problematic since users want to avoid gaps in the beam and since problematic transient RF effects in the main linac, the injector linac, and the electron source can have adverse effects on beam and operation.

#### 7.1.3.11 *Summary of Recommended Studies*

The working group on "Optics and Beam transport" encouraged further research in the following initial areas:

- Transverse beam stability
- Beam loss and halo formation in ERLs
- CSR and LSC suppressing designs
- Completion of Beam-breakup instability tests
- Ion clearing in ERLs
- Experimental verification of RF optics
- Studies of limits to multi turn ERLs

### 7.1.4 **Superconducting RF and RF Control**

M. Liepe, J. Knobloch and M. Dykes

One of the major components of an ERL is the SRF sections in the injector and the main linac, providing an energy gain of up to a few GeV. The parameter space for the main linac RF is given in Table 3, showing that ERLs are pushing the envelope in many respects. Major challenges for the superconducting (s.c.) cavity modules include among others emittance preservation of a high current beam, strong Higher-Order-Mode (HOM) damping, CW cavity operation with high cryogenic losses, and high required field stability. In addition, efficient linac operation is essential for large scale ERLs.

**Table 3:** Typical main linac parameters of existing and planned ERLs

Parameter	Min. value	Max. value
Linac energy [GeV]	0.02	10
Average current [mA]	10	1000
Bunch charge [nC]	0.01	20
Bunch length [ps]	2	100
Cavity frequency [MHz]	0.7	1.5
Cells per cavity	5	9
Acc. gradient [MV/m]	12	20
Unloaded $Q_0$	$8 \times 10^9$	$2 \times 10^{10}$
Loaded $Q_L$	$2 \times 10^7$	$1 \times 10^8$
HOM power per cavity [W]	10	> 1000
HOM spectrum, 95% upper freq. [GHz]	1	> 50
Ave/peak RF power per cavity [kW]	0.5/1	25/50
rms amplitude / phase stability	$10^{-3} / 0.1^0$	$10^{-4} / 0.02^0$

#### 7.1.4.1 *Superconducting Modules for ERLs*

Superconducting modules specifically designed from scratch for ERL applications have not been built so far. However, numerous modules, some operating CW, have been developed for other applications. In many cases these may serve as a useful starting point for ERL-module development, the required modifications being dependent on the specific application. Among the issues that must be addressed are:

- CW operation resulting in fairly high dynamic heat loads
- High-current operation and the resultant large HOM power that must be extracted to limit the cryogenic load and to ensure stable beam conditions
- Small bandwidth operation (little net beam loading), which makes the cavity operation particularly susceptible to microphonic detuning.

Currently existing superconducting modules, or modules that are presently under construction include:

- CEBAF style modules developed by TJNAF
- The 100 mA injector cryomodule presently under construction for the TJNAF FEL
- The Electron-Cooler module developed by Brookhaven National Laboratory
- ELBE module developed by FZ Rossendorf
- The TTF module developed by the TESLA Collaboration
- The 100 mA injector cryomodule presently under construction for the Cornell ERL

#### 7.1.4.2 *Cavity Designs for ERLs*

The cavity design for ERLs is driven by two considerations. First, ERLs accelerate, almost by definition, high currents with designs planned all the way up to 1 A. Thus, efficiently extracting HOMs is essential to avoid beam instabilities and excessive cryogenic loading. Secondly, dynamic losses from the accelerating cavity mode to the helium bath are also of great importance because ERLs operate CW. This becomes

particularly important for GeV class ERLs. The following is a discussion of some of the parameters that impact the above considerations.

### **Cavity frequency**

The main  $\beta=1$  SRF systems that are available or are being planned operate at 1.5 GHz (CEBAF), 1.3 GHz (TESLA, Cornell ERL), 750 MHz (CEBAF injector), 704 MHz (BNL) and 500 MHz (Cornell, KEK). There are multiple considerations that enter the choice of frequency, including: An upper bound on the frequency is given by the need to limit the amount of HOM power being excited. This favors lower frequency systems. A lower bound on the frequency is given by the fact that the total losses eventually are dominated by the temperature independent residual losses. Given the present level of technology, 700 MHz cavities represent a lower bound for the frequency of ERL cavities; this is sufficient to realize ampere-class ERLs.

### **Number of cells and cell-to-cell coupling**

The number of cells and the cell-to-cell coupling is primarily determined by the requirement that the HOMs be extracted efficiently. In particular for 1 A class machines, external Q factors of order  $10^4$  or lower must be achieved. This favors a small number of cells and a large iris radius. In conclusion, Ampere-class machines such as the BNL electron cooler use fewer (5) cells with a larger iris, whereas lower current machines can employ seven or even nine cells, with a smaller iris.

### **Cavity shape**

Much optimization is achieved through the design of the cavity shape. In the recent years, several new cell designs have been proposed, optimized for various applications. Optimization goals include low magnetic surface fields, low cryogenic losses, strong HOM damping, or low loss factors. Some of these objectives are mutually exclusive. Since the required gradients of 15-20 MV/m are moderate by present day standards, the overriding design criteria are HOM power generation/extraction (for high current) and cryogenic losses (for CW operation).

#### *7.1.4.3 Cavity Quality*

Since ERLs operate CW, the operating gradient is primarily limited by the cryogenic load, especially for larger machines. Even if high  $Q_0$  values can be achieved, operation at the state-of-the-art gradient limit (about 35 MV/m for TESLA cavities) is not an option for ERLs. Rather, the primary focus is on improving the cavity quality at lower gradient, typically in the range 15-20 MV/m. A number of factors can impact the achievable  $Q_0$  and include material, cavity preparation and magnetic shielding.

#### *7.1.4.4 HOM Damping*

Future ERLs will operate with high currents up to 1 A, thus making strong Higher-Order-Mode (HOM) damping essential. Requirements on the damping of monopole and dipole modes result from the following effects:

- The average monopole HOM power per cavity is proportional to the longitudinal loss factor of the cavity, and is also proportional to the beam current and bunch charge. This power is significant in high current ERLs (of the order of hundreds of W to several kW), and thus needs to be intercepted at a well controlled point with

good cooling efficiency. Since the longitudinal loss factor is proportional to  $1/(\text{iris radius})^2$ , 1 A ERLs use cavity frequencies below 1 GHz.

- If a beam spectrum frequency lines up with a monopole HOM frequency, resonant mode excitation occurs. For high currents the power deposited in the HOM can be very large, unless the mode has a low quality factor. This effect might be the most demanding on HOM damping for high current ERLs.

- Dipole modes can cause beam-break-up (BBU) instability, if not sufficiently damped. The BBU threshold is proportional to  $1/(R/Q \times Q)$ , so again strong HOM damping is required to push the threshold above the operating beam current.

Several methods for HOM damping have been developed and used in the past. Lower frequency modes (below some GHz) can efficiently be damped by HOM coaxial couplers. However, this type of damping does not work at high frequencies. High frequency and broadband HOM absorption is achieved by ring absorbers in the beam pipe, where the beam pipe diameter is enlarged (e.g. KEKB cavity, Cornell ERL, BNL ERL) or a fluted beam pipe (e.g. CESR cavity) is used to propagate all potential dangerous HOMs to the absorber down the beam pipe. Broadband damping is also achieved by means of waveguide HOM couplers (e.g. CEBAF cavity) and a beam pipe coaxial design (e.g. KEKB crab cavities). In all broadband damping concepts, the HOM power is absorbed by RF lossy materials. These materials are usually placed at a temperature between about 70 K and 300 K for good cooling efficiency. Detailed studies have been done to measure the RF properties of the materials over a wide frequency range and at cryogenic temperatures. Simulations have become a powerful tool in designing HOM damping for SRF cavities. Three-dimensional models allow studying HOMs and their damping in detail. The two 100 mA ERL injectors presently under construction will provide valuable opportunity to cross-check these simulations with reality.

#### 7.1.4.5 *Microphonics*

“Microphonics” refers to the detuning of an RF cavity by external sources like ground vibrations or LHe bath pressure fluctuation. These vibration sources can couple to the cavity via multiple paths. When a vibration source frequency lines up with a mechanical resonance of a cavity, particularly strong microphonics can occur.

Maintaining low cavity microphonic levels is of the utmost importance for an ERL. The main linac cavities have virtually zero beam-loading, and so for efficient cavity operation they should be operated at a very high loaded quality factor  $Q_L$ .

In the past only limited effort has been made in measuring microphonics, understanding its sources, and improving the mechanical design of the cavities and cryostat to minimize microphonics. Although proof-of-principles for low microphonics SRF cryomodules exists, with a peak detuning below 10 Hz appearing realistic, the fluctuation in microphonics level from cavity to cavity as well as temporal changes in the microphonics amplitude need to be investigated in much greater detail on large SRF installations. Likewise the sources of microphonics as well as their coupling to the cavities should be studied in more detail. This knowledge would allow improving the mechanical design of the cryostat and the cavities for lower microphonic levels in future SRF installations. A further open question is how much microphonics is correlated between cavities within a single cryomodule and between cryomodules in a large SRF machine.

Besides designing the cryomodule for minimal microphonics, a further reduction in microphonics amplitude could potentially be achieved with active control schemes, making use of a fast frequency tuner. Initial studies have shown promising results. However, active microphonics compensation is challenging, and must be supported by a good mechanical design of the cavity and its surrounding hardware.

In conclusion, low microphonics amplitudes have been demonstrated in real machine environments giving an optimal loaded  $Q_L$  of above  $5 \times 10^7$ . Further reduction of microphonics by active and passive damping schemes appears feasible.

#### 7.1.4.6 *Frequency Tuner*

Because of the small bandwidth of ERL main linac cavities, fine frequency control and good frequency stability are mandatory. The frequency tuner needs to provide sufficiently fine resolution ( $<1$  Hz), small backlash, and high stiffness. Several cavity frequency tuner have been developed over the last years. These existing and tested tuner designs can be adopted for ERLs, possibly with minor modifications.

All recent tuner designs have integrated fast frequency tuners (piezo-actuated or magnetostrictive) for fine and fast frequency control. This feature in principle allows to compensate cavity microphonics, however the required control algorithms are quite complex and only first steps in developing a controller have been demonstrated.

#### 7.1.4.7 *RF Control*

All ERLs require very stable RF fields, and ERL light sources will require the highest field stability, of the order of  $10^{-4}$  in relative amplitude and well below  $0.1^0$  in phase. This alone is challenging, and is made even more demanding by the fact that the superconducting cavities in an ERL need to be operated with a high loaded  $Q_L$  of several  $10^7$ , possibly up to  $10^8$ , for efficient operation.

This combination is challenging for the Low-Level RF (LLRF) systems for several reasons. Two ERL-specific LLRF challenges that need to be addressed are: (1) the compensation of the varying beam loading, and (2) the operation at highest loaded  $Q_L$ . The latter challenge has been studied in detail at the TJNAF FEL in collaboration between LEPP and Jefferson Lab. In a proof-of-principle experiment, Cornell's newly developed digital LLRF system has been connected to one of the FEL 7-cell cavities. With this LLRF system, excellent field stability was achieved with 5 mA beam current in energy recovery mode at loaded  $Q_L$  of about  $10^8$ . Less than 500 W of driving RF power was required for operation at a gradient of 12.3 MV/m. No dependence of the field stability on beam current (0 to 5.5 mA) and off-crest angle (between  $-40^\circ$  and  $+40^\circ$ ) was found. Even at this high loaded  $Q_L$  the cavity operated very reliably over several hours without any trips. Piezo-tuner based frequency control proved to be very effective in keeping the cavity on resonance during cavity filling. This proof-of-principle test demonstrates that no fundamental limit prohibits the cavity operation at a loaded  $Q_L$  of  $10^8$  and that high field stability is achievable at the same time. It is desirable to repeat this test with a higher beam current to fully study the impact of random beam loading in the ERL main linac cavities. Also, it is important to realize, that the required tight phase stability needs to be supported by a sufficiently stable reference RF signal generation and distribution.

#### 7.1.4.8 *Input Couplers*

The obvious purpose of couplers is to provide means of transferring power from a generator to a superconducting cavity. However, the first criteria for designing couplers are that they do not compromise the performance of the cavities they are connected to, and that they shall not negatively affect the beam. For a low energy, small emittance beam this can result in the requirement that transverse on-beam-axis field must be avoided. Asymmetric input couplers can cause time dependent kick fields, which will result in emittance growth. Main features of an input coupler are that it must provide appropriate transmission to the cavity, support of large thermal gradients and high RF power handling without transferring large amounts of heat to the cryogenic environment, and one or more vacuum barriers to atmospheric pressure. Simulations have become one of the most important tools in predicting the complex behaviors of couplers and have enormously improved reliability and shortened the time necessary to achieve successful design solutions. Such simulations include mechanical, thermal, electromagnetic, and multipacting studies.

A controversial question is whether adjustable coupling is required. Adjustability is desirable for flexibility, but it increases the complexity of the coupler, and within some limits the coupling can also be changed by means of waveguide stub-tuners. For high energy ERLs, the cost of the input couplers becomes a critical issue, and improvements in both complexity and reliability are highly desirable.

#### 7.1.4.9 *RF Power Sources*

ERLs require a large number of RF power sources. GeV scale machines have several hundreds of cavities, and each cavity is driven by its own power source. The one-source-per-cavity concept is essential, because the high loaded Q of the cavities prohibits vector sum control of multiple cavities; microphonics would cause intolerable large fluctuations of the individual fields in case of vector sum control. Requirements for the RF power sources include high efficiency, reliability and long lifetime, low pushing factors, and reasonable price. High linearity and high efficiency over the full output power range is also desirable. Two different types of RF power sources used in ERLs, klystrons and Inductive Output Tubes (IOTs), and their advantages and disadvantages were debated.

#### 7.1.4.10 *Cryogenics*

Since ERLs operate CW, the dynamic heat load from the cavities is very significant. A GeV scale ERL, if operated at 2 K, has a heat load of several kW, resulting in a cryoplant power consumption in the order of several MW. Obviously, minimizing the cryoplant power consumption becomes essential for these ERLs. This can be done by optimizing the cell shape, and by operating the cavities below 2 K. However, the latter only works for cavities with low residual surface resistance. Obviously, special care has to be taken in cavity preparation and cryomodule design (low residual magnetic fields) to achieve this. Operation below 2 K needs to be considered carefully, as it has potential impact on the cryomodule design itself as well as the cryoplant. Operation below 1.8 K needs further studies, since instabilities might occur. In any case, the design of a cryoplant should always include at least 50% overhead on all expected loads.

#### 7.1.4.11 *Injector Cryomodules*

In an ERL, the injector cryomodule needs to accelerate a “soft” low energy beam from an electron source while preserving its emittance. The energy gain in the injector RF should be high enough to make it suitable for injection into a main linac of an ERL, but low enough to avoid unnecessary waste of power. Note that the energy in the injector is not recovered. Typically the required energy gain in the injector RF is in the range 5 to 10 MeV. The two major challenges which need to be addressed especially in the injector modules are:

- Significant amount of RF power needs to be transferred to the beam. This requires high power handling by the input couplers, and usually results in short cavities (one to two cells) to limit the power per coupler.

- Optimization for emittance preservation is critical if very small emittance is required, e.g. in the Cornell ERL. This requires good HOM damping and very low transverse kick fields from beam pipe asymmetries and couplers.

These required features usually make the injector RF modules different from main linac ones. In other respects the requirements on the injector cryomodules are similar or relaxed in comparison to the main linac cryomodules. This often includes HOM damping, microphonics and tuner resolution, field control and cryogenic loads. Two major projects are underway to develop special ERL injector modules for high current beams: the 100 mA injector for the TJNAF FEL, and the 100 mA injector for the Cornell ERL. The experience from these projects will also be very valuable in designing future cryomodules for ERL main linacs.

#### 7.1.4.12 *Transfer to Industry*

Only a small number of laboratories or institutes have the infrastructure and personnel to assemble whole SRF cryomodules, e.g. DESY and TJNAF. It is therefore likely, that industry will increasingly be asked in the near future to provide large sub-assemblies of SRF cryomodules or whole modules. Different approaches can be envisioned for this, and have successfully been applied to other large-scale productions by industry for particle accelerators:

- Use of industry as job-shops or service supplier. In this case the required R&D and the design and performance risks remain by the laboratories or institutes. This approach is usually chosen for small quantities.

- Prototypes are developed by the laboratories or institutes, or jointly with industry. The established procedure and designs are then transferred to industry. The production is done in strong interaction with the laboratories or institutes, and the design and performance risks remains by the laboratories or institutes. The responsibility for faultless assembly is however with the vendors. A bonus might be offered, if certain performance specifications are surpassed.

- Prototypes are developed by the laboratories or institutes, or jointly with industry. The established procedure and designs are then transferred to industry. Production is done by industry with guaranteed performance specifications. In this approach, proof by the laboratories or institutes that procedures are mature is necessary to enable industry to give guarantee for performance. This proof can mean significant effort, including the production and tests of complete SRF cryomodules.

- Prototypes are developed by industry. Production is done by industry with guaranteed performance specifications.

Obviously, each of these approaches has significant impact on cost, which needs to be evaluated carefully for each individual project.

### 7.1.5 Synchronization, Diagnostics and Instrumentation

A. P. Freyberger and G. A. Krafft

Working Group 4 dealt with the challenging topic of beam diagnostics for ERL machines. Energy Recovery Linacs represent a challenge for beam diagnostics from several perspectives: invasive versus non-invasive diagnostics, longitudinal and transverse beam diagnostics, overall machine timing/synchronization and machine protection. Beam diagnostics for an ERL can benefit strongly from the experience at third generation light sources, recirculating linacs and presently operating ERLs. During the workshop there were presentations from all these communities, representing a large range operation experience in beam diagnostics.

The range of parameters for the different ERLs proposed or in operation is quite large and shown in Table 4.

**Table 4:** Table summarizing the beam property ranges for existing and proposed ERLs

Beam Property	Range
Current	$10^{-5} < I_{\text{beam}} < 1$ Amp
Emittance	$0.1 < \varepsilon < 30$ mm-mrad
Bunch Length	$0.1 < T_{\text{bunch}} < 100$ psec
Energy Spread	$1 < \sigma_E < 1000$ keV
Timing	$0.01 < t < 1$ psec
Beam Loss	Fractional loss $< 10^{-6}$
Position Stability	$< \mu\text{m}$

The Working Group presentations were grouped according to beam properties and this summary continues that grouping. First the transverse beam diagnostics are summarized followed by the longitudinal beam diagnostics. Within these two communities there is a strong effort on migrating from invasive techniques to non-invasive techniques that will allow for continuous monitoring of these properties. A summary of the machine timing and synchronization section follows. Improvements in timing and its distribution have implications for other diagnostics and systems notably the RF controls. The following two sections summarize the present status of beam position measurements and feedback and machine protection.

#### 7.1.5.1 Transverse Beam Profile

Measurement of the transverse beam profile is usually done in an evasive manner. Evasive techniques include wire scanners, beam viewers, optical transition radiation monitors. These techniques will work for most ERL applications however they do not provide continuous monitoring and in most cases cannot perform the measurement with the beam at full power. The discussion focused on non-invasive techniques. Lumpkin (ANL) summarized the many non-invasive techniques used at the Advanced Photon Source. Of the several interesting developments he showed, the most exciting were the new results using diffractive transition radiation to measure the beam profile. The

radiation is produced by the insertion of a metal edge near  $[\sim 10\sigma]$  the beam and the optical portion of the emitted radiation is easily observed on a CCD camera. Impedance budget and protection from high power beam strikes are a concern with such a monitor.

Synchrotron light in the optical portion of the spectrum is a convenient non-invasive beam monitor. In order to measure transverse beam sizes below the diffractive limit, interferometry is used. The synchrotron light interferometers at Jefferson Lab were presented by A. Freyberger (JLAB). These devices are based on those built by Mitsuhashi (KEK). The transverse beam size is related to the visibility of the interference pattern, and a minimum spot resolution of  $5\ \mu\text{m}$  can be achieved with a very good CCD camera. The JLAB interferometers have been used very successfully to continuously monitor the energy spread during nuclear physics experiments and are fully integrated into the machine operation.

#### 7.1.5.2 *Longitudinal Beam Profile*

During this workshop a substantial portion of the time was devoted towards discussing various methods of determining the longitudinal distribution of the bunch, or more generally the longitudinal phase space of the bunch. The techniques were largely taken from present thinking about such diagnostics from the X-ray laser community with one notable exception that is discussed below.

The electro-optic method of determining the beam time profile was discussed by Loos. The present resolution of such measurements is around 300 fsec, depending to some extent on the beam energy. This technique can also be used to determine the arrival time at the level of 30 fsec. Its principal strengths are that the measurement is nondestructive and can measure single high charge bunches. For example, at even 100 pC and 50 MeV electron beam energy, a 600 fsec FWHM bunch may be analyzed. Different crystals than are standard now may lead to improved performance in the future, and many labs are now involved in the development of electro-optic longitudinal profile diagnostics.

Longitudinal phase space tomography was discussed as a method to obtain a more complete longitudinal phase space distribution. In this method the phase space is projected on various different axes of the phase space and reconstructed using mathematical techniques already highly developed in the medical imaging field. The present resolution of the techniques is about 100 fsec in time and 3 keV (@ 100 MeV) in energy, depending in detail on the resolution of the energy spectrometer. A principal shortcoming of this technique is that it assumes, and hence requires, beam stability over the multiple shots used to make the various projections. Implementation made so far has been destructive to normal beam operation. A variant of this idea, used at Stanford to obtain detailed time profiles, is to adjust  $R_{56}$  in a bunching region and the offset phase in an accelerating cavity so the total longitudinal transfer matrix to the point where an image is made is as in a transverse focal point. Under this condition the image is completely independent of any initial energy spread in the longitudinal phase distribution.

Zero phasing profile measurements, either with a longitudinal cavity as performed at Jefferson Lab and BNL, or with a deflecting cavity as performed at SLAC, are highly destructive but offer high resolution of order 10 fsec. If the deflecting cavity method is combined with energy analysis in the plane transverse to the deflection direction, a detailed phase space distribution may be obtained simply by optical analysis of beam images produced with either transition radiation or electroluminescent viewers.

An idea extensively discussed was a way to make the destructive methods of beam analysis almost nondestructive. In an ERL with an RF CW electron beam it is possible to occasionally, that is with low duty factor, deflect a small portion of the beam off the beamline for detailed measurement. One operates under the assumption, probably good for a CW ERL, that the beam properties being measured in the deflected beam are not appreciably changed by the deflection method used and reflect the beam properties of the high duty factor undeflected portion of the electron beam in detail.

Another beam diagnostic method presented by Krafft (JLAB) is to measure the beam longitudinal transfer function. While not giving data that can easily be turned into a longitudinal bunch distribution, this device is quite useful for determining that the RF elements that are responsible for bunching are properly set. It also allows, given that a properly characterized bunching program has been achieved previously, a means to rapidly return machine conditions to its proper state. Such devices are particularly useful during the commissioning and operations phase at an operating accelerator. Such phase transfer devices have evolved into the major longitudinal dynamics diagnostic at each of the Jefferson Lab recirculated linacs.

### 7.1.5.3 *Machine Timing and Synchronization*

There are two separate, but related, issues that were discussed about machine synchronization for ERLs by Simrock (DESY). The broader of the two issues regards distributing synchronized master reference signals over substantial (of order 1 km) distances with timing errors at the level of 10 fsec. The narrower of the two issues, regards the accuracy with which one may then lock a local control system, for example the phase of an RF voltage in a cavity, to one of these stabilized reference systems. As a subset of the second class of issues one has locking laser pulses to master references at the level of tens of fsec, which is related to how precisely the beam pulses are locked to the rest of the RF systems in the extended linac.

In dealing with all of these issues much work has been accomplished as a result of work from the X-ray laser community, and it became clear during the conference that many of the solutions proposed there could be beneficially applied to ERLs. For example, if one needs a mode-locked laser as the source of electrons in an ERL beam, it makes sense to derive the laser pulses from a very high precision Optical Master Oscillator. The resolution of such clocks these days is about 50 fsec now, and should be of order 10 fsec in a few years as a result of development work for X-ray lasers (presentation by Ilday). Present examples have low noise above 10 kHz as free-running laser, and can be locked to a microwave, or other, oscillator for long term stability. Similarly, all-optical absolute clocks were discussed with 45 attosecond (rms) stability when integrated from mHz to 10 MHz (presentation by Winter). Possibly they can be developed with timing precision about 1000 times better than the best microwave oscillators, eliminating the need for a more traditional microwave master oscillator. If such devices as photocathode sources can be accomplished, then the lion's share of the rest of the synchronization problem reduces to the problem of distributing synchronization signals properly.

One of the nice features of the all-optical clock is that it supports absolute synchronization of signals at widely separated stations. For example, if the time difference between outgoing and reflected pulses on an optical fiber were continuously monitored by autocorrelation techniques and corrected to high precision, then the pulses arriving at the far end of the fiber can be absolutely synchronized as long as any time

delay mechanism experienced by the pulses happen in traversing both directions on the fiber. Presumably a complete accelerator installation would consist of several stations absolutely synchronized, which act to distribute master signals over shorter lines to control, for example, linac RF phases.

Simrock, Ludwig, and Schlarb have presented much of the most recent data on the performance of optical clocks and much greater detail than here on the ideas and the need to synchronize systems in the X-FELs. They have also given extensive information on the performance of locking of the RF phases in superconducting cavities to a given external microwave source. As a brief summary, the phase of an L-band cavity can be locked to the source such that the residual fluctuations are at the level of 0.01 degrees of RF phase using a control system that is essentially digital in nature. To summarize their main conclusions: (1) The present state-of-the art in synchronization systems is at the fsec level. At this level available commercial low noise phase and amplitude detectors contribute to jitter so a careful selection of components, low noise design, and temperature stabilizations and self-calibrating techniques are needed to achieve this level. (2) Such good performance in a realistic and noisy accelerator environment needs to be demonstrated. (3) In order to quantify, and minimize the jitter in, e.g., beam arrival time, one should develop and implement complete error budgets for all potential sources of arrival time jitter error.

#### 7.1.5.4 *Beam Position*

Measuring the centroid of the beam with stripline or button rf pick-ups is a very mature technology. Such beam position monitors (BPM) will work for an ERL as well. The improvement to BPM systems is in the new digital electronics using the new field programmable gate arrays (FPGA) to add functionality to the BPM. A talk on the digital BPM and feedback system by T. Schilcher presented some of the features of such a system installed at SLS. This system has achieved sub-micron stability and a 4 kHz sample and update rate.

Additionally, two talks on using high order modes (HOM) of the accelerating structures to measure the beam position were presented by Sawamura (JAERI) and Firsch (SLAC). This relationship between the HOM strength and beam position relative to the cavity center has two potential uses. It can be used to measure the alignment of the accelerating structures and thereby provide better modeling information. Additionally if space along the beam is so restricted [i.e. in the injector region] that there is no room for traditional BPM structures, then this HOM technique might provide an alternative.

#### 7.1.5.5 *Machine Protection*

Overview of machine protection concepts were presented by Schlarb (DESY) and Jordan (JLAB), who gave a presentation on the machine protection of the JLAB FEL. Both talks emphasized machine protection based on known concepts and technologies. An ERL would have the same concepts of different states or modes. Diagnostic mode or tune mode for establishing a good orbit through the machine before allowing CW beam delivery. Machine protection and beam loss monitors presently in use at other machines (i.e. photo-multiplier tubes and ion chambers) should work at ERL machines. It was pointed out that machine protection must include the experimental lines as well as the injector.

One of the features of an ERL is the large stored power of the beam. The peak stored power of a 100mA, 6GeV ERL is 600 MWatts and a fractional loss of 1ppm represents 600Watts of power or 100nA of beam current. Experience at JLAB has shown that a continuous loss at this level is sufficient to warm up a flange and open up a vacuum leak. Cameron (BNL) presented a proposal to perform a differential current measurement using two DC current transformer measurements on the ERL test facility at BNL which has a maximum beam energy of 40 MeV. The two transformers are electrically connected such that the current measured in the injection line nulls the signal measured in the dump line. The technique is limited by the noise and estimates suggest a 1 part in  $10^4$  measurement of the loss. This is sufficient for the ERL test facility and hopefully this effort results in some insights on how to improve loss measurements by two orders of magnitude. This is an outstanding issue for high power ERLs.

#### 7.1.5.6 *Summary*

In Working Group 4 many aspects of the electron beam diagnostics systems for new Energy Recovered Linacs were presented and reviewed. The work was divided into several broad categories: transverse diagnostics, for position, profile, and phase space; longitudinal diagnostics for time-of-arrival, longitudinal profile, and longitudinal phase space; the synchronization systems needed as a fundamental aspect of producing properly bunched beam bunches; and aspects of machine protection and beam halos, which will be especially important for high average current ERLs. Since a laser beam produces the electron beam in the first place, and thus is so instrumental in establishing the initial beam properties, more extensive discussions on laser beam diagnostic requirements and capabilities should be subjects for discussions in future meetings.

## 7.2 **Summary of the 34th ICFA Advanced Beam Dynamics Workshop “High Power Superconducting Ion, Proton, and Multi-Species Linacs - HPSL 2005”**

Petr Ostroumov

ANL, 9700 S. Cass Avenue, Argonne, IL, 60439, USA

mail to: [ostroumov@phy.anl.gov](mailto:ostroumov@phy.anl.gov)

### 7.2.1 **Introduction**

The 34th ICFA Advanced Beam Dynamics Workshop “High Power Superconducting Ion, Proton, and Multi-Species Linacs - HPSL 2005” was held in May 22-24 at the Naperville Campus of the Northern Illinois University, Illinois, USA. The Campus is located between two National Laboratories: FNAL and ANL. The conference was organized by the Members of the "Executive Committee": Court Bohn (NIU), Bill Foster (FNAL), and Petr Ostroumov (ANL). The main goal of the Workshop was to discuss common areas of beam dynamics and technology development required for a variety of next-generation high-power superconducting linacs. Currently, there are several proton and ion accelerators worldwide which are being constructed or developed based on superconducting technology. The largest projects are:

- Upgrade of the SNS (USA) and J-PARC (Japan)
- SPL – CERN
- RIA – United States
- 8-GeV Proton Driver – United States
- EURISOL – European Union.

Extensive developments of superconducting technology for accelerator applications in recent years have resulted in several significant technical advances:

- SC resonators offer significantly higher accelerating gradients than those available 5-6 years ago;
- Quality factor of SC resonators has been substantially improved and SC resonators have become more efficient;
- Both cw and pulsed regimes of proton and heavy-ion linacs can be effectively provided by SC technology;
- SC resonators have become available for acceleration of charged particles in a wide range of particle velocities from  $v \sim 0.01c$  to  $v=c$ ;
- Cost-effective techniques of rf power fan-out are being developed: single klystron can feed more than 30 resonators;
- Significant progress has been made in developing control and feedback systems for pulsed operation of high-power RF systems in proton and heavy-ion SC accelerators.

All these advances in technology require a revision of well-established techniques applied for lattice design. The program of the Workshop included four plenary sessions and four parallel sessions covering three topics:

1. Beam Dynamics.
2. Superconducting Radiofrequency Resonators for Ion Linacs.
3. RF systems.

Despite of short notice, 81 participants from 8 countries attended the Workshop. There were 19 invited talks and about 50 contributions on working group sessions. During the three months preceding the Workshop, the conveners have been able to involve accelerator physicists and engineers in the field and organize highly professional working group sessions. The interaction of experts in beam dynamics and SCRF components of proton and heavy-ion linacs was extremely fruitful and constructive.

At this occasion we thank the conveners, the local Organizing Committee as well as the Scientific Advisory Panel for their valuable input. We are especially thankful to Northern Illinois University which made a major contribution in the organization of the Workshop and showed strong accelerator physics activity.

### 7.2.2 Plenary Sessions

The Workshop begun on May 22nd at 3 pm with a plenary session where invited talks from the following facilities were presented:

1. Spallation Neutron Source      D. Olsen (SNS, Oak Ridge)
2. J-PARC                              K. Hasegawa (JAERI)

3. EURISOL	A. Facco (INFN/LNL -Legnaro)
4. CERN-SPL	K. Hanke (CERN)
5. RIA	D. Geesaman (ANL)
6. Proton Driver	G.W. Foster (FNAL)

These presentations covered the general status of the corresponding facilities with particular attention on SCRF technology being used or planned to be used in these facilities and projects. More specialized talks related to all three topics of the Workshop were presented on two other plenary sessions.

On the closeout plenary session, conveners presented summary of the working groups.

### 7.2.3 Parallel working group sessions

#### 7.2.3.1 *Beam Dynamics session*

Conveners: Jean-Michel Lagniel (CEA-Saclay), Petr Ostroumov (ANL)

18 short talks were presented on four sessions with the following sub-topics: a) beam dynamics, general; b) front end designs; b) linac commissioning and operation; c) BD simulation codes.

General beam dynamics design of several proposed H-minus linacs at BNL, FNAL and CERN were presented and discussed in detail. Extensive beam dynamics studies have been performed on CERN 3 GeV SPL and 8 GeV H-minus linac being developed at FNAL. The design philosophy of large multi-GeV linacs is based on three major recommendations:

1. Avoid instabilities by keeping the zero current phase advance (per period) in all planes below 90 deg.
2. Smooth phase advance per meter across all transitions.
3. Avoiding emittance exchange by keeping  $0.4 < \sigma_L / \sigma_T < 0.8$ . Use Hofmann's chart to control this effect.

The front end of new SC accelerators can be based on the existing designs of the SNS and J-PARC linacs. However, the transition energy between the normal conducting and SC structures can be shifted to lower energies down to  $\sim 10$  MeV for proton machines. In heavy-ion linacs SC resonators can be applied immediately after the RFQ. The transition to SC structures is cost-effective not only for cw mode but also for pulsed machines. The increasingly high accelerating gradients available from SC resonators require shorter focusing periods. Using of several different types of SC resonators along the linac results in different lattice structure. Therefore, a careful beam matching must be provided to avoid mismatch and subsequent emittance growth in the lattice transitions.

Some new approaches in the design of high-current electrostatic LEBT were discussed. Particularly, a valuable analysis was presented on using electrostatic quads for transport of low and high intensity beams with minimal aberrations.

### 7.2.3.2 *Superconducting Radiofrequency Resonators for Ion Linacs*

Conveners: Jean Delayen (JLAB), Kenneth Shepard (ANL)

The following sub-topics were presented and discussed in separate sessions: a) medium current multi-species linacs being developed worldwide (RIA, EURISOL, SPIRAL2, SARAF); b) high current pulsed and CW linacs; c) technological limits, pushing frontiers, peak fields and resonator quality factor; d) system integration, construction of facilities and their cost.

Broad issues related to design, construction and operation of various resonator types and their cryostats were presented and discussed on these sessions. The main conclusions of the “SC resonators” working group are:

- The whole velocity range of charged particles is covered by a wide variety of structures and their expected performance and operation have been demonstrated. These structures belong to the following four groups: quarter wave, half wave, multi-spoke and TM-type cavities.
- In the medium velocity range ( $0.4 \leq \beta_G \leq 0.65$ ) two classes of structures have been designed and successfully tested: multi-spoke and elliptical. Both resonators work well. The cost of the structures including cryostats is similar. Generally multi-spoke cavities operate at lower frequency and provide larger longitudinal acceptance than the elliptical cavities. In this velocity range larger longitudinal acceptance can be extremely important in several practical applications.
- Multipacting is still an issue and better simulation codes have to be developed.
- Pulsed operation in the mid-velocity range has been successfully demonstrated.
- Large scale production performance still lags behind what is demonstrated on prototypes.

### 7.2.3.3 *High-power and low level RF*

Conveners: Mark Champion (SNS), Brian Chase (FNAL)

There were four sessions each with its own sub-topic: 1) high power RF; 2) RF system integration; 3) fast phase shifters; 4) LLRF.

Broad issues related to the design and operation of RF systems were discussed on this working group:

- RF system topology. One klystron per cavity as used in SNS and CEBAF or one klystron per many cavities as proposed for FNAL’s proton driver. The RF fan-out from one klystron to many cavities is well advanced in electron linacs, particularly in the TTF for the ILC.
- How to handle a loss of single (or multiple) cavities? The loss of single RF system prevents beam operation and requires detuning of the lost cavity and re-tuning of the linac. The procedure must be done quickly.
- How to control fields at different gradients in cavities that have unique mechanical properties?
- Fast high-power RF modulators (dynamic range, bandwidth, ...).
- Piezoelectric tuners.
- Digital Low-Level RF control systems.

Valuable experience has been gained during the design, construction and initial

operation of the SNS Linac high-power RF system. More experimental data will be available during the commissioning of the SC section of the SNS linac with beam and following operation.

The major task of any accelerator system is to maximize reliability and performance while minimizing cost. This is especially true for the RF system which is a major component of the linac cost. To reduce the linac cost, the future pulsed proton drivers can be based on a fan-out of rf power from one klystron to multiple cavities. The fast phase shifters and amplitude regulators are being developed. Significant contribution to these developments have been made by recent successful testing of the 352 MHz fast ferrite RF cavity tuner at the ANL Advanced Photon Source.

#### 7.2.4 Summary

The Workshop gave an opportunity for extensive communication between accelerator physicists, engineers and accelerator designers. For cw linacs SCRF technology is the only option. The contributions and discussions at the Workshop clearly showed that new generation of linacs operating in pulsed mode can also be based on SCRF. SC resonators can provide acceleration of charged particles starting at  $\sim 30$  keV/u. However, in the energy range below  $\sim 200$  keV/u for heavy-ions and below  $\sim 10$  MeV for protons, the room temperature resonators are still cost-effective.

The rapid developments in SCRF for acceleration of heavy-ions and protons suggest to have similar Workshops biannually, for example, in connection with the next U.S. PAC in 2007.

The presentation can be downloaded from the web-site <http://www.niu.edu/clasep/HPSLconf/presentations.html>. The proceedings will also be available on the web-site and CDs will be distributed among the participants.

### 7.3 Report on the ICFA Mini-workshop on “Commissioning of X-Ray Free-Electron-Lasers” 18-22 April 2005 at DESY, Zeuthen

J. Galayda

[SLAC](http://www.slac.stanford.edu), 2575 Sand Hill Road, Menlo Park, CA 94025, USA

mail to: [galayda@slac.stanford.edu](mailto:galayda@slac.stanford.edu)

J. Rossbach

[Hamburg University and DESY](http://www.desy.de), Notkestrasse 85, 22605 Hamburg, Germany

mail to: [joerg.rossbach@desy.de](mailto:joerg.rossbach@desy.de)

#### 7.3.1 Introduction and Summary

X-ray and soft X-ray FELs like LCLS, the European XFEL and the VUVFEL are complex devices relying on proper functioning of many sub-systems as well as verification of several critical beam parameters. This calls for a well-defined commissioning strategy.

Based on the good experience with previous ICFA Mini-Workshops jointly organized by DESY and SLAC, an ICFA Beam Dynamics Mini-Workshop was held at DESY-Zeuthen, 18-22 April 2005, addressing exclusively the issue of commissioning

of X-ray FELs. The workshop was organized by SLAC and DESY, under the auspices of the ICFA Future Light Sources Subpanel. It was attended by 71 participants from 10 institutes. Information on the workshop, including all presented material, may be found at the workshop website

<http://commissioning2005.desy.de/>

### 7.3.2 Background and Goals of the Workshop

This one week invitational workshop was focused on machine commissioning plans, methods of measurement and correction, and possible strategies for the initial start-up and preliminary operations of future X-Ray Free-Electron Laser (FEL) facilities. The workshop has covered all aspects of the FEL, from photo-cathode drive laser to X-ray beam transport and diagnostics. The goals for the workshop were:

1. To discuss machine start-up strategies, parameters and expectations.
2. To highlight methods and new ideas for optimizing and characterizing the electron and X-ray beams.
3. To review previous relevant FEL commissioning experience.
4. To define the simulation tools and controls environment needed for commissioning and operations.

Of particular interest were methods to diagnose machine errors such as undulator imperfections; ideas to detect and characterize FEL radiation when systems are performing at sub-standard levels; and detailed simulations used to support machine setup, measurement and feedback strategies.

In order to facilitate a focused discussion, selected LCLS and European-XFEL subsystems were studied by the participants prior to the workshop, based on work packaged prepared by the program committee. For example, one task was the analysis of view screen images resulting from quadrupole scans done at the SLAC injector to determine the electron beam emittance. Similarly, participants were asked to determine the emittance from OTR images taken in the four-screen emittance measurement section at the VUV-FEL at DESY.

In this spirit, a total of six work packages were set up:

1. Injector commissioning:

As the requirements for brighter electron beams become more demanding, the need for accurate and detailed analysis of beam data becomes essential. Therefore it is important to review and understand the various methods used to obtain important beam properties such as emittance and others. It was with this objective in mind that the LCLS-TTF commissioning plans were discussed during the workshop. A goal of the injector commissioning working group was to compare the various methods of analysis for emittance and other beam properties. This was done by requesting the participants to analyze experimental and simulated data for six injector problems. Transverse and longitudinal emittances as well as reconstruction of the phase space using tomography were obtained and presented. Major differences between the

techniques were in the subtraction of the background and how the tails of the distribution were truncated. For the experimental data the comparison of the transverse emittances found for the various techniques were quite close, however the error bars varied considerably. Another interesting outcome concerned the analysis of simulation data with a noisy background. The analysis gave 20 to 25% smaller emittances than the known simulation values due mostly to the truncation of the tails. As a consequence, the differences in 100%-emittance values quoted by different workers were considerably larger than the (statistical) errors specified by most of them. The LCLS commissioning plans and results from injector commissioning at PITZ and TTF were also presented. A collaborative paper is in progress and a web site is planned to make these results and analysis tools (especially the tomography software) generally available.

2. Linac commissioning

3. Analysis of simulated X-ray pulses:

The most recent development in the start-end simulation effort is the integration of the X-ray beam line beyond the FEL. It includes the tracking of wavefronts, or alternatively the mutual intensity functions, through optical elements to the user's experimental station. So far only mono-chromatic beams can be transported but frequency-dependent elements such as gratings or monochromators are under development. The interface with FEL codes (Ginger and Genesis) has been established. As a supplement to FEL simulations, additional codes can calculate the spectrum and angular distribution of the full spontaneous radiation. Because the algorithm is based on Lienard-Wiechert potentials, the simulations cannot include boundary conditions such as the aperture limitation due to the vacuum chamber. The problem is solved with Monte-Carlo ray-tracing simulations, which use the results of the Lienard-Wiechert simulation as the base to generate the angular and spectral distribution of the ray traces with a uniform source along the undulator axis.

4. Analysis of TTF-II Startup

5. X-Ray Optics and End Station Commissioning

6. Undulator commissioning

The program consisted of

- A few introductory talks on the work packages,
- A number of presentations on the problems given to the participants,
- Discussions on the results, and
- Contributed talks on issues related to the respective work packages.

It should be mentioned that setting up all the work packages (dealing with non-trivial commissioning issues and real, recent measurement results) meant quite some effort for the program committee, including a number of video conferences for coordination. Finally, of course, it was the serious work of the participants devoted to the problems posted on the web which made the workshop a real success. All presented material may be found at the workshop website cited above.

## 8 Forthcoming Beam Dynamics Events

### 8.1 The 35<sup>th</sup> Advanced Beam Dynamics Workshop: The Physics and Applications of High Brightness Electron Beams

*Place and date: Erice, Sicily, October 9-14, 2005*

James Rosenzweig

[UCLA Dept. of Physics and Astronomy](#), 405 Hilgard Ave., Los Angeles, CA 90095

mail to: [rosen@physics.ucla.edu](mailto:rosen@physics.ucla.edu)

#### 8.1.1 Workshop background

This workshop represents the latest in a series that has resulted from two parent traditions: the “Arcidosso” advanced beam dynamics series, and the “High Brightness” series (e.g. UCLA, 1999). The first in the merged series, also entitled “The Physics and Applications of High Brightness Electron Beams”, took place in Sardinia, Italy, in 2002. This year’s workshop will be held in Erice, Sicily, October 10-14, 2005. It has been endorsed by both the ICFA Panels on Beam Dynamics and Advanced & Novel Accelerator. The workshop will be hosted by the “E. Majorana” Centre in Erice.

#### 8.1.2 Workshop mission

High brightness electron beams are playing an increasingly critical role in two frontier fields: radiation generation methods and advanced acceleration schemes. Such state-of-the-art radiation production methods include various types of free-electron lasers, as well as inverse Compton scattering (ICS) of intense lasers, having diverse approaches to creating high peak and average power light sources. As they are capable of harder photon production, ICS sources are candidates not only for X-ray sources, but also high-energy physics applications. Likewise, high brightness beams are at the center of future accelerator schemes, e.g. based on high gradient wakefields, and electron cooling. Indeed, possibilities exist to create unique light sources based on advanced acceleration schemes, just as intense lasers and X-ray beams enable advanced accelerator research. The goal of this workshop is to provide a comparative study of the generation, manipulating, modeling and measuring of high brightness electron beams, and the underlying methods linking the physics of these beam systems to the physics of advanced applications.

#### 8.1.3 Program

The program has been prepared, and will include invited and contributed plenary talks in the mornings, with the afternoons dedicated to working groups. Invited talks have been issued, and a full agenda will be published by the end of July 2005.

The proceedings will be published by World Scientific as dictated by the E. Majorana Centre and the workshop series traditions. Additionally, a special issue of

PRST-AB dedicated to the workshop is also planned, as was successfully done for the Sardinia workshop (<http://prst-ab.aps.org/speced/HB2002>).

The following working groups are foreseen:

1. Sources, including photoinjectors and plasma-based sources
2. Manipulation and diagnosis of high brightness beams
3. Theory and modeling, simulation challengers
4. Applications of high brightness beams in advanced accelerators and light sources.

#### 8.1.4 Contact and registration

The workshop web site is found at <http://www.physics.ucla.edu/PAHBEB2005/>. Registration is now open. As the number of attendees will be limited, early registration encouraged. The registration fee will be 600 Euro, and will include lodging, full board, travel to and from Palermo and a copy of the conference proceedings.

#### 8.1.5 Committees

The following committees are involved in organization and programming of the workshop:

##### Organizing committee

###### **Co-chairs**

**L. Palumbo (Univ. Roma)**

**J. Rosenzweig (UCLA)**

**L. Serafini (INFN-Milano)**

G. Krafft (JLAB)

H. Braun (CERN)

K-J. Kim (UC/ANL)

S. Bertolucci (INFN-LNF)

I. Ben-Zvi (BNL)

A. Renieri (ENEA)

S. Milton (ANL)

S. Chattopadhyay (JLAB)

J. Galayda (SLAC)

M. Poole (Daresbury)

C. Bocchetta (Sinc. Trieste)

K. Floettmann (DESY)

P. Krejcik (SLAC)

##### Program committee

C. Pellegrini (UCLA)

W. Barletta (LBNL)

M. Ferrario (INFN-LNF)

P. Emma (SLAC)

D. Dowell (SLAC)

L. Giannessi (ENEA)

J. Murphy (BNL)

P. O'Shea (Univ. Maryland)

J. Rossbach (DESY)

T. Garvey (LAL)

M. Eriksson (MAXLAB)

G. D'Auria (Sinc. Trieste)

D. Giulietti (Univ. Pisa)

## 8.2 The 36<sup>th</sup> ICFA Advanced Beam Dynamics Workshop: Nanobeam 2005

*Place and date: Uji-city, Kyoto, Japan, October 17-21, 2005*

Akira Noda  
Advanced Research Center for Beam Science  
Institute for Chemical Research, Kyoto University  
mail to: [noda@kyticr.kuicr.kyoto-u.ac.jp](mailto:noda@kyticr.kuicr.kyoto-u.ac.jp)

### 8.2.1 Topics

The Nanobeam 2005 workshop will focus on beam dynamics of low-emittance beam generation, tuning, feedback, beam diagnosis, ground motion, stabilization, and beam delivery system for the linear collider. In addition to these topics, related research efforts on synchrotron light sources, permanent and superconducting magnets, and photon colliders will also be included, as was already the case at the Nanobeam 2002 workshop. We foresee an additional miscellaneous session addressing cooling techniques which may produce low-emittance nanobeams, and applications of nano-scale precision beams.

### 8.2.2 Sessions

The workshop is to be composed of the following sessions.

1. Laserwire mini-workshop
2. Linear Colliders ( ILC and CLIC )
  - a) BDS-design and interaction region
  - b) stabilization and beam control
  - c) Future R&D Plans
3. Advanced Beam Science
  - a) Low emittance sources
  - b) FELs and radiation sources
  - c) Applications

### 8.2.3 Committees

#### The International Advisory Committee

P. Debu (CEA/Saclay)	D. Burke (SLAC)
J.P. Delahaye (CERN)	S. Holmes (FNAL)
S. Ozaki (BNL)	S.I. Kurokawa (KEK)
S. Myers (CERN)	A. Skrinsky (BINP)
D. Trines (DESY)	A. Wrulich (PSI)
N. Sasao (Kyoto U.)	Y. Kamiya (KEK)

#### International Program and Organizing Committee

R. Assmann (CERN)	A. Bay (Lausanne U.)
G. Blair (Royal Holloway)	R. Brinkmann (DESY)
P. Burrows (QMUL)	B. Dehning (CERN)

J.G. Dugan (Cornell U.)	Jie Gao (IHEP)
M. Harrison (BNL)	M. Hildreth (NotreDame U.)
K.J. Kim (ANL)	N. Kumagai (SPring-8)
M. Mayoud (CERN)	O. Napoly (CEA/Saclay)
A. Noda (Kyoto U.)	T. Raubenheimer (SLAC)
L. Rivkin (PSI)	S. Russenschuck (CERN)
A. Seryi (SLAC)	T. Shintake (RIKEN)
V. Shiltsev (FNAL)	D. Angal-Kalinin (Daresbury)
S. Mishra (FNAL)	J. Urakawa (KEK)
V. Telnov (BINP)	N. Toge (KEK)
N. Walker (DESY)	K. Yokoya (KEK)
L. Zhang (ESRF)	F. Zimmermann (CERN)
A. Wolski (LBNL)	

#### **Local Organizing Committee**

A. Noda (Kyoto U.)	J. Urakawa (KEK) -- Chairmen
Y. Iwashita (Kyoto U.)	T. Tauchi (KEK) -- Scientific Secretariat
T. Shirai (Kyoto U.)	T. Nomura (Kyoto U.)
M. Kumada (NIRS)	Y. Honda (KEK)
T. Sanuki (U. Tokyo)	T. Yamazaki (Kyoto U.)
H. Ohgaki (Kyoto U.)	K. Masuda (Kyoto U.)

#### **The Co-operative Organizers**

Nanobeam 2005 is organized as a workshop of the 21st Century Center of Excellence (Center for Diversity and Universality in Physics at Kyoto University) and it is jointly hosted by the following three institutes: Institute for Chemical Research, Kyoto University, High Energy Accelerator Research Organization (KEK), Yukawa Institute for Theoretical Physics.

#### **8.2.4 Contact**

Further information are available through the workshop homepage at <http://wwwal.kuicr.kyoto-u.ac.jp/nanobm/> and any questions and opinions are required to be sent to the Scientific Secretariat at [iwashita@kyticr.kuicr.kyoto-u.ac.jp](mailto:iwashita@kyticr.kuicr.kyoto-u.ac.jp).

### **8.3 The 37<sup>th</sup> Advanced Beam Dynamics Workshop: Future Light Sources 2006**

*Place and date: DESY, Hamburg, Germany, May 15-19, 2006*

Further announcements will be published in one of the next issues of the newsletter.

### **8.4 The 38<sup>th</sup> Advanced Beam Dynamics Workshop: LBI-LPA 2005, Laser-Beam Interactions and Laser Plasma Accelerators**

*Place and date: National Taiwan University, Taipei, Taiwan, Dec. 12-16, 2006*

Further announcements will be published in one of the next issues of the newsletter.

## **8.5 Mini-Workshop on Low Level RF: LLRF05**

*Place and date: CERN, Geneva, 10-13 October 2005*

T. Linnecar, P. Shinnie, CERN, Geneva  
mail to: [Ab-Rf Secretaries@cern.ch](mailto:Ab-Rf Secretaries@cern.ch)

### **8.5.1 Topics**

Sophisticated Low Level RF systems are needed in modern particle accelerators to deal with the characteristics of state-of-the-art RF accelerating structures and their power sources, and to meet unprecedented levels of performance. The goal of the LLRF05 Workshop is to share experience between linac and synchrotron projects (SNS, J PARC, ILC, LHC etc.) and to discuss the best engineering practice.

This four-day Workshop will be the 15th in the series of mini-workshops under the auspices of the ICFA Beam Dynamics Panel (<http://www-bd.fnal.gov/icfabd/>) and specifically will be the second in a series on low level RF techniques, initiated at Jefferson Lab, USA, in 2001 (<http://www.jlab.org/intralab/calendar/archive01/LLRF>).

### **8.5.2 Registration**

Workshop registration is now approaching the final date – 1 August 2005. Considerable interest has been shown in LLRF05. There are already ~ 70 participants, and we are now approaching the maximum numbers that can be accepted. If you are interested in participating please register soon at <http://cern.ch/LLRF05>. Please note also that very few CERN hostel rooms remain available and must now be booked by contacting the hostel directly at [cern.hostel@cern.ch](mailto:cern.hostel@cern.ch) (not via the LLRF05 website). Please also note that hotel rooms in Geneva are usually booked well in advance.

### **8.5.3 Programme**

We thank very much all those who have submitted abstracts. Following the closure of registration we will contact all authors individually. At the same time we will post the initial version of the complete scientific programme including posters and mini-oral talks on the web-site. This will be updated periodically as final details are known.

The definition of the programme of invited talks which will take place is well advanced, the session chairmen and the convenors of the four working groups and their scientific secretaries have been nominated.

We encourage all participants to contact the working group convenors with any ideas of subjects, controversial issues etc. that they would like to have discussed.

We remind you that talks will be made immediately available on the web and although there will be no published proceedings a CD-ROM with all the material presented at the Workshop will be distributed to the registered participants.

### 8.5.4 Contact

Please address any enquiries to [Ab-Rf Secretaries@cern.ch](mailto:Ab-Rf_Secretaries@cern.ch) to be dealt with by: Patricia Shinnie, Secretary to the Scientific Programme Committee, or Lidia Ghilardi, Secretary to the Local Organizing Committee.

### 8.5.5 Committees

#### Scientific Programme Committee

K. Akai (KEK)	C. Hovater (JLab)
M. Brennan (BNL)	M. Liepe (Cornell)
M. Champion (SNS)	T. Linnekar (CERN) (Chair)
B. Chase (FNAL)	P. Shinnie (CERN) (Secretary)
L. Doolittle (LBNL)	S. Simrock (DESY)
R. Garoby (CERN)	D. Teytelman (SLAC)

#### Local Organizing Committee

M-E. Angoletta,	L. Ghilardi (Secretary),
P. Baudreghien,	T. Linnekar,
A. Blas	F. Pedersen (Chair),
R. Garoby	P. Shinnie

## 8.6 Mini-Workshop on “The Frontier of Short Bunches in Storage Rings”

*Place and date: INFN-LNF, Frascati, Italy, November 7-9, 2005*

Mario Serio

Laboratori Nazionali di Frascati - Via E. Fermi, 40 -- I-00044 Frascati (Rome) Italy  
mail to: [mario.serio@lnf.infn.it](mailto:mario.serio@lnf.infn.it)

### 8.6.1 Topics

INFN - Laboratori Nazionali di Frascati, under the auspices of the ICFA Beam Dynamics Panel, is organizing the ICFA mini-workshop “The Frontier of Short Bunches in Storage Rings”, on November 7-9, 2005 at LNF-Frascati. The scope of the workshop is to discuss the possibility of obtaining very short bunches in e+e- colliders and synchrotron light sources and the related issues.

Since short bunches at the IP allow to lower the beta\*, possibly gaining correspondingly in luminosity, techniques to shorten bunches in storage rings are of interest for the super-factory community.

The synchrotron light community can be interested as well, since bunches in the mm scale are useful for time-resolved experiments and essential for stable production of coherent synchrotron radiation.

A web page is being prepared at the site <http://www.lnf.infn.it/conference/sbsr05>. It will be updated as the organization goes on.

## 8.6.2 Organizing Committee

Caterina Biscari *	Sasha Novokhatski, SLAC
John Byrd, LBL	Katsunobu Oide, KEK
Mario Calvetti * (LNF Director)	Miro Andrea Preger *
Alessandro Drago *	Francesco Ruggiero, CERN
Alessandro Gallo *	Claudio Sanelli *
Andrew Hutton, JLAB	Mario Serio * (Chairman)
Evgenii Levichev, BINP	Alexander Temnykh, CESR
Fabio Marcellini *	Godehard Wüstefeld, BESSY-II
Catia Milardi *	Mikhail Zobov *

\* LOCAL ORGANIZING COMMITTEE - LNF

## 8.7 An one year International Scoping Study on Neutrino Factories and Superbeams.

*Place and date of first meeting: CERN, Switzerland, September 22-24, 2005*

V. Palladino, [Univ & INFN Napoli](#), Italy  
mail to: [Vittorio.Palladino@na.infn.it](mailto:Vittorio.Palladino@na.infn.it)

### 8.7.1 Introduction

The recent undisputed evidence for transition in flight among different neutrino species, and therefore for non zero neutrino mass, strongly suggests the realization of new and superior accelerator neutrino facilities.

A strong and coherent international initiative has been taking shape in recent years. A preliminary International Scoping Study (ISS) on neutrino factory and superbeam has thus been prepared in the first half of 2005 and launched at NuFact05, the 7<sup>th</sup> International Workshop on Neutrino Factory and Superbeam, held in Frascati in June 2005.

The ISS will last one year and will report his results and proposals at NuFact06, that will be held in Irvine, California, in August 2006. The first meeting of the ISS will be held at CERN on Sep 22-24.

### 8.7.2 Neutrino Oscillation Physics today

Transition in flight of electron neutrinos to other active neutrinos, presumably muon and tau neutrinos, has been established by solar neutrino detector experiments. Its oscillatory nature, with a wavelength of about 100 Km/MeV, has also been confirmed by a terrestrial reactor experiment.

Transition in flight of atmospheric muon neutrinos, presumably into tau neutrinos, has simultaneously been demonstrated and confirmed in an accelerator experiment. Its oscillatory nature seems also established, with a wavelength of about 500 Km/GeV.

Several decades of experiments will probably be necessary to establish the common nature and the fundamental physical quantities governing these two phenomena. Presumably, they are part of a  $3 \times 3$  complex mixing matrix that predicts the detection of many additional transitions and, because of the existence of a phase, of far reaching CP and T-reversal asymmetries. As an analogy, the study of mixing among quarks has now been in progress for about 50 years.

### 8.7.3 Future Neutrino Beams

One of the necessary tools for this physics program are new superior accelerator neutrino beams. The ones presently envisaged are:

- 1) Conventional beams, based on a decay tunnel for pions (neutrino parents), of unprecedented power, several MWatts (**Superbeams**).
- 2) Novel beams, based on storage rings where neutrino parents are coasting and decaying. Two kinds have been proposed, that envisage the acceleration and storage of muons (**Neutrino Factories**) or of radioactive beta emitting ions (**Betabeams**).

Neutrino Betabeams are the subject of a complete 4 years Design Study that was approved in 2004, will last from 2005 to 2008 and produce a Conceptual Design Report (CDR) by early or mid 2009.

The ISS will continue the progress with Neutrino Factory and Superbeam (that technically largely coincides with the front end of a Factory) studies, and prepare the way for the first fully global design study for these new neutrino facilities. The goal of the ISS is to prepare a longer and more in depth, full blown Design Study, so to have a CDR ready by 2010 or so in this sector too.

A proposal for a new superior neutrino facility will become thus possible, based on these two CDRs, at about the right time for new major investments in particle physics. When presumably LHC expenditures will be completed, its first results available and a decision on the ILC taken.

### 8.7.4 The International Scoping Study

It is organized jointly by the US NuFact & Muon Collaboration, the Japanese NuFact-J Collaboration and the EU ECFA/BENE (Beams for European Neutrino Experiments) Network. CCLRC (Rutherford Lab) and the UK Neutrino Factory Collaboration [5] will be the host of the ISS. The Study Plan of the ISS will include:

- 1) study of the physics reach of future accelerator neutrino beams. Neutrino factories and superbeams will be compared to each other and to neutrino betabeams.
- 2) study of the crucial issues in the accelerator sector: proton drivers, target and collection systems (common to Factories and Superbeams) and ionization cooling, acceleration and storage of muons (specific of Factories).
- 3) study of the outstanding issues involved in the realization of neutrino detectors of adequate mass and performance for all the three beam options.

Emphasis will be on the identification of the crucial R&D areas in all sectors above, that the Design Study will have later to tackle in depth.

The first of the four meetings of the ISS will be at CERN, Sep 22-24, 2005. Its preliminary agenda is available at <http://dpnc.unige.ch/users/blondel/ISSatCERN.htm>. The following ones will be in Japan in January, at RAL in April and in California in August at the occasion of NUFAC06.

Any institute or individual interested in future neutrino physics facilities is encouraged to contribute and asked to contact any member of the Programme Committee. Reflecting the Study Plan, this consists of Yori Nagashima (Physics Group: [nagay@snow.dti2.ne.jp](mailto:nagay@snow.dti2.ne.jp)), Mike Zisman (Accelerator Group: [mszisman@lbl.gov](mailto:mszisman@lbl.gov)) Alain Blondel (Detector Group: [Alain.Blondel@cern.ch](mailto:Alain.Blondel@cern.ch)). Overall leader is Peter Dornan [P.Dornan@imperial.ac.uk](mailto:P.Dornan@imperial.ac.uk)

### 8.7.5 References

References can be found at the Web Site quoted.

## 9 Announcements of the Beam Dynamics Panel

### 9.1 ICFA Beam Dynamics Newsletter

#### 9.1.1 Aim of the Newsletter

The ICFA Beam Dynamics Newsletter is intended as a channel for describing unsolved problems and highlighting important ongoing works, and not as a substitute for journal articles and conference proceedings that usually describe completed work. It is published by the ICFA Beam Dynamics Panel, one of whose missions is to encourage international collaboration in beam dynamics.

Normally it is published every April, August and December. The deadlines are 15 March, 15 July and 15 November, respectively.

#### 9.1.2 Categories of Articles

The categories of articles in the newsletter are the following:

1. Announcements from the panel.
2. Reports of beam dynamics activity of a group.
3. Reports on workshops, meetings and other events related to beam dynamics.
4. Announcements of future beam dynamics-related international workshops and meetings.
5. Those who want to use newsletter to announce their workshops are welcome to

do so. Articles should typically fit within half a page and include descriptions of the subject, date, place, Web site and other contact information.

6. Review of beam dynamics problems: This is a place to bring attention to unsolved problems and should not be used to report completed work. Clear and short highlights on the problem are encouraged.
7. Letters to the editor: a forum open to everyone. Anybody can express his/her opinion on the beam dynamics and related activities, by sending it to one of the editors. The editors reserve the right to reject contributions they judge to be inappropriate, although they have rarely had cause to do so.
8. Editorial.

The editors may request an article following a recommendation by panel members. However anyone who wishes to submit an article is strongly encouraged to contact any Beam Dynamics Panel member before starting to write.

### 9.1.3 How to Prepare a Manuscript

Before starting to write, authors should download the template in Microsoft Word format from the Beam Dynamics Panel web site:

<http://www-bd.fnal.gov/icfabd/news.html>

It will be much easier to guarantee acceptance of the article if the template is used and the instructions included in it are respected. The template and instructions are expected to evolve with time so please make sure always to use the latest versions.

The final Microsoft Word file should be sent to one of the editors, preferably the issue editor, by email.

The editors regret that LaTeX files can no longer be accepted: a majority of contributors now prefer Word and we simply do not have the resources to make the conversions that would be needed. Contributions received in LaTeX will now be returned to the authors for re-formatting.

In cases where an article is composed entirely of straightforward prose (no equations, figures, tables, special symbols, etc.) contributions received in the form of plain text files may be accepted at the discretion of the issue editor.

Each article should include the title, authors' names, affiliations and e-mail addresses.

### 9.1.4 Distribution

A complete archive of issues of this newsletter from 1995 to the latest issue is available at

<http://icfa-usa.jlab.org/archive/newsletter.shtml>

This is now intended as the primary method of distribution of the newsletter.

Readers are encouraged to sign-up for electronic mailing list to ensure that they will hear immediately when a new issue is published.

The Panel's Web site provides access to the Newsletters, information about future and past workshops, and other information useful to accelerator physicists. There are

links to pages of information of local interest for each of the three ICFA areas.

Printed copies of the ICFA Beam Dynamics Newsletters are also distributed (generally some time after the Web edition appears) through the following distributors:

Weiren Chou	<a href="mailto:chou@fnal.gov">chou@fnal.gov</a>	North and South Americas
Rainer Wanzenberg	<a href="mailto:rainer.wanzenberg@desy.de">rainer.wanzenberg@desy.de</a>	Europe* and Africa
Susumu Kamada	<a href="mailto:Susumu.Kamada@kek.jp">Susumu.Kamada@kek.jp</a>	Asia** and Pacific

\* Including former Soviet Union.

\*\* For Mainland China, Jiu-Qing Wang ([wangjq@mail.ihep.ac.cn](mailto:wangjq@mail.ihep.ac.cn)) takes care of the distribution with Ms. Su Ping, Secretariat of PASC, P.O. Box 918, Beijing 100039, China.

To keep costs down (remember that the Panel has no budget of its own) readers are encouraged to use the Web as much as possible. In particular, if you receive a paper copy that you no longer require, please inform the appropriate distributor.

### 9.1.5 Regular Correspondents

The Beam Dynamics Newsletter particularly encourages contributions from smaller institutions and countries where the accelerator physics community is small. Since it is impossible for the editors and panel members to survey all beam dynamics activity worldwide, we have some Regular Correspondents. They are expected to find interesting activities and appropriate persons to report them and/or report them by themselves. We hope that we will have a “compact and complete” list covering all over the world eventually. The present Regular Correspondents are as follows:

Liu Lin	<a href="mailto:liu@ns.inls.br">liu@ns.inls.br</a>	LNLS Brazil
S. Krishnagopal	<a href="mailto:skrishna@cat.ernet.in">skrishna@cat.ernet.in</a>	CAT India
Sameen Ahmed Khan	<a href="mailto:rohelakhan@yahoo.com">rohelakhan@yahoo.com</a>	MECIT Middle East and Africa

We are calling for more volunteers as *Regular Correspondents*.

## 9.2 ICFA Beam Dynamics Panel Members

Caterina Biscari	<a href="mailto:caterina.biscari@lnf.infn.it">caterina.biscari@lnf.infn.it</a>	LNF-INFN, Via E. Fermi 40, C.P. 13, Frascati, Italy
Yunhai Cai	<a href="mailto:yunhai@slac.stanford.edu">yunhai@slac.stanford.edu</a>	SLAC, 2575 Sand Hill Road, MS 26 Menlo Park, CA 94025, U.S.A.
<u>Swapan Chattopadhyay</u>	<a href="mailto:swapan@jlab.org">swapan@jlab.org</a>	Jefferson Lab, 12000 Jefferson Avenue, Newport News, VA 23606, U.S.A.
Weiren Chou (Chair)	<a href="mailto:chou@fnal.gov">chou@fnal.gov</a>	Fermilab, MS 220, P.O. Box 500, Batavia, IL 60510, U.S.A.
Yoshihiro Funakoshi	<a href="mailto:yoshihiro.funakoshi@kek.jp">yoshihiro.funakoshi@kek.jp</a>	KEK, 1-1 Oho, Tsukuba-shi, Ibaraki-ken, 305-0801, Japan
Miguel Furman	<a href="mailto:mafurman@lbl.gov">mafurman@lbl.gov</a>	Center for Beam Physics, LBL, Building 71, R0259, 1 Cyclotron Road, Berkeley, CA 94720-8211, U.S.A.
Jie Gao	<a href="mailto:gaoj@ihep.ac.cn">gaoj@ihep.ac.cn</a>	Institute for High Energy Physics, P.O. Box 918, Beijing 100039, China
Ingo Hofmann	<a href="mailto:i.hofmann@gsi.de">i.hofmann@gsi.de</a>	High Current Beam Physics, GSI Darmstadt, Planckstr. 1, 64291 Darmstadt, Germany
Sergei Ivanov	<a href="mailto:ivanov_s@mx.ihep.su">ivanov_s@mx.ihep.su</a>	Institute for High Energy Physics, Protvino, Moscow Region, 142281 Russia
Kwang-Je Kim	<a href="mailto:kwangje@aps.anl.gov">kwangje@aps.anl.gov</a>	Argonne Nat'l Lab, Advanced Photon Source, 9700 S. Cass Avenue, Bldg 401/C4265, Argonne, IL 60439, U.S.A.
In Soo Ko	<a href="mailto:isok@postech.ac.kr">isok@postech.ac.kr</a>	Pohang Accelerator Lab, San 31, Hyoja- Dong, Pohang 790-784, South Korea
Alessandra Lombardi	<a href="mailto:Alessandra.Lombardi@cern.ch">Alessandra.Lombardi@cern.ch</a>	CERN, CH-1211, Geneva 23, Switzerland
Yoshiharu Mori	<a href="mailto:mori@kl.rii.kyoto-u.ac.jp">mori@kl.rii.kyoto-u.ac.jp</a>	Research Reactor Inst., Kyoto Univ. Kumatori, Osaka, 590-0494, Japan
Chris Prior	<a href="mailto:c.r.prior@rl.ac.uk">c.r.prior@rl.ac.uk</a>	ASTeC Intense Beams Group, Rutherford Appleton Lab, Chilton, Didcot, Oxon OX11 0QX, U.K.
David Rice	<a href="mailto:dhr1@cornell.edu">dhr1@cornell.edu</a>	Cornell Univ., 271 Wilson Laboratory, Ithaca, NY 14853-8001, U.S.A.
Yuri Shatunov	<a href="mailto:Yu.M.Shatunov@inp.nsk.su">Yu.M.Shatunov@inp.nsk.su</a>	Acad. Lavrentiev, prospect 11, 630090 Novosibirsk, Russia
Junji Urakawa	<a href="mailto:junji.urakawa@kek.jp">junji.urakawa@kek.jp</a>	KEK, 1-1 Oho, Tsukuba-shi, Ibaraki-ken, 305-0801, Japan
Jie Wei	<a href="mailto:wei@bnl.gov">wei@bnl.gov</a>	BNL, Bldg. 911, Upton, NY 11973- 5000, U.S.A.
Jiu-Qing Wang	<a href="mailto:wangjq@mail.ihep.ac.cn">wangjq@mail.ihep.ac.cn</a>	Institute for High Energy Physics, P.O. Box 918, 9-1, Beijing 100039, China
Rainer Wanzenberg	<a href="mailto:Rainer.wanzenberg@desy.de">Rainer.wanzenberg@desy.de</a>	DESY, Notkestrasse 85, 22603 Hamburg, Germany

*The views expressed in this newsletter do not necessarily coincide with those of the editors. The individual authors are responsible for their text.*